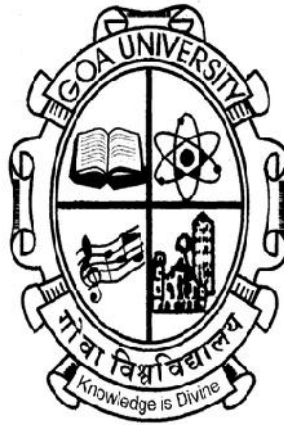


**GEOLOGY AND CHARACTERISTICS OF METAGREYWACKE
AND ASSOCIATED ROCKS OF GOA GROUP, INDIA**

A THESIS SUBMITTED TO
GOA UNIVERSITY
FOR THE AWARD OF THE DEGREE OF
DOCTOR OF PHILOSOPHY
IN
GEOLOGY



BY
Ms. GLANCIA Q. FERNANDES

Research Guides

Prof. KOTHA MAHENDER

Goa University,
Taleigao, Goa

Dr. SRIDHAR D. IYER

CSIR-National Institute of Oceanography,
Dona Paula, Goa

March 2018

DEDICATED
TO
MY PARENTS
&
TEACHERS

CERTIFICATE

This is to certify that the thesis entitled “**Geology and Characteristics of Metagreywacke and Associated Rocks of Goa Group, India**” submitted to Goa University, by Ms. Glancia Q. Fernandes for the award of the degree of **Doctor of Philosophy in Geology** is a record of original and independent work carried out by her during the period of December 2012- March 2018 under my supervision and the same has not been previously submitted for the award of any diploma, degree, associateship or fellowship or any other similar title.

Goa University

March 2018

Prof. Kotha Mahender

(Research Guide)

Dr. Sridhar D. Iyer

(Research Co-Guide)

DECLARATION

I hereby declare that the matter embodied in this thesis entitled “**Geology and Characteristics of Metagreywacke and Associated Rocks of Goa Group, India**” submitted to Goa University, for the award of the degree of **Doctor of Philosophy in Geology** is a record of original and independent work carried out by me during the period of December 2012- March 2018 under the supervision of Prof. Kotha Mahender, Department of Earth Science, Goa University and Dr. Sridhar D. Iyer, CSIR-National Institute of Oceanography, Dona Paula and that it has not been previously formed the basis for award of any diploma, degree, associateship or fellowship or any other similar title.

Goa University

March 2018

Ms. Glancia Q. Fernandes

(Research Scholar)

ACKNOWLEDGEMENT

I would like to express my sincere gratitude to Prof. Kotha Mahender and Dr. Sridhar D. Iyer for their wise counsel, guidance and co-operation. They constantly and patiently guided and encouraged me during the course of the work. I take this opportunity to express my gratitude to them for their constant involvement in the study, valuable suggestions, critical evaluation of the findings and patient review of the manuscript.

I gratefully acknowledge Dr. J. N. Pattan (V.C. Nominee) for constantly evaluating my progress during my study and also for valuable suggestions given to improve the study. I am also thankful to him for providing ICP-MS facilities at CSIR-NIO, Dona Paula.

I acknowledge Vice Chacellor, Goa University and the Director, CSIR-NIO for the various permissions to carry out this work. I would like to thank Director, Mr. Prasanna Acharya and staff of Directorate of Mines and Geology, Panaji, Goa. My grateful thanks to Director, Fr. Kinley D'Cruz and staff of Don Bosco College of Engineering for the help rendered to me. I owe special thanks to Dr. Abhay Mudolkar, CSIR-NIO, Dona Paula, Goa for providing

me with XRF analysis. My gratitude also goes to Dr. Thamban Melloth, National Centre for Antarctic and Ocean Research (NCAOR), Mormugao, Goa, for providing me ICP-MS facilities. I would also like to thank Dr. Brenda Mascarenhas e Pereira (CSIR-NIO, Dona Paula, Goa) for providing the facilities for ICP-MS analysis. My thanks are also due to Dr. G. Parthiban for conducting the ICP-MS analysis and also Mr. V.M. Khedekar (CSIR-NIO, Dona Paula) for conducting EPMA analysis.

I also take this opportunity to thank my teachers from the Department of Earth Science, Goa University Dr. A. Dessai, Dr. A.G. Chachadi, Dr. T.A. Vishwanath and Dr. Anthony Viegas and also teachers from Smt. Parvatibai Chowgule College of Arts and Science, Prof. H. Nadkarni, Prof. Katti, Prof. Allan Rodrigues and Prof. Meghana Devli for their support and guidance during the work.

I would like to express my gratitude to Purshottam Verlekar, Sanford Mascarenhas, Malcolm Afonso, Richard Lobo, my brother Johan Fernandes and my father Gromiko Fernandes for accompanying me in the field, without which this study would not have been possible.

Special thanks to Milind Naik, Ankeeta Amonkar, Jubi Thomas, Sufiyan Shaikh, Pooja Shirodkar, Clyde Antao, Svetlana Fernandes, Mahesh Mayekar and Raghav Gadgil for their assistance during the laboratory work and also for rendering help during the various stages of my work.

I also extend my gratitude to the non - teaching staff of Department of Earth Science, Goa University, Mr. Premakant Gawas, Ms. Sangita Tilve, Mr. Tilve and Mr. Devidas Gawade for their assistance during the laboratory work. I would also like to thank Dr. Reshma Raut Dessai, Dr. Niyati Kalangutkar and Mr. Vasant Karelkar for their constant support and assistance.

I express my profound gratitude to my parents, Mr. Gromiko and Mrs. Leonora Fernandes and brother Johan who supported me without any boundaries throughout the completion of the work, without which this would not have been possible. They are the pillars of support at all times and also a continual encouragement. I would also like to thank my husband Mr. Allison Mascarenhas for supporting and helping me in completion of this thesis.

Above all, I thank the Almighty for showering me with His Grace.

Glancia Queenie Fernandes

INDEX

| Chapter No. | Contents | Page No. |
|--------------------|--|-----------------|
| 1 | INTRODUCTION | |
| | 1.1 Prologue | |
| | 1.2 Background to the problem | |
| | 1.3 Previous work | |
| | 1.4 Aim and objectives | |
| | 1.5. Study area | |
| | 1.5.1 Location | |
| | 1.5.2 Accessibility | |
| | 1.5.3 Climate | |
| | 1.5.4 Physiography | |
| | 1.5.5 Drainage | |
| 2 | METHODOLOGY AND TECHNIQUES | |
| | 2.1 Field methods | |
| | 2.2 Laboratory methods | |
| | 2.2.1 Petrography and modal analysis | |
| | 2.2.2 Electron Probe Micro-Analysis (EPMA) | |
| | 2.2.3 Whole rock geochemistry | |
| | 2.2.3.1 X Ray Fluorescence (XRF) | |
| | 2.2.3.2 Induced Coupled Plasma- Mass Spectrometry (ICP-MS) | |
| | 2.3 Summary | |

| | |
|----------|--|
| 3 | GEOLOGICAL SETTING AND STRATIGRAPHY |
| | 3.1 General |
| | 3.2 Geological setting and stratigraphy |
| | 3.3 Field occurrence and structural description of metagreywacke and associated rocks |
| | 3.3.1 Metagreywacke |
| | 3.3.1.1 Primary depositional structures |
| | 3.3.1.2 Diagenetic structure |
| | 3.3.1.3 Soft Sediment Deformation Structures (SSDS) |
| | 3.3.1.4 Deformational structures |
| | 3.3.1.5 Erosional structures |
| | 3.3.2 Associated Rocks |
| | 3.3.3 Summary |
| 4 | PETROGRAPHY OF METAGREYWACKE AND ASSOCIATED ROCKS |
| | 4.1 Metagreywacke |
| | 4.2 Associated rocks |
| | 4.2.1 Dykes of dolerite and hornblende schist |
| | 4.3 Summary |
| 5 | GEOCHEMISTRY OF METAGREYWACKE AND ASSOCIATED ROCKS |
| | 5.1 Metagreywacke |
| | 5.2 Associated rocks |
| | 5.3 Summary |

6.1 Metagreywacke**6.1.1 Formational mechanism of structures**

6.1.1.1 Primary depositional structures

6.1.1.2 Diagenetic structures

6.1.1.3 Soft Sediment Deformation Structures (SSDS)

6.1.1.4 Deformational structures

6.1.1.5 Erosional structures

6.1.2 Diagenesis**6.1.3 Metamorphic modification****6.1.4 Provenance, paleoweathering and tectonic setting**

6.1.4.1 Provenance

6.1.4.2 Paleoweathering

6.1.4.3 Tectonic setting

6.1.5 Bouma sequence**6.2 Associated rocks**

6.2.1 Crystallization trend of dolerite dyke

6.2.2 Petrogenesis

6.3 Summary**SUMMARY AND CONCLUSION****7.1 Epilogue****REFERENCES****RESEARCH PUBLICATION**

LIST OF FIGURES

| Figure No. | Title |
|------------|---|
| 1.1 | Geological map of Goa (modified after GSI) with the location of the sampling sites. |
| 3.1 | Geological map of Dharwar craton with different greenstone belts and Clospet Granite. Dharwar craton bounded by Deccan Traps, Granulite terrane and Cudappah basin (Chadwick et al., 1996). |
| 3.2 | Field photographs of primary depositional structures in metagreywacke. |
| 3.3 | Field photographs of SSDS in metagreywacke. |
| 3.4 | Field photographs of metagreywacke. |
| 3.5 | Field photographs of dolerite dyke and quartz veins. |
| 4.1 | Photomicrographs of metagreywacke. |
| 4.2 | Photomicrographs of metagreywacke. |
| 4.3 | Photomicrographs of metagreywacke. |
| 4.4 | Ternary diagrams based on modal analysis of metagreywacke. |
| 4.5 | Photomicrographs of dolerite. |
| 4.6 | Photomicrographs of dolerite. |
| 4.7 | Photomicrographs of dolerite and hornblende schist. |
| 5.1 | Compositional variation trend of major oxides of metagreywacke. |
| 5.2 | Plots for classification of metagreywacke. |
| 5.3 | A) Chondrite normalised rare earth element patterns showing the trend of argillite. B) Chondrite normalised rare earth element patterns showing the trend of metagreywacke. |

-
- 5.4 A) Binary plot of Cr against Ni (after Condie, 1993).
B) Plot of Eu/Eu* against (Gd/Yb)_N ratio (after Taylor and McLennan, 1985).
C) Binary plot of LREE/HREE against (Gd/Yb)_N (after Taylor and McLennan, 1985).
- 5.5 A) Total alkalis versus silica diagram (after Le Maitre et al., 1989) of dolerite samples.
B) Ternary diagram of AFM (A= Na₂O+K₂O ; F= FeOt ; M= MgO).
- 5.6 Variation diagrams of dolerite with MgO against oxides such as TiO₂, FeOt, Ni and Al₂O₃.
- 5.7 Variation diagrams of dolerite plotted with Mg# against oxides such as SiO₂, FeO, Al₂O₃ and TiO₂.
- 5.8 Geochemical plots of dolerite.
- 5.9 Variation diagram of dolerite. The large ion lithophile elements (LILE) such as Cr, Ni, Sr, Co, V and La are plotted against Zr (ppm).
- 5.10 A) Plot of CaO/ Al₂O₃ against Mg# for dolerite samples.
B) Binary plot of Ce against Nd for dolerite samples.
- 5.11 Chondrite normalized rare earth element patterns showing the trend of dolerite.
- 5.12 Tectono-magmatic ternary discrimination diagram of MgO-Al₂O₃-FeOt (Pearce et al., 1977).
- 6.1 Schematic illustration showing the development of pseudonodule from a load structure.
- 6.2 Plots for provenance of metagreywacke.
-

-
- 6.3 Plots for paleoweathering of metagreywacke.
 - 6.4 Tectonic setting diagrams of metagreywacke (Bhatia, 1983).
 - 6.5 Tectonic setting diagrams of metagreywacke.
 - 6.6 Tectonic setting discriminant diagrams of metagreywacke after Bhatia and Crook (1986).
 - 6.7 Sketch of the Bouma units in an ideal sequence (Bouma, 1962; Walker, 1965; Middleton and Hampton, 1973).
 - 6.8 Schematic illustration of a model depicting the phases of basin development in the study area.
-

LIST OF TABLES

| Table No. | Title |
|-----------|--|
| 1.1 | Stratigraphy of Goa Group after Gokul et al. (1985) and Dessai (2011). |
| 3.1 | Deccan continental flood basalt province stratigraphy (Subbarao and Hooper, 1988). |
| 4.1 | EPMA data of different minerals present in argillite, metagreywacke, dolerite and hornblende schist. |
| 4.2A | Modal composition (%) of various minerals present in metagreywacke, quartzo-feldspathic metagreywacke and metagreywacke with biotite. |
| 4.2B | Modal composition (%) of various minerals present in dolerite. |
| 5.1 | Major oxide (wt%) of argillite, metagreywacke, quartzose-feldspathic metagreywacke, metagreywacke with biotite and metagreywacke cataclasite of the present study area. |
| 5.2 | Trace and REE (ppm) of argillite, metagreywacke, quartzose-feldspathic metagreywacke, metagreywacke with biotite and metagreywacke cataclasite of the present study area. |
| 5.3 | Ratios of various oxides, trace elements and REE of argillite, metagreywacke, quartzose-feldspathic metagreywacke, metagreywacke with biotite and metagreywacke cataclasite of the present study area. |
| 5.4 | Values of Pearson's coefficient of correlation of major elements of metagreywacke. |
| 5.5 | Average composition of metagreywacke of the study area and related greywacke from other areas for comparison. |

-
- 5.6 Major (wt %), minor, trace and rare earth elements (ppm) of dolerite dykes of the study area and related reported dolerite from Merces, Goa (Widdowson et al., 2000) and Desur Lava, Karnataka (Hegde et al., 2014).
- 6.1 Interpretation of the process of formation of anideal Boumasequence (Bouma, 1962; Walker, 1965; Middleton and Hampton, 1973) and also of the study area.
- 6.2 Sedimentary structures and their inferred depositional processes of the heterolithic succession of metaconglomerate and metagreywacke sequence of the study area (Sanvordem Formation).
-

Chapter 1
INTRODUCTION

1.1 Prologue

Fine grained clastic sedimentary rocks are known to preserve geochemical signatures of their source rocks and so are important to decipher the nature of the upper continental crust from which they were derived (Dayal and Murthy, 2006). Evolution of continental crust during the early history of the Earth has received considerable attention (Kröner, 1984). The upper crust composition during the Archean can be obtained by analyzing the sediments deposited during that time. Hence, the knowledge of the composition of Archean sediments can make an important contribution to understand the tectonic setting during the time of sediment deposition (Naqvi et al., 1988) and help unravel the depositional history and processes.

A systematic study of the various structures in sedimentary rock yield significant details about the depositional environment that affected the sediment during and after their deposition. Since the framework mineralogy and composition of the sediments are altered and recycled due to metamorphism, the sedimentary structures are reliable features to provide important information not only about the depositional environment of sediments but also of the post-depositional processes and evolution of the basin of deposition (Fernandes et al., 2016a).

The petrology of clastics is controlled by provenance which in turn is a function of tectonic setting. The modal mineralogy of the framework components of sedimentary rock helps to decipher the tectonic (Dickinson and Suczek, 1979). Post-depositional modification of mineralogy during diagenesis of sandstone includes authigenic mineral development and detrital mineral alteration. Various factors such as basinal setting, palaeoenvironmental conditions of source and deposition followed by subsequent

diagenetic modification have an impact on the sedimentary rock composition (Fadipe et al., 2011).

The detrital sediment composition is significantly controlled by the source rock composition which is in turn followed by weathering and diagenetic processes (Armstrong-Altrin, 2009). The compositional characteristics of source rock are well recorded and act as valuable tools to decipher the tectonic setting of the sediment emplacement (Maravelis and Zelilidis, 2009; Bakkiaraj et al., 2010). However, the other factors controlling the mineralogical and chemical composition of sedimentary rocks are environmental conditions influencing source rock weathering, duration of weathering, mode and distance of transport of clastic materials, depositional environment and post-depositional processes (Hayashi et al., 1997; Moosavirad et al., 2012). Some of these factors are controlled by plate tectonic setting of the depositional basin (Dickinson and Suczek, 1979; Armstrong-Altrin et al., 2004; Dey et al., 2009; Moosavirad et al., 2012). Thus, the terrigenous sediments preserve a record of their source rock, weathering conditions, hydraulic sorting and tectonic setting during deposition.

Greywacke and fine grained argillite is widely used to decipher the evolution of upper continental crust and also to model the composition of Archean crust (Taylor and McLennan, 1985). The geochemical and petrographical signatures of fine grained rocks of younger ages are found to reasonably define their tectonic settings (Dickinson and Suczek, 1979; Dickinson and Valloni, 1980; Bhatia, 1983; Bhatia and Crook, 1986; Naqvi et al., 1988).

1.2 Background to the problem

The abundance, composition and size of the framework grains along with the matrix components and cement type greatly control the texture of metagreywacke. The diagenetic modifications are used to demonstrate the various stages that represent the progress of sediments to a rock. After lithification, additional changes that persisted in mineralogy are regarded to be the products of the various degrees of metamorphism. Due to burial and metamorphism, the framework mineralogy of these rocks is significantly altered (Fernandes et al., 2016a). The morphology of structure, its extent and lithological associations are used as tools to identify and evaluate their process of formation. Turbidite deposits ideally represent Bouma sequence and also exhibit Soft Sediment Deformation Structures (SSDS) (Valente et al., 2014).

Many studies are conducted using the major, trace and Rare Earth Elements (REE) geochemistry as they provide clues to characterize provenance, paleoweathering, tectonic setting and climatic variability from the terrigenous sediments. The geochemical modifications occurring during the exogenic processes tend to mask the influence of provenance (McLennan and Taylor, 1991). However, the Rare Earth Elements (REE) are more reliable than the major and trace elements to decipher the provenance, since REE concentrations are not affected during erosion, sedimentation and diagenesis (Sinha et al., 2007). These modifications are dependent on the clay minerals which host the REE. Since REE's are relatively immobile during diagenetic and metamorphic processes, REE's along with Th and Sc are widely used to trace the evolutionary history of the sedimentary rocks and upper crust in general (Taylor, 1964; Nance and Taylor, 1976; McLennan et al., 1980; McLennan, 1989; McLennan and Taylor, 1991; Prame and Pohl, 1994).

1.3 Previous work

The lithounits of Goa were geologically examined by Fermor (1909) followed by Dunn (1942) and later by Dhepe (1953). However, Oertal (1958) reported the rocks of Goa to belong to Dharwar System and divided them into two groups: (i) the lower infraconglomerate group and (ii) the upper metalliferous group. A scheme of stratigraphic classification was proposed by Gokul et al., (1985), which is further revised by Dessai, (2011) and is presented in Table 1.1.

Widdowson (2009) described in detail the mineralogical and compositional changes observed in a 40 m high laterite profile that is present at the Mercedes quarry, Goa. This profile, of probable Miocene age (Schmidt et al., 1983) overlies fresh greywacke and portrays seven weathered zones indicating the parent rock of laterite to be greywacke. These zones identified from the bottom to the top are: altered greywacke, reddened greywacke, saprolite with Fe-rich mottling and/or segregations, Fe-Al segregations and nodular concretions, laterite with fretworks of Fe-rich segregations, semi-indurated Fe-rich tubular textured laterite and indurated laterite cap. Below the fretworks, a palaeo-water-table occurs.

The petrology and geochemistry of the greywacke of the Dharwar-Goa sector belonging to the Late Archaean Supracrustal composing of a thick sequence of greywacke with intercalations of quartzite, BIF and carbonates were studied by Devaraju et al. (2010). The geochemical data of this greywacke indicates the deposition of sediments in a progressively changing basin from a passive to active continental margin and island arc setting.

These are the only studies that pertain to the characteristics of the greywacke of Goa and so far the origin, formation mechanism and evolution of the greywacke of Goa have not been reported.

Further, Auden (1949) reported a series of dyke intrusions in the Indian shield particularly along the coastal regions and these dykes were considered to be feeders to the Deccan Trap basaltic flows. However, the trend of a few basic dykes is reported to be comparable with the major lineaments. This probably suggests two episodes of volcanism during which the dykes were emplaced along the Goa coast and is indicative of a thin continental crust along the coast (Iyer et al., 1990). Further, Widdowson et al. (2000) reported that the coastal dykes of Goa represent the youngest phase of mafic intrusive forming a pre-Deccan basement of Peninsular India. The major, trace, rare earth elements and $^{87}\text{Sr}/^{86}\text{Sr}$ ratios of these dykes are consistent with Deccan basalts while the $^{40}\text{Ar}/^{39}\text{Ar}$ age data indicate Palaeocene age. Patil and Rao (2002) conducted palaeomagnetic studies of the dolerite dykes in Goa and proved them to be contemporaneous to the Deccan traps.

Table 1.1 Stratigraphy of Goa Group after Gokul et al. (1985) and Dessai (2011).

| After Gokul et al. (1985) | | | Dessai (2011) | | |
|----------------------------|--------------------------|--|-----------------------------------|---------------------|--|
| | | | Basic Intrusives | | Metadolerite/Dolerite |
| | | | Canacona Granite | 2395±390 (?) Ma | |
| | | | Mafic-ultramafic layered complex | | |
| | | Metadolerite | | Vagheri Formation | Metabasalt, Argillite and metagreywacke |
| Basic Intrusives | | Dolerite, Gabbro | Ponda Group (= Chitradurga Group) | Bicholim Formation | Banded ferruginous quartzite Manganeferous chert breccia with pink ferruginousphyllite Limestone Pink ferruginous phyllite Quartz-chlorite- amphibolite-schist |
| Chandranath Granite Gneiss | 2600±100 Ma | Granodiorite | | Sanvordem Formation | Metagreywacke, Argillite, quartzite, tilloid |
| | Vagheri Formation | Metabasalt, Argillite and metagreywacke | ~~~~~ Unconformity ~~~~~ | | |
| | Bicholim Formation | Banded ferruginous quartzite Manganeferous chert breccia with pink ferruginousphyllite Limestone Pink ferruginous phyllite Quartz-chlorite- biotite-schist | Barcem Group (= Bababudan Group) | Barcem Formation | Matagabbro Peridotite, talc-chlorite schist, Quartzite, quartz-sericite schist, Red Phyllite, Quartz porphyry Massive, schistose and vesicular metabasalt |
| | Sanvordem Formation | Argillite, quartzite, tilloid | ~~~~~ Unconformity ~~~~~ | | |
| | Barcem Formation | Metagabbro Peridotite, talc-chlorite-schist Quartzite, quartz- sericite-schist Phyllite Quartz-porphyry Massive, schistose and vesicular basalt | Chandranath Granite Gneiss | 2700-2900 Ma | Granodiorite |
| | Basement: not identified | | Anmode Ghat trondhjemite gneiss | 3300-3400 Ma | Basement: trondhjemite-tonalite granodiorite |

1.4 Aim and objectives

The primary aim of the study is to acquire and analyse the petrology and geochemical data of the metagreywacke of Sanvordem Formation, Goa Group, Goa, India so as to understand the process of formation and evolution. Hence, to fulfill the aim, following are the objectives:

1. To study the distribution, extent and sedimentologic nature of metagreywacke and associated rocks of the Goa Group, India.
2. To determine and understand the petrographic and geochemical characteristics of the metagreywacke.
3. To study the diagenetic changes and establish the sequence of diagenetic events so as to understand the process of formation of metagreywacke.
4. To integrate the data in order to understand the tectonic setting, origin and evolution of the metagreywacke.

Petrography and petrochemistry is used to interpret diagenesis and deformation microstructures. An in-depth account of the diagenetic and metamorphic processes that produced various microstructures is discussed. However, various depositional, diagenetic, deformational and erosional structures exhibited by the rocks are also studied and presented. In this background, I have outlined the structural details, petrology and geochemistry of metagreywacke of the Sanvordem Formation of Goa Group, India to understand the interplay between diagenesis and low grade metamorphism, evolution, tectonic setting and provenance. Intrusions of dolerite dykes associated with the country rocks of metagreywacke are also studied for their petrology, petrogenesis and for their relation with metagreywacke.

1.5 Study area

1.5.1 Location

All along the west coast of Goa, extensive exposures of metagreywacke are present that belong to the Sanvordem Formation of Goa Group. The areas under investigation are the coastal stretch of Pernem, Bardez, Tiswadi and Mormugao Talukas. The outcrops at Pernem, Bardez and Mormugao Talukas are exposed along the coast as cliffs and headlands (Fig. 1.1). The outcrops in Tiswadi Taluka are present in the hinterland and are best exposed in the various quarries.

Besides metagreywacke, the study area has presence of various outcrops of dykes of dolerite intruding these country rocks.

1.5.2 Accessibility

The study areas are well connected by road network. The areas are accessible from the important towns like Pernem, Mapusa, Panaji and Vasco. However, since a majority of the outcrops are present along the coast, these outcrops can be approached by walking all along the coast. The quarries in Tiswadi Taluka can be approached by road from Panaji.

1.5.3 Climate

Goa experiences a tropical monsoon climate and is warm and humid throughout the year. The relative humidity during the monsoon period is high and range from 90% to 95% while during rest of the year it ranges from 80 to 85%. The state has a low diurnal variation in temperature as it is located proximal to the Arabian Sea. On an average, the minimum temperature in winter is about 18°C and during summer it reaches upto 36°C. Goa is bestowed by abundant rainfall from the Southwest monsoon during the months from June to September.

1.5.4 Physiography

The study area forms a part of the western coastal plains with plateaus. This terrain comprises of low-lying stretches of sandy beaches, khazan lands, estuarine mudflats, mangroves, fields, saltpans and settlement areas. The two largest estuaries of Goa lie within this stretch which includes Mandovi and Zuari rivers. The North Goa coastal plains are interrupted by low (less than 100 meters high) laterite topped plateaus. The plateaus comprise of rocky headlands towards the sea front, between which lies the sandy beaches. The coastal stretch of South Goa (Quepem and Canacona coasts) are much isolated and limited in extent, wherein the terrain is hilly and mountainous even near the coast (Wagle, 1982; Fernandes, 2009).

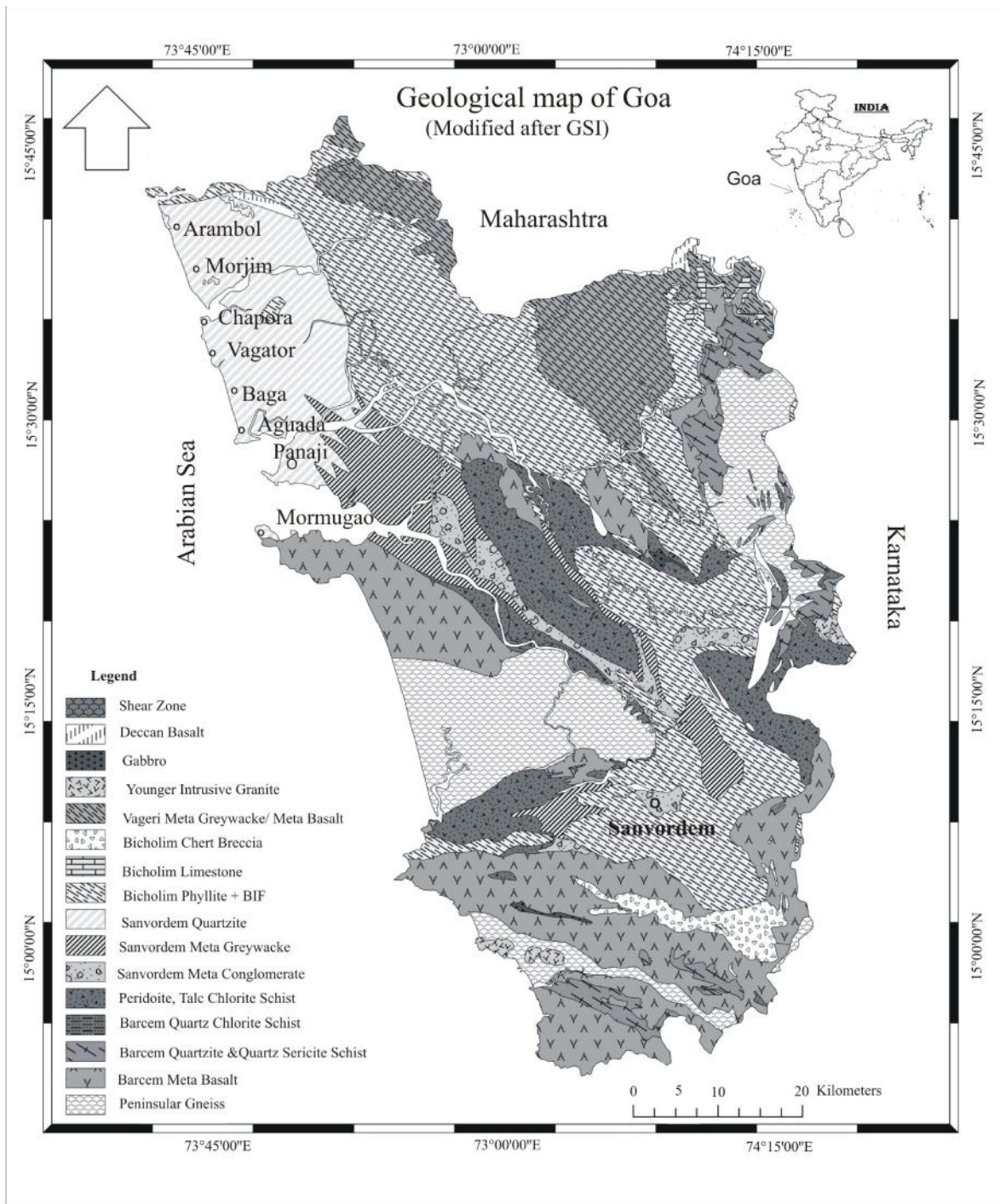


Fig. 1.1: Geological map of Goa (modified after GSI) with the location of the sampling sites.

1.5.5 Drainage

The important rivers draining the state of Goa from north to south are Terekhol, Chapora, Mandovi, Zuari, Sal, Talpona and Galjibaga. These rivers are under the tidal influence for a few kilometers along their length near the coast. The rivers have tremendous capacity to erode headward, due to heavy rainfall. The drainage is predominant in two directions: N-W and E-W. These trends follow the regional trend and coincide with the faults, fractures and shear zones (Iyer and Wagle, 1987).

Chapter 2

METHODOLOGY AND TECHNIQUES

To accomplish the objectives of the study, several methods of investigation were undertaken to understand the tectonic setting, origin and evolution of metagreywacke and the associated rocks of the Sanvordem Formation of Goa Group, India. The methods employed include sampling, petrographic studies including modal analysis as well as electron probe micro-analysis (EPMA). The whole-rock geochemistry was carried out for major elements by X-Ray Fluorescence (XRF), while the minor and trace elements including Rare Earth Elements (REE) were determined by Induced Coupled Plasma - Mass Spectrometry (ICP-MS). Data plotting by the use of SigmaPlot on binary and ternary diagrams is carried out. Further, the data of metagreywacke of the study area is interpreted and compared with similar and related rocks of greywacke from Dharwar (Devaraju et al., 2010), Late Archaean greywacke (Condie, 1993) and also greywacke from Fig Tree, Barberton (South Africa) (Toulkeridis et al., 1999). While, the dolerite dykes of the study area are compared with dolerite dykes of Goa (Widdowson et al., 2000) and of Desur Lavas, Deccan Traps (Belgaum district, Karnataka) (Hegde et al., 2014).

2.1 Field methods

Before the commencement of fieldwork, the topographic and geologic maps were studied to identify areas of probable rock exposures. Google maps also gave valuable information during the course of fieldwork to identify the exposures for a detailed study. Fieldwork consisted of observation of geologic relationships and of structural data such as attitude of bedding planes, fold and shear zone. Rock samples were collected for petrographic, micro-structural study and also for whole-rock geochemistry. The study area is marked in the map (Fig. 1.1). Further, during the compilation of data, field visits were conducted in the same study area, to verify the details described for its confirmation.

The outcrops in the study area were mainly present as cliffs and headlands along the coast. Outcrops were also located in the hinterlands and in various quarries. Rock samples of

metagreywacke and also of the associated dykes were collected throughout the study area in order to provide a complete representation of the rock types present. Sampling of metagreywacke was done especially across the contours (especially at the quarries), so as to get a vertical variation. The dyke samples obtained were from the margin as well as from the center of the dyke body.

2.2 Laboratory methods

2.2.1 Petrography and modal analysis

Petrographic observations served to either confirm or correct the rock descriptions made during fieldwork and to detect textures and minor phases not observable in hand specimen. The samples were examined in transmitted light for the petrographic study using Leica DMLP (at CSIR-NIO, Dona Paula, Goa) and Nikon Eclipse E200 (at Department of Earth Science, Goa University, Goa) polarizing microscopes. A total of 49 samples were collected from the study area of metagreywacke and associated rocks. Thin sections (36 metagreywacke and 13 associated dyke samples) were used for the petrographic study.

Specific attributes that were documented during the petrographic study include mineralogy, visual estimates of mineral modes and textural information. Petrographic studies help to understand the composition and textural parameters such as grain size, sorting and mutual relationship among grains. During petrographic analysis, particular attention was given to the textural pattern of metagreywacke to understand the diagenetic process. The mineralogy of framework grains, cement and matrix were essential for reconstructing the diagenetic history of the metagreywacke while the textural pattern of the associated dykes helped to delineate the crystallization history.

Modal analysis produces a representation of the distribution and volume percent of minerals within the thin section. In this method, rocks from different areas can be compared with the

help of thin sections, using a petrological microscope. It also helps in giving the maximum and minimum grain sizes. The delimitation of modal analysis is when the rock has a preferred orientation of one or more minerals. The total area of sample must be sufficiently larger than the maximum diameter of the smallest grain size.

Modal analysis was conducted by measuring the surface area of mineral grains of the same mineral relative to the total surface area of the thin section. This was done using the software NIS-Element D coupled to the NIKON Eclipse E200 microscope. At least two points were analysed for each thin section for the volume percent and average value was considered.

2.2.2 Electron Probe Micro-Analysis (EPMA)

Electron probe micro-analysis (EPMA) is an analytical tool used to non-destructively determine the chemical composition of small volumes of solid materials. Minerals preserve chemical information adopted during their formation and subsequent alteration. This information helps to understand the geologic processes such as crystallization, lithification, volcanism, metamorphism and tectonic setting. EPMA works by bombarding a small area of a sample or mineral with an electron beam resulting in X-rays that are emitted at wavelengths typical to the elements being analysed. Hence the sample composition can be easily identified by recording the wavelength using a Wavelength Dispersive Spectroscopy (WDS) system.

Mineral analyses were obtained employing an SX5 CAMECA at CSIR-NIO, Goa and were performed at 15 kV accelerating potential and with beam current of 12 nA. The standards used for the analysis were natural silicate and oxide minerals.

2.2.3 Whole rock geochemistry

Of the 49 samples used for petrographic studies, 27 samples (22 metagreywacke and 5 associated dykes) were analysed for X-ray fluorescence (XRF) and inductively coupled plasma - mass spectrometry (ICP-MS). The samples were powdered using an agate mortar.

2.2.3.1 X-Ray Fluorescence (XRF)

X-ray fluorescence (XRF) is the emission of characteristic X-rays (or fluorescence) from a material that has been excited by bombarding with high-energy X-rays or gamma rays. One gram of each powdered samples were made into glass pellets and analysed for major and minor elements employing a Philips X-ray Fluorescence Spectrometer at CSIR-NIO, Goa. The standards used were Japanese gabbro (JGb-2), dolerite (WS-E), quartz latite (QLo) and Japanese sediment (JSd-1). The accuracy for major oxides is within ± 5 .

2.2.3.2 Inductively Coupled Plasma-Mass Spectrometry (ICP- MS)

Trace and rare earth element (REE) concentrations were determined with inductively coupled plasma - mass spectrometry (ICP-MS) following the standard procedure of Balaram and Rao (2003). Finely ground rock samples were digested by dissolving 50 mg powder in a mixture of HF, HNO₃ and HClO₄. A minimum of two cycles of drying of the acid and sample mixture were carried out during the digestion. A few samples underwent a third cycle. Rhodium was used as an internal standard. Finally, the solution was made up to 100 ml using distilled water. The standard reference materials used were Icelandic basalt (BIR-1) and dolerite (DNC-1). The precision for trace elements is less than 1% and the accuracy is within ± 5 . The REE data were normalized using the chondrite values (after Sun and McDonough, 1989).

The analyses were conducted employing an Inductively Coupled Plasma-Mass Spectrometry (ICP-MS) at CSIR-NIO, Dona Paula, Goa and at IsoTrace Laboratory (Agilent ICP- MS), National Centre for Antarctic and Ocean Research (NCAOR), Mormugao, Goa.

2.3 Summary

This chapter provides a brief description about the various methods used, beginning with the sampling, petrographic description, modal analysis and EPMA. Methods employed for whole-rock geochemistry of XRF and ICP-MS analyses are also given.

Chapter 3

GEOLOGIC SETTING AND STRATIGRAPHY

3.1 General

The Indian peninsular shield is composed of Archean formations comprising the cratons of Singhbhum, Aravalli, Bastar and Dharwar. The Dharwar Craton lies between latitudes 12° 00' and 18° 00' and longitudes 74° 00' and 80° 00' E. The northern part of the Dharwar Craton is capped by 66 Ma old continental flood basalts of the Deccan Traps and towards the East, the craton is masked by Proterozoic sediments of the Cuddappah Supergroup (Fig. 3.1).

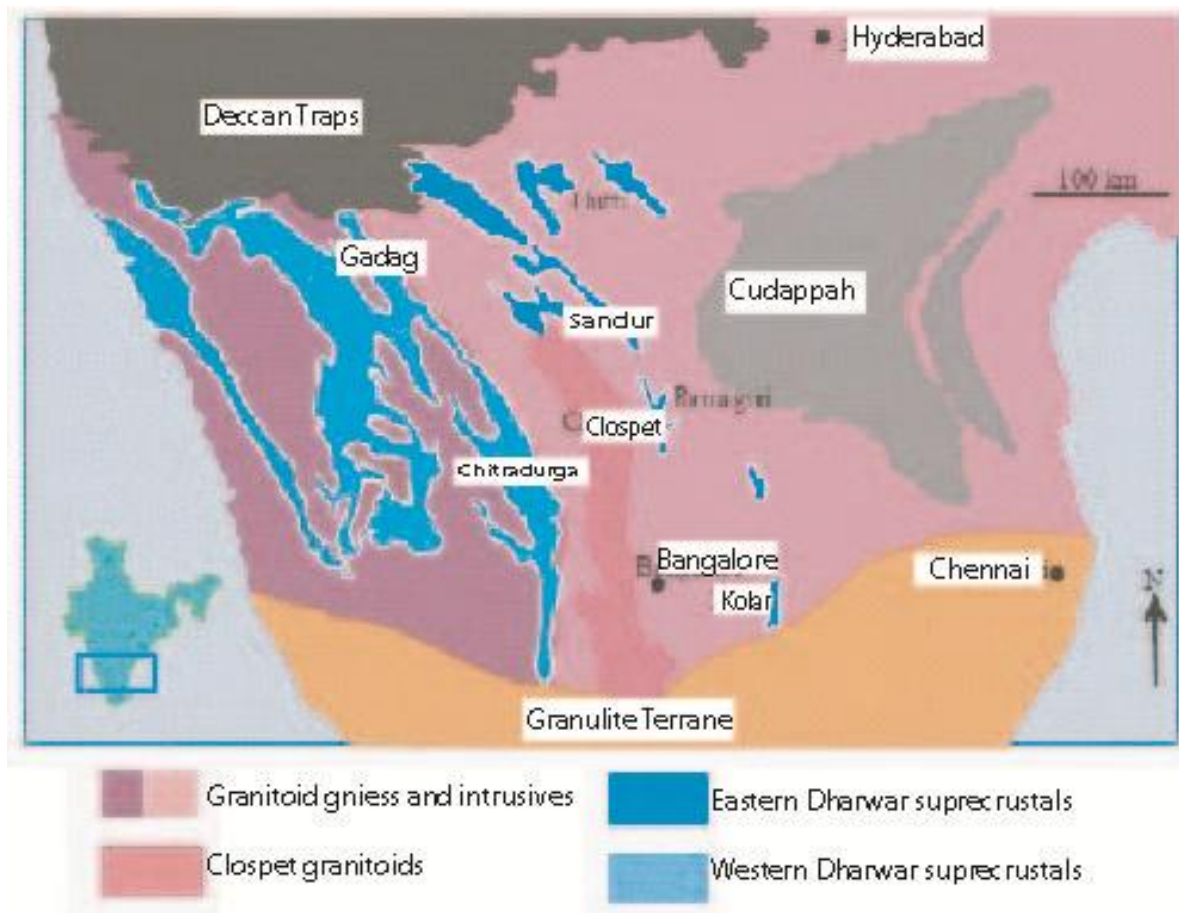


Fig. 3.1: Geological map of Dharwar craton with different greenstone belts and Clospet Granite. Dharwar craton bounded by Deccan Traps, Granulite terrane and Cudappah basin (Chadwick et al., 1996).

Based on dominant lithologies, age, abundance of greenstones and degree of regional metamorphism, the Dharwar Craton is subdivided into the western and eastern blocks. The Western Dharwar Craton (WDC) is mainly composed of Tonalite Trondjemite Granodiorite (TTG) suite as old as 3.4 Ga (Peucat et al., 1993). The highly deformed and metamorphosed

Sargur Group greenstone belt (>3.0 Ga) is unconformably overlain by Dharwar Supergroup supracrustal (3.0–2.6 Ga) (Nutman et al., 1996). The sedimentary basin of the northern part of the Dharwar-Shimoga greenstone belt of the western Dharwar craton (Archean crust) consists of a succession of quartz-pebble conglomerate and quartz arenite which is overlain by the turbidite sequence (Srinivasan and Naqvi, 1990; Hegde and Chavadi, 2009). The Eastern Dharwar craton (EDC) comprises of late Archean monzo-diorite, granodiorite and granite suite. The age of the EDC ranges from 2.7 to 2.55 Ga (Balakrishnan et al., 1990; Krogstad et al., 1991; Vasudev et al., 2000). Metamorphism in the WDC varies from low-temperature greenschist to amphibolites facies, whereas the EDC exhibits high-temperature greenschist to amphibolites facies (Chadwick et al., 1997).

Goa covering an area of about 3,702 km² is situated along the central west coast of India between the Arabian Sea and the Western Ghats. The Goa Group comprises of the greenschist facies of metamorphic rocks belonging to the Dharwar Supergroup (Gokul et al., 1985). The widely exposed Archean metasedimentary rock is metagreywacke. Although these rocks have undergone low grade metamorphism, various sedimentary structures are still preserved in the rocks (Fernandes et al., 2016a).

This study examines the metagreywacke of the Sanvordem Formation and also the associated dykes intruding them. Metagreywacke form the most abundant and dominant lithology of the WDC and occupy around 30,000 km² and are affected by regional low grade metamorphism resembling greenschist assemblage, the other processes involved are silicification, carbonatization and widespread formation of secondary sericite and chlorite. Yet, with this extent of metamorphism and alteration a range of primary minerals, textures and structures are still preserved in the WDC (Devaraju et al., 2010).

3.2 Geologic setting and stratigraphy

The Indian peninsular shield which is characterised by cratons is mainly composed of tonalite trondjemite granodiorite (TTG) suite, greenstone belt and granitoid. In Goa, the Dharwar Craton extends between latitude 14°53'54" N and 15°48'00" N and longitude 73°40'33" E and 74°20'13" E. Goa is situated towards the north-western part of the WDC and form a part of the Shimoga-Goa supracrustal belt with a trend of NNW-SSE. The extent of Dharwar Craton in Goa is concealed beneath the Arabian Sea in the west and Deccan Trap in the north-west. The Shimoga-Goa supracrustal belt continues beneath the Trap and terminates upto Narmada along the Narmada-Son lineament (Dessai, 2011). The general trend of the Dharwar Craton is NW-SE, representing sediments at the base and superimposed by metamorphosed basic and acid volcanic rocks. These are overlain by greywacke, followed by pyroclasts and tuffs associated with precipitates of chemogenic lime, iron and manganese. These are in turn overlain by another greywacke suite of rocks. This heterogeneous assemblage has suffered greenschist facies of metamorphism and as they are found in Goa, they are termed as the Goa Group (Gokul et al., 1985).

The stratigraphic sequence of the Goa Group consists of the metavolcanic and metasedimentary assemblage (Archean to Proterozoic), mafic and ultra-mafic complexes and intrusive granite (Lower Proterozoic), Deccan Trap (Upper Cretaceous to Eocene), laterite (Cenozoic) and beach sand and estuarine alluvium (Quaternary) (Geological Survey of India, 1996). The meta-sedimentary assemblage of the Archean to Proterozoic age is divided in the order of superposition as: Barcem, Sanvordem, Bicholim and Vageri Formation in the ascending order. Gokul et al. (1985) correlated the Goa Group with the rocks from Chitradurga Group of the Dharwar Supergroup that is dominantly of metagreywacke and tilloid. The tilloid demarcates a basal conglomerate indicating a break in sedimentation episode. The underlying acidic and basic metavolcanics are included in lower Bababudan

Group. However, in Goa Group, the tilloid is assigned the status of para-conglomerate hence the tilloid along with the metavolcanic are included in Goa Group. Further, Dessai (2011) divided the rocks of Goa into two lithostratigraphic sequences: Barcem Group and Ponda Group which corresponds to Bababudan and Chitradurga Group of the Dharwar Supergroup, respectively. The Barcem Group comprises of Barcem Formation while the Ponda Group comprises of Sanvordem, Bicholim and Vageri Formations (Refer Fig. 1.1).

As reported by the Geological Survey of India (1996), the Barcem Formation comprises of basic and acid metavolcanics with associated meta-tuff and meta-sediment. The Sanvordem Formation comprises of metagreywacke, tilloid and argillite. The Bicholim formation is represented by metapyroclast and tuff with calcareous, manganiferous and ferruginous chemical precipitate. The Vageri Formation comprises of metagreywacke and metabasalt. Acidic and basic intrusions followed the sedimentation phases. Deccan Trap of about 60 m cap the north-eastern corner of Goa and are of Upper Cretaceous to Lower Eocene age (Gokul et al., 1985; Fernandes et al., 2016a). The stratigraphic sequence of Goa group is given in table 1.1 and figure 1.1.

Based on Rb/Sr whole-rock measurements, the oldest known rock in Goa is the Anmod trondjhemitic gneiss of 3400 ± 140 Ma age (Dhondial et al., 1987). Later work reported on age is 3300 Ma using the Sm-Nd and U-Pb signatures (Devaraju et al., 2007). The Anmod trondjhemitic gneiss forms the basement for the Goa Group of rocks and is correlated with the older parts of the Peninsular gneiss of South India.

The various acidic intrusives exposed in the form of granitic gneisses in Goa (Fig. 1.1) are based on localities and are referred to as (i) Chandranath granite gneiss, (ii) Tamdi feldspathic gneiss, (iii) Dudhsagar granite and (iv) Canacona granite. These granitic-gneisses are reported to be either syntectonic or post-tectonic in relation to the deformational episodes exhibited by the supracrustals (Harinadha Babu et al., 1981; Gokul et al., 1985; Dessai,

2011). The Chandranath granite gneiss is reported to be syntectonic with the first phase of folding while the Dudhsagar granite and Tamdi feldspathic gneiss are synkinematic with the second phase of folding and the Canacona granite is post-tectonic emplacement. However, the relationship between granite gneisses and supracrustals is not yet delineated (Gokul et al., 1985; Dessai, 2011).

Gokul et al. (1985) identified three cycles of folding. The first cycle of folding is observed towards the south-western part of Goa, wherein the fold movement had resulted in asymmetrical folds with the axis trending E-W. The syncline of the fold extends from Nuvem to Morpirla and its corresponding anticline is occupied by Chandranath granite which is syntectonic with the first phase of folding. The second cycle of folding was the most powerful and its evidences are present all over the territory. These folds are doubly plunging with NW-SE axis trend. Various macro- scale and meso- scale folds are present to the east and north of Sanvordem. The secondary planar structure resulted from this fold movement led to the formation of prominent schistosity in the area. The third cycle of folding had resulted in a major syncline in the north-eastern part of Goa around Valpoi. The axis of the fold has NNW-SSE trend with a plunge of 12-15° due NNW. This fold movement resulted in the S-shaped bend in the Bicholim ore formation. It is also reported that the trend of a few basic dykes is comparable with the lineaments. This probably suggests two episodes of volcanism during which the dykes were emplaced along the Goa coast and is indicative of a thin continental crust along the coast (Iyer et al., 1990).

The prominent straight west coast of India represents a major fault (Gokul et al., 1985). The various fault planes perpendicular to the major west coast fault in Goa are attributed to have developed in W-WSW direction. Along these fault planes the rivers of Chapora, Tiracol, Mandovi and Zuari flow in to the Arabian Sea. Numerous minor faults are present in the coastal area that trend NE-SW and NW-SE and are widely reported from the ore quarries.

Besides, significant evidences of shearing and tectonisation are reported along the ghat section of the Goa-Karnataka border. The probable time of formation of faults and its correlation with the formation of western ghat is not known (Gokul et al., 1985). Iyer et al. (1989) reported that the lineaments of Goa were correlated with the three cycles of tectonic activity, with the east-west direction being the most prominent.

The emplacement of basic intrusives followed the event of mafic-ultramafic layered complex and Canacona granite (2395 ± 390 Ma), thus, the injection of the dykes is the last event (Dessai, 2011; Fernandes et al., 2016a). These dykes could be either related to post- Deccan Trap that occurred at 63 Ma corresponding to the end of Deccan volcanism and/or to the initiation of Mesozoic rift of western India and the splitting of India and Madagascar at 89 Ma. Palaeomagnetic and radiometric dating study has indicated that the dyke swarms in SW peninsular India is older and is of Precambrian age (Widdowson et al., 2000) whereas the younger swarms are related to the late Mesozoic tectonism (Storey et al., 1995; Patil and Rao, 2002; Fernandes et al., 2016a).

Geochemical studies and $^{40}\text{Ar}/^{39}\text{Ar}$ data indicated that the dykes of Goa were feeders to the younger formations of the Wai subgroup of Deccan basalts that are of Early Palaeocene age (Widdowson et al., 2000). However, palaeomagnetic studies of Patil and Rao (2002) suggested the dykes to be contemporaneous to the Deccan traps.

The lithospheric extension and rifting which occurred between ~180 and 64 Ma between India and Madagascar were associated with two or more hotspots and resulted in extensive volcanism of:

- 1) the Rajmahal, Sylhet and Bengal Traps (~117 Ma; Bakshi, 1995);
- 2) widespread magmatism in Madagascar (92-84 Ma; Storey et al., 1997);

- 3) St Mary's Island off the west coast of India (~90 Ma; Torsvik et al., 2000; Pande et al., 2001);
- 4) the Deccan Traps in India (~64 to 66 Ma; Widdowson et al., 2000).

Among these, the Deccan Trap is the largest covering an area of about 500,000 km², extending into the Arabian Sea to the west, having an estimated original erupted volume of as much as 1.3 x 10⁶ km³ (Naqvi 2005; Jay and Widdowson, 2008; Hegde et al., 2014). Some workers (eg., Richards et al., 1989; Campbell and Griffiths, 1990) have considered these Continental Flood Basalt (CFB) as a product of mantle plume heads. Morgan (1981) reported that the Deccan basalts were a consequence of the northerly drifting Indian subcontinent over the Reunion plume in the Late Cretaceous. Vanderkluyesen et al. (2011) have reported three dyke systems exposed in Deccan Traps flood basalt province of India: 1) north-south trending west coast swarm; 2) east-west trending Narmada-Tapi swarm in the north-central Deccan; 3) Nasik-Pune swarm in the central western Deccan. The three volcanic events of the Deccan occurred during 68-67 Ma, 65 Ma and finally at 62 Ma, with maximum activity at the ca. 65 Ma event. However, the arrival of Reunion plume at the base of the Indian lithosphere occurred at ~70 Ma (Roy 2003; Collier et al., 2008; Kerr et al., 2010; Rao et al., 2011).

Based on geochemical characteristics and field markers the Deccan CFB is divided into three subgroups and eleven formations (Table 3.1). The succession thins towards south-east displaying the older formations (Watts and Cox, 1989; Mitchell and Widdowson, 1991; Widdowson et al., 2000), while the youngest formation occurs at Belgaum, Karnataka, India which also caps the Western Ghats escarpment and the elevated plateau region of Goa (Widdowson et al., 2000).

Table 3.1: Deccan continental flood basalt province stratigraphy (Subbarao and Hooper, 1988)

| Group | Subgroup | Formation |
|---------------|----------|---|
| Deccan Basalt | Wai | Panhala Mahabaleshwar Ambenali Poladpur |
| | Lonavala | Bushe Khandala |
| | Kalsubai | Bhimashankar Thakurvadi Neral Igatpuri Jawhar |

All along the length of Goa, the original basalt overburden that might have been existed could have been removed due to the eastward recession of the Western Ghat scarps as such the link between the dykes and the lava flows that might have existed in Goa is not demonstrated in the field presently (Widdowson et al., 2000). Chemo-stratigraphical studies implies that the exposures of dolerite dykes present along the coastal plains of North Goa and also the flows capping the eastern ghat escarpment consists of successions of the Ambenali, Mahabaleshwar and Panhala Formations (Devey and Lightfoot, 1986; Mitchell and Widdowson, 1991; Widdowson et al., 2000).

3.3 Field occurrence and structural description of metagreywacke and associated rocks

Structures developed in sedimentary rocks during the process of their formation act as clues to decipher the sedimentary environment at the time of deposition of sediments. This research deals with a new finding of the various depositional, diagenetic, deformational and erosional structures exhibited by the rocks of Sanvordem Formation, Goa Group. In this present study

the morphology, extent and lithological associations of the structures are used as tools to identify and evaluate the process of formation of the structures. Further, Bouma sequence representing turbidite deposit is also reported to occur in metagreywacke rocks of the study area. The formation and the importance of the various structures that represent turbidite deposits are reported for the first time in the Goa Group.

3.3.1 Metagreywacke

The rock exposure along the coast of North Goa is mainly metagreywacke and is about 1 to 6 m in thickness while a maximum thickness of 30 m occurs in the hinterland quarries. The reduced thickness of the coastal outcrops is perhaps either due to marine erosion or due to the decrease of the basin depth. At several places, the outcrops are capped by lateritic tablelands.

The sedimentary structures identified in the study area are categorised into five groups:

- 1) Primary depositional structures
- 2) Diagenetic structure
- 3) Soft Sediment Deformation Structures (SSDS)
- 4) Deformational structures
- 5) Erosional structures

3.3.1.1 Primary depositional structures

Primary depositional structures are known to have formed during deposition of the sediments. The metagreywacke of the study area have a strike of NE-SW and an average dip of 30°. The primary structures in the study area comprise of laminations, dropstone, graded bedding and cross lamination and also liesegang rings (diagenetic structure), while, the SSDS

identified in the study area are convolute, flame and load, ball and pillow (pseudonodule), slump fold and syn-sedimentary fault which form during lithification process.

Laminations are dominant and are easily recognizable in the study area. These are characteristically continuous, parallel and have sharp boundaries. A horizon of metagreywacke with biotite layers is identified at the Morjim road junction (Fig. 1.1). It is identified by the presence of a film of mica flakes and clay minerals (Fig. 3.2A, 4.1F).

Dropstone structure

The conglomerate at the base of the Sanvordem Formation comprises of sand to silt sized matrix that cements the quartzitic and granitic pebbles that range in size from 10 to 15 cm. Dropstone structure is exhibited by the pebble present in conglomerate (Fig. 3.2 B, C). The pebble has a broad and convex base at the bottom and is almost flat at the top. The laminations above the pebble are present without any disturbance while the laminations below the pebble, are distorted while in the mid- region of the pebble laminations are discontinuous and broken. Some exposures of conglomerate interbedded with argillite as well as intercalations of fine grained clayey laminated argillites in the form of lensoid pockets are also noticed (Fig. 3.2 D, E). Also, at places lineation in conglomerate is prominent with a trend of N 310°.

Graded bedding

Small-scale rhythmic upward fining sequences in metagreywacke are identified at microscopic scale (Fig. 4.3B).

Cross lamination

Cross lamination (Fig. 3.2F) is noticed within a bed of metagreywacke lithofacies with the foreset having an angular truncation with the topset and a tangential contact with the bottomset bounding surface of the beds.

3.3.1.2 Diagenetic structure

Liesegang rings

Liesegang rings in metagreywacke have characteristic concentric or ring-like appearance with band thickness ranging between 2 and 5 mm and are bounded by cracks and fissures and are perpendicular to the bedding planes (Fig. 3.4A).

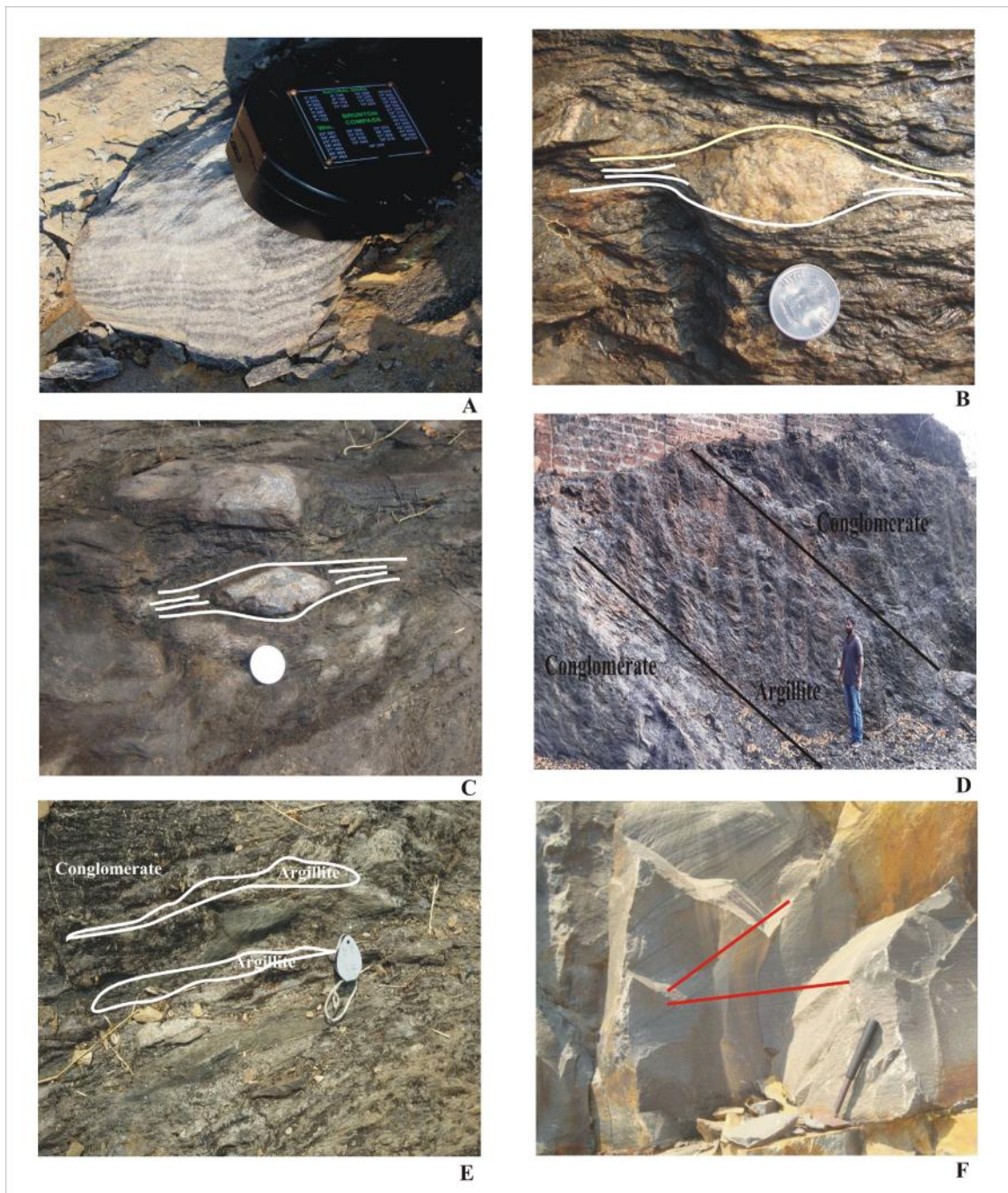


Fig. 3.2: Field photographs of primary depositional structures in metagreywacke:

A) 'Metagreywacke with biotite' horizon identified by presence mica (biotite) flakes and clay minerals.

B, C) Dropstone structure in matrix-supported metaconglomerate unit with pebbles of quartzite and granite. (White lines indicate the laminations).

D) Argillite interbedded between metaconglomerate.

E) Metaconglomerate with intercalations of argillites in the form of lensoid pockets.

F) Metagreywacke with cross laminations.

3.3.1.3 Soft Sediment Deformation Structures (SSDS)

The SSDS are also called as penecontemporaneous features, formed before lithification in clastic sediments (Van Loon, 2009) and reflect deformational processes that occur in unlithified sediments or in sedimentary rocks that are unlithified before the deformation started (Lowe, 1975; Mills, 1983; Müller et al., 2000; Collinson, 2003; Van Loon, 2009). The SSDS are indicators of the early consolidation history of sediments rather than their depositional environment (Allen, 1982) and these early diagenetic features form due to liquefaction in water saturated unconsolidated sediments (Owen, 1987; Topal, 2014). The SSDS are related either to sedimentary or tectonic features and are controlled by the degree of compaction of the sediments (Owen, 1995; Mazumder et al., 2009; Kundu et al., 2011). The main factors involved in the formation of the SSDS are; rapid deposition, differential loading in adjacent parts of the sediment and gravity controlled density currents (Bowman et al., 2004). The SSDS are commonly observed in Quaternary and Phanerozoic deposits and are very rarely found in Precambrian deposits (Ghosh, 2012), such as those reported from Chaibasa Formation in Eastern India that was deposited between 2100 and 1600 Ma during Proterozoic (Mazumder et al., 2006).

SSDS are formed either by gravitational movements, density differences or by movement of intergranular fluid. The SSDS are recorders of the environmental condition which occurred between the sediment deposition events. The SSDS are associated with muds and muddy sands as water does not dissipate rapidly in low-permeability muds (Potter et al., 1984; Valente et al., 2014). Several SSDS such as convolute laminations, flame and load, ball and pillow (pseudonodules), slump fold and syn-sedimentary fault that were observed in the study area are now discussed.

Convolute laminations

Convolute laminations occur as a 50 cm thick layer, sandwiched between undeformed sedimentary layers in metagreywacke (Fig. 3.3A). The convolute laminations are associated with load and flame structures which occur as crenulations that are present at the top and bottom of the convolute bedding. The convolute lamination exhibit flame structures of about 3-5 cm thick.

Flame and Load structures

The load structure shows coarse-denser sediment that has sunk into the underlying finer-lighter material while the flame structure shows the rise of the underlying finer-lighter sediments into the overlying coarse-denser sediments. This structure is possibly formed by a process of density gravity settling (Fig. 3.3B).

Ball and pillow structures

Ball and pillow structures occur as fine grained sediment nodules of almost circular to elliptical shape. Since these structures appear as irregular bulbous nodular features they are also called as **pseudonodules** (Fig. 3.3C, D).

Slump fold structures

The slump fold structures occur in single strata of metagreywacke with broad, U-shaped and have an almost vertical axial plane. Slump folds are seen bounded by undisturbed sediments above and below (Fig. 3.3E).

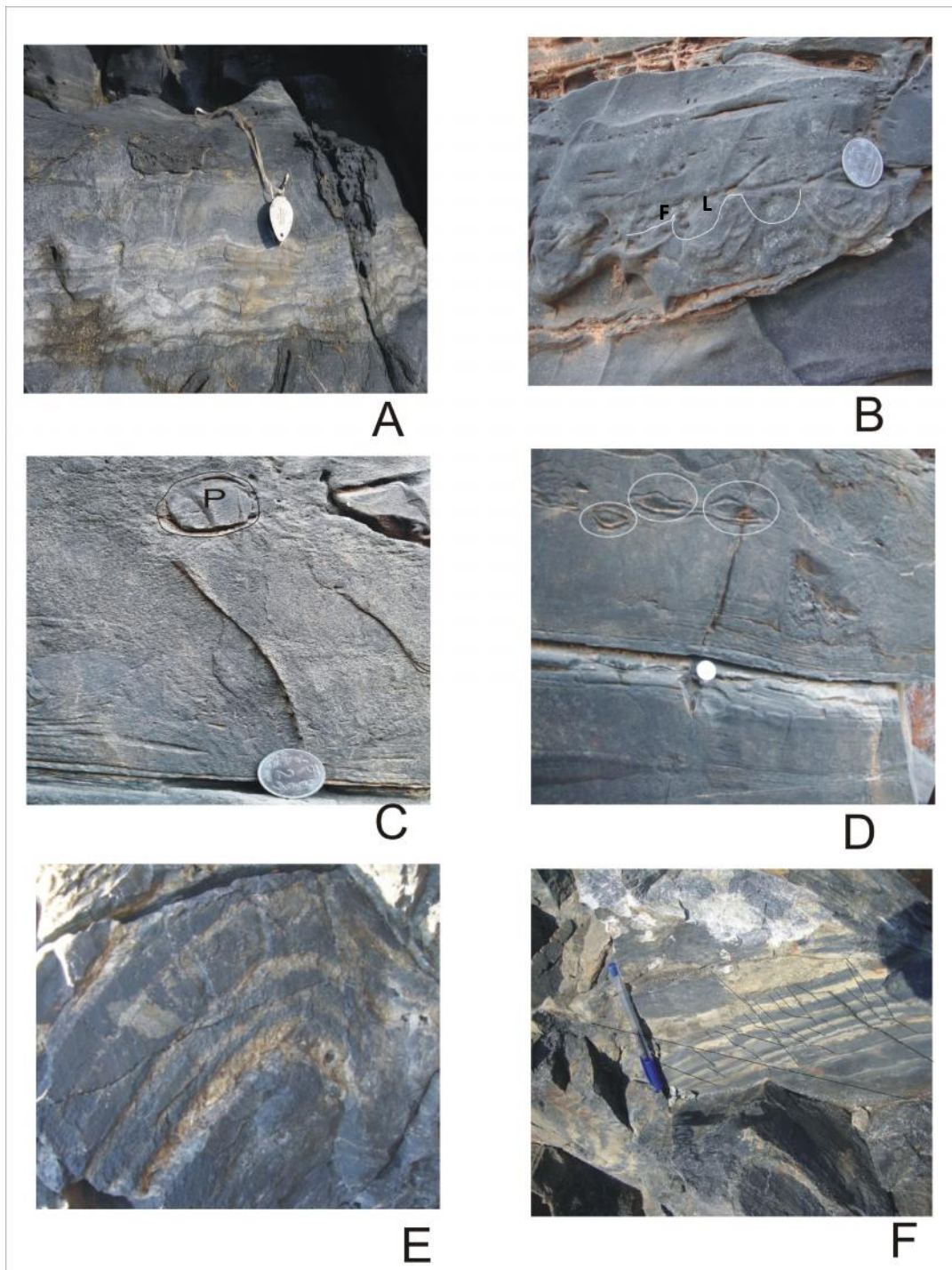


Fig. 3.3: Field photographs of SSDS in metagreywacke:

A) Convolute lamination in metagreywacke sandwiched between undeformed layered sedimentary strata.

B) Load (L) and Flame (F) structure occur as crenulations or wavy undulations having about 3-5 cm thickness. (White lines indicate the laminations).

C, D) Pseudonodules (P) seen as circular to elliptical shape (marked by circle).

E) Slump folds bounded by undisturbed sediments above and below, having a broad and U-shape and with a near vertical axial plane.

F) Syn-sedimentary faults truncate against undeformed continuously layered strata above and below them (Fault planes are marked by black lines).

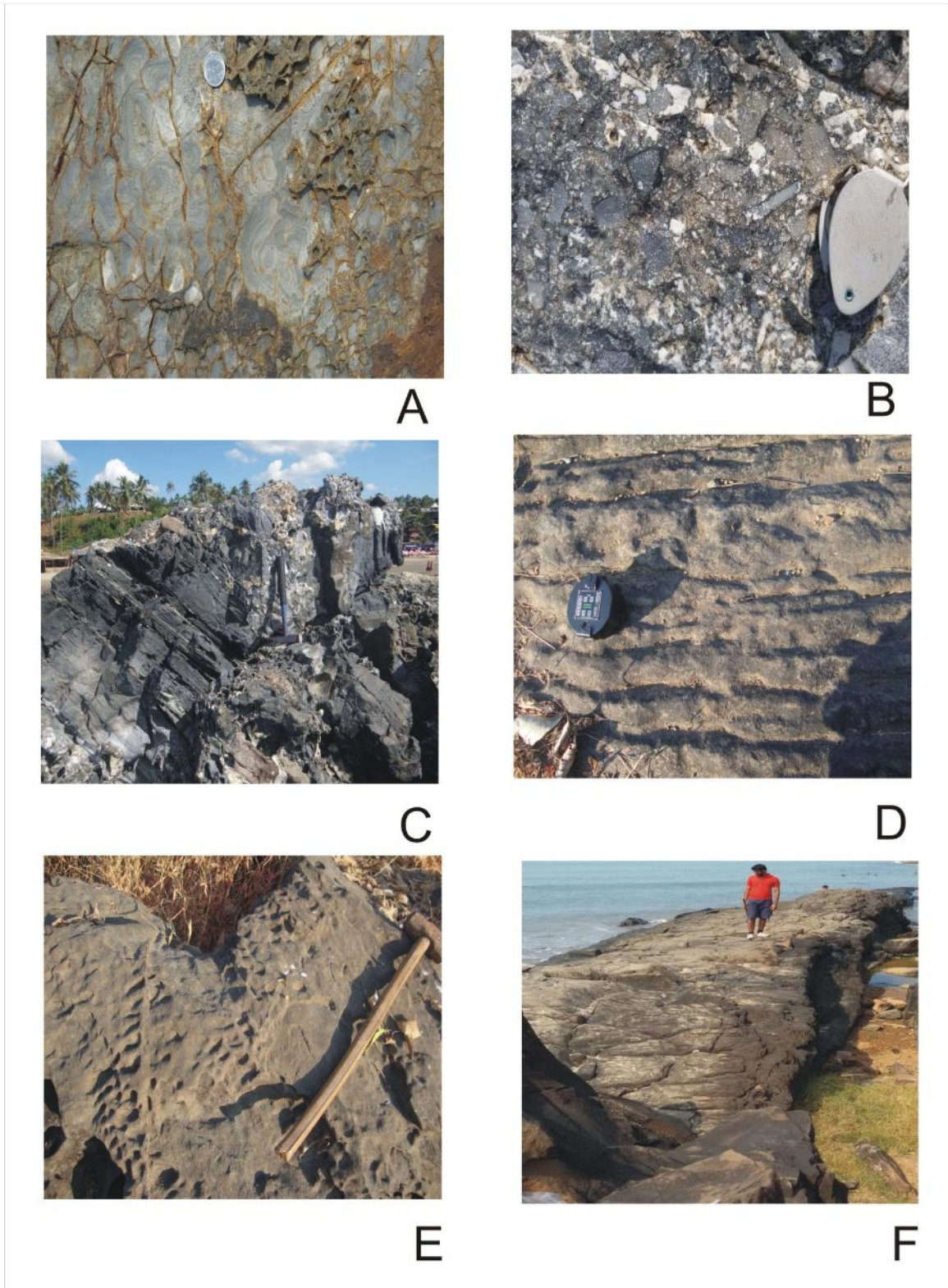


Fig. 3.4: Field photographs of metagreywacke:

A) Liesegang rings with characteristic concentric or ring-like appearance.

B, C) Shear zone in metagreywacke forming metagreywacke cataclasite.

D) Erosional ridges and furrows on horizontal surface of the tilted strata with a dip of about 34° .

E) Honeycomb structure with pits of varying sizes in metagreywacke.

F) Field photograph of dolerite dyke emplaced into metagreywacke.

Syn-sedimentary faults

Faults are identified truncating the undeformed continuously layered strata of metagreywacke above and below them wherein the hanging wall of the fault exhibits thickening or growth representing syn-sedimentary faults (Fig. 3.3F).

3.3.1.4 Deformational structures

The deformational structures identified in the study area are fold and shear zone.

Fold

A major anticlinal fold is delineated using the structural data at Vagator with one limb dipping due North and other in South direction. The fold axis lies approximately along an E-W direction i.e., along the reported regional fold axis.

Shear zone

A shear zone is observed at Vagator wherein the metagreywacke is sheared along with quartz veins to form 'metagreywacke cataclasite' (described in chapter 4). This occurs as a narrow zone with a trend of N 150° (Fig. 3.4B, C).

3.3.1.5 Erosional Structures

Besides the various structures that were formed due to primary, diagenetic and deformational processes there are some features formed due to the erosional process in the study area.

Erosional furrows

This structure occurs as furrows and ridges on the horizontal surface of the tilted strata of metagreywacke that has a dip of about 34° (Fig. 3.4D).

Honeycomb structure

This structure is seen as pits of varying sizes on the rock surface (Fig. 3.4E).

3.3.2 Associated Rocks

The metagreywacke of the study area is identified to be associated with dykes of dolerite (Figs. 3.4F, 3.5A, B), quartz veins (Figs. 3.5C, D) as well as with a presence of a dyke of hornblende schist.

Several dolerite dykes have intruded the country rock of metagreywacke. The grain size varies from the margin to the centre of the dyke. The margin of the dyke is fine grained and host closely spaced joints while towards centre the grain size progressively increases and the joints reduce. A majority of the dykes trend between N 295° and N 320° giving a general trend of NW-SE which is the dominant trend. The cross-cutting relation observed among dykes at the coast of Aguada indicates that the dykes are of two generations. The trend of the older dyke is N 345° while that of the younger dyke is N 315°. This indicates that the younger dyke trend ranges within the general trend of the dyke (i.e. between N 295° to N 320°) as mentioned above (Fig. 3.5B).

Besides the dykes, various quartz veins are present in the metagreywacke, ranging in size from millimeters to several centimetres. At places, pinching and swelling of quartz veins are seen, also exhibiting partly hummocky type of pattern of the veinlets (Fig. 3.5C, D). An outcrop of dyke of hornblende schist is reported at Mormugao which is seen to have intruded the country rock of metagreywacke.

The importance and formation of the above detailed structures and features would be later discussed (Chapter 6).



A



B



C



D

Fig. 3.5: Field photograph of dolerite dykes and quartz veins:

A) Dyke emplaced into metagreywacke exposed in a 10 m high section.

B) Cross-cutting dykes with trend of older dyke N 345° and that of the younger dyke is N 315° (marked by two red lines).

C) Numerous quartz veins ranging in size from millimeters to several centimetres present in metagreywacke.

D) Quartz veins exhibiting partly hummocky type of pattern of the veinlets.

3.3.3 Summary

In this chapter, the various indentified structures of metagreywacke are categorised into five groups:

Primary depositional structures

- Laminations, dropstone, graded bedding and cross laminations.

Diagenetic structure

- Liesegang rings.

Soft Sediment Deformation Structures (SSDS)

- Convolute, flame and load, ball and pillow (pseudonodules), slump fold, and syn-sedimentary fault.

Deformational structures

- Fold and shear zone.

Erosional structures

- Erosional furrows and honey comb structures.

The associated dolerite dykes are described with respect to their trend and the presence of quartz veins.

Hornblende schist dyke is also reported in the study area.

Chapter 4

PETROGRAPHY OF METAGREYWACKE

AND

ASSOCIATED ROCKS

The abundance, composition and size of the framework grains along with the matrix components and cementing material control the texture of sedimentary rocks. Hence petrography and modal composition of the metagreywacke of the Sanvordem Formation, Goa Group are used to interpret their diagenesis and deformation microstructures. Here an in-depth account of the diagenetic and metamorphic processes that produced various microstructures are discussed. The diagenetic modifications are used to demonstrate the various stages that represent the process of lithification. Additional changes that persisted in mineralogy are regarded to be the products of the various degrees of metamorphism. Due to burial and metamorphism in metagreywacke of Goa Group, the framework mineralogy of rocks is significantly altered.

4.1 Metagreywacke

The metagreywacke exhibits immature, poorly sorted texture with angular to sub-angular shaped components. The framework components comprise of quartz, feldspar, mica and relict detrital rock fragments (Fig. 4.1 to 4.3). The matrix is fine grained comprising of clay minerals with a variable amount of comminuted quartz, biotite, muscovite, chlorite and calcite. Micas occur as framework grains and also as matrix component. Recrystallization in quartz is identified with lobate contact grain boundaries in the quartz fabric and also from the 120° triple junction contact of the grains (Fig. 4.1A). Frosted and pitted appearance in quartz grains is common (Fig. 4.1A). Ductile deformation is identified in orthoclase and plagioclase with undulose extinction also plagioclase exhibit tapering deformed twins (Fig. 4.1A, B, C, D), while brittle deformation is evident in fragmented orthoclase (Fig. 4.1C, 4.2F). Orthoclase commonly exhibits saussuritization and carlsbad twin. Besides, perthitic feldspars are also found (Fig. 4.1 C).

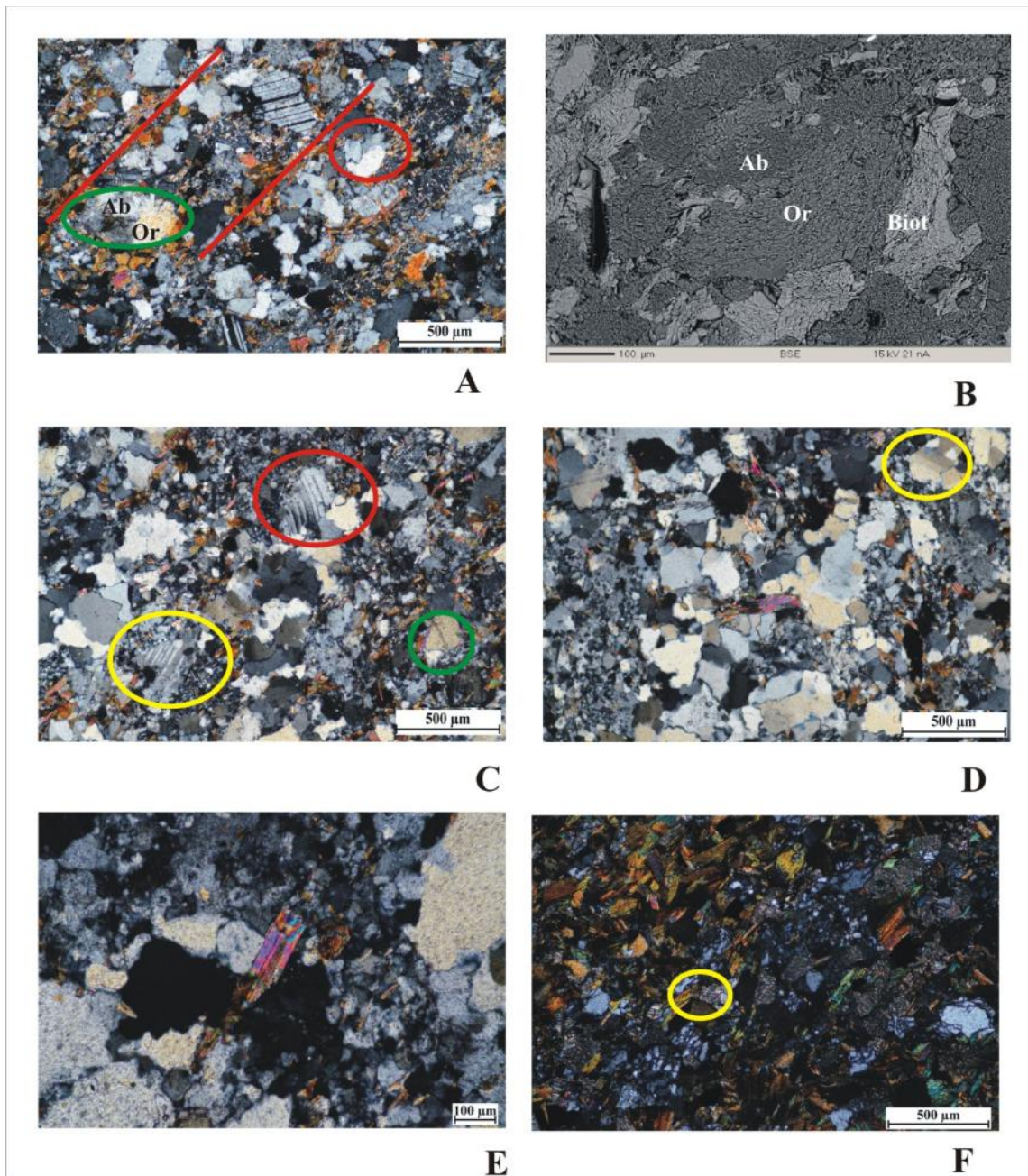


Fig. 4.1: Photomicrographs of metagreywacke:

A) Metagreywacke: Quartz grains with 120° triple junctions (red circle). Deformed orthoclase (Or) with albite (Ab) (green circle) (Back scattered image shown in fig 2B). Schistosity is marked by white line.

B) Back scattered image of metagreywacke exhibiting deformation of orthoclase (Or) grain. Adjacent to this grain, albite (Ab) and biotite (Biot) is identified.

C) Metagreywacke: Plagioclase with undulose extinction, tapering deformed twins (red circle). Perthite feldspar present (yellow circle). Fragmented orthoclase grain (green circle).

D) Quartzo-feldspathic metagreywacke: Fine grained mosaic of new recrystallized quartz grains is seen (left). Orthoclase grains with undulose extinction (yellow circle).

E) Quartzo-feldspathic metagreywacke with biotite flake embedded in quartz (middle part of photograph).

F) Metagreywacke with Biotite: Alternate biotite layer and quartz rich layer with calcite (yellow circle) and clayey material is identified.

Geochemistry of various minerals present in metagreywacke of the study area are studied using EPMA (Table 4.1). Further, although the rocks of the study area have undergone low-grade metamorphism with presence of biotite and chlorite as well as development of schistosity, an attempt is made to understand the modal data as sedimentary features still persists in the rocks. On the basis of the petrological attributes and by modal counts (Table 4.2A) of various detrital components, the metagreywacke of the study area is grouped into five distinctive petrofacies described as follows:

- 1) **Metagreywacke:** Metagreywacke comprises of quartz (av ~42%) and feldspars (orthoclase, plagioclase) (av ~13%). The matrix is mainly of clayey matter with subordinate amount of quartz and mica with an average of 31% of the total rock volume (Fig. 4.1 A to C, Table 4.2A). Using EPMA data the feldspars identified are of orthoclase and albite composition (Table 4.1).

- 2) **Quartzo-feldspathic metagreywacke:** This rock type is exposed at a hillock at Morjim (Fig. 1.1) and differs from the others by their coarse texture and dominance of quartz (av ~ 49%) and feldspar (av ~21%). Biotite is more abundant (8%) than muscovite (0.85%). Matrix (av 17%) is dominantly of clayey material with subordinate amount recrystallized quartz (Fig. 4.1D, E, Table 4.2A).

Table 4.1: EPMA data of different minerals present in argillite, metagreywacke, dolerite and hornblende schist.

| Oxides (%) | Argillite | | | Argillite | | | Metagreywacke | | | Dolerite | | | | Hornblende schist | | | | Hornblende schist | | | |
|--------------------------------|-----------|---------|--------|-----------|---------|---------|---------------|------------|--------|----------|-------------------------|---------------------------|--------|-------------------|--------|--------|----------------|-------------------|-------------------------|----------|----------------|
| | Pyrite | Apatite | Quartz | Chlorite | Apatite | Biotite | Allophane | Orthoclase | Albite | Biotite | Fe-rich Lithic fragment | Labradorite (plagioclase) | Augite | Ilmenite | Albite | Quartz | Ferromagnesian | Ilmenite | Fe-rich Lithic fragment | Ilmenite | Ferromagnesian |
| SiO ₂ | | 0.58 | 99.26 | 37.57 | 0.20 | 37.53 | 37.31 | 49.41 | 67.31 | 38.74 | 50.96 | 53.21 | 49.38 | 3.73 | 66.21 | 99.58 | 42.15 | 1.74 | 56.80 | 3.97 | 41.71 |
| Al ₂ O ₃ | | 0.09 | 0.10 | 23.88 | 0.11 | 16.48 | 61.89 | 32.36 | 18.97 | 16.89 | 3.38 | 28.00 | 2.55 | 1.74 | 19.34 | 0.05 | 12.60 | 0.33 | 15.23 | 0.54 | 13.77 |
| TiO ₂ | | 0.00 | 0.01 | 0.16 | 0.01 | 0.44 | 0.03 | 0.00 | 0.00 | 1.65 | 0.05 | 0.14 | 0.84 | 25.65 | 0 | 0.03 | 0.34 | 45.77 | 0.29 | 44.48 | 0.38 |
| Fe ₂ O ₃ | | 0.10 | 0.26 | 2.78 | 0.05 | 19.30 | 0.05 | 3.05 | 0.10 | 20.35 | 40.76 | 1.43 | 13.68 | 64.30 | 0.25 | 0.21 | 25.76 | 44.69 | 23.09 | 41.67 | 25.42 |
| MnO | | 0.00 | 0.01 | 0.00 | 0.00 | 0.00 | 0.00 | 0.06 | 0.01 | 0.39 | 0.15 | 0.00 | 0.29 | 0.59 | 0.02 | 0.00 | 0.24 | 1.62 | 0.05 | 1.60 | 0.20 |
| MgO | | 0.05 | 0.03 | 33.69 | 0.04 | 16.55 | 0.17 | 1.96 | 0.04 | 11.09 | 3.07 | 0.37 | 15.10 | 0.71 | 0.09 | 0.02 | 4.01 | 0.17 | 0.90 | 0.52 | 4.54 |
| CaO | | 58.49 | 0.13 | 0.38 | 57.45 | 0.52 | 0.02 | 0.08 | 0.30 | 0.01 | 0.62 | 12.25 | 15.50 | 0.39 | 0.71 | 0.06 | 10.63 | 0.78 | 0.92 | 2.44 | 10.29 |
| Na ₂ O | | 0.10 | 0.09 | 0.13 | 0.13 | 0.29 | 0.02 | 0.41 | 11.32 | 0.05 | 0.28 | 4.30 | 0.27 | 0.19 | 9.43 | 0.05 | 1.10 | 0.06 | 0.71 | 0.18 | 1.79 |
| K ₂ O | | 0.06 | 0.02 | 1.15 | 0.02 | 9.59 | 0.00 | 12.65 | 0.17 | 10.64 | 0.67 | 0.22 | 0.04 | 0.04 | 0.24 | 0.00 | 0.77 | 0.12 | 1.55 | 0.11 | 0.81 |
| P ₂ O ₅ | | 40.44 | 0.00 | 0.09 | 41.97 | 0.40 | 0.00 | 0.00 | 0.00 | 0.00 | 0.01 | 0.05 | 0.03 | 0.05 | 0.14 | 0.00 | 0.04 | 0.02 | 0.11 | 0.04 | 0.00 |
| V ₂ O ₃ | | 0.00 | 0.03 | 0.03 | 0.00 | 0.10 | 0.05 | 0.00 | 0.05 | 0.18 | 0.00 | 0.01 | 0.20 | 2.99 | 0.01 | 0.00 | 0.14 | 4.85 | 0.13 | 4.34 | 0.13 |
| SO ₂ | | 0.11 | 0.04 | 0.16 | 0.03 | 0.03 | 0.00 | 0.03 | 0.01 | 0.01 | 0.06 | 0.01 | 0.04 | 0.05 | 0.03 | 0.03 | 0.02 | 0.01 | 0.22 | 0.11 | 0.05 |
| Total | | 100 | 100 | 100 | 100 | 101.23 | 99.53 | 100 | 98.26 | 99.99 | 100.01 | 100 | 97.92 | 100.43 | 96.47 | 100 | 97.78 | 100.16 | 100 | 99.99 | 99.07 |
| S | 55.69 | | | | | | | | | | | | | | | | | | | | |
| Fe | 44.88 | | | | | | | | | | | | | | | | | | | | |
| Total | 100.57 | | | | | | | | | | | | | | | | | | | | |

Table 4.2A: Modal composition (%) of various minerals present in metagreywacke, quartzo-feldspathic metagreywacke and metagreywacke with biotite. (Q-quartz, KF- K-feldspar, PF-plagioclase feldspar, F- total feldspar, RF- rock fragment, M- matrix).

| Sample Number | 08 | 09 | 10 | 12 | 22B | 21A | 21B | 22C | 21C |
|------------------|---------------|-------|-------|-------|-------|-----------------------------------|-------|-------|-----------------------------|
| | Metagreywacke | | | | | Quartzo-feldspathic metagreywacke | | | Metagrey-wacke with biotite |
| Q | 50.81 | 34.11 | 43.71 | 44.35 | 40.37 | 47.41 | 56.48 | 44.54 | 16.44 |
| KF | 9.45 | 6.08 | 6.24 | 4.20 | 18.28 | 33.43 | 19.44 | 7.01 | - |
| PF | 7.74 | 6.93 | 4.68 | 2.06 | 1.82 | - | 1.69 | 2.28 | - |
| F | 17.19 | 13.01 | 10.92 | 6.27 | 20.10 | 33.43 | 21.13 | 9.29 | - |
| Biotite | 7.96 | 16.30 | 12.99 | 12.54 | 3.27 | 2.91 | 3.20 | 18.08 | 27.22 |
| Muscovite | - | - | 0.73 | 0.55 | 0.12 | 1.53 | 1.02 | - | 13.92 |
| Mica | 7.96 | 16.30 | 13.72 | 13.09 | 3.39 | 4.44 | 4.22 | 18.08 | 41.14 |
| RF | 1.27 | 0.79 | 2.01 | 2.23 | - | 7.08 | 0.53 | 1.69 | 1.29 |
| M | 22.77 | 35.78 | 29.64 | 34.06 | 36.14 | 7.63 | 17.65 | 26.39 | 41.14 |

Table 4.2B: Modal composition (%) of various minerals present in dolerite.

| Sample Number | 20 | 32B | 33 | 29 |
|--------------------------------|----------|-------|-------|-------|
| | Dolerite | | | |
| Plagioclase | 49.88 | 56.86 | 63.21 | 46.91 |
| Pyroxene | 36.81 | 32.97 | 30.73 | 50.06 |
| opaque (illmenite) | 4.54 | 5.85 | 3.36 | 3.03 |
| uralite | 8.77 | - | - | - |
| Fe rich lithic fragment | - | 4.31 | 2.70 | - |

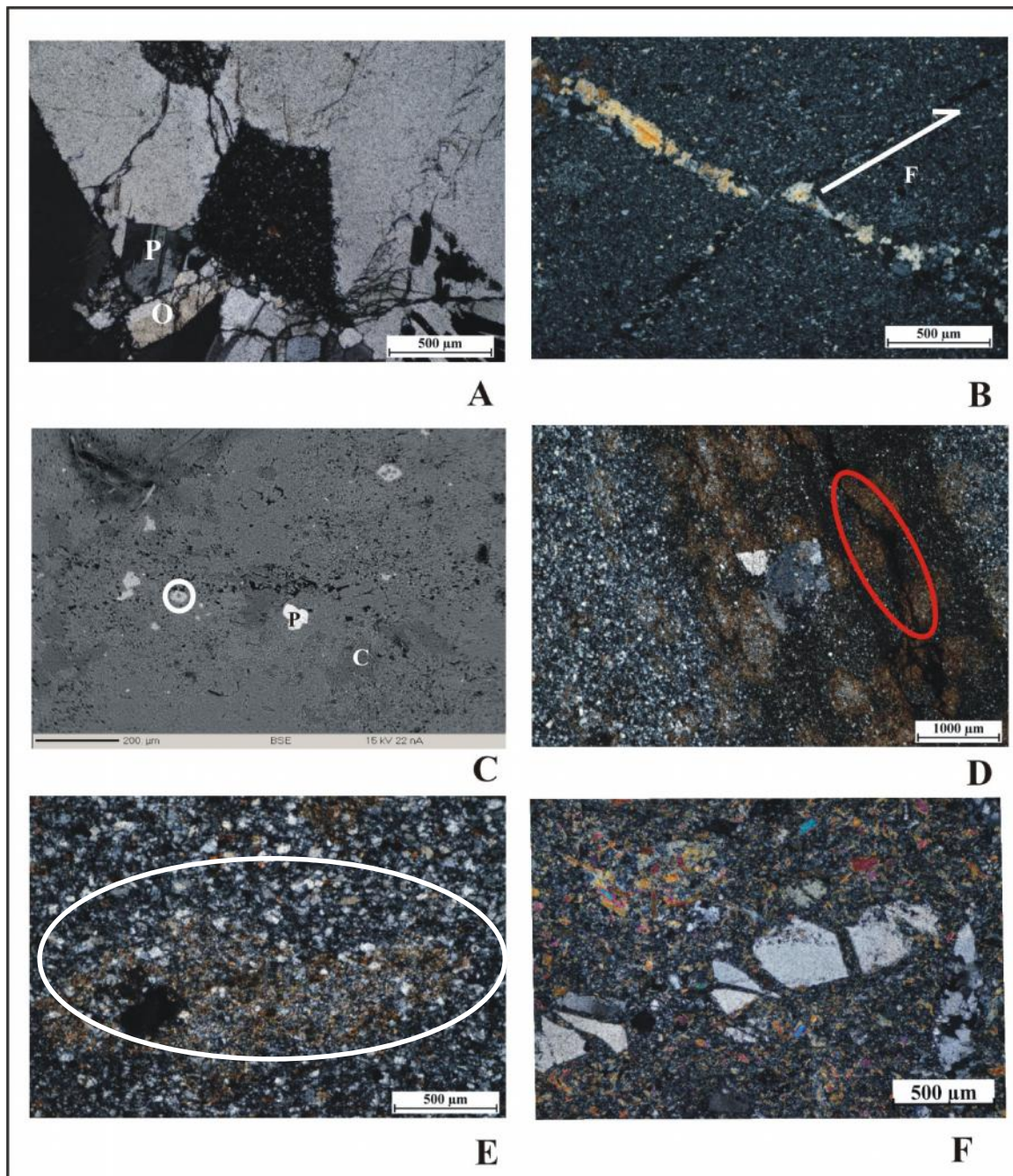


Fig. 4.2: Photomicrographs of metagreywacke:

A) Metagreywacke Cataclasite: Plagioclase (P) with tapering lamellar twins. Orthoclase (O) as well as opaques are present with clayey material.

B) Metagreywacke Cataclasite: Micro-faulting (F) of quartz-chlorite vein wherein the fault plane comprises of clayey matrix and recrystallized quartz.

C) Back scattered image (BSE) of argillite showing pyrite (P), apatite (white circle) and chlorite (C).

D) Argillite: Ovoid clast of mica formation (magnified image of clast in fig 3E seen at white circle). Styolites associated with clayey matter and micas (red circle).

E) Argillite: Ovoid clast of mica formation (white circle).

F) Argillite: Fragmentation of large quartz grain.

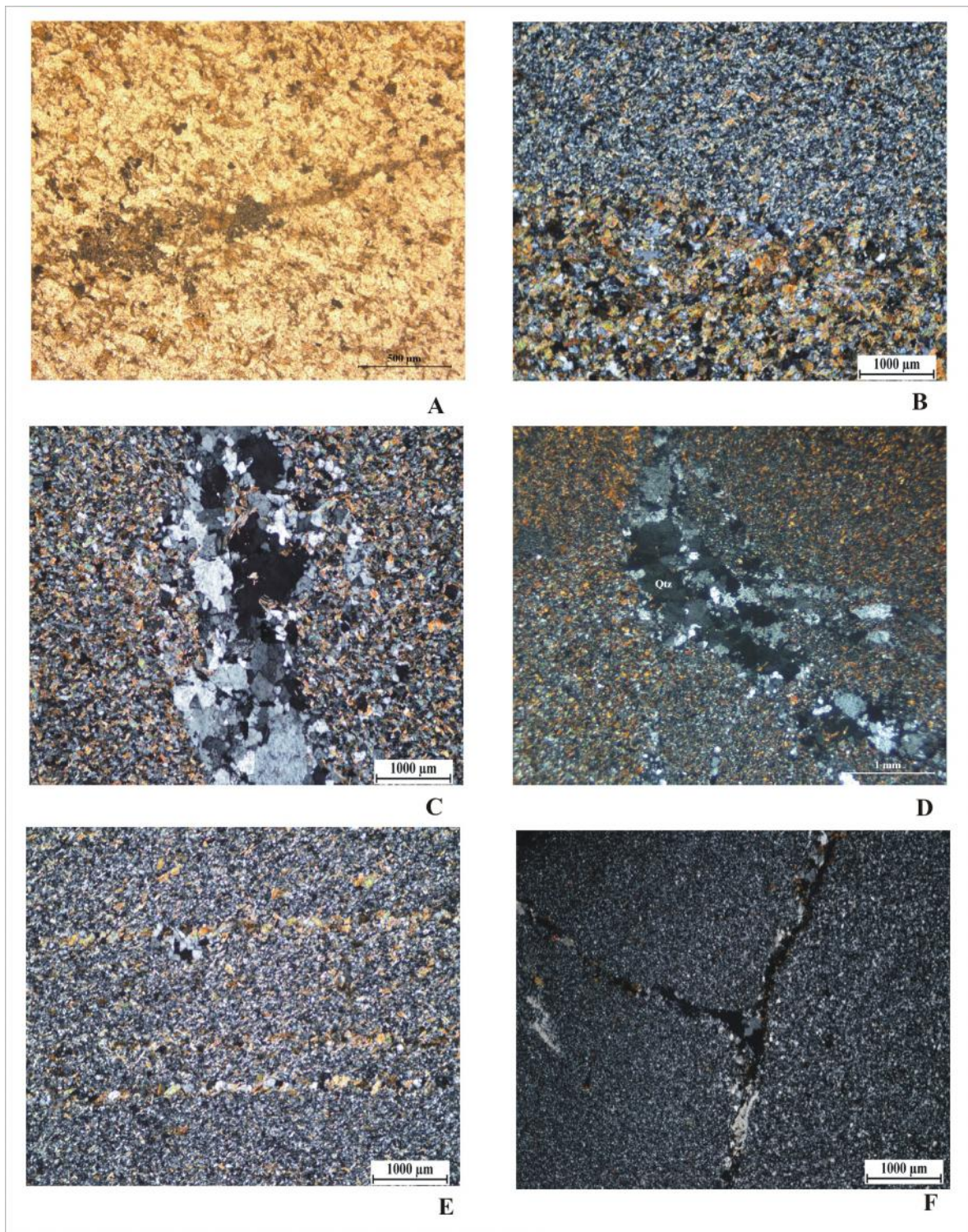


Fig. 4.3: Photomicrographs of metagreywacke:

A) Band of chlorite and biotite exhibiting pinching and swelling (plane polarised light) in metagreywacke.

B) Graded bedding (in plane polarised light) in metagreywacke.

C, D) Quartz veins with dissipation of quartz into the country rock evident by decrease in quartz concentration away from the quartz vein and entrapped mica into the veins.

E) Numerous veins of quartz, biotite and chlorite in various combinations are seen in metagreywacke.

F) Vein intersecting at a T-shaped junction, with recrystallization of quartz at the locus of junction.

- 3) **Metagreywacke with Biotite:** This is exposed at the base of the hillock at Morjim (Fig. 1.1) and resembles a horizon that was identified by the presence of layers of mica flakes and clay minerals which are absent at the other locations. Biotite-rich layer alternates with quartz-clay-rich layer (Fig. 4.1F). Overall the rock shows a dominance in micas (27% of biotite and 13% of muscovite) and also has quartz (av 16%) and matrix (av 41%) (Table 4.2A). Orthoclase is undeformed. Calcite with two sets of rhombohedral cleavage occurs (Fig. 4.1F).
- 4) **Metagreywacke Cataclasite:** This rock type is exposed at the coast of Chapora (Fig. 1.1) as a cataclastic shear zone. It comprises of detrital quartz, feldspar and opaque with abundant clayey matrix (Fig. 4.2A, B). The varying grain size of quartz with undulose extinction owes its occurrence from quartz veins of the shear zone (described in chapter 3). Brittle deformation of a vein of quartz and chlorite is defined by micro-faulting wherein the fault plane is marked by matrix and recrystallized quartz (Fig. 4.2B).
- 5) **Argillite:** These are very fine grained rocks with no clear distinction between matrix and clasts. With the help of EPMA data, components of quartz, chlorite, biotite, apatite, pyrite and allophone were identified (Fig. 4.2 C to F, Table 4.1). Ovoid clasts of irregular biotite mica indicate the commencement of mica formation (Fig. 4.2D, E). Schistosity is seen from the alignment of biotite. Pressure solution stylolites (Fig. 4.2D) in the form of suture-like penetrations are identified in mosaic texture of quartz and mica. These stylolites are highly prominent in argillite associated with micas and clayey matter. Detrital quartz grains have undergone brittle deformation, leading to their fragmentation (Fig. 4.2F).

In this thesis, all 5 types are broadly referred to as metagreywacke, unless they are mentioned with quotes ('...').

Various other textures are identified in these petrofacies. A band of chlorite and biotite exhibits pinch and swell texture, due to deformation (Fig. 4.3A). Graded bedding is identified in metagreywacke (Fig. 4.3B).

Injection of silica fluids leading to formation of quartz veins (Fig. 4.3C, D) led to dissolution of quartz into the country rock. Hence, at instances various mineral grains of micas are seen as if they are entrapped into the veins. This is also evident by the decrease in quartz concentration away from the quartz vein. Besides, numerous veins comprising of quartz, biotite and chlorite are also found (Fig. 4.3E). A vein intersecting at a T-shaped junction is seen, with recrystallization of quartz at the locus of junction (Fig. 4.3 F).

For a better understanding of the modal data (Table 4.2A), the bulk composition of the metagreywacke has been expressed in two ternary diagrams of Q-KF-PF (quartz - K feldspar - plagioclase feldspar) and Q-F-M (quartz - feldspar - matrix) (Bruck, 1972; Fig. 4.4A, B). In figure 4.4A the samples of 'metagreywacke' and 'quartzo-feldspathic metagreywacke' show dominance of quartz. In figure 4.4B a widespread scatter of points is noted almost at the central portion towards the matrix line of the triangle. The modal data can be used in sandstone classification diagram, given by Q-F-RF (quartz-feldspar-rock fragments) (Folk et al., 1970) (Fig. 4.4C) and also in provenance discrimination diagram of Q-F-RF plot (Dickinson, 1985) (Fig. 4.4D). In the figure 4.4C, the 'metagreywacke' and 'quartzo-feldspathic metagreywacke' samples plot in the field of subarkose and arkose field, 'metagreywacke with biotite' plots in the field of sublitharenite field. In ternary Q-F-RF plot, the modal data shows transitional continental to craton interior provenance (Fig. 4.4D). As such from the plots it is delineated that the samples from the study area indicate 'greywacke' rock type and a continental provenance.

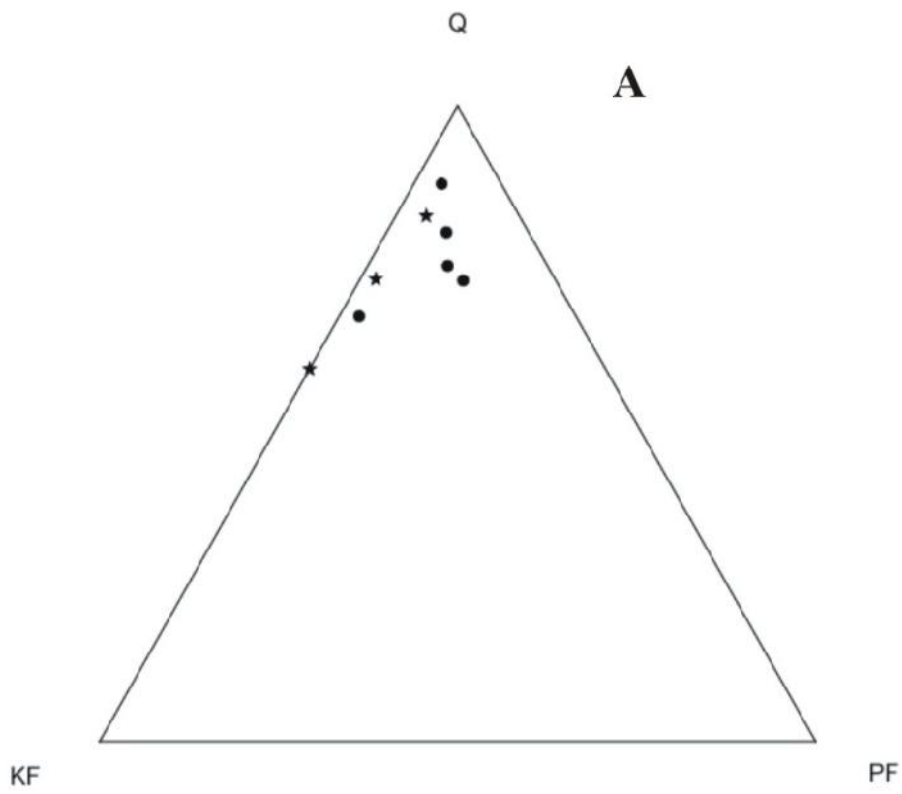
4.2 Associated rocks

As described in chapter 3, the metagreywacke is associated with dykes of dolerite and numerous quartz veins. Dyke of hornblende schist is also reported from the study area.

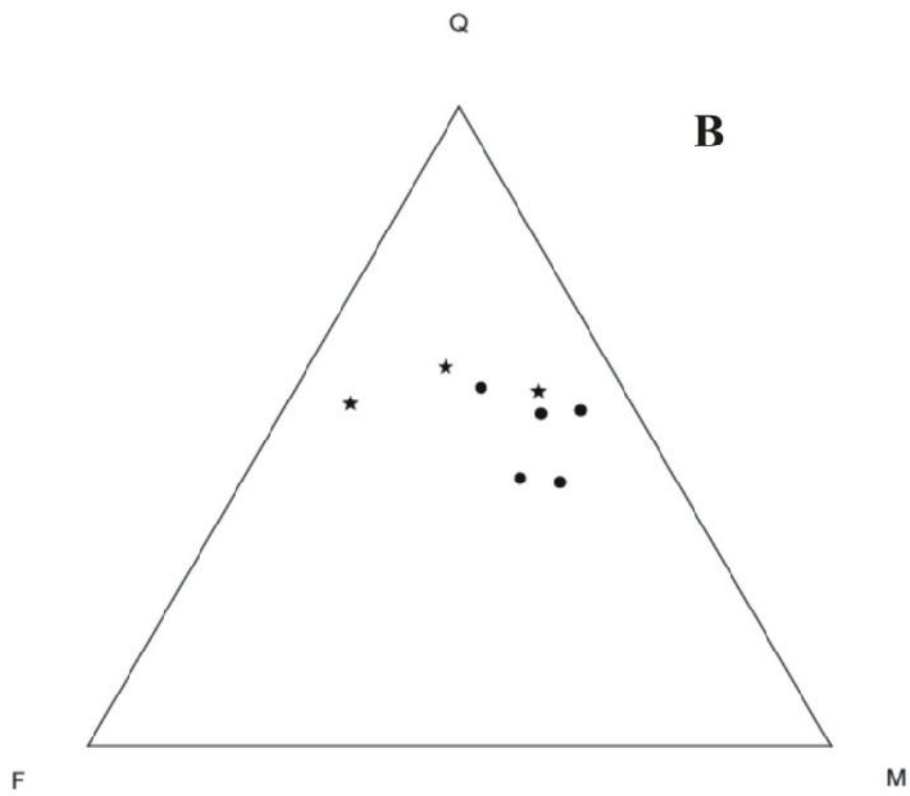
4.2.1 Dykes of dolerite and hornblende schist

The dolerite dykes are medium grained at the central part of dyke and fine grained at the marginal part of the dyke. This texture resulted as quenching commenced from the marginal portion of the intrusion towards the interior. Dolerites comprise of plagioclase (av 54%), pyroxene (augite) (av 38%) and with accessory apatite, Fe-rich lithic fragment (av 2%) and ilmenite (av 4%) (Figs. 4.5, 4.6, 4.7 and Table 4.2B). The dykes are texturally porphyritic with coarse phenocrysts dominantly of plagioclase and with significant amount of augite embedded in medium grained groundmass of plagioclase and augite.

Using the EPMA data (Table 4.1), it is reported that the plagioclase is labradorite in composition and pyroxene present is augite while the opaque is ilmenite. Fe-rich lithic fragment (Fig. 4.5A, B), is present in the dykes of Aguada and Mormugao and occur as dark brown grains, which is verified using Back Scattered image (BSE) (Fig. 4.5B) and EPMA data (Table 4.1). Besides, opaques of ilmenite and elongated needles of apatite (Fig. 4.5C) are found associated with plagioclase.

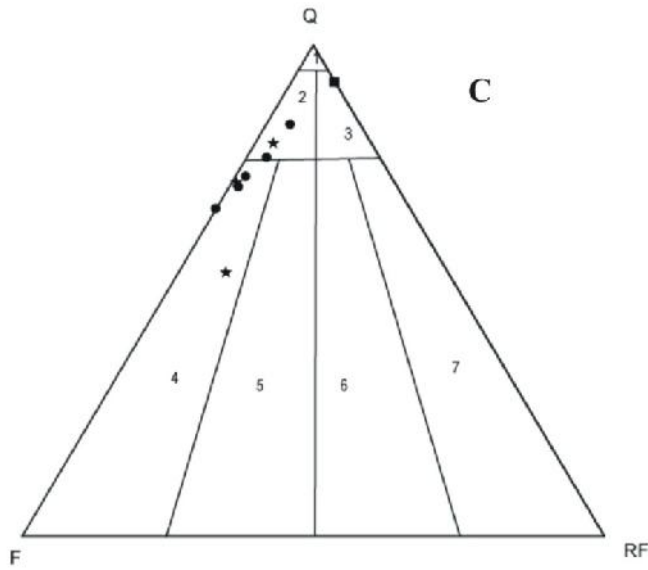


(Bruck, 1972)

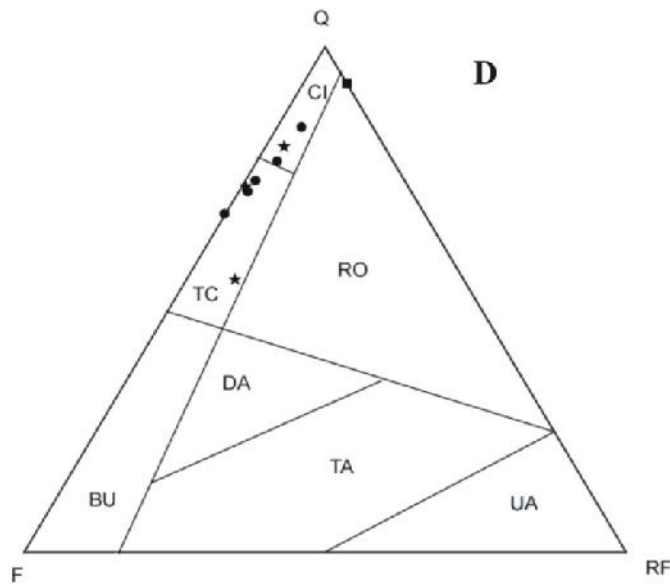


(Bruck, 1972)

Contd...



(Folk et al., 1970)



(Dickinson, 1985)

- Metagreywacke
- ★ Quartzo-feldspathic metagreywacke
- Metagreywacke with biotite

Fig. 4.4: Ternary diagrams based on modal analysis of metagreywacke:
 A) Ternary diagram of Q-KF-PF (quartz - K feldspar - plagioclase feldspar) (Bruck, 1972).
 B) Ternary diagram of Q-F-M (quartz – feldspar – matrix) (Bruck, 1972).
 C) Ternary diagram Qt-F-RF (quartz – feldspar – rock fragment) of sandstone classification sandstone (after Folk et al., 1970). (1. Quartz arenite; 2. Subarkose; 3. Sublitharenite; 4. Arkose; 5. Lithic arkose; 6. Feldspathic litharenite; 7. Litharenite.)
 D) Qt-F-RF discrimination diagram of provenance fields (after Dickinson, 1985).
 (BU – basement uplift; TC – transitional continental; CI – craton interior; RO – recycled orogen; DA – dissected arc; TA – transitional arc; UA – undissected arc).

Plagioclase and augite are the most dominant mineralogy of dolerite dykes of the study area. Some plagioclase grains exhibit deformation twins that have lenticular lamellae that taper at their ends (Fig. 4.5D). Deformation of plagioclase has resulted in undulose extinction and kink folds (Fig. 4.5E). Hour glass or sector zone is seen in plagioclase (Fig. 4.5F), wherein the opposite sectors are identical optically and are distinct from the other opposite pair. Poikilitic inclusions are seen in which the columnar plagioclase crystals depict inclusions of glass, plagioclase (Fig. 4.6A), augite (Fig. 4.6B). At places, penetrating twin is noticed in plagioclase (Fig. 4.6C). Trachytoid texture consisting of platy plagioclase phenocryst stacked one above the other (Fig. 4.6D) and gives a parallel alignment of minerals in the rock. The plagioclase grains are aligned in the magmatic flow and are devoid of any evidence of internal plastic deformation.

The plagioclases identified are of two generations:

- 1) Plagioclase occurs as medium grained ground mass and mostly exhibit simple polysynthetic twins.
- 2) Plagioclase occurs as coarse grained phenocrysts that have oscillatory zones.

The pyroxene is augite in composition occurring as groundmass and as phenocryst. Pyroxene with oscillatory zone is identified (Fig. 4.6E). Pyroxene with melt inclusions are present (Fig. 4.6F). Plagioclase and pyroxene exhibits simple carlsbad twin (Fig. 4.6B, 4.7A). Oscillatory zoning is illustrated by plagioclase and pyroxene (Fig. 4.6A, E). Glomeroporphyritic texture is exhibited (Fig. 4.6D) in which the many phenocrysts are clustered as aggregates of plagioclase laths (glomerocrysts), present in medium grained groundmass of plagioclase and pyroxene.

The presence of chert vein in dolerite exhibits comb structure wherein the fibre texture (plane polarized light in thin section, see Fig. 4.7B) have grown perpendicular to the vein walls. In

figure 4.7B the first layer is of dolerite (D) and the second layer is the transition of dolerite to chert (D-C) layer indicating the boundary/fringe undergone silicification. And the third layer is that of chert (C). A relict phenocryst of plagioclase is replaced by chert and the replacement is very dominant along the twin plane (Fig. 4.7C).

The fine grained dolerite typically exhibit plagioclase symplectic texture with vermicular (wormy) intergrowth (Fig. 4.7D) in plagioclase indicating a replacement as pyroxene embays into plagioclase.

The petrographic description along with EPMA data (Table 4.1) and Back Scattered images (BSE) were conducted to examine the composition of hornblende schist (Fig. 4.7E, F). It is observed that the dyke of hornblende schist comprises of ferrohornblende, quartz and feldspar (albite) and has accessory biotite and illmenite. Ferrohornblende occurs as sheafs which taper into quartz-albite aggregates and at instances show kink folds.

Fe-rich lithic fragment was identified in dolerite and in hornblende schist with brown colour in plane polarized light. Using EPMA, it was observed that it is enriched in Fe_2O_3 (avg ~40% in dolerite dyke and ~ 23% in hornblende schist) and SiO_2 (avg ~50% in dolerite dyke and ~ 57% in hornblende schist) (Table 4.1).

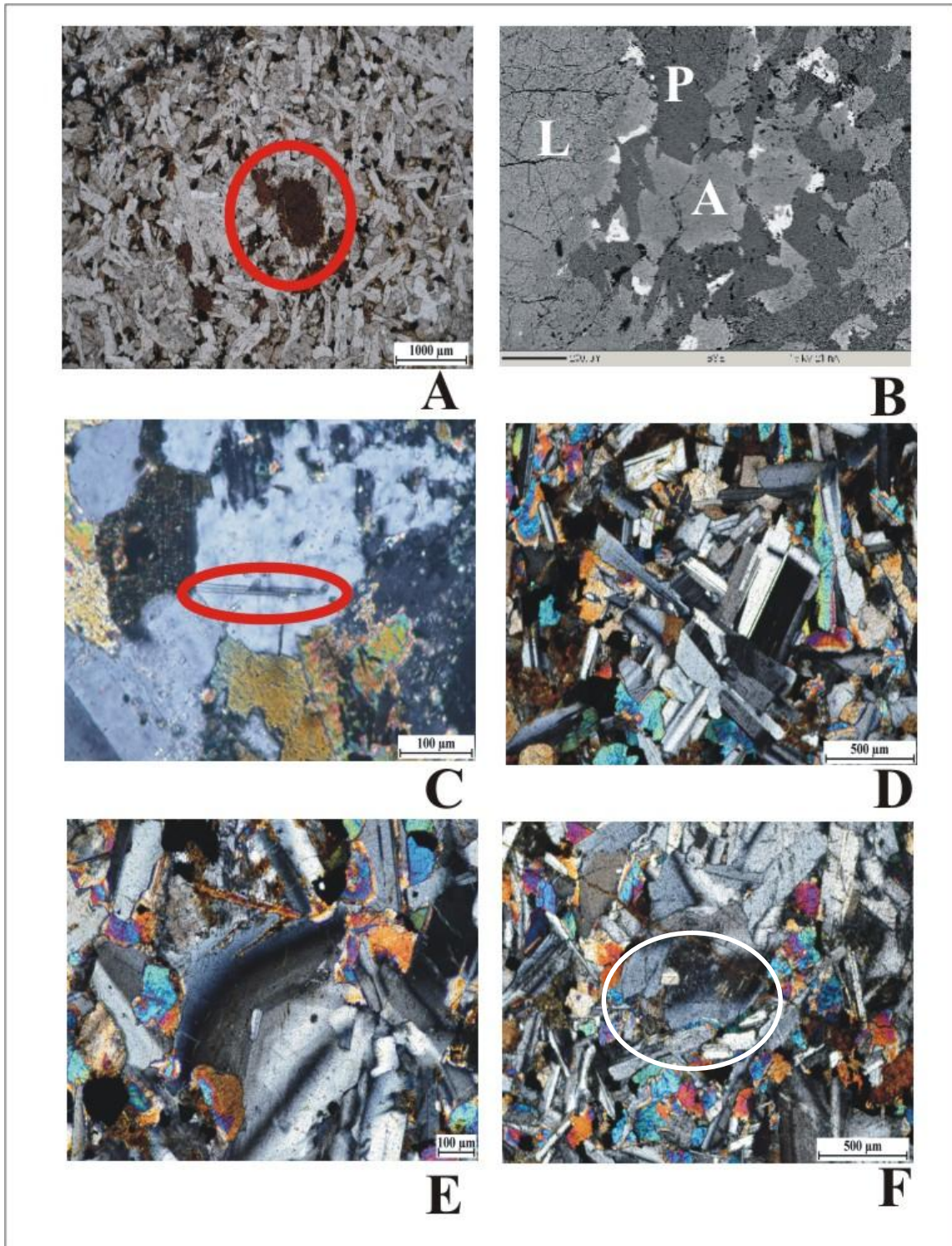


Fig. 4.5: Photomicrographs of dolerite:

A) Fe-rich lithic fragment (red circle) in dolerite.

B) Back Scattered Image of dolerite (L- lithic fragment, P- Plagioclase, A- Augite).

C) Elongate needle of apatite (red circle) along with plagioclase and augite.

D) Plagioclase exhibiting simple carlsbad twin. Plagioclase exhibiting deformation twins having lenticular lamellae's and seen to taper at its termination.

E) Plagioclase with kink folding.

F) Hour glass or sector zoning is seen in plagioclase, wherein opposite sectors are identical optically and are distinct from the other opposite pair (white circle).

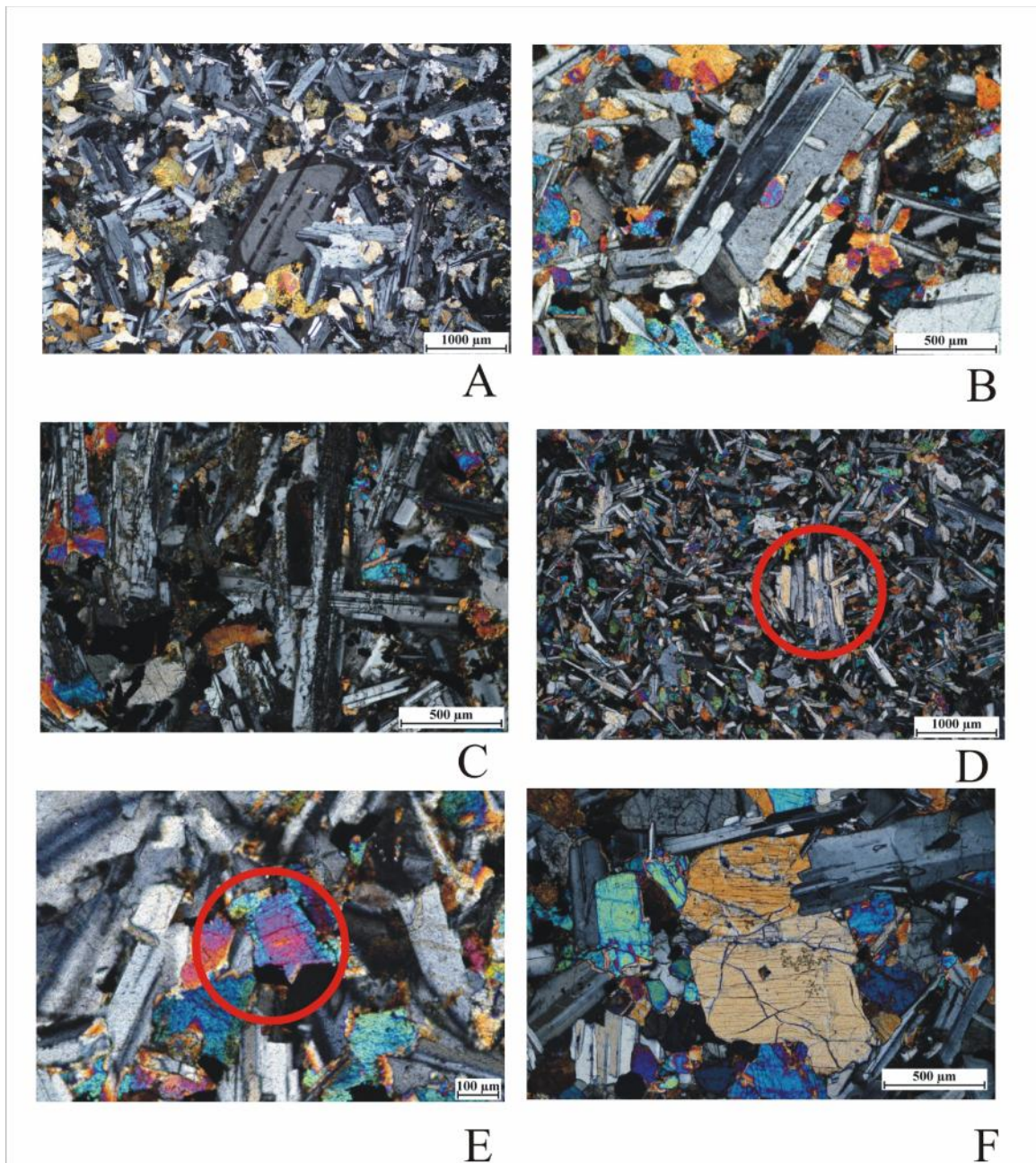


Fig. 4.6: Photomicrograph of dolerite:

A) Oscillatory zoning is illustrated by plagioclase.

B) Poikilitic inclusions are seen wherein the columnar plagioclase crystal is bearing inclusions of plagioclase and augite.

C) Plagioclase penetrating twin is noticed.

D) Trachytoid texture consisting of platy plagioclase phenocryst stacked one above the other giving a parallel alignment of minerals in the rock, which also indicates a glomeroporphyritic texture (red circle).

E) Oscillatory zoning (red circle) is illustrated by pyroxene.

F) Melt inclusions identified in pyroxene.

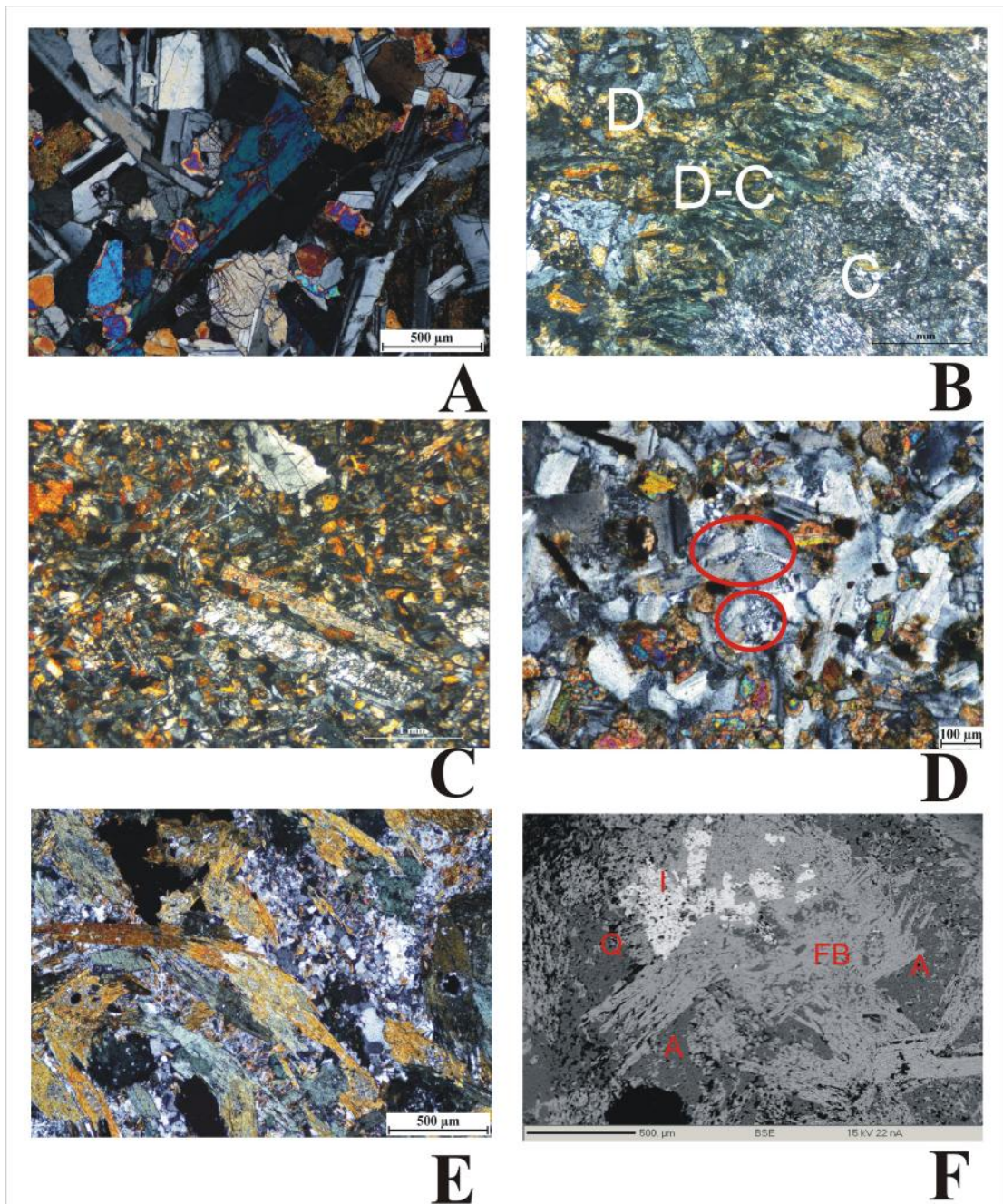


Fig. 4.7: Photomicrograph of dolerite (from A to D) and hornblende schist (from E to F):

A) Pyroxene exhibiting simple carlsbad twin.

B) Presence of fibrous chert vein in dolerite exhibits comb structure wherein fibres have grown perpendicular to the vein walls. First layer is of dolerite (D), the second layer is the transition of dolerite to chert layer (D-C) indicating the boundary/fringe undergoing silicification. The third layer is that of chert (C).

C) Relict phenocryst of plagioclase is replaced by chert and the replacement is very dominant along the twin plane.

D) Plagioclase exhibiting symplectic texture with vermicular (wormy) intergrowth (red circle).

E) Hornblende schist with ferrohornblende sheafs which tapers into quartz-albite aggregates.

F) Back Scattered Image of Hornblende schist (FB- Ferrohornblende, A- Albite, I- Ilmenite, Q- Quartz).

4.3 Summary

In this chapter, in addition to petrographic description, EPMA data and BSE is given to verify the presence of various minerals. With the help of foregoing observations, the immature and poorly sorted metagreywacke rocks are grouped into five distinctive petrofacies: metagreywacke; quartzo-feldspathic metagreywacke; metagreywacke with biotite; metagreywacke cataclasite and argillite. The petrographic description of each of these rock types is given in detail. The modal analysis data of the metagreywacke is plotted using various discrimination diagrams for sandstone classification as well as for provenance.

Further, dykes of dolerite and hornblende schist intrude the country rocks of metagreywacke which are also described in detail to understand its mineralogy and texture.

Chapter 5

GEOCHEMISTRY OF METAGREYWACKE

AND

ASSOCIATED ROCKS

It is well recognized that the crustal evolution and the tectonic setting can be indicated from the geochemistry of clastic sedimentary rocks (Lahtinen, 2000). Geochemical data of sedimentary rocks provides vital clues on paleoweathering conditions, provenance and tectonic setting which are interrelated (Condie et al., 2001; Khudoley et al., 2001; Armstrong-Altrin et al., 2004; Chakrabarti et al., 2007; Chakrabarti et al., 2009; Carranza-Edwards et al., 2009; Araújo et al., 2010).

In this chapter, besides the geochemistry of metagreywacke, the associated rocks of dolerite are also discussed. The geochemical studies of dykes are used to focus on petrogenesis by studying the tectonic context of magma genesis and its emplacement (Balakrishnan et al., 1999; Moyen et al., 2003; Jayananda et al., 2006; Rogers et al., 2007; Dey et al., 2012; Sarma et al., 2012).

5.1 Metagreywacke

The geochemistry of Archaean sedimentary rocks has been studied by many workers to understand their mode of origin and emplacement (Condie et al., 1970; Bavinton and Taylor, 1980; Jenner et al., 1981; Bhatia and Crook, 1986). The geochemical data of major, minor as well as trace elements and REE of the 22 metagreywacke samples of the study area of Sanvordem Formation, Goa Group are presented in table 5.1, 5.2 and 5.3. Correlation coefficient data of major elements is given in table 5.4.

The average value of major oxide composition of argillite is as follows (Table 5.1, 5.2 and 5.5): $\text{SiO}_2 \sim 66.67\%$, $\text{Al}_2\text{O}_3 \sim 15.7\%$, $\text{K}_2\text{O} \sim 2.49\%$, $\text{CaO} \sim 1.11\%$, $\text{TiO}_2 \sim 0.63\%$, $\text{Fe}_2\text{O}_3 \sim 5.33\%$, $\text{MgO} \sim 3.52\%$, $\text{MnO} \sim 0.06\%$, $\text{Na}_2\text{O} \sim 3.39\%$ and $\text{P}_2\text{O}_5 \sim 0.11\%$. The average values of trace elements of argillite are as follows: Cr ~ 123.26 ppm, Zr ~ 149.65 ppm, Sr ~ 111.96 ppm and tREE ~ 195.69 ppm. And, the average value of major oxide composition of metagreywacke is as follows (Table 5.1, 5.2 and 5.5): $\text{SiO}_2 \sim 69.31\%$, $\text{Al}_2\text{O}_3 \sim 13.71\%$, K_2O

~ 2.82%, CaO ~ 0.92%, TiO₂ ~ 0.50%, Fe₂O_{3t} ~ 5.32%, MgO ~ 2.54%, MnO ~ 0.08%, Na₂O ~ 3.24% and P₂O₅ ~ 0.09%. The average values of trace elements of metagreywacke are as follows: Cr ~ 77.38 ppm, Zr ~ 104.83 ppm, Sr ~ 140.66 ppm and tREE ~ 139.22 ppm.

In order to understand better the geochemistry of metagreywacke of the present study, the data is compared with that of:

- 1) greywacke from Merces, Goa (Widdowson, 2009);
 - 2) greywacke with biotite of Goa-Dharwar sector (Devaraju et al., 2010);
 - 3) greywacke with chlorite-sericite of Goa-Dharwar sector (Devaraju et al., 2010);
 - 4) fine-grained greywacke of Goa-Dharwar sector (Devaraju et al., 2010);
 - 5) Late Archaean (3.5-2.5 Ga) greywacke (Condie, 1993);
 - 6) Archaean greywacke of Fig Tree, Barberton (South Africa) (Toulkeridis et al., 1999)
- (Table 5.5).

Table 5.1: Major oxide (wt%) of argillite (Sr. no. 1 to 14), metagreywacke (Sr. no. 15 to 19), quartzose-feldspathic metagreywacke (Sr. no. 20), metagreywacke with biotite (Sr. no. 21) and metagreywacke cataclasite (Sr. no. 22) of the present study area.

| Sr.no. | 1 | 2 | 3 | 4 | 5 | 6 | 7 | 8 | 9 | 10 | 11 | 12 | 13 | 14 | 15 | 16 | 17 | 18 | 19 | 20 | 21 | 22 |
|--------------------------------|-----------|-------|-------|-------|-------|-------|-------|-------|-------|--------|--------|-------|--------|--------|-------|-------|-------|-------|--------|--------|--------|--------|
| Sample no. | 01 | 01B | 02 | 05 | 06 | 06B | 07 | 13 | 15 | 16A | 17A | 23B | 28A | 31 | 08 | 09 | 10 | 12 | 22B | 21B | 21C | 27B |
| SiO ₂ | 62.8 3 | 78.57 | 64.43 | 64.36 | 65.01 | 59.87 | 56.34 | 66.38 | 66.85 | 75.20 | 74.34 | 68.02 | 67.66 | 63.54 | 74.92 | 54.73 | 69.30 | 68.93 | 78.65 | 81.11 | 49.06 | 68.50 |
| Al ₂ O ₃ | 15.3 5 | 10.56 | 14.93 | 14.00 | 14.01 | 16.55 | 17.48 | 14.56 | 13.89 | 16.37 | 16.32 | 17.48 | 20.72 | 17.61 | 11.66 | 18.47 | 13.56 | 13.81 | 11.04 | 10.29 | 12.90 | 20.58 |
| TiO ₂ | 0.70 | 0.29 | 0.62 | 0.60 | 0.68 | 0.73 | 0.71 | 0.57 | 0.72 | 0.67 | 0.60 | 0.69 | 0.76 | 0.55 | 0.41 | 0.72 | 0.49 | 0.54 | 0.36 | 0.31 | 3.03 | 0.22 |
| Fe ₂ O ₃ | 7.57 | 3.11 | 6.85 | 7.43 | 7.50 | 7.99 | 10.04 | 6.29 | 6.15 | 0.90 | 1.04 | 1.12 | 1.26 | 7.35 | 3.94 | 8.92 | 5.38 | 5.22 | 3.15 | 2.04 | 11.23 | 1.35 |
| MnO | 0.08 | 0.03 | 0.11 | 0.11 | 0.09 | 0.08 | 0.12 | 0.04 | 0.09 | 0.00 | 0.00 | -0.01 | -0.01 | 0.09 | 0.03 | 0.12 | 0.08 | 0.09 | 0.06 | 0.04 | 0.56 | 0.00 |
| MgO | 3.02 | 1.12 | 2.37 | 2.69 | 2.70 | 3.36 | 3.85 | 3.07 | 2.86 | 5.59 | 6.21 | 8.75 | 0.77 | 2.99 | 1.81 | 4.48 | 2.62 | 2.40 | 1.38 | 0.79 | 5.29 | 0.86 |
| CaO | 0.99 | 0.82 | 1.34 | 2.86 | 1.94 | 1.61 | 1.46 | 0.57 | 1.54 | 0.30 | 0.33 | 0.28 | 0.38 | 1.10 | 0.73 | 1.36 | 0.77 | 0.86 | 0.86 | 0.95 | 11.86 | 0.26 |
| Na ₂ O | 3.78 | 3.87 | 4.59 | 3.71 | 3.86 | 3.97 | 2.72 | 2.90 | 3.32 | 0.66 | 1.01 | 0.65 | 9.51 | 2.97 | 3.26 | 3.70 | 3.30 | 3.64 | 2.27 | 3.16 | 1.11 | 9.72 |
| K ₂ O | 3.02 | 1.30 | 2.23 | 1.77 | 2.10 | 2.99 | 3.97 | 3.49 | 2.64 | 2.62 | 2.19 | 2.43 | 0.34 | 3.86 | 1.94 | 4.54 | 3.01 | 2.48 | 2.15 | 1.26 | 4.62 | 0.22 |
| P ₂ O ₅ | 0.14 | 0.06 | 0.17 | 0.13 | 0.16 | 0.14 | 0.14 | 0.04 | 0.13 | 0.03 | 0.07 | 0.10 | 0.13 | 0.13 | 0.08 | 0.12 | 0.08 | 0.11 | 0.06 | 0.05 | 0.35 | 0.05 |
| Sum | 97.4 8 | 99.73 | 97.62 | 97.65 | 98.03 | 97.29 | 96.82 | 97.91 | 98.19 | 102.35 | 102.11 | 99.50 | 101.52 | 100.19 | 98.78 | 97.15 | 98.58 | 98.07 | 100.00 | 100.00 | 100.00 | 101.76 |

Table 5.2: Trace and REE (ppm) of argillite (Sr. no. 1 to 14), metagreywacke (Sr. no. 15 to 19), quartzose-feldspathic metagreywacke (Sr. no. 20), metagreywacke with biotite (Sr. no. 21) and metagreywacke cataclasite (Sr. no. 22) of the present study area. (nd=not determined)

| Sr.no. | 1 | 2 | 3 | 4 | 5 | 6 | 7 | 8 | 9 | 10 | 11 | 12 | 13 | 14 |
|------------|-----------|--------|--------|--------|--------|--------|--------|--------|--------|--------|--------|--------|--------|--------|
| Sample no. | 01 | 01B | 02 | 05 | 06 | 06B | 07 | 13 | 15 | 16A | 17A | 23B | 28A | 31 |
| | Argillite | | | | | | | | | | | | | |
| Li | 47.31 | 19.99 | 34.97 | 30.17 | 34.02 | 53.83 | 56.35 | 49.38 | 40.52 | nd | nd | nd | nd | nd |
| Be | 12.70 | 13.82 | 12.50 | 11.00 | 10.81 | 12.48 | 12.78 | 11.92 | 10.53 | nd | nd | nd | nd | nd |
| Sc | 17.21 | 5.89 | 14.40 | 14.64 | 15.08 | 18.39 | 17.68 | 12.76 | 15.23 | nd | nd | nd | nd | nd |
| Ti | 4310 | 1740 | 4040 | 3810 | 4120 | 4460 | 4390 | 3610 | 4560 | nd | nd | nd | nd | nd |
| V | nd | nd | nd | nd | nd | nd | nd | nd | nd | 81.39 | 80.26 | 117.64 | 61.60 | 93.93 |
| Cr | 135.30 | 29.73 | 87.54 | 163.10 | 184.40 | 146.60 | 152.60 | 95.98 | 143.30 | 122.97 | 108.67 | 132.56 | 111.52 | 111.32 |
| Co | 22.61 | 6.36 | 24.67 | 19.30 | 20.30 | 24.96 | 19.61 | 16.79 | 51.94 | 2.51 | 9.03 | 4.76 | 1.86 | 14.67 |
| Ni | 57.01 | 12.74 | 39.33 | 53.68 | 51.62 | 57.04 | 57.92 | 34.15 | 107.80 | 45.62 | 37.42 | 20.06 | 1.92 | 39.48 |
| Cu | 41.51 | 9.32 | 108.50 | 64.98 | 68.11 | 47.25 | 35.69 | 33.96 | 69.37 | 14.70 | 6.84 | 3.94 | 4.00 | 73.61 |
| Zn | 77.19 | 28.93 | 81.58 | 66.29 | 76.70 | 56.62 | 85.10 | 44.98 | 126.00 | nd | nd | nd | nd | nd |
| Ga | 48.63 | 21.16 | 39.42 | 31.06 | 32.99 | 37.44 | 54.70 | 43.34 | 36.06 | nd | nd | nd | nd | nd |
| Rb | 168.60 | 86.79 | 128.30 | 81.11 | 99.77 | 177.00 | 207.60 | 148.30 | 131.50 | nd | nd | nd | nd | nd |
| Sr | 131.00 | 117.30 | 157.00 | 233.20 | 212.50 | 154.70 | 130.10 | 125.40 | 110.50 | 14.03 | 10.34 | 7.24 | 16.04 | 148.16 |
| Y | 23.50 | 25.32 | 23.22 | 23.93 | 23.16 | 22.32 | 21.51 | 17.81 | 25.34 | nd | nd | nd | nd | nd |
| Zr | 146.30 | 150.70 | 171.30 | 141.40 | 144.30 | 160.40 | 147.10 | 137.80 | 202.30 | 124.05 | 145.39 | 135.94 | 138.66 | 149.52 |
| Nb | 18.51 | 12.29 | 18.88 | 13.33 | 16.05 | 18.78 | 16.26 | 17.73 | 29.51 | nd | nd | nd | nd | nd |
| Sn | 2.56 | 1.68 | 2.06 | 1.77 | 1.80 | 2.03 | 2.52 | 2.62 | 2.94 | nd | nd | nd | nd | nd |
| Sb | 0.19 | 0.25 | 0.31 | 0.45 | 0.25 | 0.23 | 0.09 | 0.16 | 0.21 | 0.49 | 0.30 | 0.20 | 0.08 | 0.58 |
| Cs | 7.78 | 4.38 | 7.86 | 5.30 | 6.56 | 11.89 | 12.79 | 5.85 | 6.87 | nd | nd | nd | nd | nd |
| Ba | 846.60 | 264.50 | 675.60 | 405.10 | 460.20 | 516.70 | 909.80 | 757.30 | 585.70 | 76.31 | 56.52 | 69.60 | 26.40 | 763.59 |
| Pb | 2.97 | 7.37 | 4.41 | 4.30 | 3.47 | 5.06 | 4.48 | 1.67 | 4.70 | nd | nd | nd | nd | nd |
| Th | 7.61 | 6.79 | 8.07 | 7.31 | 7.50 | 8.56 | 6.39 | 7.62 | 20.73 | nd | nd | nd | nd | nd |
| U | 3.24 | 2.78 | 3.40 | 3.47 | 3.40 | 3.58 | 2.69 | 3.82 | 10.48 | nd | nd | nd | nd | nd |
| | | | | | | | | | | | | | | |
| La | 36.83 | 41.81 | 46.01 | 44.36 | 56.73 | 43.68 | 34.17 | 18.72 | 47.13 | 6.39 | 57.61 | 3.40 | 0.84 | 33.83 |
| Ce | 84.22 | 103.00 | 100.70 | 91.73 | 111.40 | 90.35 | 72.44 | 43.63 | 99.66 | 14.46 | 119.38 | 8.00 | 2.14 | 71.06 |
| Pr | 7.60 | 9.44 | 9.34 | 8.73 | 10.37 | 8.96 | 7.08 | 4.41 | 10.69 | nd | nd | nd | nd | nd |
| Nd | 31.36 | 39.46 | 38.68 | 36.96 | 44.56 | 38.44 | 30.46 | 19.26 | 46.72 | 7.47 | 57.42 | 4.78 | 1.94 | 27.41 |
| Sm | 4.30 | 4.76 | 4.79 | 4.86 | 5.40 | 5.26 | 4.48 | 3.13 | 6.48 | nd | nd | nd | nd | nd |
| Eu | 1.05 | 0.86 | 1.20 | 1.24 | 1.34 | 1.33 | 1.17 | 0.81 | 1.49 | 0.24 | 0.83 | 0.24 | 0.12 | 1.26 |
| Gd | 4.33 | 4.94 | 4.72 | 5.02 | 5.65 | 5.31 | 4.54 | 3.27 | 6.26 | 1.85 | 8.35 | 1.70 | 0.64 | 5.41 |
| Tb | 0.61 | 0.68 | 0.65 | 0.69 | 0.74 | 0.71 | 0.63 | 0.47 | 0.83 | nd | nd | nd | nd | nd |
| Dy | 3.40 | 3.68 | 3.51 | 3.85 | 3.86 | 3.70 | 3.43 | 2.69 | 4.58 | nd | nd | nd | nd | nd |
| Ho | 0.72 | 0.77 | 0.74 | 0.80 | 0.77 | 0.74 | 0.70 | 0.59 | 0.93 | nd | nd | nd | nd | nd |
| Er | 2.26 | 2.47 | 2.37 | 2.48 | 2.29 | 2.20 | 2.10 | 1.84 | 2.89 | nd | nd | nd | nd | nd |
| Tm | 0.35 | 0.40 | 0.38 | 0.39 | 0.35 | 0.34 | 0.31 | 0.30 | 0.49 | nd | nd | nd | nd | nd |
| Yb | 2.18 | 2.75 | 2.45 | 2.48 | 2.13 | 2.07 | 1.91 | 2.00 | 3.31 | 1.63 | 1.57 | 2.02 | 0.86 | 2.16 |
| Lu | 0.33 | 0.46 | 0.38 | 0.38 | 0.32 | 0.32 | 0.29 | 0.32 | 0.49 | nd | nd | nd | nd | nd |

Cont (Table 5.2)....

| Sr.no. | 15 | 16 | 17 | 18 | 20 | 19 | 21 | 22 |
|------------|---------------|--------|--------|--------|--------|--|-------------------------------|------------------------------|
| Sample no. | 08 | 09 | 10 | 12 | 22B | 21B | 21C | 27B |
| | Metagreywacke | | | | | Quartzo- feldspathic metagreywacke | Metagreywacke with biotite | Metagreywacke Cataclasite |
| Li | 20.92 | 64.83 | 38.89 | 31.13 | nd | nd | nd | nd |
| Be | 8.51 | 17.24 | 10.09 | 11.45 | nd | nd | nd | nd |
| Sc | 9.09 | 16.98 | 11.24 | 11.81 | nd | nd | nd | nd |
| Ti | 2470 | 4680 | 3070 | 3340 | nd | nd | nd | nd |
| V | nd | nd | nd | nd | 50.50 | 38.89 | 217.81 | 67.87 |
| Cr | 58.98 | 108.70 | 75.59 | 85.68 | 57.93 | 48.40 | 850.75 | 101.60 |
| Co | 10.94 | 29.53 | 15.68 | 16.37 | 8.35 | 5.49 | 90.24 | 1.70 |
| Ni | 21.99 | 55.09 | 30.14 | 31.59 | 35.76 | 22.06 | 347.13 | 1.15 |
| Cu | 60.31 | 89.46 | 65.91 | 39.83 | 41.41 | 12.40 | 290.97 | 4.39 |
| Zn | 23.02 | 107.50 | 87.16 | 54.16 | nd | nd | nd | nd |
| Ga | 31.13 | 57.92 | 37.15 | 37.10 | nd | nd | nd | nd |
| Rb | 57.33 | 225.80 | 138.00 | 92.79 | nd | nd | nd | nd |
| Sr | 108.80 | 220.30 | 117.80 | 143.70 | 112.71 | 133.45 | 183.89 | 10.42 |
| Y | 21.45 | 26.26 | 13.51 | 20.88 | nd | nd | nd | nd |
| Zr | 91.68 | 150.80 | 105.30 | 115.20 | 61.18 | 57.88 | 942.53 | 97.94 |
| Nb | 13.79 | 31.37 | 19.14 | 20.11 | nd | nd | nd | nd |
| Sn | 2.02 | 3.56 | 2.23 | 2.28 | nd | nd | nd | nd |
| Sb | 0.17 | 0.22 | 0.21 | 0.35 | 0.08 | 0.20 | 0.75 | 0.04 |
| Cs | 1.75 | 11.58 | 5.68 | 4.23 | nd | nd | nd | nd |
| Ba | 519.40 | 784.70 | 629.50 | 628.90 | 659.14 | 474.30 | 534.33 | 10.47 |
| Pb | 3.00 | 4.70 | 3.02 | 2.20 | nd | nd | nd | nd |
| Th | 5.57 | 10.92 | 7.04 | 8.09 | nd | nd | nd | nd |
| U | 2.29 | 5.80 | 2.66 | 3.94 | nd | nd | nd | nd |
| | | | | | | | | |
| La | 32.21 | 37.00 | 15.18 | 32.61 | 24.70 | 8.55 | 1061.56 | 0.26 |
| Ce | 66.22 | 73.67 | 30.38 | 69.77 | 41.71 | 17.56 | 1963.95 | 0.81 |
| Pr | 6.52 | 7.33 | 3.31 | 7.20 | nd | nd | nd | nd |
| Nd | 27.78 | 31.60 | 14.35 | 31.14 | 18.17 | 8.30 | 594.37 | 1.46 |
| Sm | 3.81 | 4.52 | 2.17 | 4.55 | nd | nd | nd | nd |
| Eu | 0.90 | 1.04 | 0.55 | 1.09 | 1.14 | 0.73 | 9.49 | 0.14 |
| Gd | 3.93 | 4.69 | 2.22 | 4.51 | 4.26 | 2.02 | 102.61 | 0.65 |
| Tb | 0.54 | 0.67 | 0.32 | 0.63 | nd | nd | nd | nd |
| Dy | 2.98 | 3.75 | 1.95 | 3.42 | nd | nd | nd | nd |
| Ho | 0.64 | 0.81 | 0.45 | 0.70 | nd | nd | nd | nd |
| Er | 1.98 | 2.54 | 1.54 | 2.12 | nd | nd | nd | nd |
| Tm | 0.31 | 0.41 | 0.28 | 0.35 | nd | nd | nd | nd |
| Yb | 2.00 | 2.76 | 1.89 | 2.25 | 1.97 | 1.39 | 28.91 | 0.89 |
| Lu | 0.30 | 0.45 | 0.30 | 0.33 | nd | nd | nd | nd |

Table 5.3: Ratios of various oxides, trace elements and REE of argillite (Sr. no. 1 to 14), metagreywacke (Sr. no. 15 to 19), quartzose-feldspathic metagreywacke (Sr. no. 20), metagreywacke with biotite (Sr. no. 21) and metagreywacke cataclasite (Sr. no. 22) of the present study area. (nd=not determined)

| Sr.no. | 1 | 2 | 3 | 4 | 5 | 6 | 7 | 8 | 9 | 10 | 11 | 12 | 13 | 14 | 15 | 16 | 17 | 18 | 20 | 19 | 21 | 22 |
|---|---------|----------|---------|---------|---------|----------|---------|---------|---------|--------|--------|--------|--------|--------|---------|---------|---------|---------|--------|--------|---------|--------|
| Sample no. | GA - 01 | GA - 01B | GA - 02 | GA - 05 | GA - 06 | GA - 06B | GA - 07 | GA - 13 | GA - 15 | Ga 16A | Ga 17A | Ga 23B | Ga 28A | Ga 31 | GA - 08 | GA - 09 | GA - 10 | GA - 12 | Ga 22B | Ga 21B | Ga 21C | Ga 27B |
| LREE | 169.68 | 204.27 | 205.43 | 192.90 | 235.44 | 193.32 | 154.34 | 93.24 | 218.43 | 30.39 | 243.60 | 18.12 | 5.68 | 138.98 | 141.37 | 199.84 | 68.16 | 150.88 | 89.98 | 37.17 | 3731.98 | 3.32 |
| HREE | 9.84 | 11.21 | 10.48 | 11.07 | 10.45 | 10.07 | 9.36 | 8.19 | 13.52 | 1.63 | 1.57 | 2.02 | 0.86 | 2.16 | 8.75 | 11.38 | 6.72 | 9.79 | 1.97 | 1.39 | 28.91 | 0.89 |
| La/Sm | 8.57 | 8.78 | 9.62 | 9.13 | 10.51 | 8.31 | 7.63 | 5.97 | 7.28 | nd | nd | nd | nd | nd | 8.45 | 8.19 | 7.01 | 7.16 | nd | nd | nd | nd |
| Gd/Yb | 1.99 | 1.79 | 1.92 | 2.03 | 2.65 | 2.56 | 2.38 | 1.64 | 1.89 | nd | nd | nd | nd | nd | 1.97 | 1.70 | 1.17 | 2.01 | 2.16 | nd | nd | nd |
| LREE/HREE | 17.24 | 18.22 | 19.60 | 17.42 | 22.53 | 19.20 | 16.49 | 11.38 | 16.16 | 18.64 | 155.10 | 8.97 | 6.60 | 64.21 | 16.17 | 14.05 | 10.14 | 15.42 | 45.63 | 26.81 | 129.08 | 3.73 |
| Eu/Eu* | 0.75 | 0.54 | 0.77 | 0.77 | 0.74 | 0.77 | 0.79 | 0.77 | 0.72 | nd | nd | nd | nd | nd | 0.71 | 0.69 | 0.77 | 0.73 | nd | nd | nd | nd |
| La/Yb | 16.92 | 15.18 | 18.76 | 17.92 | 26.67 | 21.08 | 17.91 | 9.38 | 14.24 | 3.92 | 36.68 | 1.68 | 0.98 | 15.63 | 16.12 | 13.43 | 8.02 | 14.53 | 12.53 | 6.17 | 36.72 | 0.29 |
| Sm/Nd | 0.14 | 0.12 | 0.12 | 0.13 | 0.12 | 0.14 | 0.15 | 0.16 | 0.14 | nd | nd | nd | nd | nd | 0.14 | 0.14 | 0.15 | 0.15 | nd | nd | nd | nd |
| Cr/Th | 17.77 | 4.38 | 10.85 | 22.31 | 24.58 | 17.12 | 23.89 | 12.59 | 6.91 | nd | nd | nd | nd | nd | 10.59 | 9.95 | 10.74 | 10.59 | nd | nd | nd | nd |
| Cr/Sc | 7.86 | 5.05 | 6.08 | 11.14 | 12.23 | 7.97 | 8.63 | 7.52 | 9.41 | nd | nd | nd | nd | nd | 6.49 | 6.40 | 6.73 | 7.25 | nd | nd | nd | nd |
| Th/Sc | 0.44 | 1.15 | 0.56 | 0.50 | 0.50 | 0.47 | 0.36 | 0.60 | 1.36 | nd | nd | nd | nd | nd | 0.61 | 0.64 | 0.63 | 0.68 | nd | nd | nd | nd |
| Cl A | 66.33 | 63.80 | 64.67 | 62.70 | 63.96 | 65.89 | 68.22 | 67.64 | 64.93 | 82.06 | 82.24 | 83.88 | 66.95 | 68.95 | 66.28 | 65.79 | 65.72 | 66.45 | 67.61 | 65.68 | 42.32 | 66.85 |
| K ₂ O/Al ₂ O ₃ | 0.20 | 0.12 | 0.15 | 0.13 | 0.15 | 0.18 | 0.23 | 0.24 | 0.19 | 0.16 | 0.13 | 0.14 | 0.02 | 0.22 | 0.17 | 0.25 | 0.22 | 0.18 | 0.20 | 0.12 | 0.36 | 0.01 |
| Th/U | 2.35 | 2.44 | 2.37 | 2.11 | 2.21 | 2.39 | 2.37 | 2.00 | 1.98 | nd | nd | nd | nd | nd | 2.43 | 1.88 | 2.65 | 2.05 | nd | nd | nd | nd |
| La/Th | 4.84 | 6.16 | 5.70 | 6.07 | 7.56 | 5.10 | 5.35 | 2.46 | 2.27 | nd | nd | nd | nd | nd | 5.78 | 3.39 | 2.16 | 4.03 | nd | nd | nd | nd |

Table 5.4: Values of Pearson's coefficient of correlation of major elements of metagreywacke petrofacies.

| Variable | SiO ₂ | Al ₂ O ₃ | TiO ₂ | Fe ₂ O ₃ | MnO | MgO | CaO | Na ₂ O | K ₂ O | P ₂ O ₅ | CIA | K ₂ O/Al ₂ O ₃ |
|---|------------------|--------------------------------|------------------|--------------------------------|-------|-------|-------|-------------------|------------------|-------------------------------|-------|---|
| SiO ₂ | 1.00 | | | | | | | | | | | |
| Al ₂ O ₃ | -0.42 | 1.00 | | | | | | | | | | |
| TiO ₂ | -0.6 | -0.03 | 1.00 | | | | | | | | | |
| Fe ₂ O ₃ | -0.83 | -0.06 | 0.52 | 1.00 | | | | | | | | |
| MnO | -0.67 | -0.21 | 0.92 | 0.70 | 1.00 | | | | | | | |
| MgO | -0.32 | 0.26 | 0.38 | 0.05 | 0.17 | 1.00 | | | | | | |
| CaO | -0.59 | -0.22 | 0.95 | 0.58 | 0.97 | 0.20 | 1.00 | | | | | |
| Na ₂ O | -0.01 | 0.45 | -0.28 | -0.17 | -0.26 | -0.67 | -0.24 | 1.00 | | | | |
| K ₂ O | -0.67 | -0.01 | 0.52 | 0.74 | 0.58 | 0.51 | 0.45 | -0.60 | 1.00 | | | |
| P ₂ O ₅ | -0.78 | 0.03 | 0.87 | 0.71 | 0.88 | 0.20 | 0.86 | -0.09 | 0.46 | 1.00 | | |
| CIA | 0.48 | 0.33 | -0.60 | -0.65 | -0.79 | 0.42 | -0.76 | -0.20 | -0.22 | -0.70 | 1.00 | |
| K ₂ O/Al ₂ O ₃ | -0.53 | -0.32 | 0.61 | 0.73 | 0.72 | 0.37 | 0.60 | -0.66 | 0.93 | 0.51 | -0.42 | 1.00 |

Table 5.5: Average composition of metagreywacke of the study area and greywacke from other areas for comparison (the numbers within the brackets indicate the number of samples averaged). 1) greywacke from Merces, Goa (Widdowson, 2009); 2) greywacke with biotite of Goa-Dharwar sector (Devaraju et al., 2010); 3) greywacke with chlorite-sericite of Goa-Dharwar sector (Devaraju et al., 2010); 4) fine-grained greywacke of Goa-Dharwar sector (Devaraju et al., 2010); 5) Late Archaean (3.5-2.5 Ga) greywacke (Condie, 1993); 6) Archaean greywacke of Fig Tree, Barberton (South Africa) (Toulkeridis et al., 1999); 7) argillite (study area); 8) metagreywacke (study area); 9) quartzo-feldspathic metagreywacke (study area); 10) metagreywacke with biotite (study area); 11) metagreywacke cataclasite (study area). (nd = not determined; na = not available)

| Sr.no. | 1 (1) | 2 (6) | 3 (13) | 4 (8) | 5 (1) | 6 (12) | 7 (14) | 8 (5) | 9 (1) | 10 (1) | 11 (1) |
|--------------------------------|--------|--------|--------|--------|--------|--------|---------|--------|--------|---------|--------|
| SiO ₂ | 67.77 | 67.31 | 63.03 | 63.13 | 65.00 | 63.41 | 66.67 | 69.31 | 81.11 | 49.06 | 68.50 |
| Al ₂ O ₃ | 14.65 | 12.13 | 14.16 | 15.18 | 15.20 | 11.85 | 15.70 | 13.71 | 10.29 | 12.90 | 20.58 |
| TiO ₂ | 0.56 | 0.79 | 0.59 | 0.61 | 0.61 | 0.54 | 0.63 | 0.50 | 0.31 | 3.03 | 0.22 |
| Fe ₂ O ₃ | 6.08 | 7.67 | 7.06 | 7.19 | 5.90 | 8.15 | 5.33 | 5.32 | 2.04 | 11.23 | 1.35 |
| MnO | 0.13 | 0.08 | 2.93 | 3.27 | na | 0.18 | 0.06 | 0.08 | 0.04 | 0.56 | 0.00 |
| MgO | 3.07 | 3.90 | 0.11 | 0.11 | 3.30 | 6.16 | 3.52 | 2.54 | 0.79 | 5.29 | 0.86 |
| CaO | 0.95 | 1.37 | 2.83 | 2.22 | 2.60 | 2.48 | 1.11 | 0.92 | 0.95 | 11.86 | 0.26 |
| Na ₂ O | 3.31 | 2.10 | 3.51 | 2.65 | 3.10 | 1.68 | 3.39 | 3.24 | 3.16 | 1.11 | 9.72 |
| K ₂ O | 3.68 | 3.30 | 1.92 | 3.17 | 2.10 | 1.85 | 2.49 | 2.82 | 1.26 | 4.62 | 0.22 |
| P ₂ O ₅ | 0.12 | 0.11 | 0.14 | 0.16 | 0.14 | 0.09 | 0.11 | 0.09 | 0.05 | 0.35 | 0.05 |
| Sum | 100.32 | 98.76 | 96.28 | 97.69 | 97.95 | 96.39 | 99.03 | 98.52 | 100 | 100 | 101.76 |
| Li | na | na | na | na | na | na | 40.73 | 38.94 | nd | nd | nd |
| Be | na | na | na | na | na | na | 12.06 | 11.82 | nd | nd | nd |
| Sc | 14 | 17 | 14 | 14 | 15 | 14 | 14.59 | 12.28 | nd | nd | nd |
| Ti | na | na | na | na | na | na | 3893.33 | 3390 | nd | nd | nd |
| V | na | na | na | na | na | na | 86.96 | 50.50 | 38.89 | 217.81 | 67.87 |
| Cr | 108 | 152 | 108 | 108 | 175 | 539 | 123.26 | 77.38 | 48.40 | 850.75 | 101.60 |
| Co | na | 38 | 25 | 28 | 30 | 30 | 17.10 | 16.17 | 5.49 | 90.24 | 1.70 |
| Ni | 33 | 58 | 52 | 54 | 75 | 336 | 43.98 | 34.91 | 22.06 | 347.13 | 1.15 |
| Cu | 41 | 64 | 47 | 69 | na | 31 | 41.55 | 59.38 | 12.40 | 290.97 | 4.39 |
| Zn | 109 | 58 | 78 | 91 | na | 90 | 71.49 | 67.96 | nd | nd | nd |
| Ga | na | na | na | na | na | na | 38.31 | 40.83 | nd | nd | nd |
| Rb | 118 | 106 | 80 | 161 | 70 | 94 | 136.55 | 128.48 | nd | nd | nd |
| Sr | 114 | 90 | 292 | 390 | 265 | 77 | 111.96 | 140.66 | 133.45 | 183.89 | 10.42 |
| Y | 15 | 24 | 23 | 27 | 25 | 16 | 22.90 | 20.53 | nd | nd | nd |
| Zr | 191 | 166 | 215 | 271 | 160 | 111 | 149.65 | 104.83 | 57.88 | 942.53 | 97.94 |
| Nb | 13 | 9 | 9 | 14 | 11 | 7 | 17.93 | 21.10 | nd | nd | nd |
| Sn | na | na | na | na | na | na | 2.22 | 2.52 | nd | nd | nd |
| Sb | na | na | na | na | na | na | 0.27 | 0.21 | 0.20 | 0.75 | 0.04 |
| Cs | na | na | na | na | na | na | 7.70 | 5.81 | nd | nd | nd |
| Ba | 721 | 356 | 419 | 713 | 390 | 291 | 458.14 | 644.33 | 474.30 | 534.33 | 10.47 |
| Pb | 12 | 7 | 12 | 14 | 20 | 15 | 4.27 | 3.23 | nd | nd | nd |
| Th | 16 | 8 | 10 | 13 | 8 | 5 | 8.95 | 7.90 | nd | nd | nd |
| U | 6 | 2 | 3 | 5 | 2 | 1 | 4.10 | 3.67 | nd | nd | nd |
| La | na | 25.70 | 30.94 | 35.10 | 26 | 16.21 | 33.68 | 28.34 | 8.55 | 1061.56 | 0.26 |
| Ce | na | 57.98 | 72.12 | 85.16 | 52 | 31.76 | 72.30 | 56.35 | 17.56 | 1963.95 | 0.81 |
| Pr | na | 4.83 | 6.38 | 7.09 | | 3.55 | 8.51 | 6.09 | nd | nd | nd |
| Nd | na | 20.07 | 24.74 | 23.70 | 22 | 14.08 | 30.35 | 24.61 | 8.30 | 594.37 | 1.46 |
| Sm | na | 3.69 | 4.58 | 3.11 | 3.90 | 2.86 | 4.83 | 3.76 | nd | nd | nd |
| Eu | na | 1.02 | 1.28 | 0.69 | 1.10 | 0.68 | 0.94 | 0.94 | 0.73 | 9.49 | 0.14 |
| Gd | na | 3.76 | 4.27 | 4.95 | 3.69 | 2.59 | 4.43 | 3.92 | 2.02 | 102.61 | 0.65 |
| Tb | na | 0.61 | 0.60 | 0.44 | 0.58 | 0.47 | 0.67 | 0.54 | nd | nd | nd |
| Dy | na | 4.32 | 3.40 | 4.27 | na | 2.85 | 3.63 | 3.02 | nd | nd | nd |
| Ho | na | 0.76 | 0.65 | 0.49 | na | 0.61 | 0.75 | 0.65 | nd | nd | nd |
| Er | na | 2.27 | 1.83 | 0.01 | na | 1.77 | 2.32 | 2.04 | nd | nd | nd |
| Tm | na | 0.35 | 0.26 | 0.22 | na | 0.28 | 0.37 | 0.34 | nd | nd | nd |
| Yb | na | 2.20 | 1.71 | 1.33 | 1.40 | 1.67 | 2.11 | 2.17 | 1.39 | 28.91 | 0.89 |
| Lu | na | 0.33 | 0.24 | 0.19 | 0.25 | 0.26 | 0.36 | 0.34 | nd | nd | nd |
| Total REE | na | 127.89 | 153.00 | 166.75 | 110.92 | 79.64 | 195.69 | 139.22 | nd | nd | nd |

The variable trends observed on the variation diagrams with SiO_2 at the X-axis and various oxides (TiO_2 , Al_2O_3 , Fe_2O_3 , Na_2O , CaO and MgO) on the y-axis (Fig. 5.1), indicates mixing of the different constituents of the sediment and a poor mineralogical maturity (Fernandes et al., 2016a). The plots of SiO_2 with TiO_2 , Al_2O_3 , Fe_2O_3 , MgO and CaO indicates a negative correlation, while the plots of SiO_2 with Na_2O are almost scattered which may result from the presence of variable feldspar proportions within the rocks (Table 5.4). In figure 5.1B, the 'argillite' and 'metagreywacke cataclasite' have a comparative higher content of Al_2O_3 with respect to the other categories, indicating significant occurrence of clayey matrix (cf. Cullers, 1995). The presence of clay is indicated by enhanced Al_2O_3 content (10.28-20.71%) and $\text{K}_2\text{O}/\text{Al}_2\text{O}_3$ (0.02 to 0.36).

Major element and trace element data have been used to classify the sandstones (Pettijohn et al., 1972; Marston, 1978; Bhatia and Crook, 1986; Herron, 1988; Le Maitre et al., 1989). A binary variation diagram of $\text{SiO}_2/\text{Al}_2\text{O}_3$ vs $\text{K}_2\text{O}/\text{Na}_2\text{O}$ (after Wimmenauer, 1984) (Fig. 5.2A) indicates that majority of the samples of the study area plot in greywacke field, while, 'quartzo-feldspathic metagreywacke' plots in quartz-rich greywacke, and 'metagreywacke with biotite' plots in pelitic greywacke field.

The plot of $\log (\text{Na}_2\text{O}/\text{K}_2\text{O})$ against $\log (\text{SiO}_2/\text{Al}_2\text{O}_3)$, (after Pettijohn et al., 1972) (Fig. 5.2B) also emphasizes the greywacke field, but some samples of the study area plot in the litharenite and arkose field. The above variation diagram of Pettijohn et al., (1972) is modified by Herron (1988) (Fig. 5.2C) as a binary plot of $\log (\text{Fe}_2\text{O}_3/\text{K}_2\text{O})$ against $\log (\text{SiO}_2/\text{Al}_2\text{O}_3)$. Here the samples plot in the shale and wacke fields along with the various reference greywacke samples while, 'quartzo-feldspathic metagreywacke' plot in the field of litharenite.

On the ternary diagram of $\text{Fe}_2\text{O}_3+\text{MgO} - \text{Na}_2\text{O} - \text{K}_2\text{O}$ (after Marston, 1978) (Fig. 5.2D), a majority of the samples of the study area, plots in the field of greywacke and some in Fe-Mg

potassic sandstones. The average of Archaean greywacke of Fig Tree, Barberton (Toulkeridis et al., 1999) and the average of greywacke with biotite from Goa-Dharwar sector (Devaraju et al., 2010) plots in the field of Fe-Mg potassic sandstone (Fig. 5.2D). Hence, from all the plots (Fig. 5.2), it is evident that our samples study based on major oxide studies indicate a greywacke composition.

In the K_2O vs Na_2O bivariate diagram of Crook (1974), the metagreywacke samples of the study area plots dominantly in quartz intermediate to quartz-rich field (Fig. 5.2E). Further, the value of K_2O/Al_2O_3 ratio is less than 0.3 for clays and range from 0.3 to 0.9 for feldspars (Cox and Lowe, 1995; Moosavirad et al., 2012). However, the value of K_2O/Al_2O_3 ratio of metagreywacke of the study area is (average) 0.17 (range from 0.02 to 0.36), reveal a dominance of clay minerals.

The study of REE is more reliable than the major and trace elements as they are not affected during the erosion, sedimentation and diagenetic processes. The elemental concentration of REE of metagreywacke petrofacies is normalized using the chondrite values of Sun and McDonough (1989) (Fig. 5.3). The 'metagreywacke' samples have a lower tREE (avg ~139 ppm), as compared to 'argillite' with a high content of tREE (avg ~195 ppm). This indicates that although there is dominance of clay minerals, there is much higher content of clay minerals in 'argillites' than the 'metagreywacke'.

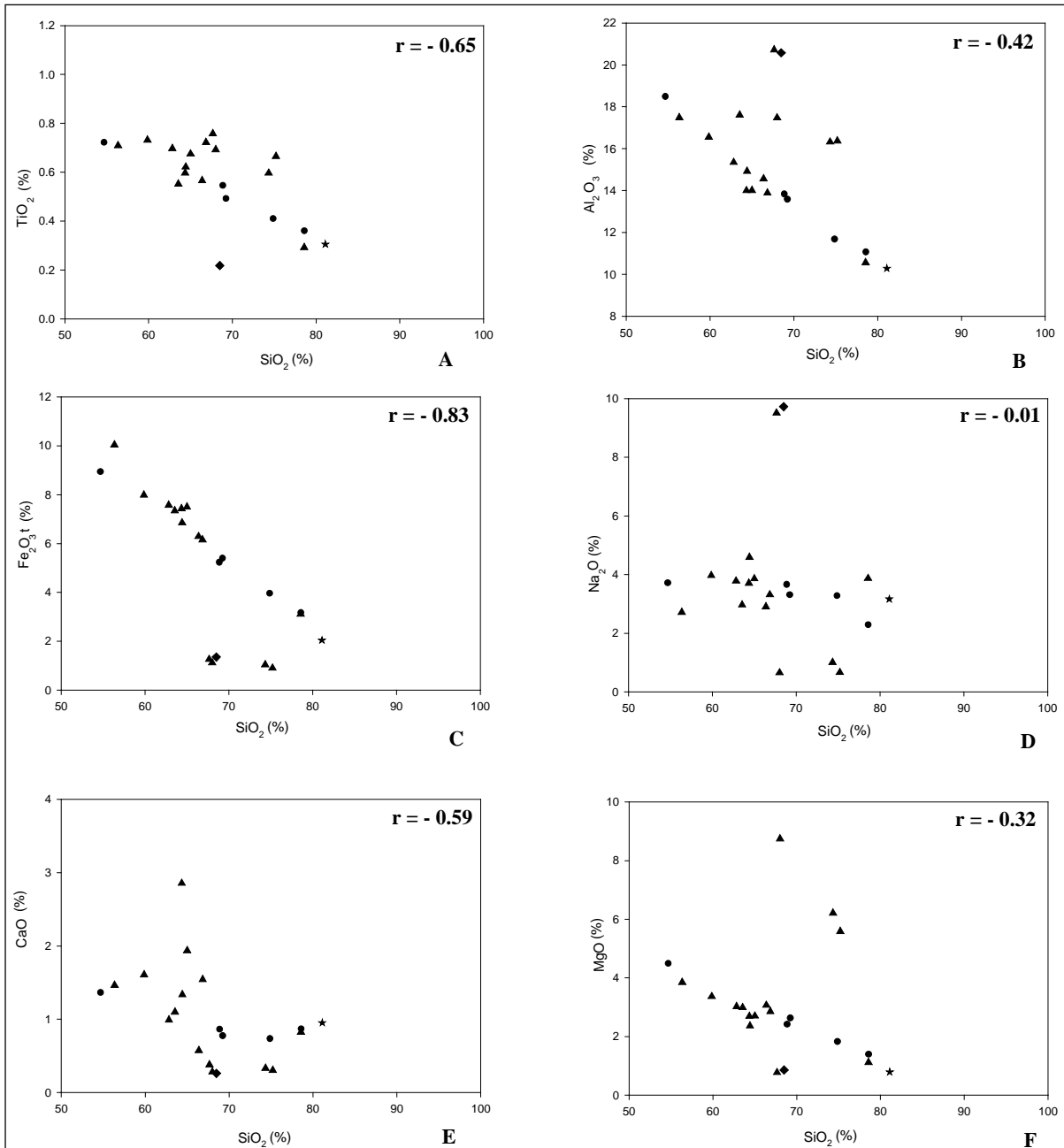
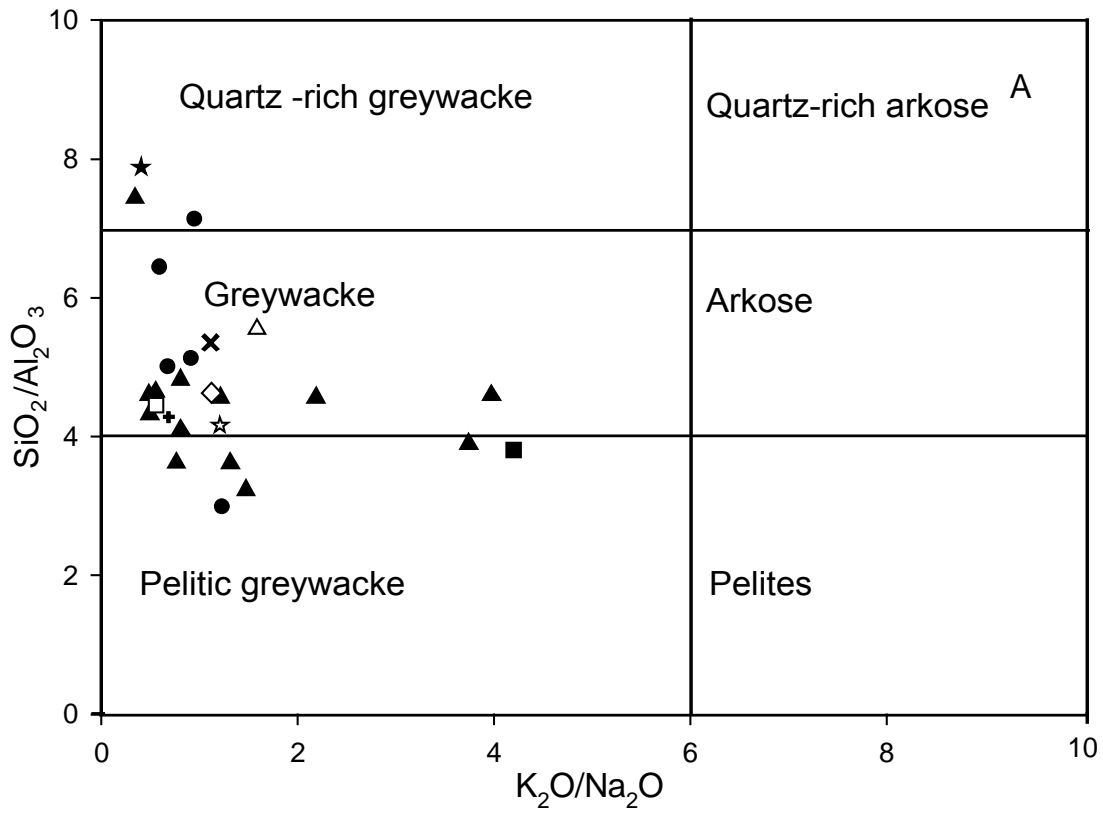


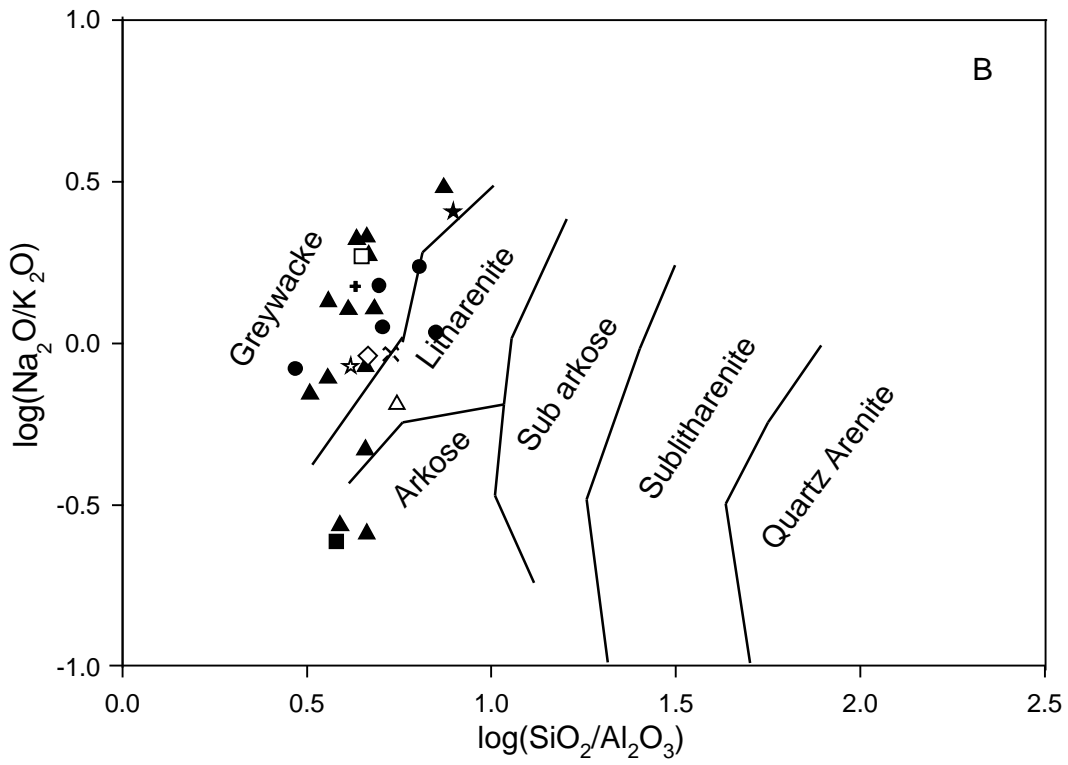
Fig. 5.1: Compositional variation trend of major oxides of metagreywacke.

Chondrite normalized REE patterns of 'argillite' (Fig. 5.3A) show light REE (LREE) enrichment with an $(La/Sm)_N$ ratio of 5.97 to 10.51 and relatively flat heavy REE (HREE) with an $(Gd/Yb)_N$ ratio of 1.64 to 2.65. A negative Eu anomaly is exhibited with $Eu/Eu^* = 0.54$ to 0.79 with an average of 0.74 . The samples of 'argillite' exhibit a strongly fractionated REE pattern with $(La/Yb)_N = 0.98$ to 36.68 with an average of 15.50 .

Similarly, the chondrite normalized REE patterns of 'metagreywacke' (Fig. 5.3B) show light REE (LREE) enrichment with an $(La/Sm)_N$ ratio of 7.01 to 8.45 and relatively flat heavy REE (HREE) with an $(Gd/Yb)_N$ ratio of 1.17 to 2.01 . A negative Eu anomaly is exhibited with $Eu/Eu^* = 0.69$ to 0.77 with an average of 0.73 . The samples of quartzo-feldspathic metagreywacke, metagreywacke with biotite and metagreywacke cataclasite also exhibit a strongly fractionated REE pattern with $(La/Yb)_N = 0.29$ to 36.72 with an average of 13.47 .

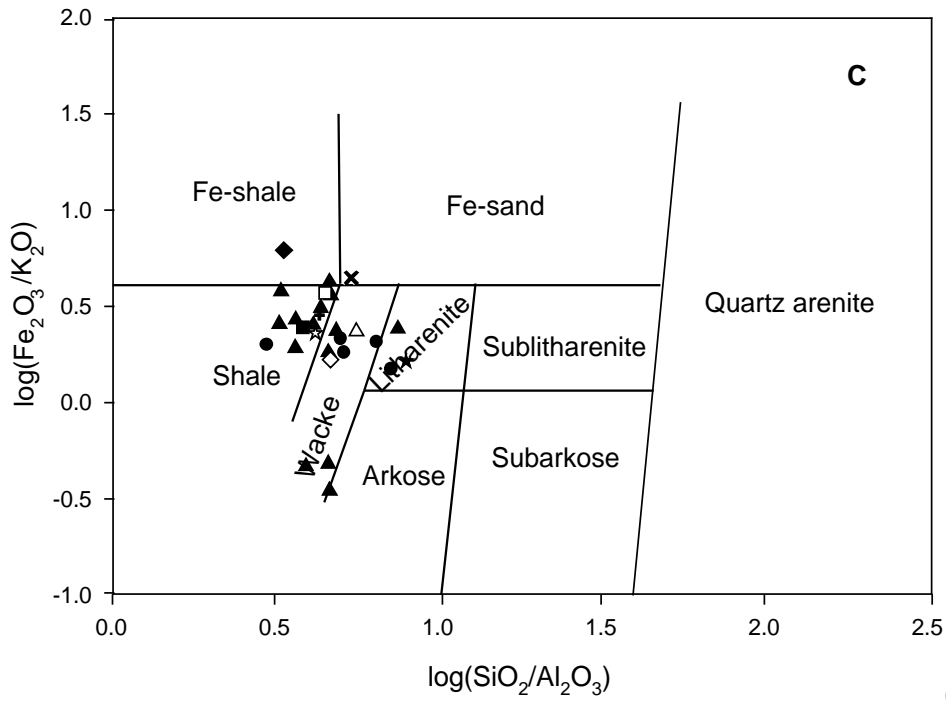


(after Wimmenauer, 1984)

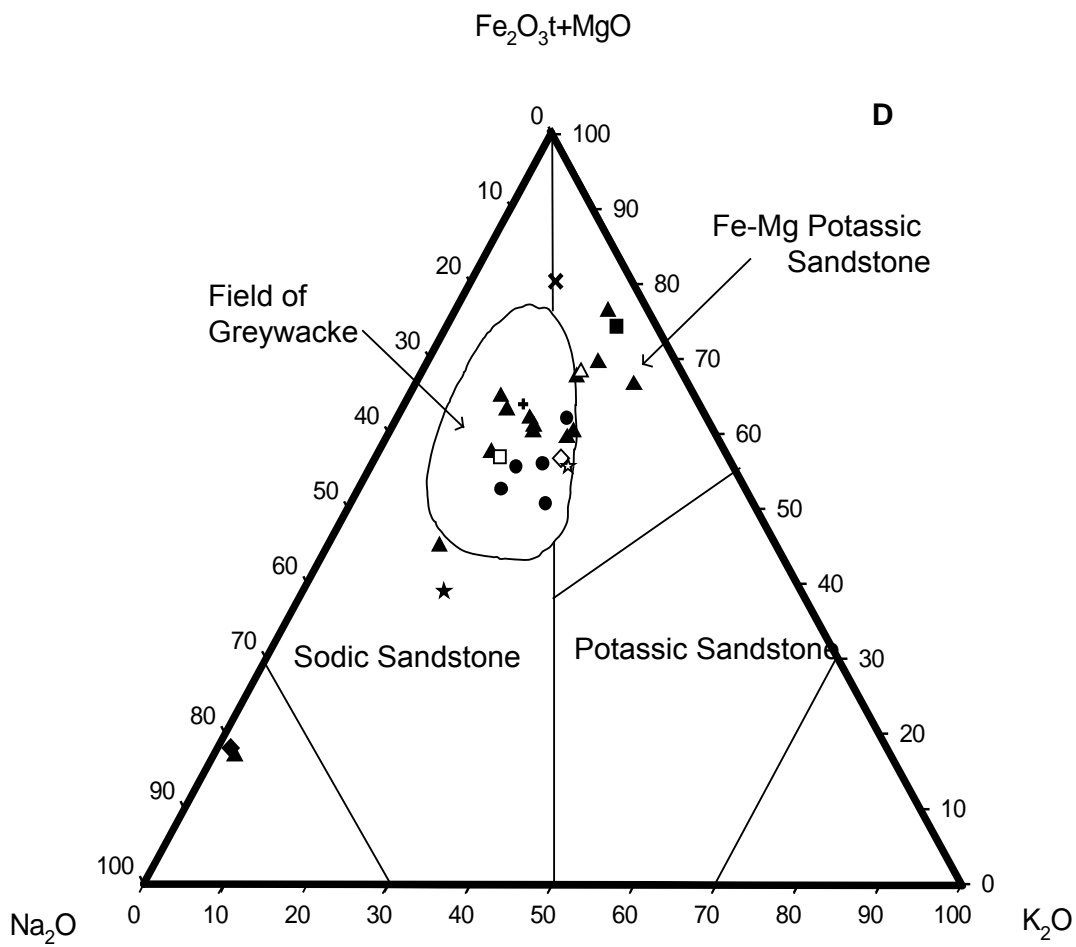


(after Pettijohn et al., 1972)

Contd..

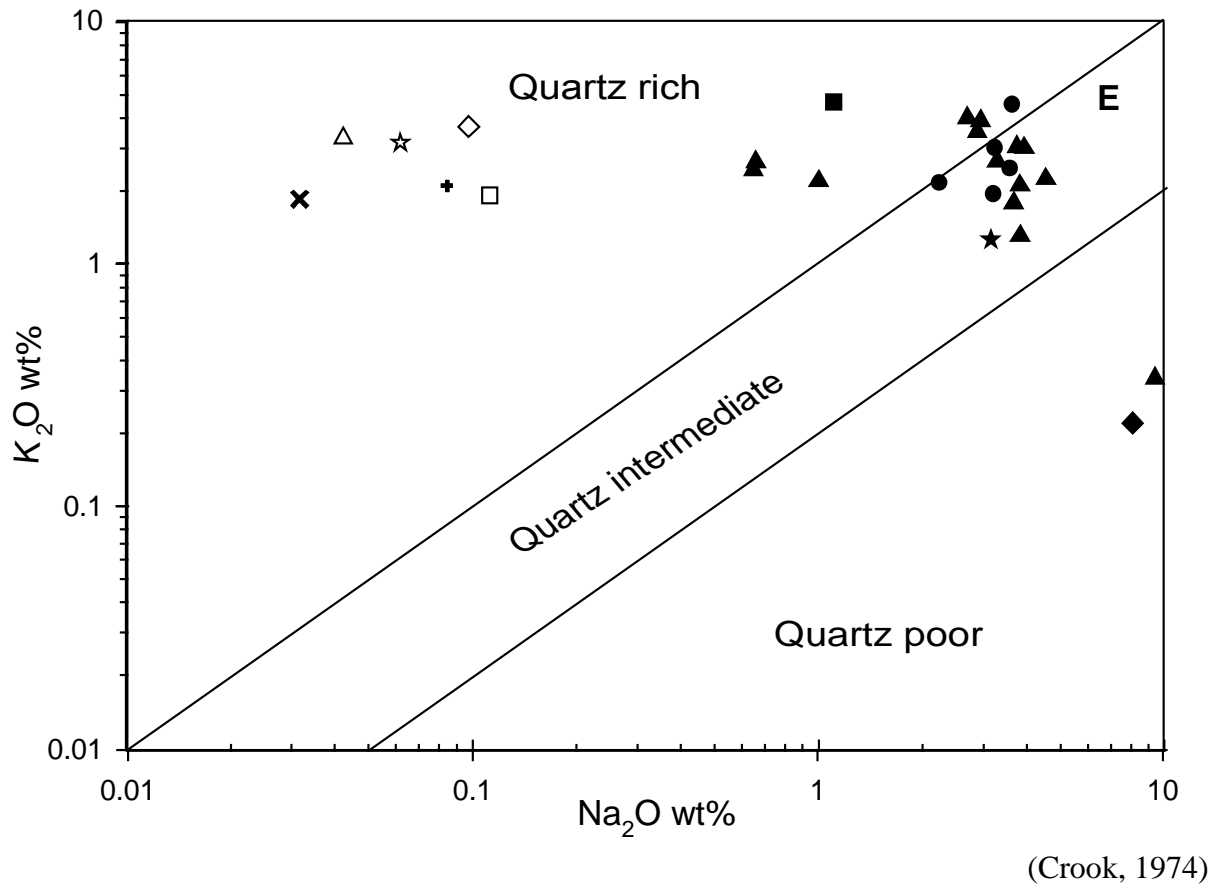


(after Herron, 1988)



(after Marston, 1978)

Contd..



- ▲ Argillite
- Metagreywacke
- ★ Quartzo-feldspathic metagreywacke
- Metagreywacke with biotite
- ◆ Metagreywacke cataclasite
- ◇ Greywacke from Merces quarry (Widdowson, 2009)
- △ Greywacke with biotite (Devaraju et al., 2010)
- Greywacke with chlorite-sericite (Devaraju et al., 2010)
- ☆ Fine grained greywacke (Devaraju et al., 2010)
- + Greywacke (Condie, 1993)
- × Greywacke of Fig Tree, Barberton (Toulkeridis et al., 1999)

Fig. 5.2: Plots for classification of metagreywacke.

- A) Binary plot of $\text{SiO}_2/\text{Al}_2\text{O}_3$ vs $\text{K}_2\text{O}/\text{Na}_2\text{O}$ (after Wimmenauer, 1984).
- B) Binary plot of $\log(\text{Na}_2\text{O}/\text{K}_2\text{O})$ against $\log(\text{SiO}_2/\text{Al}_2\text{O}_3)$ (after Pettijohn et al., 1972).
- C) Binary plot of $\log(\text{Fe}_2\text{O}_3/\text{K}_2\text{O})$ against $\log(\text{SiO}_2/\text{Al}_2\text{O}_3)$ (after Herron, 1988).
- D) Ternary diagram of $\text{Fe}_2\text{O}_3+\text{MgO}-\text{Na}_2\text{O}-\text{K}_2\text{O}$ (after Marston, 1978).
- E) Plot of K_2O vs Na_2O bivariate diagram of Crook (1974).

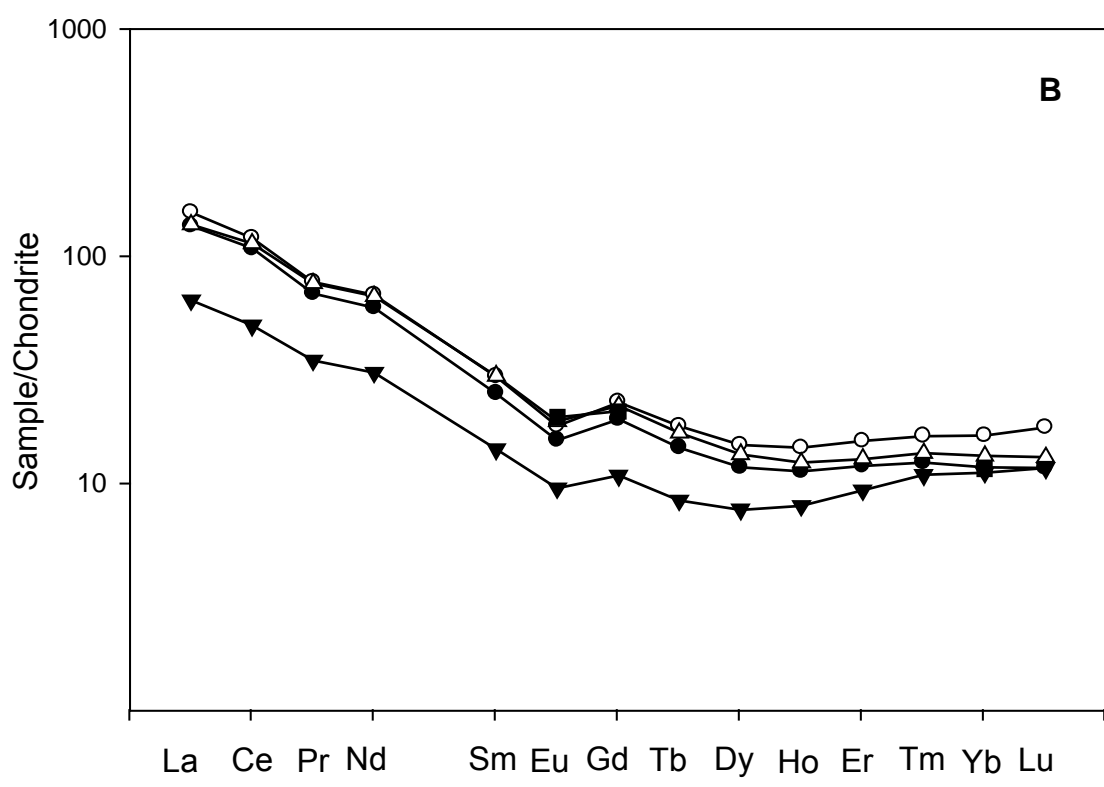
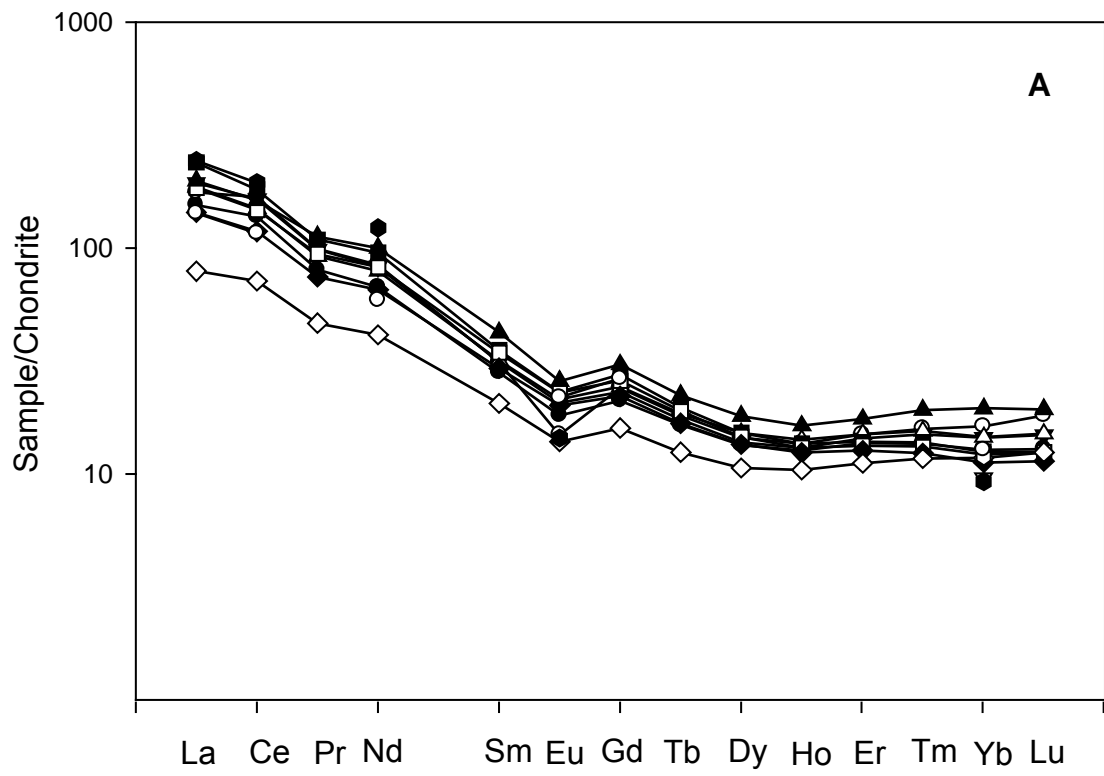
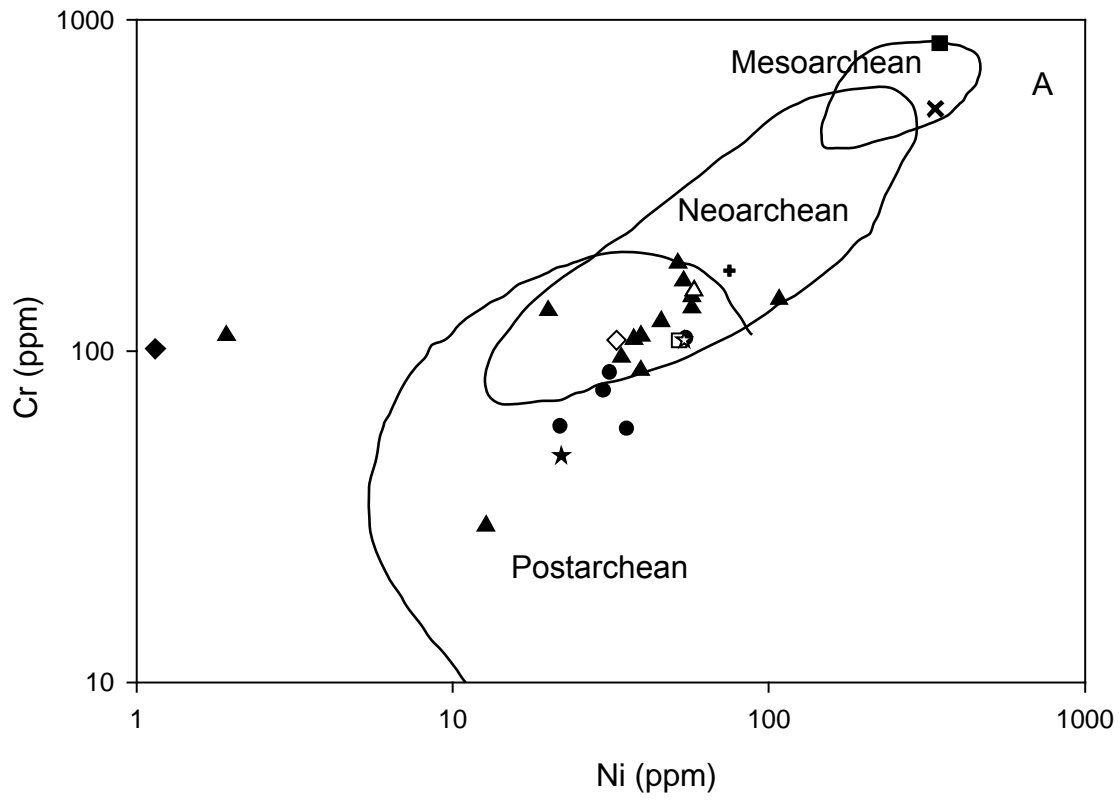
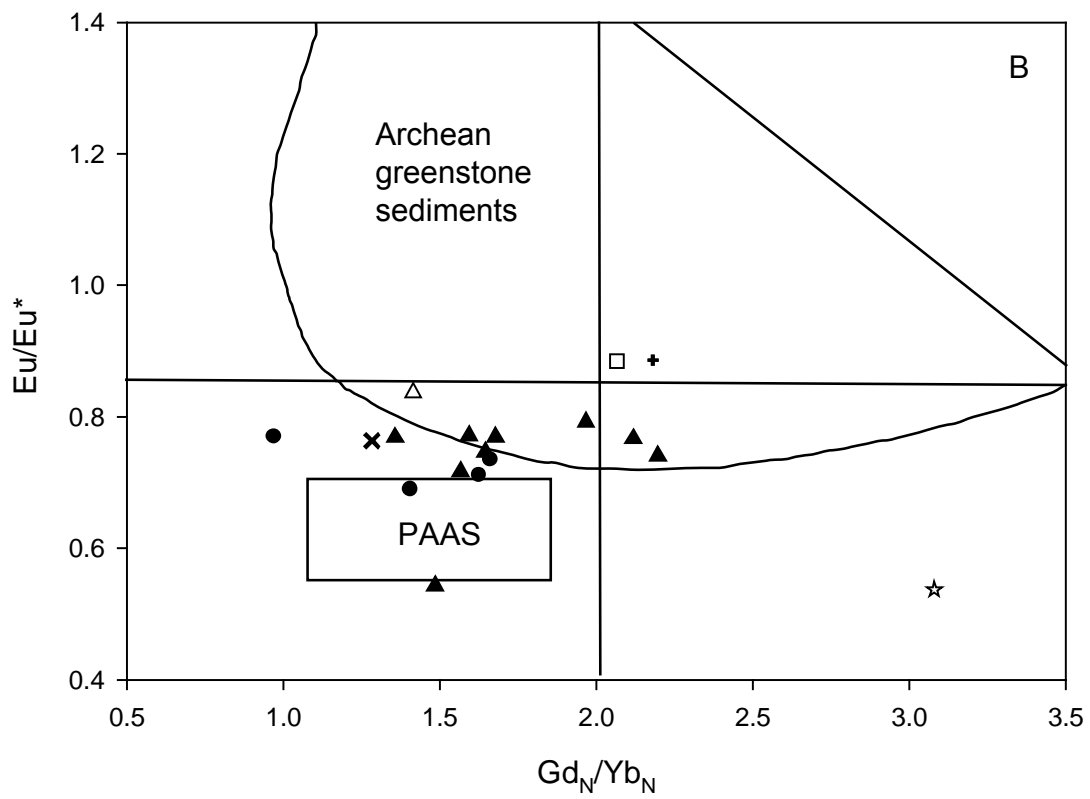


Fig. 5.3: A) Chondrite normalised rare earth element patterns showing the trend of argillite. B) Chondrite normalised rare earth element patterns showing the trend of metagreywacke.

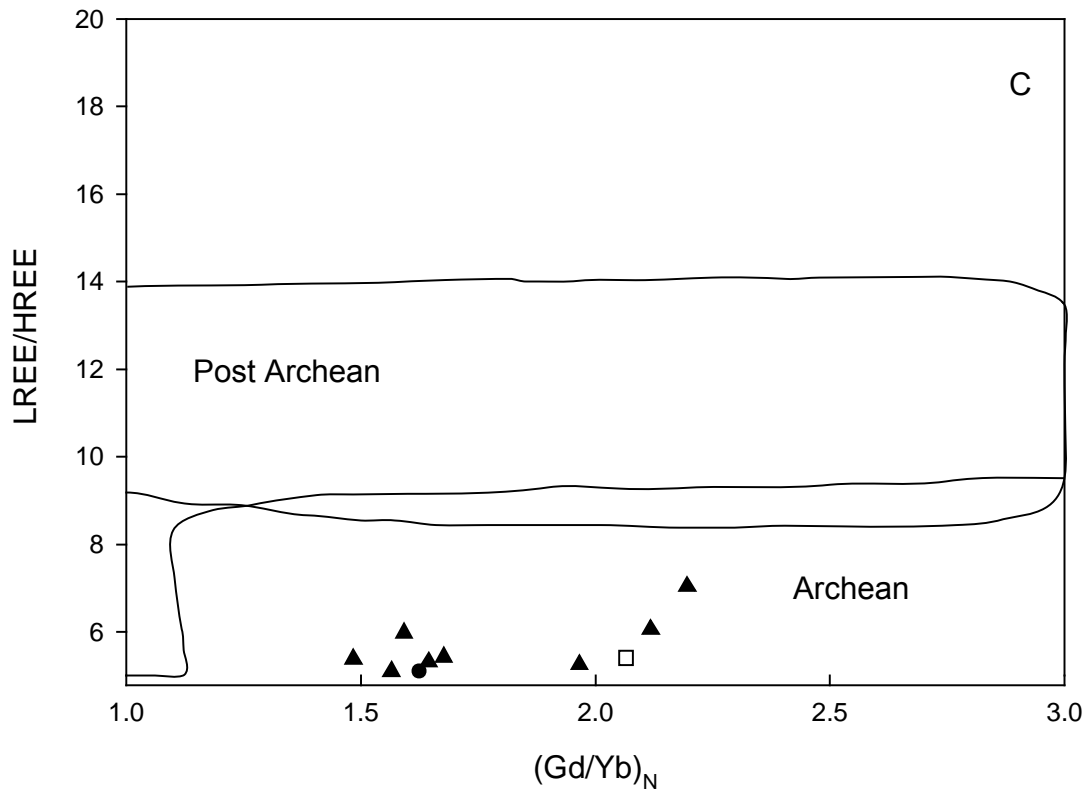


(after Condie, 1993)



(after Taylor and McLennan, 1985)

Contd..



(after Taylor and McLennan, 1985)

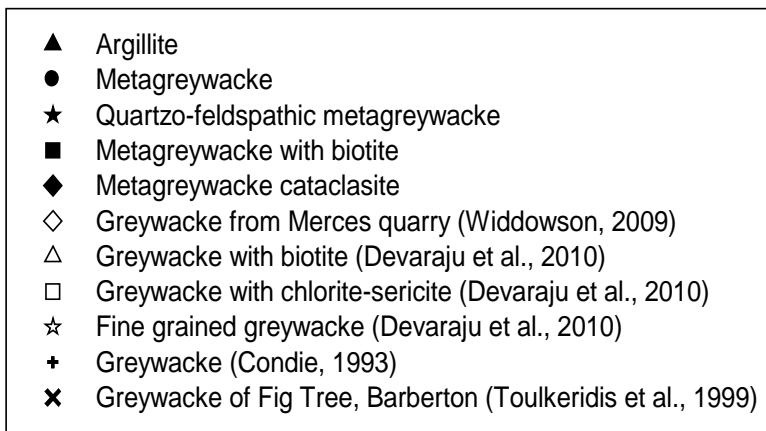


Fig. 5.4: A) Binary plot of Cr against Ni (after Condie, 1993).
 B) Plot of Eu/Eu^* against $(\text{Gd}/\text{Yb})_N$ ratio (after Taylor and McLennan, 1985).
 C) Binary plot of LREE/HREE against $(\text{Gd}/\text{Yb})_N$ (after Taylor and McLennan, 1985).

Sedimentary rocks have been used to constrain the average composition of the terrains exposed at the time of deposition. Studies have shown that the Archean upper crust is generally different from the post-Archean upper crust in chemical composition. The chemical difference between Archean and post-Archean upper crust have been recorded in REE of sedimentary rocks. The Archean greywackes are reported to be enriched in Mg, Cr, Co, Ni and Pd and they are depleted in Ti, K, P, Nb, Ba, Sr, Rb, Th, U and REE compared to the post-Archean greywackes (Taylor and McLennan, 1985; Condie, 1993; Asiedu et al., 2004).

Archean sedimentary rocks are observed to be inherently richer in Ni and Cr than those of post-Archean (Condie, 1993). In the binary diagram of Cr against Ni (after Condie, 1993), the samples of the study area plot in Neoproterozoic overlapping the post-Archean (Fig. 5.4A). Since it is difficult to derive the crustal abundances of sediments using Cr and Ni due to its complex behaviour during weathering, erosion and sedimentation, as such, relatively immobile elements such as REE and Th are commonly used (Taylor and McLennan, 1983). The Archean upper crust is differentiated from the post-Archean upper crust by the following (Asiedu et al., 2004): (1) a decrease in negative Eu-anomaly, (2) a decrease in $(Gd/Yb)_N$ ratio 2.0 to 1.0–2.0, (3) a decrease in Sm/Nd ratio from about 0.21 to 0.19 (4) a decrease in Cr/Th ratio about 20 to 5.7, (5) a decrease in Cr/Sc ratio 13 to 4.1, (6) an increase in Th/Sc ratio from about 0.5 to 1.0.

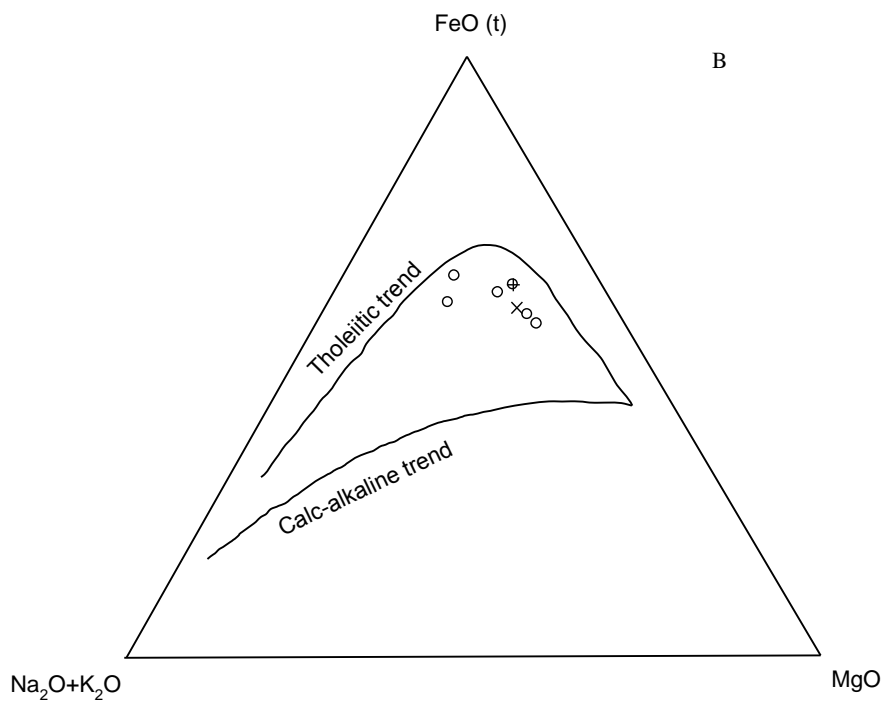
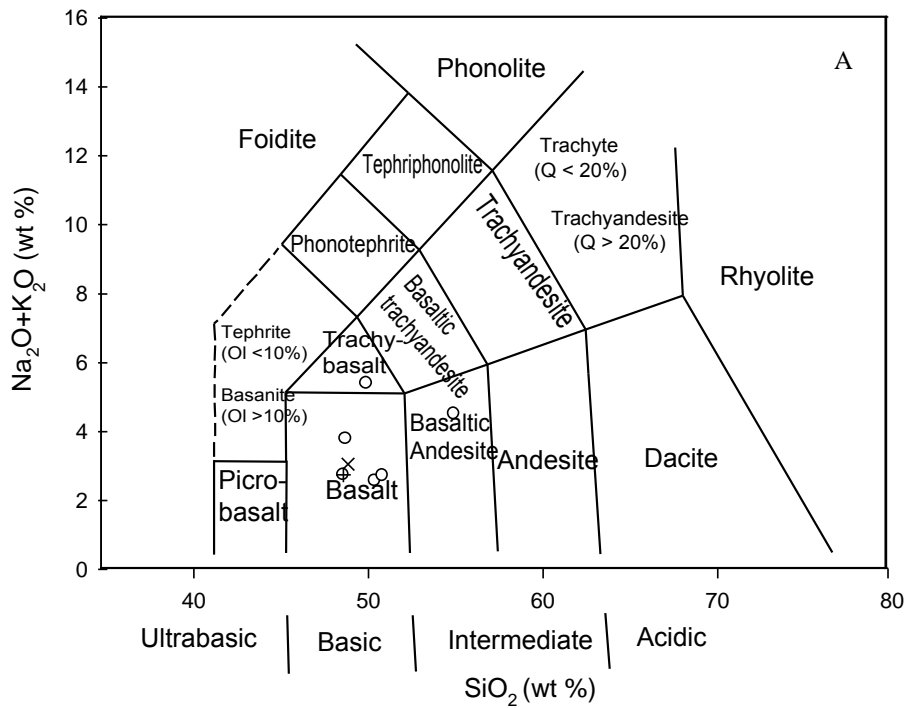
Since the ratios of ‘metagreywacke’ and ‘argillite’ are comparably similar, the values here are considered for the entire range of metagreywacke petrofacies of the study area. The analyzed metagreywacke petrofacies samples of the study area shows typical Archean signatures with negative Eu-anomaly of avg ~ 0.73 ; a decrease in $(Gd/Yb)_N$ ratio from 2.65 to 1.17; a decrease in Sm/Nd ratio from 0.16 to 0.12 ; a decrease in Cr/Th ratio about 24 to 4.3; a decrease in Cr/Sc ratio from about 12 to 5; an increase in Th/Sc ratio from about 0.3 to 1.3. In addition, the plot of Eu/Eu^* against $(Gd/Yb)_N$ ratio (after Taylor and McLennan, 1985), a

majority of the samples attest to the Archean greenstone sediments (Fig 5.4B). Also, in terms of the plot of LREE/HREE against $(Gd/Yb)_N$ plot (after Taylor and McLennan, 1985), the metagreywacke samples of the study area plot in Archean field (Fig 5.4C).

5.2 Associated rocks

Geochemistry of dykes of dolerite associated with the metagreywacke is studied for its major and trace elements. Various geochemical signatures were used to understand the evolution of magma. In order to have a better understanding of the geochemistry of dolerite dykes from the study area, the data was compared with those of: 1) dolerite Deccan-type feeder dyke, Goa (Widdowson et al., 2000) and 2) Desur Lavas, Deccan Traps (Belgaum district, Karnataka) (Hegde et al., 2014).

The major and trace element analyses are presented in table 5.6. The major element composition is as follows: SiO_2 ~ 49 - 55%, Al_2O_3 ~ 12 - 14%, K_2O ~ 0.38 - 2.18%, TiO_2 ~ 1 - 2%, Fe_2O_3t ~ 12 - 17%, MgO ~ 3 - 6%, MnO ~ 0.17 - 0.27%, Na_2O ~ 2 - 3%. The analysed samples of the dyke range in composition from basalt to basaltic andesite as plotted in the total alkalis (Na_2O+K_2O) vs silica diagram (Fig. 5.5A) and in the AFM (A= Na_2O+K_2O ; F= FeO; M= MgO) diagram (Fig. 5.5B), the samples follow the tholeiitic trend. Dolerites with <10 wt% MgO are classified as tholeiitic basalts, while with >10 wt% MgO are classified as picrite basalts (Dessai et al., 2008). The analysed samples of dolerite of the study area are tholeiitic basalts as the MgO content range from 3.45 to 6.42.



- Dolerite of the study area
- × Goa dykes (Widdowson et al., 2000)
- ⊕ Dessur lava (Hegde et. al., 2014)

Fig. 5.5:
 A) Total alkalis versus silica diagram (after Le Maitre et al., 1989) of dolerite samples.
 B) Ternary diagram of AFM (A= Na₂O+K₂O ; F= FeOt ; M= MgO).

The analysed dolerites samples of the study area are plotted on variation diagrams, with MgO plotted at the X-axis and various oxides/elements (TiO_2 , FeOt, Ni (ppm) and Al_2O_3) plotted at the Y-axis (Fig. 5.6). This variation diagram is widely used for basaltic rocks to understand the differentiation of magma. MgO exhibits negative correlation trend with TiO_2 and FeOt indicating decrease in TiO_2 and FeOt as basalts differentiate. The plot of MgO against Ni and Al_2O_3 shows positive correlation indicating enrichment in Ni and Al_2O_3 during magma differentiation. With reference to TiO_2 against MgO diagram (Fig. 5.6A) the sample of dolerite dyke from Arambol and Sada headland have plotted in the Poladpur Formation, while one plots in Bushe and the other two outside the field area. This data is comparable with the reference data of Goa dyke (Widdowson et al., 2000) and Desur Lava (Hegde et al., 2014), wherein it lies within the range on the samples of the study area.

Table 5.6: Major (wt %), minor, trace and rare earth elements (ppm) of dolerite dykes of the study area (Sr. no. 1 to 5) and related reported dolerite from Merces, Goa (Widdowson et al., 2000) (Sr. no. 6) and Desur Lava, Karnataka (Hegde et al., 2014) (Sr. no. 7). The numbers within the brackets indicate the sample number. (nd= not determined; na= not available).

| Sr.no. | 1 | 2 | 3 | 4 | 5 | 6 | 7 |
|--------------------------------|------------------|-----------------|--------------|-----------------|--------------|-------------|----------------|
| Sample no. | Ribandar (04) | Chimbel (14) | Baga (29) | Arambol (20) | Sada (33) | Goa Dyke | Dessur Lava |
| SiO ₂ | 49.02 | 50.20 | 55.21 | 50.68 | 51.12 | 49.26 | 49.01 |
| Al ₂ O ₃ | 12.23 | 12.98 | 12.91 | 14.47 | 14.47 | 13.90 | 13.45 |
| TiO ₂ | 1.37 | 2.95 | 1.89 | 1.70 | 1.78 | 2.32 | 3.75 |
| Fe ₂ O ₃ | 17.00 | 15.49 | 16.05 | 12.98 | 13.53 | 14.51 | 15.65 |
| FeO | 14.78 | 13.47 | 13.96 | 11.29 | 11.76 | 12.62 | 13.61 |
| MnO | 0.27 | 0.17 | 0.20 | 0.19 | 0.19 | 0.20 | 0.25 |
| MgO | 5.70 | 3.87 | 3.45 | 6.42 | 6.07 | 5.93 | 5.46 |
| CaO | 8.12 | 5.89 | 7.24 | 11.54 | 11.16 | 10.40 | 10.13 |
| Na ₂ O | 2.88 | 3.18 | 2.96 | 2.15 | 2.19 | 2.56 | 2.47 |
| K ₂ O | 0.88 | 2.18 | 1.52 | 0.38 | 0.50 | 0.47 | 0.30 |
| P ₂ O ₅ | 0.20 | 0.86 | 0.21 | 0.14 | 0.15 | 0.26 | 0.47 |
| Sum | 97.66 | 97.77 | 101.63 | 100.66 | 101.17 | 99.81 | 114.55 |
| Li | 18.70 | 25.09 | nd | nd | nd | na | na |
| Be | 4.42 | 8.61 | nd | nd | nd | na | na |
| Sc | 37.97 | 31.41 | nd | nd | nd | 31.40 | 34.00 |
| Ti | 8240 | 18330 | nd | nd | nd | na | na |
| V | nd | nd | 267.82 | 327.73 | 316.79 | na | 464 |
| Cr | 88.76 | 25.07 | 34.53 | 173.18 | 176.77 | 106 | na |
| Co | 78.35 | 52.57 | 46.05 | 44.02 | 43.86 | 59.57 | 48 |
| Ni | 84.13 | 52.68 | 38.20 | 90.80 | 88.52 | 71.29 | 62 |
| Cu | 49.98 | 41.01 | 215.43 | 176.04 | 169.61 | 186.71 | 330 |
| Zn | 93.56 | 112.10 | nd | nd | nd | 106.14 | 123.00 |
| Ga | 30.51 | 46.19 | nd | nd | nd | 23.10 | na |
| Rb | 31.39 | 78.19 | nd | nd | nd | 12.86 | 7.10 |
| Sr | 257 | 428.20 | 247.25 | 154.47 | 185.39 | 225 | 222 |
| Y | 31.47 | 67.94 | nd | nd | nd | 36.14 | 43.40 |
| Zr | 117.10 | 200.50 | 174.69 | 111.09 | 109.86 | 146 | 219 |
| Nb | 8.54 | 28.77 | nd | nd | nd | 11.43 | 23.40 |
| Sn | 1.37 | 2.63 | nd | nd | nd | na | na |
| Sb | 0.10 | 0.38 | 0.24 | 0.20 | 0.04 | na | na |
| Cs | 0.62 | 5.69 | nd | nd | nd | 0.27 | na |
| Ba | 436.60 | 768.80 | 383.31 | 98.29 | 134.76 | 133.43 | 222.00 |
| Pb | 3.19 | 5.15 | nd | nd | nd | 2.40 | na |
| Th | 2.67 | 2.41 | nd | nd | nd | 1.14 | 2 |
| U | 1.27 | 0.91 | nd | nd | nd | 0.35 | na |
| La | 13.52 | 50.50 | 25.05 | 8.83 | 11.16 | 8.96 | 18.50 |
| Ce | 33.46 | 115.50 | 52.75 | 20.40 | 25.20 | 22.77 | 44.30 |
| Pr | 4.02 | 14.40 | nd | nd | nd | 2.95 | 6.40 |
| Nd | 17.47 | 70.92 | 29.94 | 14.49 | 15.91 | 15.11 | 28.10 |
| Sm | 3.97 | 12.36 | nd | nd | nd | 3.90 | 7.26 |
| Eu | 1.19 | 3.40 | 2.04 | 1.35 | 1.38 | 1.28 | 2.32 |
| Gd | 4.76 | 13.86 | 7.94 | 5.17 | 5.02 | 4.13 | 7.87 |
| Tb | 0.81 | 1.96 | nd | nd | nd | 0.71 | 1.26 |
| Dy | 4.89 | 10.63 | nd | nd | nd | 4.27 | 7.49 |
| Ho | 1.06 | 2.15 | nd | nd | nd | 0.85 | 1.48 |
| Er | 3.23 | 6.04 | nd | nd | nd | 2.29 | na |
| Tm | 0.50 | 0.86 | nd | nd | nd | 0.35 | 0.57 |
| Yb | 3.10 | 5.12 | 3.01 | 2.84 | 2.81 | 2 | 3.60 |
| Lu | 0.48 | 0.75 | nd | nd | nd | 0.34 | 0.55 |
| Mg# | 40.72 | 33.87 | 30.58 | 50.36 | 47.93 | 45.59 | 41.69 |
| Ti/Zr | 70.37 | 91.42 | nd | nd | nd | | |
| La/Sc | 0.36 | 1.61 | nd | nd | nd | | |
| Zr/10 | 11.71 | 20.05 | nd | nd | nd | | |
| Ba/Zr | 3.73 | 3.83 | 2.19 | 0.88 | 1.23 | | |

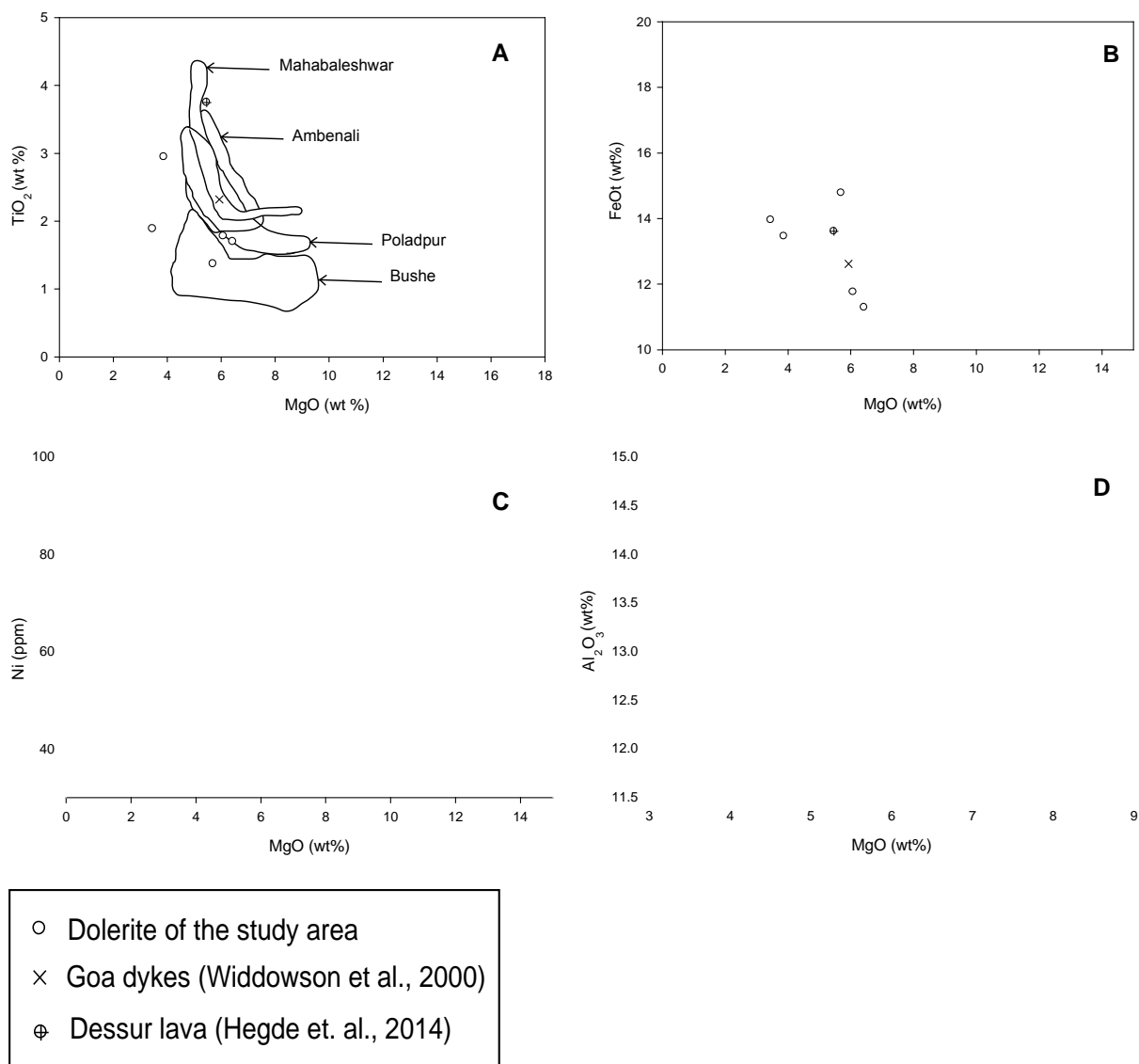


Fig. 5.6: Variation diagrams (A, B, C and D) of dolerite with MgO against oxides such as TiO₂, FeOt, Ni and Al₂O₃.

The Mg number (Mg#) value is calculated as $Mg\# = [Mg^{2+}/(Mg^{2+} + Fe^{2+})]*100$. The rocks with high Mg# (>57) values were derived by higher amounts of magma melting or may represent high temperature magmas, hence, may tend to have high Ni (>100 ppm) values than those with lower Mg# (<57) values and lower Ni (< 100 ppm) values (Lightfoot et al., 1993; Xu et al., 2001). It is also observed that more primitive rocks with high Mg# and Ni, tend to be of more contaminated magmas (Cox and Clifford, 1982; Mahoney et al., 1982; Mahoney, 1988).

The Mg# values of the analyzed dolerite samples range from 30.58 to 50.36 (avg 40.69) as shown in the variation diagram (Fig. 5.7) of Mg# against SiO₂, FeO, Al₂O₃ and TiO₂. The plot of Mg# against Al₂O₃ and SiO₂ exhibits a positive correlation and in the plot of Mg# against FeO exhibit a negative correlation. While, the plot of Mg# against TiO₂ exhibits a scatter plot. The lower Ni values (~avg 70.87) indicates lower temperature magmas and its less evolved and less contaminated nature. The positive correlation between Mg# and SiO₂ of the samples clearly indicate the Si-rich nature of the rocks (cf. Dessai et al., 2008) (Fig 5.7A). The Mg# of Arambol, Sada and Ribandar has a close affinity to the dykes of Goa (Widdowson et al., 2000) and Desur Lava (Hegde et al., 2014) (Table 5.6).

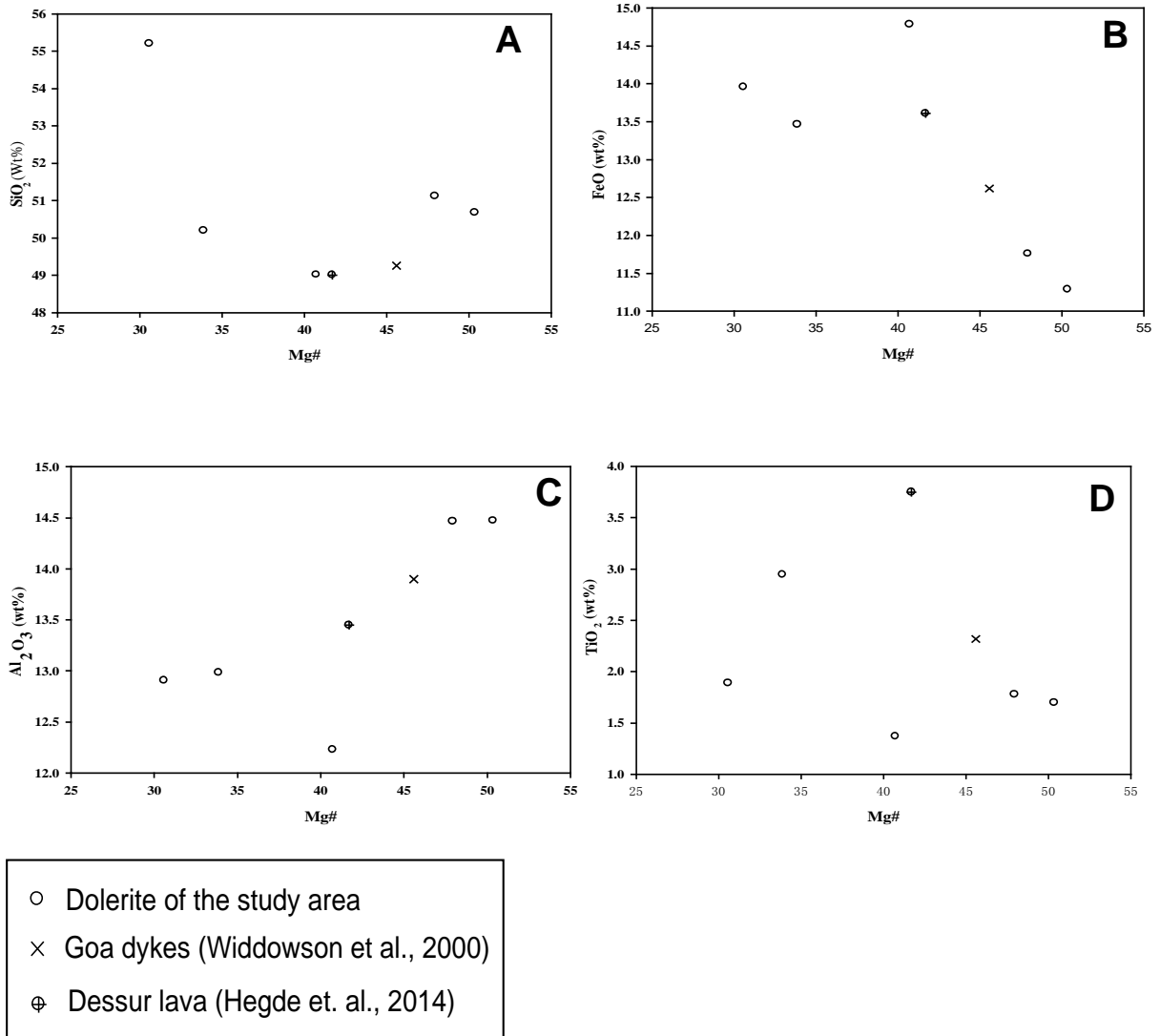


Fig. 5.7: Variation diagrams of dolerite plotted with Mg# against oxides such as SiO₂, FeO, Al₂O₃ and TiO₂.

The abundance of trace elements of the dolerite dyke of the study area are variable with Zr from 109 to 200 ppm, Sr shows a large range from 154-428 ppm while the compatible elements such as Ni ranges between 38 and 90 ppm and Cr from 25 to 176 ppm. However, the Cr value of dyke from Arambol and Sada are in close range (173 to 176 ppm respectively) and dykes from Chimbhel and Baga are in close range (25 to 34 ppm respectively). While the value of dyke from Ribandar is intermediate (88 ppm). The incompatible high field strength elements (HFSE) such as Ti, Zr are primarily used as discriminants between magma types and are immobile during low-temperature alteration processes (Peate, 1997; Riley et al., 2005) and are not largely modified by moderate amount of fractional crystallization or susceptible to variable degree of partial melting (Luttinen and Furnes, 2000; Riley et al., 2005). Zr is an effective index of differentiation in magmas that do not crystallize zircon (Riley et al., 2005). Based on TiO_2 vs Zr plot (Fig. 5.8A), a low Ti-Zr group is identified. Using the chemostratigraphic classification of upper stratigraphic horizon ie. Wai Sub-Group of Deccan (Devey and Lightfoot, 1986; Jay and Widdowson, 2008; Rao, et al., 2011), the data is plotted on Sr vs Ba discriminate diagram (Fig. 5.8B). In the diagram, the sample of dolerite dyke from Arambol and Sada headland plot in the Poladpur Formation field along with the average of the Goa dykes of Widdowson et al. (2000).

The large ion lithophile elements (LILE) such as Cr, Ni, Sr, Co, V and La are incompatible in gabbroic assemblage and hence are plotted against Zr (Fig. 5.9). La shows positive correlations with Zr while Cr, Ni, Sr and Co shows a negative correlation. The higher Sr contents 154-428 ppm indicates mafic granulites accompanied with high MgO content reflecting accumulation of Sr-rich calcic-plagioclase (cf. Dessai et al., 2008).

The plot of $\text{CaO}/\text{Al}_2\text{O}_3$ against Mg# indicates plagioclase fractionation (Fig 5.10A). Further, in the Ce against Nd diagram, the samples plot along melting path between 1% to 5% of primitive mantle (Fig. 5.10B). The chondrite normalized REE pattern of the dolerite sample (Fig. 5.11) shows LREE enrichment, HREE depletion along with a weak negative Eu anomaly.

The tectono-magmatic ternary discrimination diagram of $\text{MgO}-\text{Al}_2\text{O}_3-\text{FeO}t$ (Pearce et al., 1977) (Fig. 5.12) indicates that the dolerites are correlated to the continental basalts and to a lesser extent to ocean island basalt suggesting a continental tectonic setting.

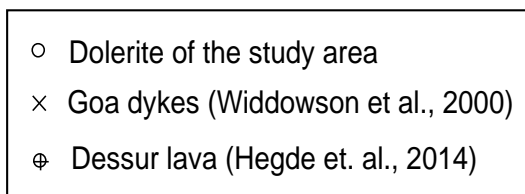
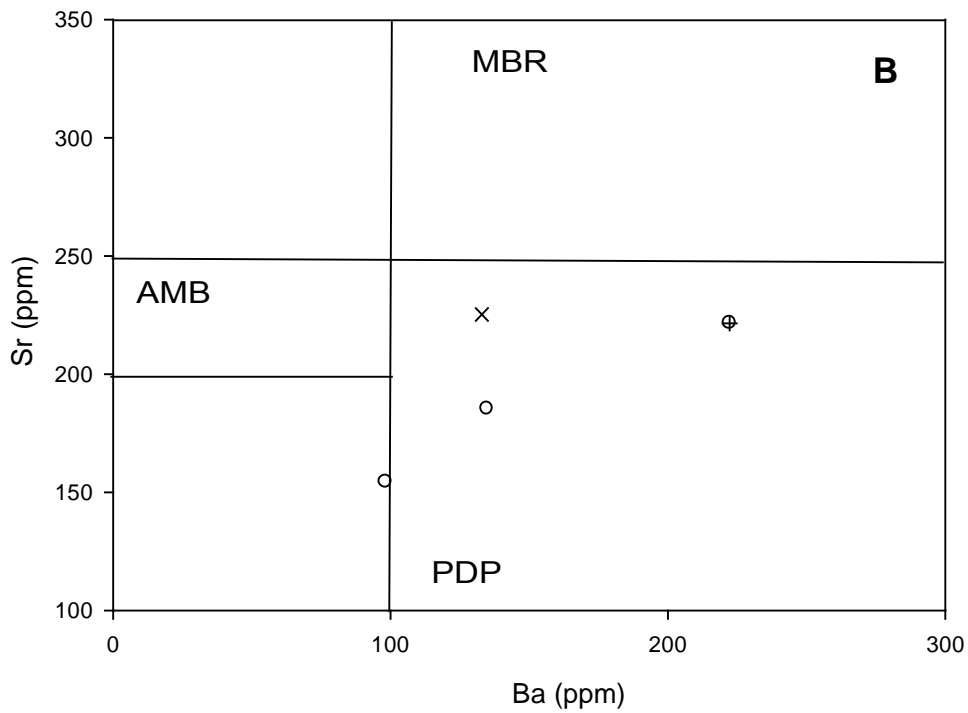
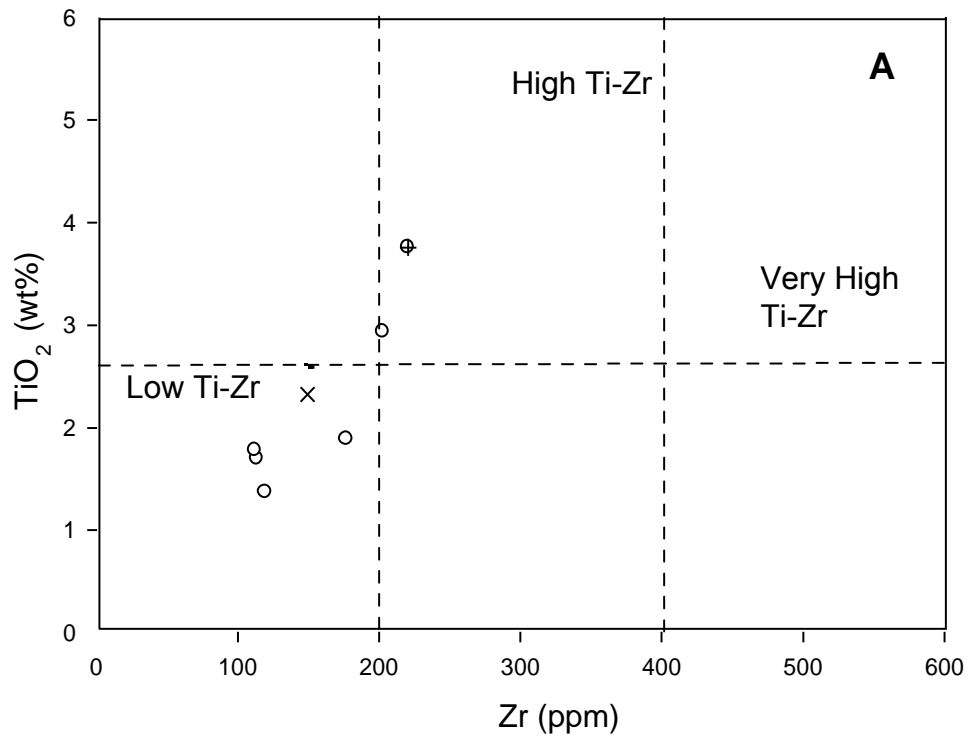


Fig. 5.8: Geochemical plots of dolerite:
 A) Binary plot of TiO₂ vs Zr plot.
 B) Binary plot of Sr vs Ba discriminate diagram (MBR- Mahabaleshwar Formation; AMB- Ambenali Formation; PDP- Poladpur Formation).

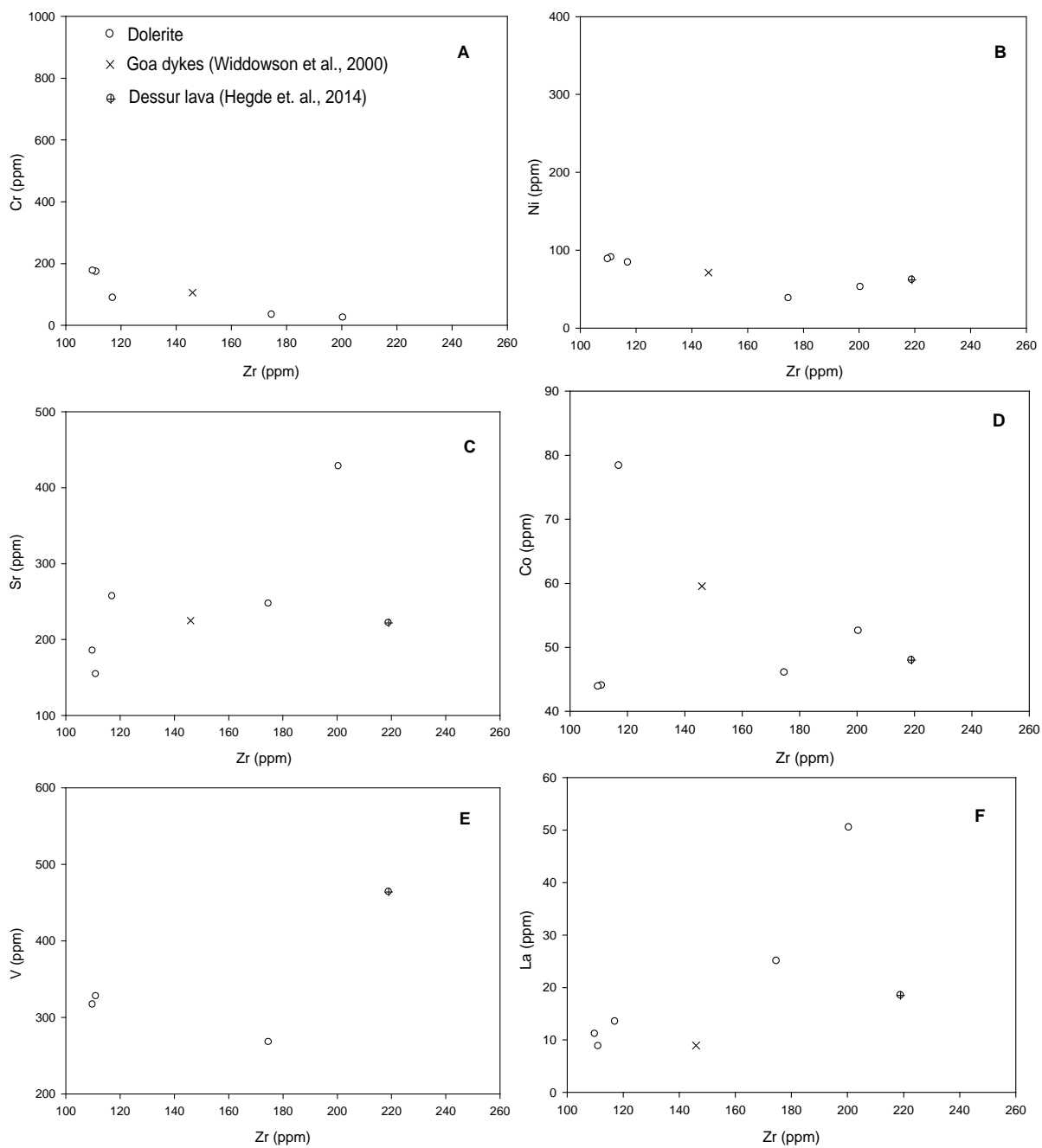
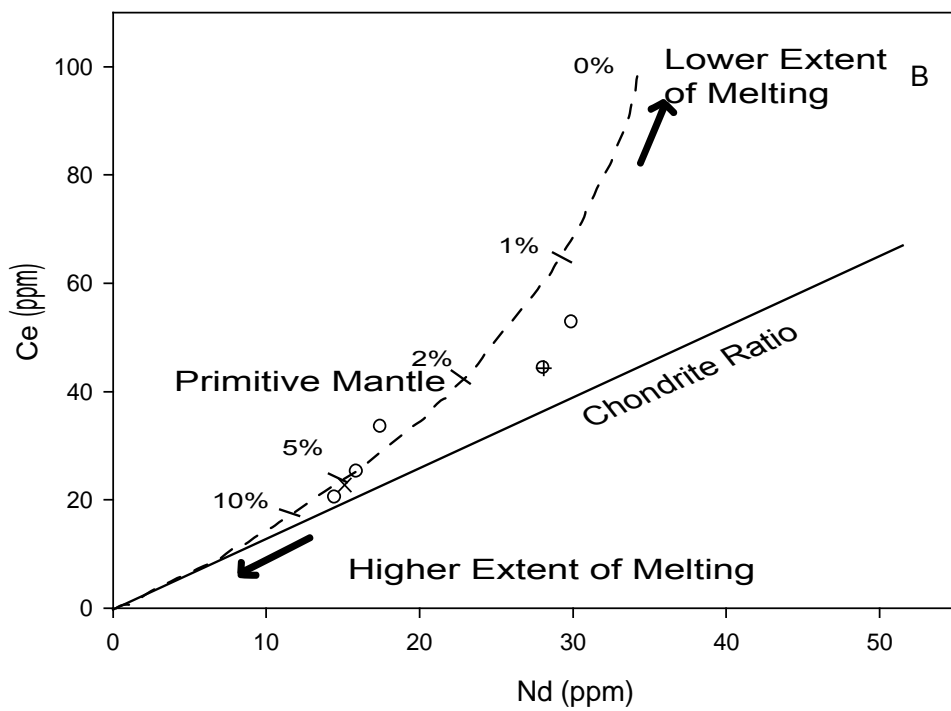
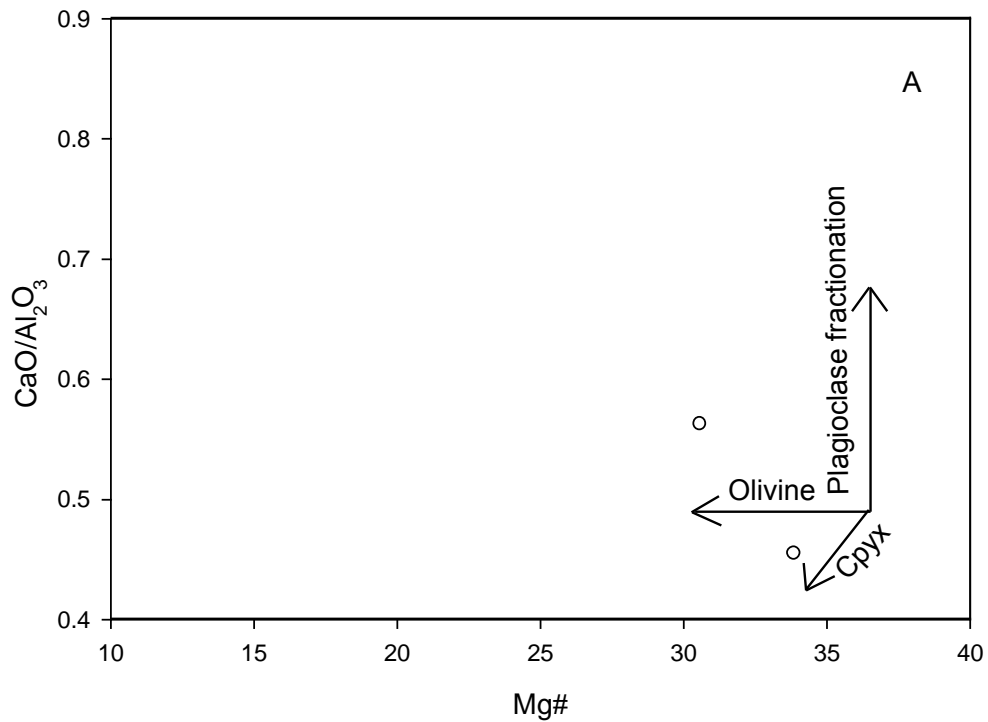


Fig. 5.9: Variation diagram of dolerite. The large ion lithophile elements (LILE) such as Cr, Ni, Sr, Co, V and La are plotted against Zr (ppm).



- Dolerite of the study area
- × Goa dykes (Widdowson et al., 2000)
- ⊕ Dessur lava (Hegde et. al., 2014)

Fig. 5.10: A) Plot of CaO/ Al₂O₃ against Mg# for dolerite samples.
 B) Binary plot of Ce against Nd for dolerite samples.

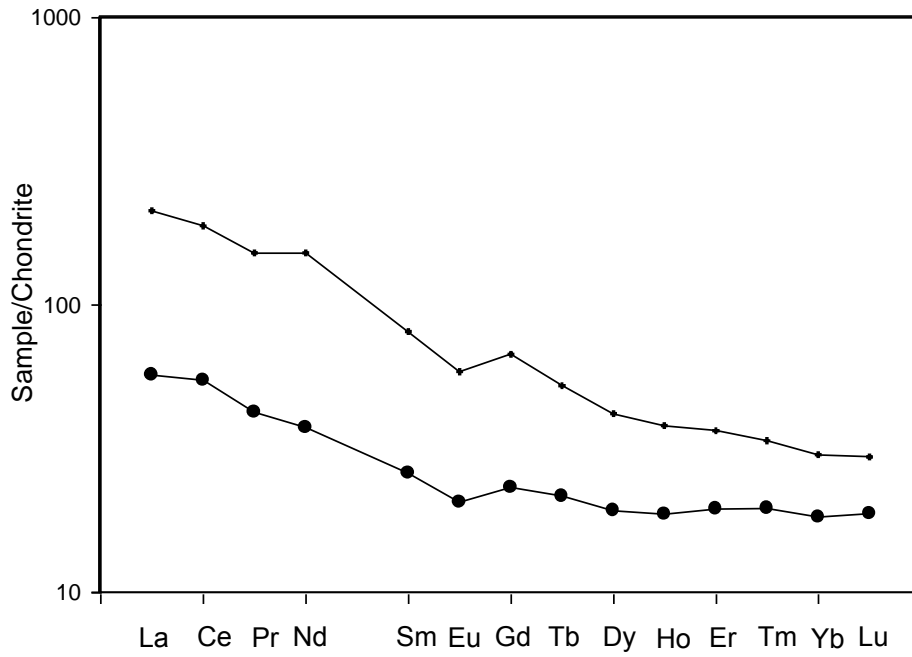


Fig. 5.11: Chondrite normalized rare earth element patterns showing the trend of dolerite.

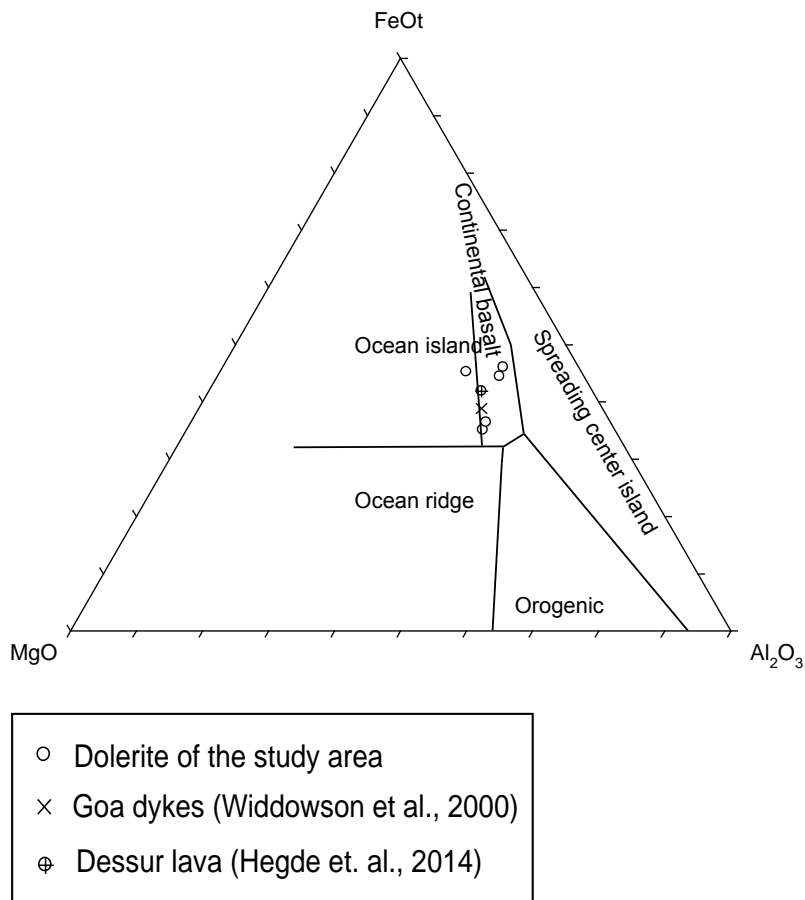


Fig. 5.12: Tectono-magmatic ternary discrimination diagram of MgO-Al₂O₃-FeOt (Pearce et al., 1977).

5.3 Summary

In this chapter whole rock geochemistry of metagreywacke and associated rocks (dolerite dykes) is presented using the major, trace and RE elements.

The metagreywacke of Sanvordem Formation is compared with the average data of the following: 1) greywacke from Merces, Goa (Widdowson, 2009); 2) greywacke with biotite of Goa-Dharwar sector (Devaraju et al., 2010); 3) greywacke with chlorite-sericite of Goa-Dharwar sector (Devaraju et al., 2010); 4) fine-grained greywacke of Goa-Dharwar sector (Devaraju et al., 2010); 5) Late Archaean (3.5-2.5 Ga) greywacke (Condie, 1993); 6) Archaean greywacke of Fig Tree, Barberton (South Africa) (Toulkeridis et al., 1999). The metagreywacke samples of the study area are comparable in geochemical composition to the greywackes as mentioned above.

The metagreywacke samples of the study area are plotted on various sandstone classification diagrams using major oxides, the majority plots indicates greywacke composition. Using silica variation diagram a poor mineralogical maturity was observed. Various geochemical signatures were used to understand the behaviour of minerals. The analyses of the trace and REE constrain the average composition of the terrains exposed at the time of deposition of the rocks to be that of Archean.

Further, in this chapter the geochemistry of the associated dolerite dykes of Goa are compared to those of: 1) dolerite Deccan-type feeder dyke, Goa (Widdowson et al., 2000) and 2) Desur Lavas, Deccan Traps (Belgaum district, Karnataka) (Hegde et al., 2014). It is studied that a few dykes of the study area have a close affinity to the dykes of Goa (Widdowson et al., 2000) and Desur Lava (Hegde et al., 2014), representing its relation to Deccan volcanism while others are of older generation.

The dolerites exhibit a tholeiitic trend in the AFM diagram. Major oxides along with Mg# are studied using various binary plots to understand the geochemical nature of rocks, suggesting lower temperature and less evolved nature of the magma. Tectono-magmatic ternary discrimination diagram suggests the dolerites have affinity to continental basalts and to a lesser extent to ocean island basalt.

Chapter 6

DATA INTERPRETATION AND DISCUSSION

This chapter deals with the interpretation and discussion and is divided into two sections: Metagreywacke and Associated rocks. The metagreywacke section discusses the structural data, petrographic observations and geochemical analyses. Here, the mechanism of formation of the various structures is interpreted with the help of the field structural data. Diagenesis of metagreywacke as well as the metamorphic modifications are studied using the petrographic details. With the aid of geochemistry and geochemical signatures, the provenance, paleoweathering and tectonic setting are deciphered. Further, summarizing the data, the occurrence of a Bouma sequence is delineated and a model for the basin development of metagreywacke and the evolution of the basin is proposed.

In the other section of associated rocks, dolerite dykes intruding the metagreywacke are studied to understand their trend of magma evolution. With the help of mineralogy and textural attributes, the various processes occurring during the crystallization of magma are deduced to understand its cooling behaviour. Using the major, trace and REE data various plots are constructed in order to understand the behaviour of the various geochemical signatures.

6.1 Metagreywacke

It is well recognised that sedimentary structures are reliable tools to delineate the environment and the history of deposition of the sediments. The transport of terrigenous clastic particles from the source terrain to the depositional basin is mainly by hydraulic suspension (Potter et al., 1984). The various structures are classified based on the morphology and deformation style and these depend on the driving force, sediment rheology, mechanism and timing of deformation relative to sedimentation. The sedimentary processes involving the deposition of metagreywacke and interbedded argillite (originally shale) in the Goa Group plays significant role in influencing the chemical composition of metagreywacke (cf. Hegde and Chavadi, 2009). The association of metagreywacke along with argillite in the

Goa Group is very helpful to model intracrustal processes, evolution, tectonic setting and provenance (cf. Condie and Wronkiewicz, 1990; McLennan and Taylor, 1991; Feng et al., 1993; Fedo et al., 1996; Manikyamba et al., 1997).

Based on the data from the previous chapters, here the formation of structures, diagenesis as well as provenance, paleoweathering and tectonic setting are now discussed.

6.1.1 Formational mechanism of structures

The formation processes of the various structures in metagreywacke are reported for the first time. The structures are classified based on process of formation and are discussed below.

The various structures identified in the study area are categorised into five groups namely:

- 1) primary depositional structures (laminations, dropstone, graded bedding, cross lamination);
- 2) diagenetic structure (liesegang rings);
- 3) Soft Sediment Deformation Structures (SSDS) (convolute, flame and load, ball and pillow (pseudonodule), slump fold, and syn-sedimentary fault);
- 4) deformational structures (fold and shear zone) and
- 5) erosional structures (erosional furrows and honeycomb structure).

Here, the process of formation of these structures is discussed.

6.1.1.1 Primary depositional structures

The presence of **laminations** in the metagreywacke of the study area (Fig. 3.2A) are suggestive of uniform and regular type of deposition of sediments and represents quiet water condition in which silt and clay sized particles accumulated.

The medium to fine grained metagreywacke with conglomerate at its base (Fig. 3.2B, C), suggests the role of turbidite gravity flow sedimentation deposited by the same sediment flow mechanism as that of metagreywacke (cf. Feary, 1979, Leggett, 2012).

Dropstone structure (Fig. 3.2B, C) in conglomerate is formed due to the sinking of quartzitic and granitic pebbles into the underlying soft sediment because of density difference. This causes a local distortion and bending of the laminae beneath the load protuberance (cf. Stow, 2010).

Graded bedding (Fig. 4.3B) is an intrabed structure with an upward fining sequence implying deceleration of sediment-laden current with the coarsest grains settling first representing normal sedimentation in the sedimentary basin and is formed both due to mass-flow and distal turbidites or by low-density turbidity flows.

Cross lamination (Fig. 3.2F) present in the study area implies a low flow regime (cf. Stow et al., 1996).

Besides, the presence of these various structures, an association of argillite in conglomerate (Fig. 3.2D, E) is identified as interlayer and intercalated lensoid pockets. The presence of argillaceous derivation within the conglomerates indicates that there were periods when either the transport mechanism of sediments were inactive or some areas of the depositional basin were isolated from the rapid downslope movement of coarser materials or due to local shallow environment in the depositional basin.

Argillite is also observed to be associated with metagreywacke in the study area (refer chapter 4). The presence of fine-grained argillite associated with metagreywacke indicates turbidite sequence representing suspension type of sedimentation and reflects lower flow energy regimes. A horizon of 'metagreywacke with biotite' strata is identified by the presence of a film of mica flakes and clay minerals which is absent at other locations (Fig.

3.2A, 4.1F). The presence of this horizon may be interpreted to be the contact of the coarse and fine grained strata in a turbidite sequence (cf. Bouma, 2004).

6.1.1.2 Diagenetic structure

The **liesegang rings** (Fig. 3.4A) occur as concentric rings in metagreywacke, bounded by fissures (cracks) which acted as conduits for the solutions and the rock porosity led to mass transport of ions generating a rhythmic precipitation. Each joint compartment bounded by fissures behaved as an independent cell. Liesegang rings either formed during diagenesis or because of rhythmic precipitation or by diffusional processes, occurring as precipitates in porous media (cf. Henisch, 1988; McBride, 2003). Liesegang (1913) suggested the diffusion of cells from inside to outside whereas Carl and Amstutz (1958) opined that the diffusion occurs from outside to inside. Since in the study area, the bands are perpendicular to the bedding planes, it indicates the diffusion to have occurred parallel to the bedding planes. The absence of a nucleus indicates the inception of the rings to be from the rim and not from the center.

6.1.1.3 Soft Sediment Deformation Structures (SSDS)

Water saturated sediments often result in a variety of SSDS ranging from load, flame, pseudonodules, slump folds and syn-sedimentary faults (McDonald and Shilts 1975; Brodzikowski et al., 1987; Chunga et al., 2007; Gruszka and Van Loon, 2007; Van Loon, 2009). The significant controls leading to the formation of deformation structures are rapid deposition, slope and gravity controlled density currents (Bowman et al., 2004) and also differential compaction (Mazumder et al., 2009).

The metagreywacke in the study area are massive and laminated while at certain outcrops mainly at the cliffs of Aguada and at headlands of Arambol, various SSDS are preserved which possibly could be due to the deformation of the original laminations. The destruction

of laminations leading to the formation of SSDS is attributed to various reasons: intense reworking of sediments due to organisms, rapid deposition by suspension, disruption of sediments due to liquefaction and movement of sediment in the water logged state (cf. Collinson and Thompson, 1982). Ortner (2007) explained that the SSDS could form during sediment gravity flow and due to rapid deposition of water and sediments. Due to the rapid deposition, water is trapped in the interstitial pores of sediments resulting in unstable pore pressure. During the course of burial and compaction, the interstitial water escapes leading to the formation of the various styles of SSDS. In the present study area the SSDS could be a result of these factors associated with the early stages of sediment consolidation. These SSDS are records of events and conditions between two or more depositional events.

Most of the SSDS such as flame, load and pseudonodules observed in the study area (Fig. 3.3) needs density contrast within the sediment layers. The SSDS mostly results when liquidised or hydroplastic and more competent sediments are stressed during or shortly after deposition. Here, the processes of formation of the various SSDS are discussed, of which the observations of the given structures are reported in Chapter 3.

Convolute laminations (Fig. 3.3A) identified in the study area, probably occur due to the shear stresses which are set by the turbidity flow which in turn leads to dewatering of sediments. The structure is known to form due to penecontemporaneous dewatering during fluidisation – liquefaction processes and expulsion of pore water (cf. Cojan and Thiry, 1992; Owen, 1996; Rossetti, 1999; Samaila et al., 2006, Kundu et al., 2011). Convolute laminations are typical of turbidites, which involves deformation of laminated and cross-laminated Bouma units (Bouma units are discussed later in this chapter) (cf. Selley, 2000).

Flame structures (Fig. 3.3B, Fig. 6.1) Kundu et al. (2011) listed five processes for the formation of flame structures: 1) fluvial current drag (Kuenen and Menard, 1952), 2) action of pressure due to loading (Anketell et al., 1970), 3) slope controlled movement of sediment

load (Brenchley and Newall, 1977), 4) earthquake shock (Visher and Cunningham, 1981; Sukhija et al., 1999; Li et al., 2008) and 5) differences in dynamic viscosity between sediment layers (Anketell et al., 1970) when the fine grained sediments behave as diapiric intrusions (Mills, 1983). The formation of flame structures in the study area is attributed either to differences in dynamic viscosity between the sediment layers and overlying pressure of the sediment or slope controlled movement of the sediment deposit due to the difference in the grain size.

Load structures (Fig. 3.3B, Fig. 6.1) in the study area were seen associated to be with the flame structures. They have formed as the denser sediments settle into lighter sediments as there is a gravitational readjustment due to the instability of strata. Owen (2003) observed that when the substrate is liquified, it loses its capacity to support sediments and hence there is a lateral redistribution of the sediment load and these are associated with flame structures.

The schematic illustration (Fig. 6.1) shows the development of flame and load structure into the pseudonodule. The initial formation of load and flame structure is followed by prominent load structure, which sinks into the underlying strata to form ball and pillow (pseudonodule).

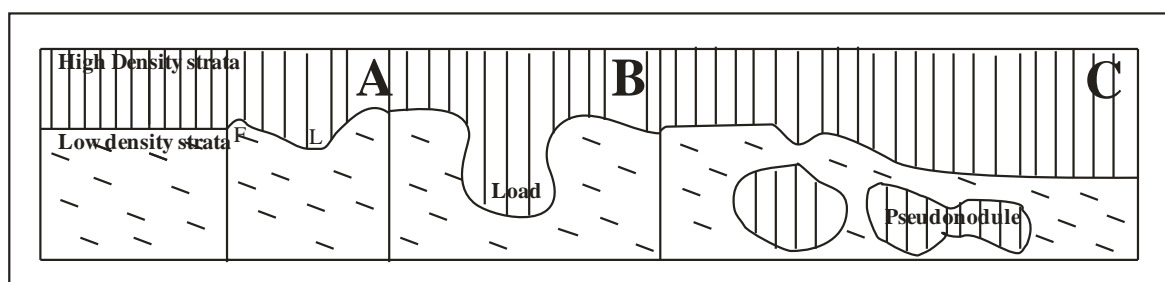


Fig. 6.1: Schematic illustration showing the development of pseudonodule from a load structure. Load and flame structures are formed (A), followed by prominent load structures (B), these load structures sink into the underlying strata (B) to form ball and pillow or pseudonodule (C). (F-Flame structure; L-Load structure).

Ball and pillow structures (Pseudonodules) (Fig. 3.3C, D, 6.1) are seen as isolated masses with variable morphologies in the underlying less dense strata when the load structures detached from the parent sedimentary bed during liquefaction. The load structure separates from the overlying sediments as the load bearing strength of liquefied sediment is lost (cf. Kundu and Goswami, 2008), resulting in sinking of the load cast or denser sediment into the underlying strata (cf. Kuenen, 1958). This leads to the formation of ball and pillow (pseudonodules) structure.

The **slump folds** (Fig. 3.3E) occur as folds in strata bounded by undisturbed sediments above and below within a sedimentary unit. As such, their formation due to tectonic activity is not possible. The folds possibly formed when the sediment layers behaved as plastic or semi-consolidated media and due to gravity the sediments moved down slope (cf. Kundu et al., 2011), either as the slope exceeds the angle of repose of the sediments (cf. Mills, 1983) or under the influence of large-scale water movements (cf. Siegenthaler et al., 1987) or an exceptionally low angle (<1°) subaqueous slopes (Alsop and Marco 2013).

Syn-sedimentary faults are small scale faults bounded by undeformed sedimentary strata above and below (Fig. 3.3F) indicating their syn-sedimentary origin. These types of faults and their association with undeformed strata are evident of brittle deformation when the sediments were partly consolidated (cf. Rossetti and Góes, 2000). Syn-sedimentary faults can also develop during the late stage of deformation due to a sudden increase in pore water pressure by the application of stress (cf. Pandey and Pandey, 2015).

The SSDS are observed along a horizon of the Sanvordem Formation which is exposed along the coast of North Goa at Aguada and Arambol and were probably formed in a single instantaneous event. These above discussed SSDS are overlain and underlain by undisturbed sediment and so may not be related to regional tectonics. These undeformed sediments (above and below SSDS) mark a period of quiescence before and after the growth of the

SSDS. These might have been as a result of a short natural trigger for the SSDS formation which disturbed the water saturated semi-consolidated sediments and this is attested by the limited lateral extent and less thickness of the SSDS strata.

6.1.1.4 Deformational structures

The **shear zone** (Fig. 3.4B, C) could have possibly formed due to faulting which occurred contemporary to the major fault of the west coast of India during which time several fault planes developed in W to WSW direction (cf. Gokul et al., 1985; Iyer et al., 1990). The presence of quartz veins is due to the emplacement of dolerite dykes when silicic fluids were injected into the country rock of metagreywacke. Due to faulting, the quartz veins were sheared and the metagreywacke was mylonitised by ductile deformation leading to haphazard arrangement of quartz grains within the country rock leading to the formation of 'metagreywacke cataclasite' (described in chapter 4).

6.1.1.5 Erosional structures

The erosional structures are formed as a result of different mechanisms such as stream currents, current-generated microturbulence, obstacle-generated microturbulence and abrasive action of current-transported debris and sediment. However, most of the structures formed are soon exposed and destroyed (High and Picard, 1973; Selley 2000).

Erosional furrows are noted in the study area as furrows and ridges (Fig 3.4D). These structures are formed due to differences in erosional effect on tilted strata of alternate soft and resistant rock surface which has carved them into a landscape of ridges and furrows.

Honeycomb structure (Fig 3.4E) in the study area is commonly seen along the sea coast. This results from the percolation of salty sea water through the pore spaces of rocks and evaporates at the surface forming tiny salt crystals on the surface of the rocks. The growth of

the salt crystals separates the sand particles from the cementing material, eventually creating a small depression in the rock. Due to the constant action of salty water the cavity enlarges at a faster rate creating pits in the rock.

6.1.2 Diagenesis

The framework components of metagreywacke of Sanvordem Formation such as quartz, feldspar and mica, exhibit various textural features indicating their process of formation. The metagreywacke is grouped into five distinctive types based on the mineralogy and also is supported by its geochemistry. They are: metagreywacke; quartzo-feldspathic metagreywacke; metagreywacke with biotite; metagreywacke cataclasite; argillite. Various processes which resulted in the mineralogical and diagenetic textural patterns in the metagreywacke are discussed here.

Quartz present in metagreywacke typically exhibits three habits (Fig. 4.1, 4.2, 4.3):

- 1) quartz grains with original detrital shape;
- 2) quartz grains locally interlocked by overgrowth into a quartzitic mosaic, wherein the original detrital boundaries are not identifiable;
- 3) quartz grains with denticulated fringe of secondary quartz, which welds them together.

This variation in texture is mainly due to diagenetic reorganization and as silica readily alters into other forms, it also dissolves and reprecipitates repeatedly (cf. Larsen and Chilingarian, 1967; Devaraju et al., 2010). Detrital minerals such as quartz and orthoclase (Fig. 4.1) exhibit pits which may have resulted during transportation of sand grains or may be due to their formation at high temperatures and then exposed to low temperatures with aqueous solutions creating disequilibrium but favored dissolution (cf. Milliken, 2003). The framework grains of

quartz and feldspar exhibit 'chevaux-de-frise' texture (Fig. 4.1) which is a diagenetic encroachment of the matrix over the detrital quartz and feldspar grains giving a hazy outline (cf. Carozzi, 1960; Devaraju et al., 2010). The abundant quantity of feldspar in 'metagreywacke' and 'quartzo-feldspathic metagreywacke' (Table 4.2A; Fig. 4.1) suggests that either feldspar grains have been able to resist decomposition during transportation or had been transported from a proximal source. The fragmentation seen in grains (Fig. 4.1C, 4.2F) of orthoclase and quartz can be recognized as due to compactional mechanism during diagenesis (cf. Chuhan et al., 2000; Milliken, 2003).

The formation of mica is well seen in 'argillites' (Fig. 4.2D, E) wherein the inception of mica crystallization occurs as ovoid clast which is formed from clay. This stage is the most advanced stage of diagenesis in progression towards metamorphism and transitional into low-grade metamorphism and is called as the phyllo-morphic stage (cf. Brown and Thayer, 1963; Chamley, 2013). 'Quartzo-feldspathic metagreywacke' and 'metagreywacke with biotite' have significant amount of muscovite (Fig. 4.1, Table 4.2) as, either its lattice is more readily developed from the clay minerals or perhaps it is stable in most of the burial conditions. The occurrence of muscovite surrounded by quartz (Fig. 4.1E) is a result of the resistance of the mineral to deformation. It is noted that rocks with higher clay content especially 'argillite' are mica-dominant.

The 'metagreywacke with biotite' (Fig. 4.1F) exhibits growth of mica, wherein the size of mica increases to occupy more of the matrix material. Calcite in 'metagreywacke with biotite' (Fig. 4.1F), may have formed due to precipitation which readily occur upon release of pressure and decrease in temperature (cf. Carozzi, 1960). Pyrite in 'argillite' occurring as isolated crystals (Fig. 4.2C) owes its formation to oxidation and reduction reactions involving iron and sulphur which occur late in the rock history. This suggests that sulphur had been previously held close to the site of pyrite attached to clay and hence late reducing conditions

resulted in crystallization of pyrite. However, due to groundwater the occurrence of dissolved oxygen and the oxidizing conditions are restricted to near-surface positions (cf. Milliken, 2003).

Stylolites identified in 'argillite' (Fig. 4.2D) occur under conditions of strong pressure solution which is dominated in rocks bearing argillaceous matrix. Among the micaceous minerals muscovite is rather resistant to pressure solution while biotite yields more easily to pressure solution. Pressure solution stylolites is an important cause of intergranular volume reduction which occurs during compaction process of diagenesis (cf. Milliken, 2003).

6.1.3. Metamorphic modification

In the study area, the late diagenetic processes were succeeded by early stages of metamorphism that gave rise to low grade greenschist facies of rocks (Fernandes et al., 2016a, b). Metagreywacke association displays textural characteristics from diagenesis to metamorphism. Recrystallization of detrital quartz imparts a major reorganization in texture related to grains, cement and the interstitial pore space elimination.

The presence of biotite and muscovite alignment in metagreywacke (Fig. 4.1A) indicates schistosity of the rocks. In 'metagreywacke with biotite', well developed alternate layers of micas and quartz gives it a schistose texture (Fig. 3.2A, 4.1F). The presence of chlorite as well as biotite owes their formation to greenschist facies of metamorphism. Intracrystalline deformation also is evident by tapering deformed twin lamellae indentified in feldspar (Fig. 4.1C, 4.2A). Undulatory extinction in detrital grains of quartz and feldspar (Fig. 4.1A, C) may be due to intracrystalline plastic deformation. Recrystallization is prominent in 'quartzo-feldspathic metagreywacke' (Fig. 4.1D) wherein quartz is recognized by presence of a mosaic of new grains owing its formation to grain boundary migration (cf. Blenkinsop, 2000).

6.1.4 Provenance, paleoweathering and tectonic setting

The geochemical composition of terrigenous sedimentary rocks is a function of the complex interplay of variables, such as provenance, paleoweathering, transportation and diagenesis. The framework mineralogy, provenance and the tectonic setting of sedimentary basins are interrelated (Bhatia, 1983; Banerjee and Banerjee, 2010; Devaraju et al., 2010). Thus, the composition of sedimentary rocks is useful to recognize the nature of ancient continental and oceanic basins. Furthermore, the relationship between attributes of the plate tectonic setting and factors such as relief, physical sorting and diagenesis also govern the composition of clastic sedimentary rocks (Pettijohn et al., 1972; Blatt et al., 1980; Fernandes et al., 2016a). The diagenetic process of metagreywacke of the Goa Group is obscured by the effect of low grade metamorphism but a record of the geological history can be inferred as it is retained in the detrital sediments (Fernandes et al., 2016a). Trace elements such as La, Ce, Nd, Y, Th, Zr, Hf, Nb, Ti and Sc which are regarded as insensitive to alteration and have low mobility during sedimentary processes and also low residence time in water (Holland, 1978; Ma Yanping and Zhao Jingzhou, 2015) are well-suited to decipher the origin of metagreywacke. Some of these elements are useful to plot various discriminant diagrams that help to characterize the tectonic setting of metagreywacke (Bhatia and Crook, 1986). Similarly, the REE are also very useful to determine the origin of the metagreywacke as these are incorporated into the sedimentary rocks during the recycling of sediments and get preserved in them as a record of the average upper crustal elemental abundances (Rashid, 2005; Fernandes et al., 2016a).

Therefore, on the above basis, I now discuss the provenance, paleoweathering and tectonic setting of metagreywacke of the Goa Group.

6.1.4.1 Provenance

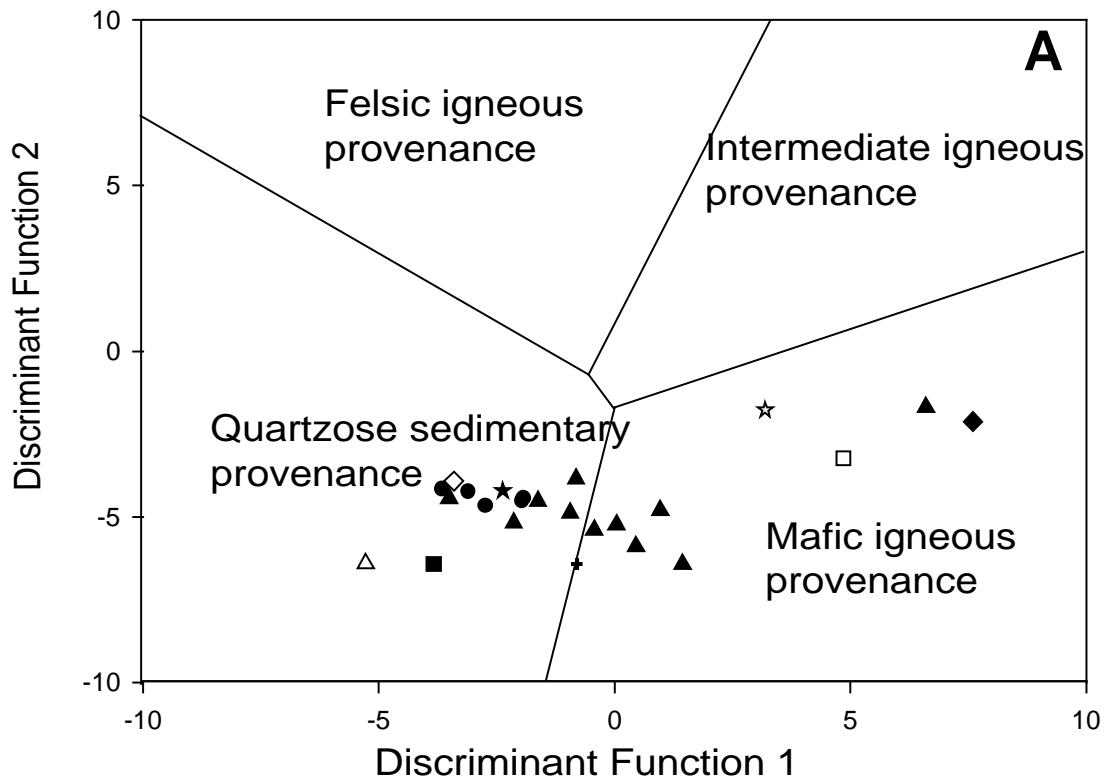
The mineralogical and chemical composition of siliciclastic sedimentary rocks are widely used to investigate their source rocks (Kalsbeek and Frei, 2010; Moosavirad et al., 2012). Hence, the detrital framework composition of such rocks is a reliable indicator of the tectonic setting of the provenance.

For the present study, modal analysis of framework components of metagreywacke is carried out (Table 4.2A) and the data obtained has been plotted on discrimination diagrams. The ternary Quartz (Q)- Feldspar (F)- Rock fragment (RF) plot (Dickinson, 1985) of the framework mode shows various provenance fields which includes basement uplift, transitional continental, craton interior, recycled orogen, dissected arc, transitional arc and undissected arc. In this plot, the metagreywacke samples of the study area indicates a craton interior to transitional continental (Fig. 4.4D) reflecting high percentage of quartz grains representing a typical continent provenance.

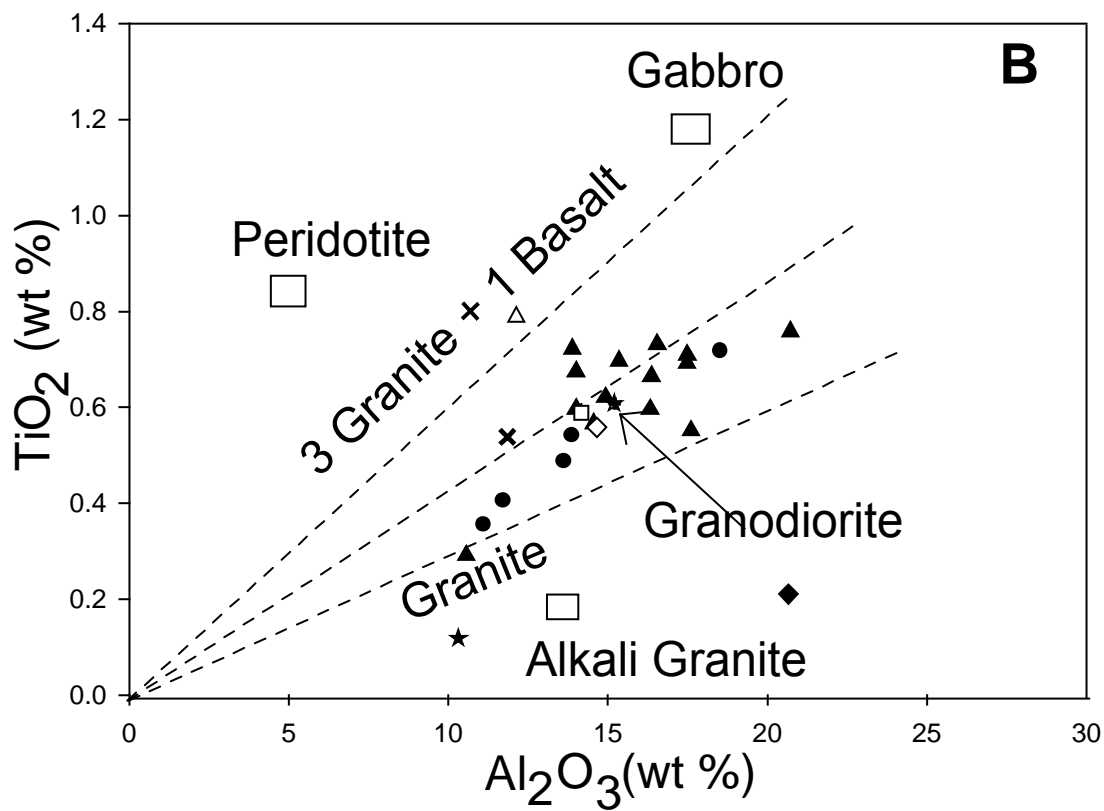
A discriminant function diagram (Fig. 6.2A) based on major element oxides of Ti, Al, Fe, Mg, Ca and K by Roser and Korsch (1988) is effective in distinguishing between the felsic igneous, intermediate igneous, mafic igneous and quartzose sedimentary provenances. In this plot, the metagreywacke samples of the study area indicate a dominance of quartzose sedimentary provenance, while a few samples plot in mafic igneous provenance. Detrital components for the quartzose sedimentary provenance were possibly derived from either a specific crystalline (igneous source) or another sedimentary source.

However, the ultimate crystalline source for the rocks of the present study can be inferred from their Al_2O_3 and TiO_2 contents. Since Al and Ti are essentially immobile elements and due to the low solubility of their oxides and hydroxides in low temperature aqueous solutions, the Al_2O_3 and TiO_2 contents of the siliciclastic rocks can be assumed as practically equal to

those of their source (Stumm and Morgan, 1981; Sugitani et al., 1996; Moosavirad et al., 2012). To constrain the provenance of siliciclastic sedimentary rocks, McLennan et al. (1980), proposed a TiO_2 versus Al_2O_3 bivariate discrimination diagram (Fig. 6.2B). On this diagram the samples plot among the granite and granodiorite line except a few 'argillite' samples plot among the granodiorite and (3 granite + 1 basalt) line indicating a mixed composition.

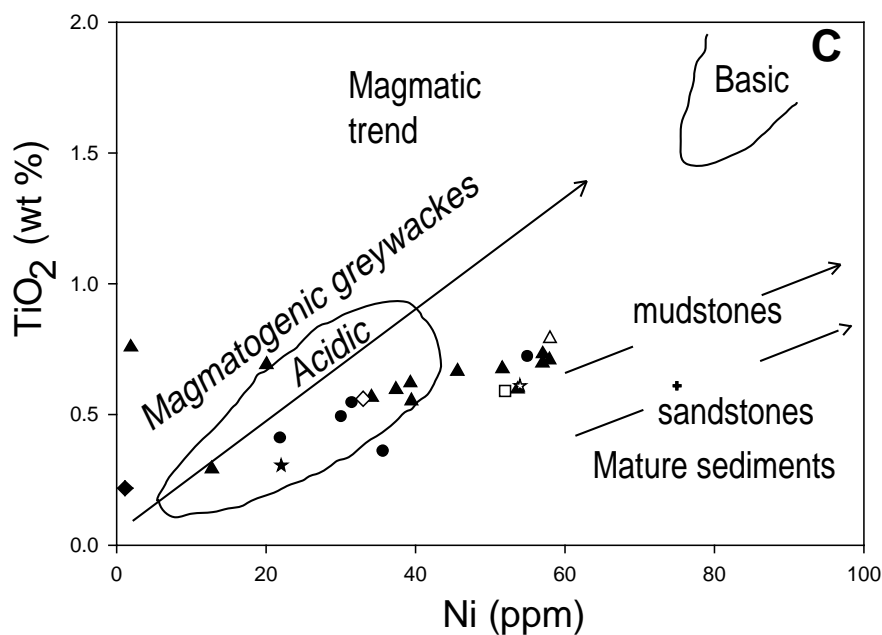


(Roser and Korsch, 1988)

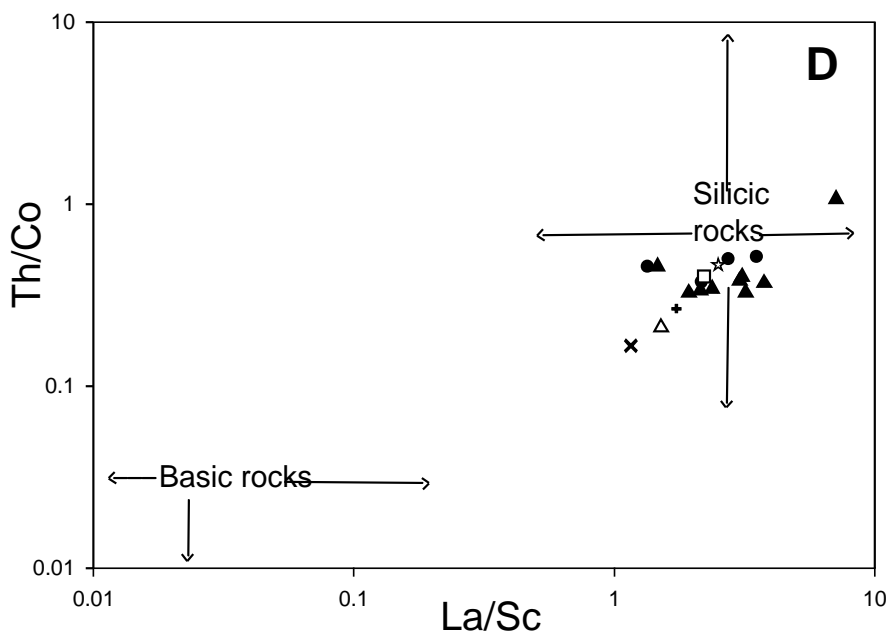


(McLennan et al., 1980)

Contd...



(Floyd et al., 1989)



(McLennan and Taylor, 1991; Cullers, 2002)

Fig. 6.2: Plots for provenance of metagreywacke:

A) Discriminant function diagram of metagreywacke based on major element oxides of Ti, Al, Fe, Mg, Ca and K by Roser and Korsch (1988).

B) TiO_2 versus Al_2O_3 bivariate discrimination diagram (McLennan et al., 1980).

C) Binary plot of TiO_2 (wt%) vs Ni (ppm) (Floyd et al., 1989).

D) Bivariate plot of Th/Co vs La/Sc (McLennan and Taylor, 1991; Cullers, 2002).

| | |
|---|---|
| ▲ | Argillite |
| ● | Metagreywacke |
| ★ | Quartzo-feldspathic metagreywacke |
| ■ | Metagreywacke with biotite |
| ◆ | Metagreywacke cataclasite |
| ◇ | Greywacke from Merces quarry (Widdowson, 2009) |
| △ | Greywacke with biotite (Devaraju et al., 2010) |
| □ | Greywacke with chlorite-sericite (Devaraju et al., 2010) |
| ☆ | Fine grained greywacke (Devaraju et al., 2010) |
| + | Greywacke (Condie, 1993) |
| × | Greywacke of Fig Tree, Barberton (Toulkeridis et al., 1999) |

The abundances of Ni (~avg 53 ppm) and TiO₂ (~avg 0.68%) in siliciclastic sediments are useful indicators in provenance studies. Hence, in the binary plot (Fig. 6.2C) of TiO₂ (wt%) vs Ni (ppm) (after Floyd et al., 1989), the source composition of the rocks indicate acidic igneous rocks and mudstones.

The High Field Strength Elements (HFSE) such as Zr, Nb, Hf, Y, Th and U elements are enriched in felsic sources rather than the mafic sources as they are preferentially partitioned into melts during crystallization (Feng and Kerrich, 1990). Zr, Hf and Y reflect provenance compositions due to their immobile behavior (Taylor and McLennan, 1985; Bakkiaraj et al., 2010). The ratios of La/Sc, La/Cr, La/Co, Th/Sc, Th/Cr, Th/Co and Eu/Eu* are important to constraint the average provenance composition (Cullers and Podkoyrov, 2000) as they are significantly different in felsic and mafic rocks (Cox and Lowe, 1995; Cullers, 1995; 2000). Variation in Th and La is indicative of felsic while Sc and Co are indicative of mafic and so is used to differentiate between felsic and mafic provenance (McLennan et al., 1980; Nagarajan et al., 2007a, b; Kasanzu et al., 2008; Bakkiaraj et al., 2010). As such a bivariate plot of Th/Co vs La/Sc (cf. McLennan and Taylor, 1991; Cullers, 2002) (Fig. 6.2D) is used to plot the samples of the present study and this suggests a high ratio of Th/Co and La/Sc indicating a felsic nature of the source rocks.

The REE pattern and Eu anomaly provide significant clues of the source rock characteristics (Taylor and McLennan, 1985). Generally, high LREE/HREE ratio and a high negative Eu anomaly are found in felsic rocks, while the mafic rocks have low LREE/HREE ratio and a low negative Eu anomaly (Taylor and McLennan, 1985; Cullers, 1994). Archean sedimentary rocks exhibit a less uniform REE pattern as compared to those typical of post-Archean (Taylor and McLennan, 1983). In our present study, the analysed samples exhibit negative Eu anomaly of average 0.73 suggests its derivation from felsic rocks (Fig. 5.3). The steep (abundant) LREE-enriched pattern indicates Archean sediment derivation from acidic parent

rocks. This felsic source indicates feldspar-bearing granodiorite rocks to be the main source of the provenance. Similar findings of the REE patterns were reported by Taylor and McLennan (1985).

6.1.4.2 Paleoweathering

Paleoweathering is an important factor affecting the composition of sedimentary rocks. As sedimentary rocks *sensu stricto* are composed of weathered products they reflect the weathered profile rather than the parent rock (Nesbitt et al., 1996). Source rock composition, duration of weathering, climatic conditions and rate of tectonic uplift of source region are the factors that govern the intensity of chemical weathering of source rocks (Wronkiewicz and Condie, 1987). Due to chemical weathering, elements such as Ca, Na and K are largely removed from the source rocks. Hence the proportion of these elements surviving in the soil profiles is an index of the intensity of chemical weathering (Nesbitt et al., 1997; Moosavirad et al., 2012).

Various parameters such as chemical index of alteration (CIA, Nesbitt and Young, 1982), K_2O/Na_2O (Nesbitt and Young, 1984), Rb/Sr (McLennan et al., 1993) and Th/U ratios (McLennan et al., 1993) are used to determine the alteration of sedimentary rocks. However, the widely used and reliable parameter for influence of source rock weathering is estimated by calculating the CIA (Nesbitt and Young, 1982):

$$CIA = [Al_2O_3 / (Al_2O_3 + CaO + Na_2O + K_2O)] \times 100$$

Where, CaO is the amount of CaO incorporated in the silicate fraction of the rock.

The high CIA values reflect the removal of liable cations such as Ca^{2+} , Na^+ and K^+ relative to the static residual constituents (Al^{3+}) during weathering, conversely, low CIA values indicate the near absence of chemical alteration and consequently might reflect cool and/or arid

conditions. The average CIA values are higher in Fe-sand (78), wacke (76), sub-litharenite (55), arkose (53), sub-arkose (36), and quartz arenite (31) while typical shales average about 70 to 75. In unweathered igneous rocks the CIA values are close to 50 whereas the intensely weathered residual rock with presence of kaolinite and gibbsite has values ~100 (Nesbitt and Young, 1982; Fedo et al., 1995). The lower average CIA values in arkose, sub-arkose and quartz arenite is due to direct input of immature continent detrital minerals into the depositional system which does not reflect the general chemical weathering conditions in the source region. Also, the CIA value variation indicates the sediment sorting effect. Concentration of quartz and feldspar along with heavy minerals are present in the coarse fraction while weather-able minerals present in the suspended load sediments is due to physical sorting of sediments during transportation and deposition (Garcia et al., 2004; Bakkiaraj et al., 2010).

The CIA values of metagreywacke samples of the study area range from 63 to 84 with an average of 73. The average CIA value of fine grained 'argillite' (69) is slightly more than the coarser 'metagreywacke' association (66). In order to understand the extent of alteration in the above equation a plot of Al_2O_3 against $Al_2O_3+CaO+Na_2O+K_2O$ is drawn (Fig.6.3A) indicating moderate leaching. The plot of SiO_2 versus CIA shows a consistent trend of CIA with SiO_2 ($r=0.48$) (Fig.6.3B) wherein with increasing silica content CIA is constant during alteration.

The nature of weathering and the post-depositional modifications leading to the mobility of elements could be evaluated by plotting Al_2O_3 (A), $(CaO+Na_2O)$ (CN) and K_2O (K) on an A-CN-K ternary diagram (Fig.6.3C) (after Nesbitt and Young, 1982; 1984). A majority of the samples of the study area plot away from the plagioclase – K feldspar join line, indicating moderate to intense chemical weathering in the source area. A few 'argillite' plot towards illite on the A-K edge which do not incline towards the K apex, indicating the presence of

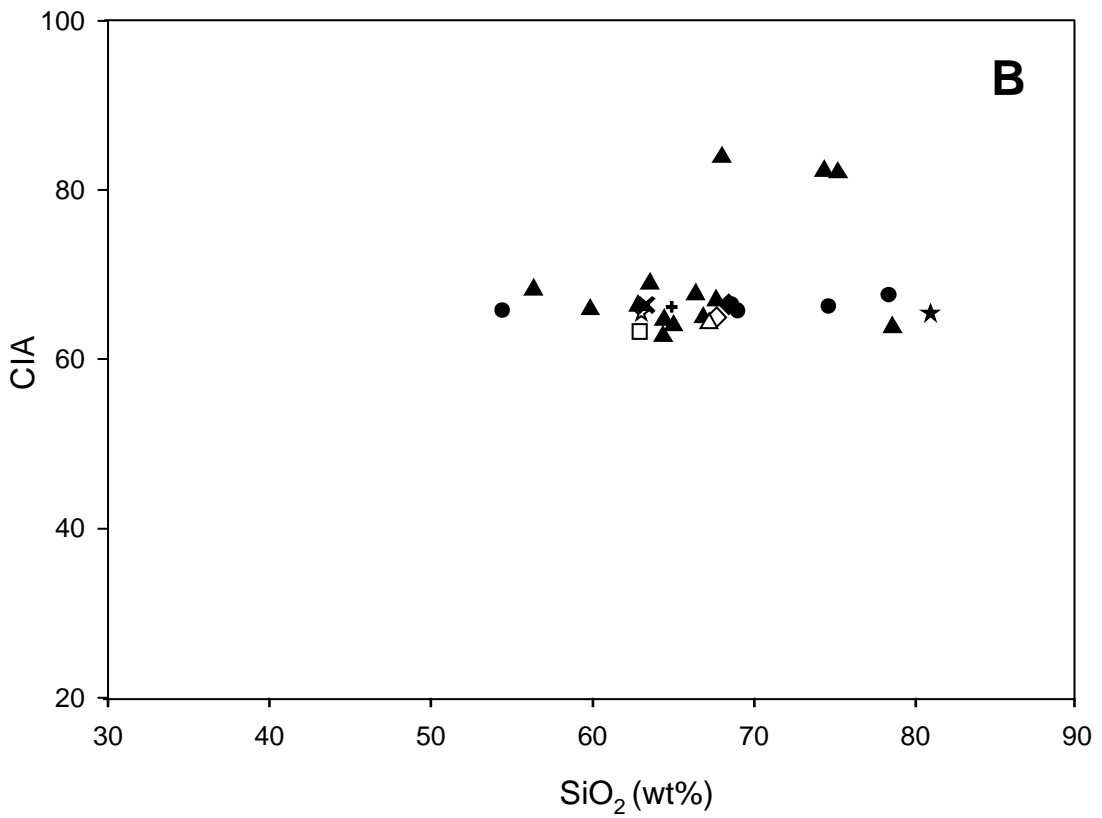
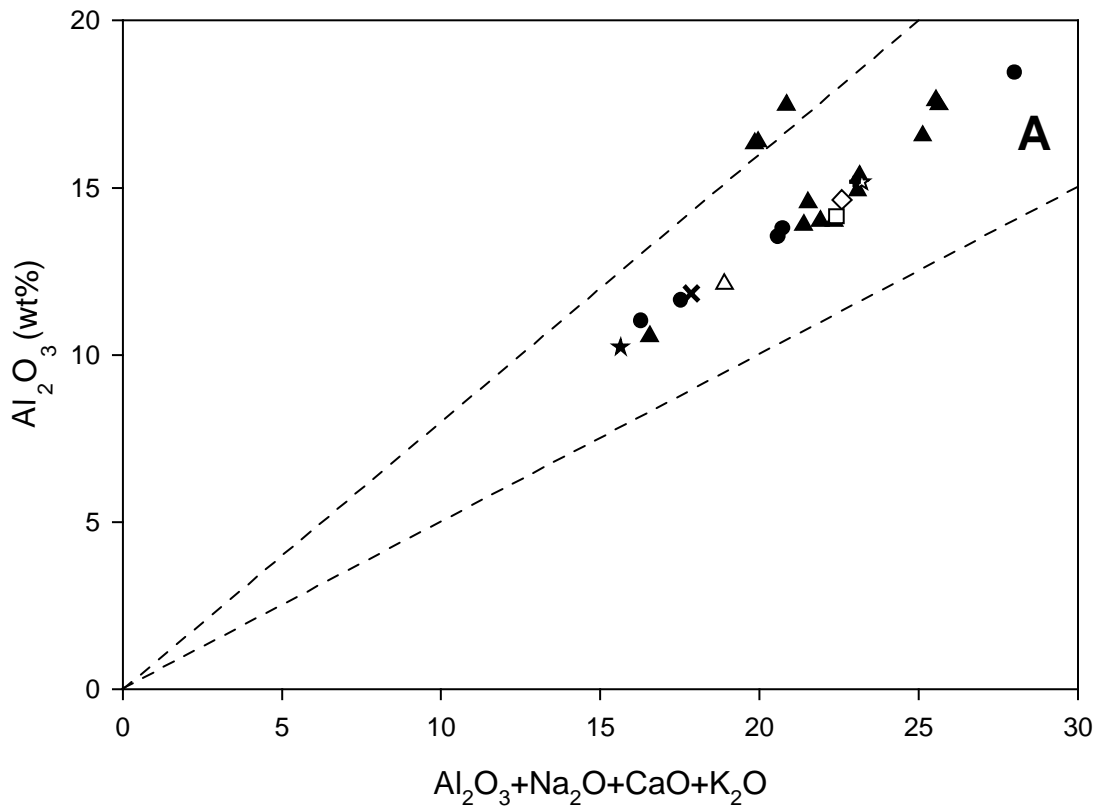
more illite than kaolinite which probably could be an effect of potash metasomatism, where post depositional processes convert kaolinite to illite (cf. Nagarajan et al., 2015). However, the slight amount of added potassium is due to the presence of clastic grains of K-feldspar, that provide an evidence for detrital nature of K-bearing phases. A 'metagreywacke cataclasite' and an 'argillite' plot on the A-CN line while 'metagreywacke with biotite' plot below the plagioclase– K-feldspar join near the field of tonalite-granodiorite. This suggests different weathering rates of rocks of the metagreywacke as the plots of samples in the diagram are not concentrated in a single field (Fig. 6.3C).

The characteristic source of clastic sedimentary rocks can be studied using the Th/U ratio as the ratio increases with increasing weathering (Taylor and McLennan, 1985; McLennan and Taylor, 1991; McLennan et al., 1990). High Th/U ratio indicates oxidative weathering and removal of U, also Th/U increases with kaolinite content in highly weathered rocks (McLennan et al., 1980). Th/U ratio equal to or greater than 4 indicates the derivation of sediments from the upper crust whereas a value lower than 4 is related to mantle contribution (Roddaz et al., 2006; Bakkiaraj et al., 2010). Th/U ratio is also a sensitive indicator of metamorphism and it may reach 8-10 in amphibolites facies and as high as 25 in the granulite facies (Wedephol, 1991). Bhatia and Taylor (1981) observed that the Th/U ratio for most of the sedimentary rocks remains uniform at 4.5, while for sediments derived from andesitic and dacitic rocks the La/Th ratios are 6.7 and 4.5 respectively. This ratio remains constant at 2.6 for most quartzose sedimentary rocks.

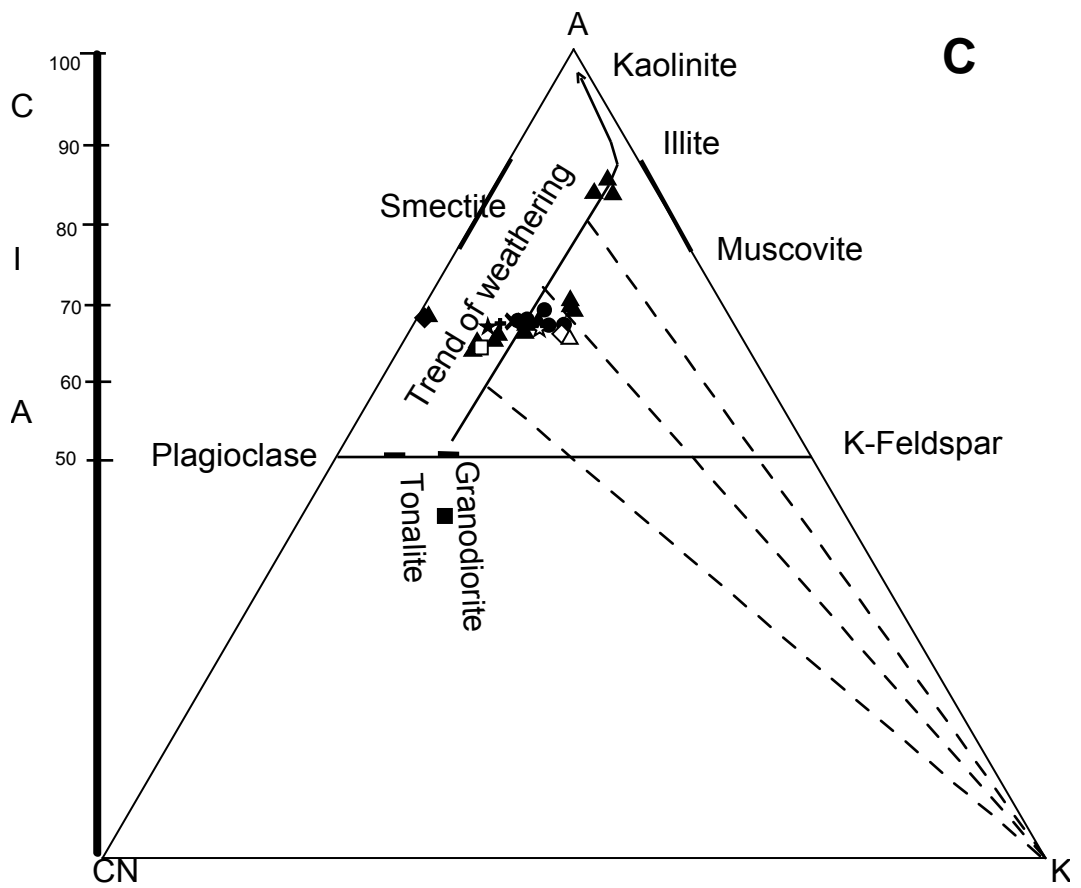
The analyzed metagreywacke samples of the study area show Th/U ratio an average of 2.25 (range from 1.88 to 2.65) and the average of La/Th ratio is 4.683 (range from 2.16 to 7.56), indicating a provenance closer to dacitic to quartzose sedimentary rocks composition. In Figure 6.3D of Th/U against Th, metagreywacke lie below value 4, in the depleted mantle source. The low Th/U exists due to sedimentary process and is likely to have resulted from U

enrichment (avg ~3.96) and hence is accompanied by high U content reflecting the greater mobility of this element and also reflects the geochemically depleted nature of such reservoirs (cf. Newman et al., 1984).

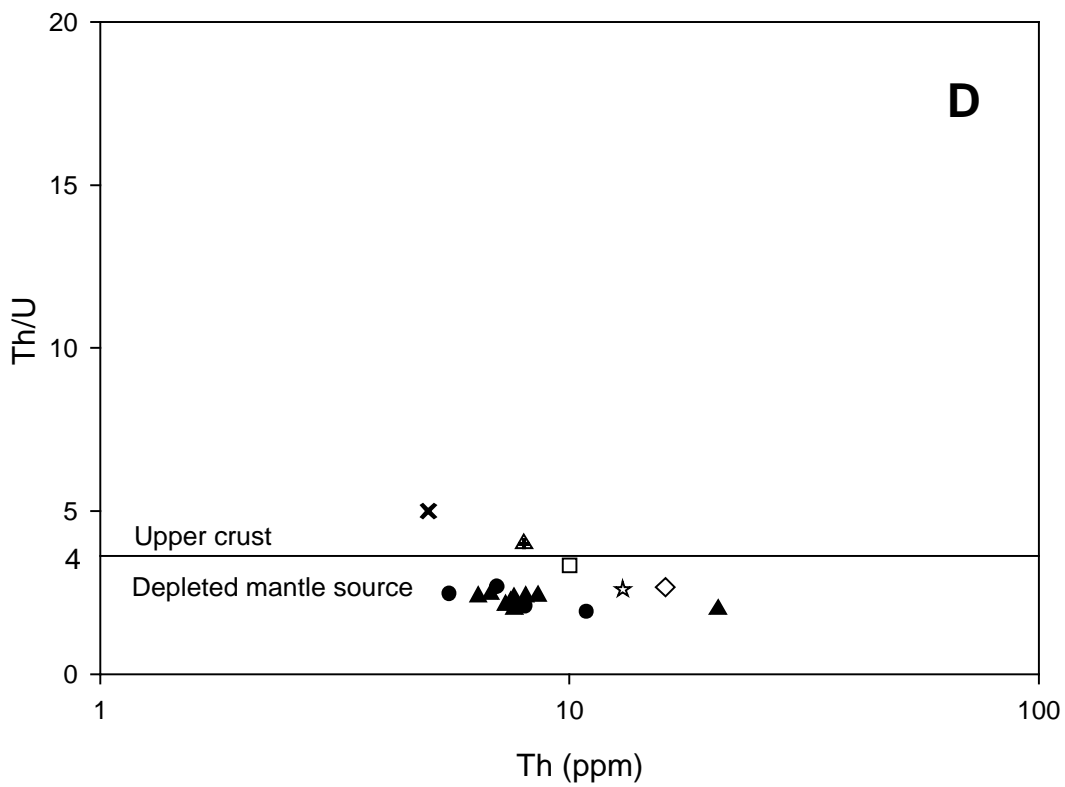
The distribution of major elements (P_2O_5 and TiO_2), trace elements (Th, U, Zr, Hf and Nb) and REE significantly influences the chemical composition of terrigenous sediments. The average content of Zr (169 ppm) in the metagreywacke samples of the study area is lower than Post Archean Australian Shale (PAAS) value (210; McLennan et al., 1983) and also Upper Continental Crust (UCC) value (190; Taylor and McLennan, 1985). Weathering indices of sedimentary rocks are useful tools to understand the tectonic activity and climatic conditions of the source region. To understand the climatic condition during sedimentation of siliciclastic sedimentary rocks Suttner and Dutta (1986) proposed a binary plot of SiO_2 wt% versus $(Al_2O_3 + K_2O + Na_2O)$ wt%. The analysed samples in this binary plot indicate essentially arid climatic condition (Fig. 6.3E).



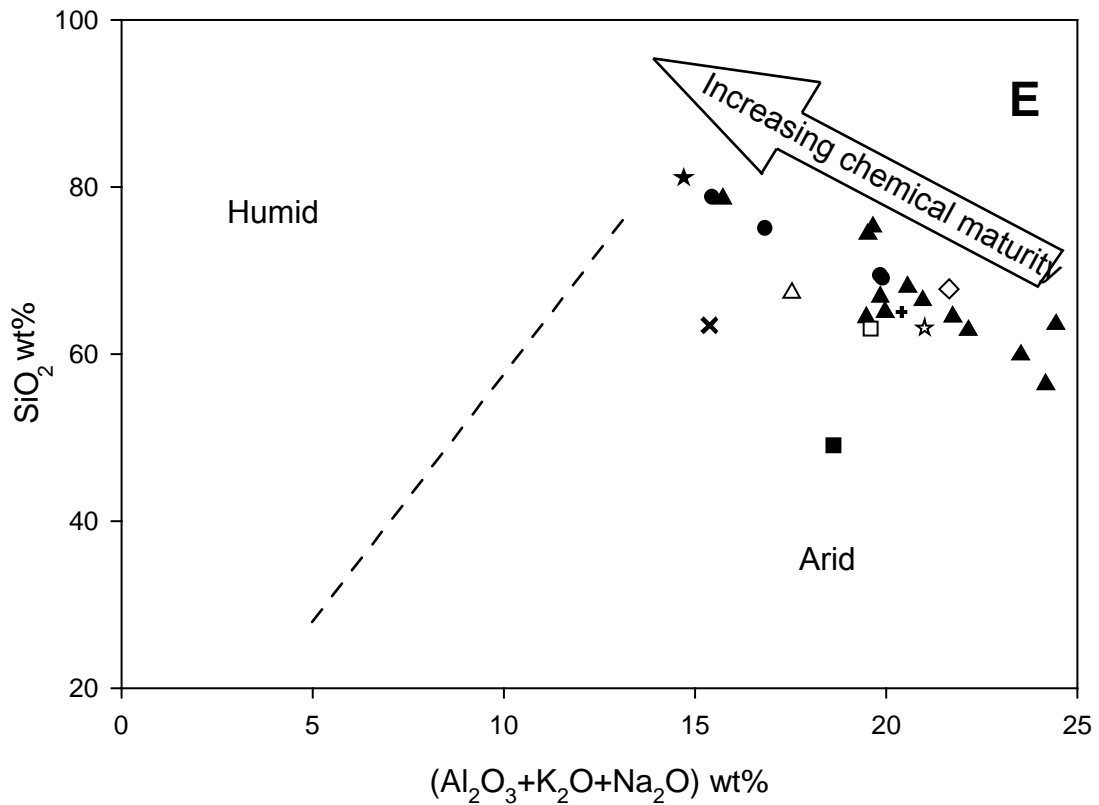
Contd...



(Nesbitt and Young, 1982; 1984)



Contd...



(Suttner and Dutta, 1986)

- ▲ Argillite
- Metagreywacke
- ★ Quartzo-feldspathic metagreywacke
- Metagreywacke with biotite
- ◆ Metagreywacke cataclasite
- ◇ Greywacke from Merces quarry (Widdowson, 2009)
- △ Greywacke with biotite (Devaraju et al., 2010)
- Greywacke with chlorite-sericite (Devaraju et al., 2010)
- ☆ Fine grained greywacke (Devaraju et al., 2010)
- + Greywacke (Condie, 1993)
- × Greywacke of Fig Tree, Barberton (Toulkeridis et al., 1999)

Fig. 6.3: Plots for paleoweathering of metagreywacke:

A) Plot of Al_2O_3 against $\text{Al}_2\text{O}_3 + \text{CaO} + \text{Na}_2\text{O} + \text{K}_2\text{O}$.

B) Plot of SiO_2 versus CIA ($r=0.48$).

C) Ternary diagram plot of Al_2O_3 (A), $(\text{CaO} + \text{Na}_2\text{O})$ (CN) and K_2O (K) (Nesbitt and Young, 1982; 1984).

D) Plot of Th/U against Th.

E) Plot of SiO_2 wt% versus $(\text{Al}_2\text{O}_3 + \text{K}_2\text{O} + \text{Na}_2\text{O})$ wt% (Suttner and Dutta, 1986).

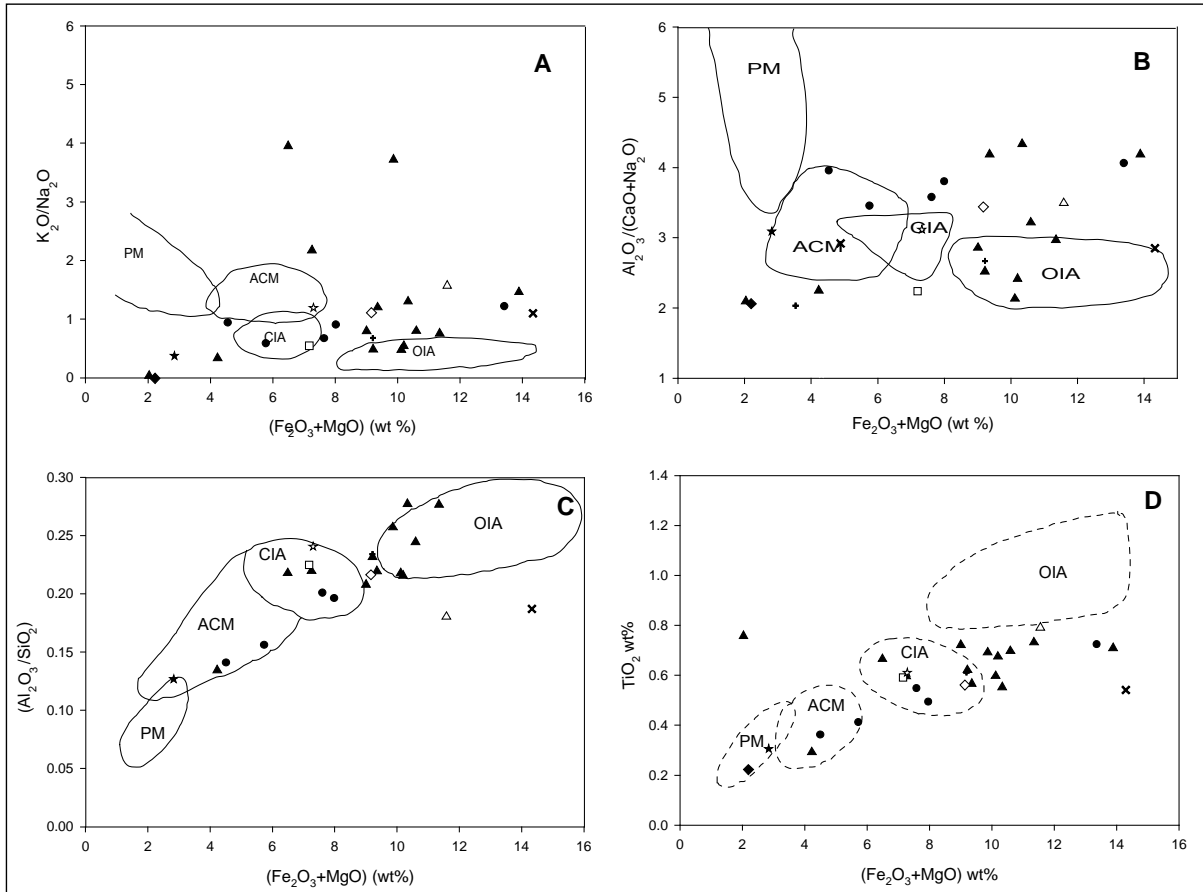
6.1.4.3 Tectonic setting

It is well recognized that the crustal evolution and the tectonic setting can be indicated from the geochemistry of clastic sedimentary rocks (Lahtinen, 2000). The chemical composition of siliciclastic sedimentary rocks is influenced by plate tectonic setting and depositional basin and as such the rocks possess different terrain-specific geochemical signatures (Bhatia, 1983; Bhatia and Crook, 1986; Roser and Korsch, 1986). To delineate the tectonic setting, several major, trace and REE based discrimination diagrams have been proposed (Maynard et al., 1982; Bhatia, 1983; Bhatia and Crook, 1986; Roser and Korsch, 1986; McLennan et al., 1990; McLennan and Taylor, 1991; Floyd et al., 1991; Murphy, 2000). Diagenesis also influences the bulk composition of sandstones, but the nature of diagenesis depends on the tectonic setting of the basin (Siever, 1979; Bhatia, 1983; Fernandes et al., 2016a).

Tectonic setting discrimination diagrams for siliciclastic sedimentary rocks of Bhatia (1983) and Roser and Korsch (1986) are based on immobile and also mobile major elements such as Na_2O and K_2O . Bhatia (1983) used parameters such as $\text{Fe}_2\text{O}_3+\text{MgO}$, TiO_2 , $\text{Al}_2\text{O}_3/\text{SiO}_2$, $\text{K}_2\text{O}/\text{Na}_2\text{O}$ and $\text{Al}_2\text{O}_3/(\text{CaO}+\text{Na}_2\text{O})$ to classify tectonic setting namely: Oceanic Island Arc (OIA), Continental Island Arc (CIA), Active Continental Margin (ACM) and Passive Margin (PM). In $\text{K}_2\text{O}/\text{Na}_2\text{O}$ versus $(\text{Fe}_2\text{O}_3+\text{MgO})$ and $\text{Al}_2\text{O}_3/(\text{CaO}+\text{Na}_2\text{O})$ versus $\text{Fe}_2\text{O}_3+\text{MgO}$ diagrams, the analysed samples of the study area show a scatter at the Ocean Island Arc (OIA), Continental Island Arc (CIA), Active Continental Margin (ACM) fields (Fig. 6.4A, B). In the $\text{Al}_2\text{O}_3/\text{SiO}_2$ versus $\text{Fe}_2\text{O}_3+\text{MgO}$ and TiO_2 versus $\text{Fe}_2\text{O}_3+\text{MgO}$ diagrams (Fig. 6.4C, D) the majority samples show a scatter and plot in CIA and a few in ACM. The source of the rocks that plot in CIA has dominant contribution from felsic volcanic rocks provenance while those in ACM are derived from granitic gneisses and granites of the uplifted basement provenance (cf. Bhatia, 1983).

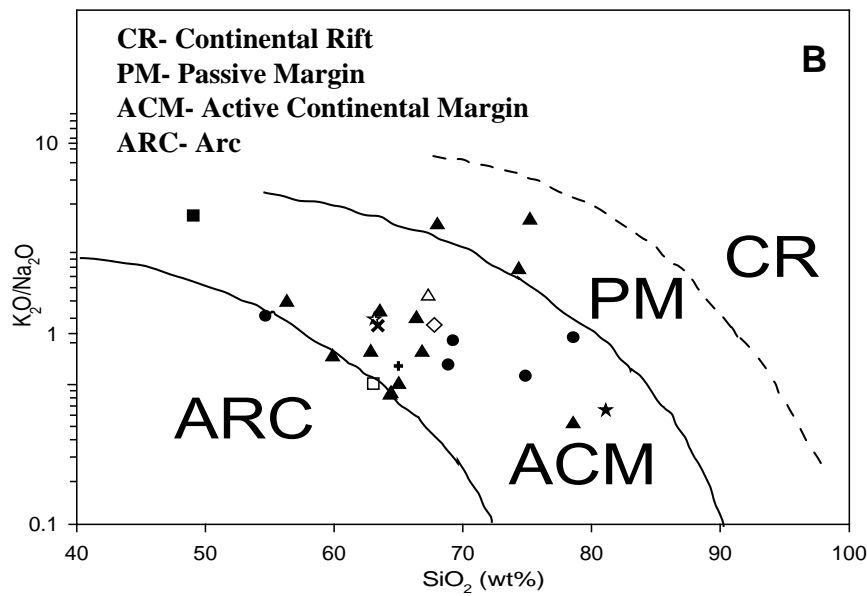
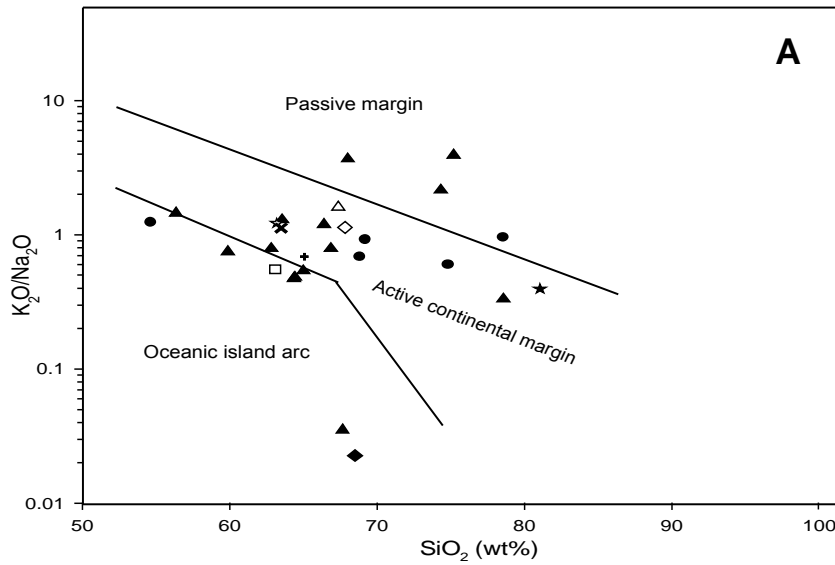
Armstrong-Altrin and Verma (2005) reported that the tectonic setting discrimination diagram proposed by Roser and Korsch (1986) is more reliable than the plate tectonic setting of sedimentary basin proposed by Bhatia (1983). Hence, to improve the discrimination of the tectonic setting, a plot of K_2O/Na_2O against SiO_2 proposed after Roser and Korsch (1986) (Fig. 6.5A) is used. In this plot, the samples indicate ACM type of tectonic setting (Fig. 6.5A). This observation is similar to the plot of K_2O/Na_2O versus SiO_2 diagram (Roser and Korsch, 1986), modified after Murphy (2000), indicating ACM (Fig.6.5B).

Immobile trace elements such as La, Ce, Nd, Y, Th, Zr, Hf, Nb, Ti and Sc are most appropriate to help discriminate the tectonic setting of siliciclastic sedimentary rocks which is in turn influenced by parameters such as provenance, relief, weathering, physical sorting and diagenesis (Devaraju et al., 2010; Fernandes et al., 2016a). The Ti/Zr versus La/Sc binary plot (after Bhatia, and Crook, 1986) (Fig. 6.6A) indicates that the deposition of the metagreywacke essentially took place in a Continent Island Arc tectonic setting with a subordinate tectonic setting of an Active Continental Margin. The ternary discriminant diagram of CaO- Na_2O - K_2O , La-Th-Sc and Th-Sc-Zr/10 (after Bhatia, and Crook, 1986) (Fig. 6.6B to D) attests to the fact that an overwhelming deposition occurred in a Continental Island Arc setting. This can be noted in the plot of CaO- Na_2O - K_2O (Fig. 6.6B) that shows the sediments were not only deposited in a Continental Island Arc set-up but also in an Active Continental Margin setting.



- ▲ Argillite
- Metagreywacke
- ★ Quartzo-feldspathic metagreywacke
- Metagreywacke with biotite
- ◆ Metagreywacke cataclasite
- ◇ Greywacke from Merces quarry (Widdowson, 2009)
- △ Greywacke with biotite (Devaraju et al., 2010)
- Greywacke with chlorite-sericite (Devaraju et al., 2010)
- ☆ Fine grained greywacke (Devaraju et al., 2010)
- + Greywacke (Condie, 1993)
- × Greywacke of Fig Tree, Barberton (Toukeridis et al., 1999)

Fig. 6.4: Tectonic setting diagrams of metagreywacke (Bhatia, 1983). (Oceanic Island Arc (OIA), Continental Island Arc (CIA), Active Continental Margin (ACM) and Passive Margin (PM)).



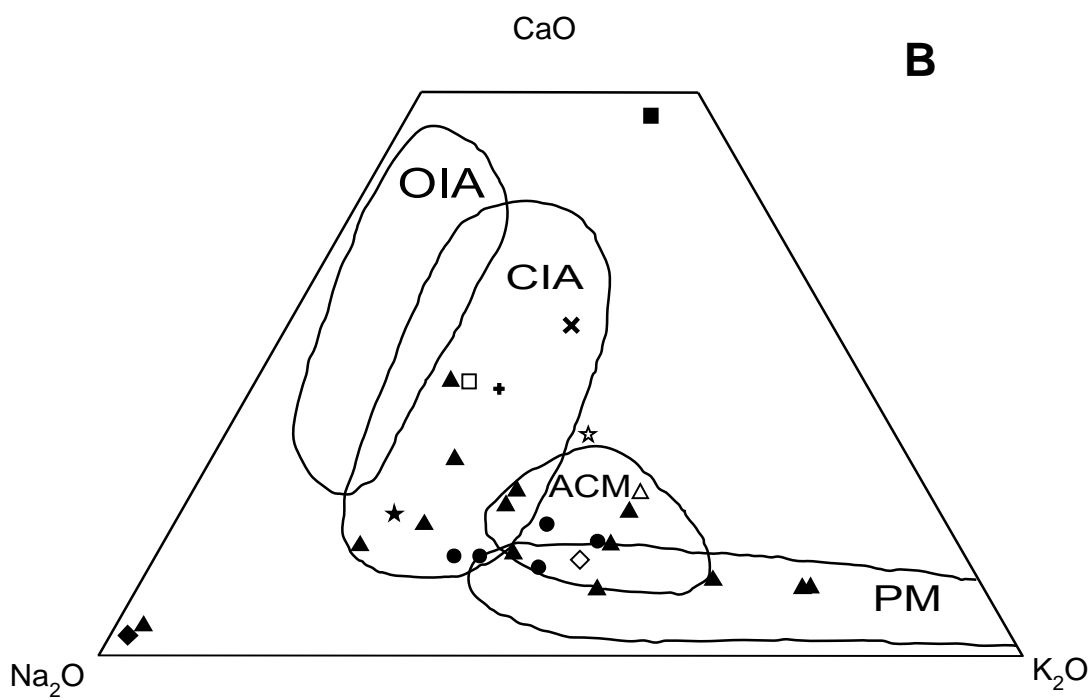
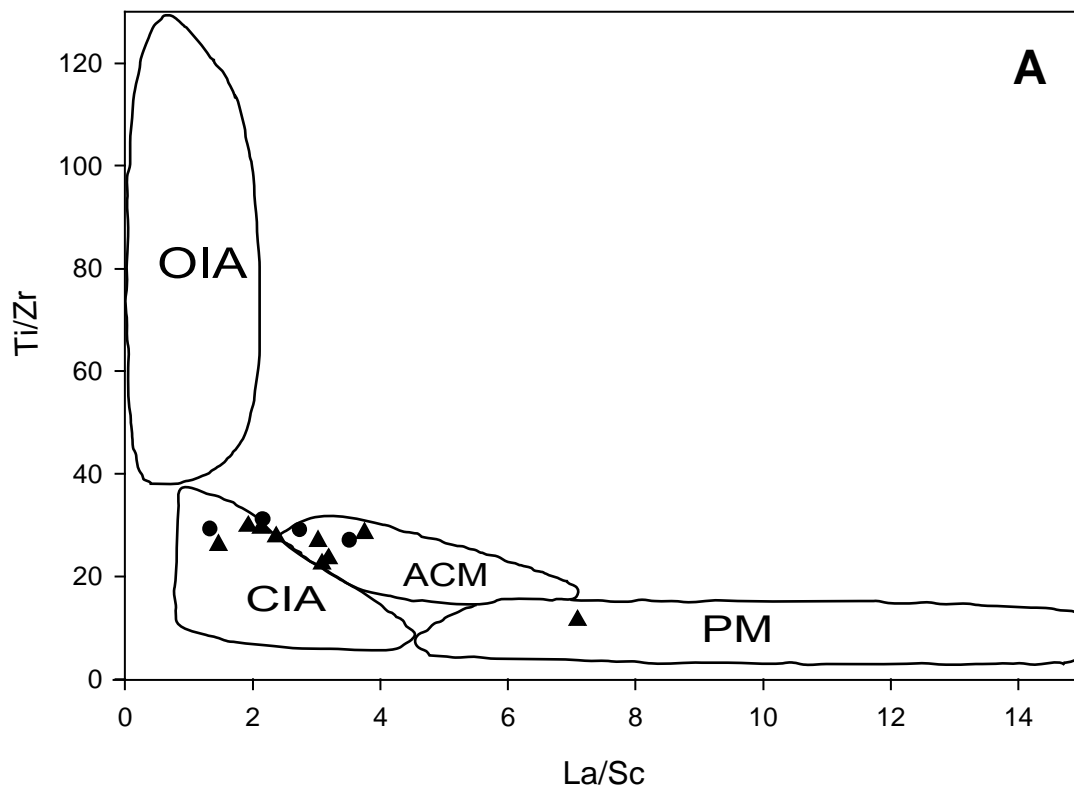
- ▲ Argillite
- Metagreywacke
- ★ Quartzo-feldspathic metagreywacke
- Metagreywacke with biotite
- ◆ Metagreywacke cataclasite
- ◇ Greywacke from Merces quarry (Widdowson, 2009)
- △ Greywacke with biotite (Devaraju et al., 2010)
- Greywacke with chlorite-sericite (Devaraju et al., 2010)
- ☆ Fine grained greywacke (Devaraju et al., 2010)
- + Greywacke (Condie, 1993)
- × Greywacke of Fig Tree, Barberton (Toulkeridis et al., 1999)

Fig. 6.5: Tectonic setting diagrams of metagreywacke:
 A) Plot of K_2O/Na_2O versus SiO_2 (Roser and Korsch, 1986).
 B) Plot of K_2O/Na_2O versus SiO_2 diagram (Roser and Korsch, 1986), modified after Murphy (2000).

The tectonic setting can be inferred from the REE distribution (McLennan et al., 1990; McLennan and Taylor, 1991; Asiedu et al., 2000; Bakkiaraj et al., 2010). The characteristics of rocks from continental margin have LREE $(La/Sm)_N$ enrichment and high total rare earth elements (REE), while rocks from undifferentiated oceanic arc have low $(La/Sm)_N$ ratio, REE content, and lack of negative Eu anomaly. Active Continental Margin have variable negative Eu anomaly in the range of 0.6-1.0 (McLennan, 1989). The present study shows an average of ~ 5 $(La/Sm)_N$ and Eu/Eu^* ratio of 0.73. Hence, these values suggest an Active Continental Margin setting for the metagreywacke of the study area.

Petrological evidence and geochemical data of metagreywacke of the study area suggest that the deposition of the metagreywacke largely occurred in a deep basin which progressively changed to shallow basin of a Continental Island Arc to an Active Continental setting. However, both settings attest to active margin settings, wherein the sediments were either deposited at subduction arc basins, strike-slip margin or in proximal portions in back-arc basins (cf. Alvarez and Roser, 2007).

The Sanvordem Formation is characterized by a basement of conglomerate which is unconformable with thick beds of basal massive metagreywacke and is in turn overlain by graded metagreywacke and argillite. These beds have structural features such as parallel laminations and SSDS.



Contd...

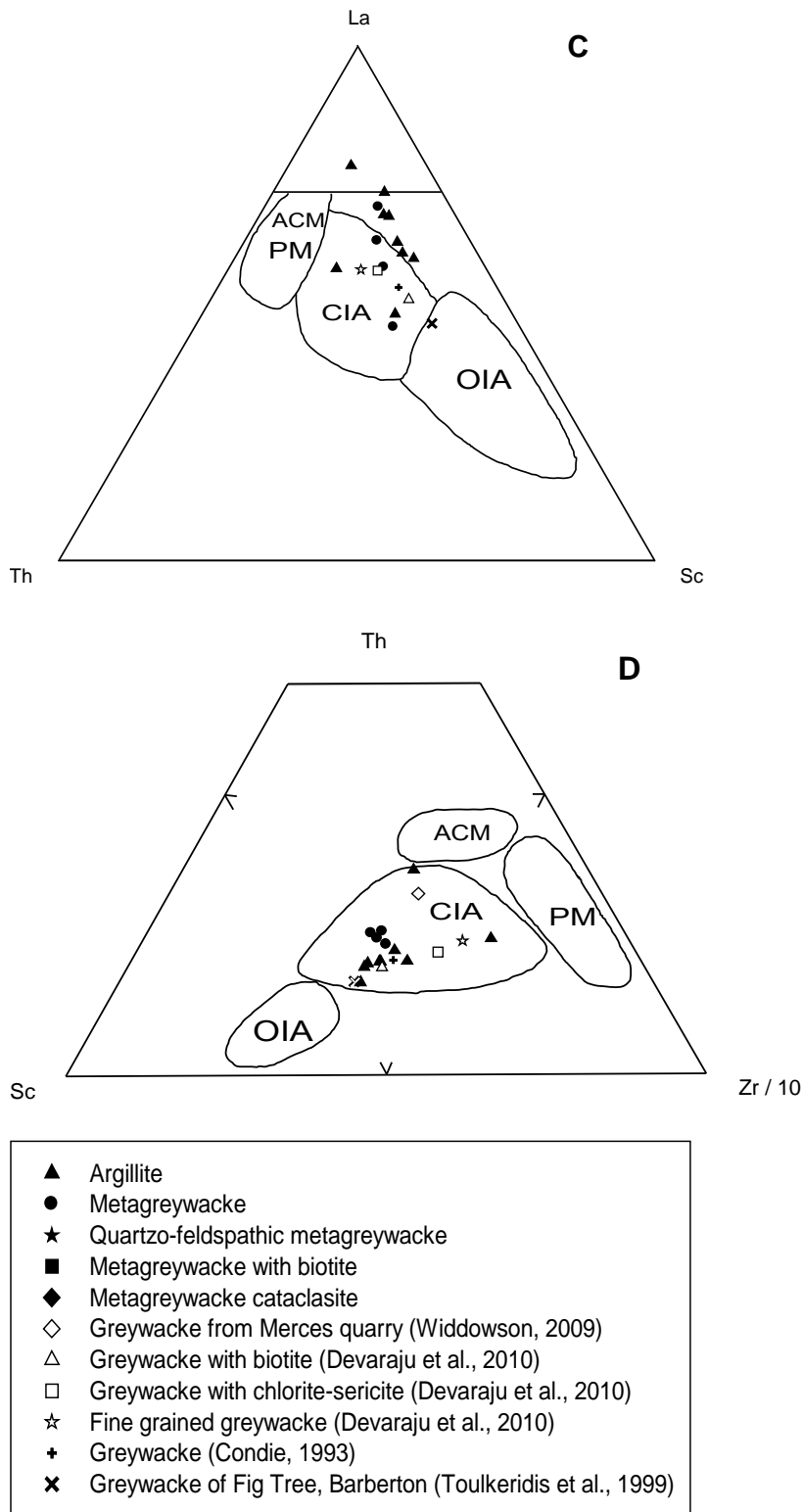


Fig. 6.6: Tectonic setting discriminant diagrams of metagreywacke (after Bhatia and Crook (1986). (OIA = oceanic island arc, CIA = continental island arc, ACM = active continental margin, PM = passive margin):

(A) Ti/Zr vs La/Sc binary plot.

(B) Ternary discriminant diagram of CaO–Na₂O–K₂O.

(C) Ternary discriminant diagram of La–Th–Sc.

(D) Ternary discriminant diagram of Th–Sc–Zr/10.

6.1.5 Bouma sequence

Turbidity current is a mixture of water and detritus flow comprising of mud, silt and sand, which remains in suspension by turbulence. Due to the force of gravity there is downslope movement of the flow creating turbidity current which follows the basin floor. As the turbulence of current decays, sedimentation commences. This resulting facies distribution represents deposition from turbidity currents (cf. Bouma, 1962; Mutti and Ricchi-Luchi, 1978; Valente et al., 2014) and the various structures can be sequentially arranged to form regular units of a Bouma sequence. In the study area, the SSDS are associated with the metagreywacke and are arranged in a regular fashion to obtain a Bouma sequence with 5 ideal units (A to E) (Fig. 6.7, Table 6.1).

The Bouma sequence consists of texture and bedding subdivisions which result from changing hydraulic regimes (Potter et al., 1984; Larsen, 1986; Potter et al., 2012). The various structures exhibited by this entire succession of metagreywacke can be integrated to portray the internal structure of the Bouma sequence in which each surge of turbidite flow produces an individual graded sequence or a turbidite. The SSDS, typically the convolute laminations, are characteristics of turbidites, which imply deformation of either massive or laminated or cross laminated Bouma units. The deformation results due to the dewatering of sediment aided by shear stresses set up by the turbidity flow (Collinson and Thompson, 1982; Valente et al., 2014).

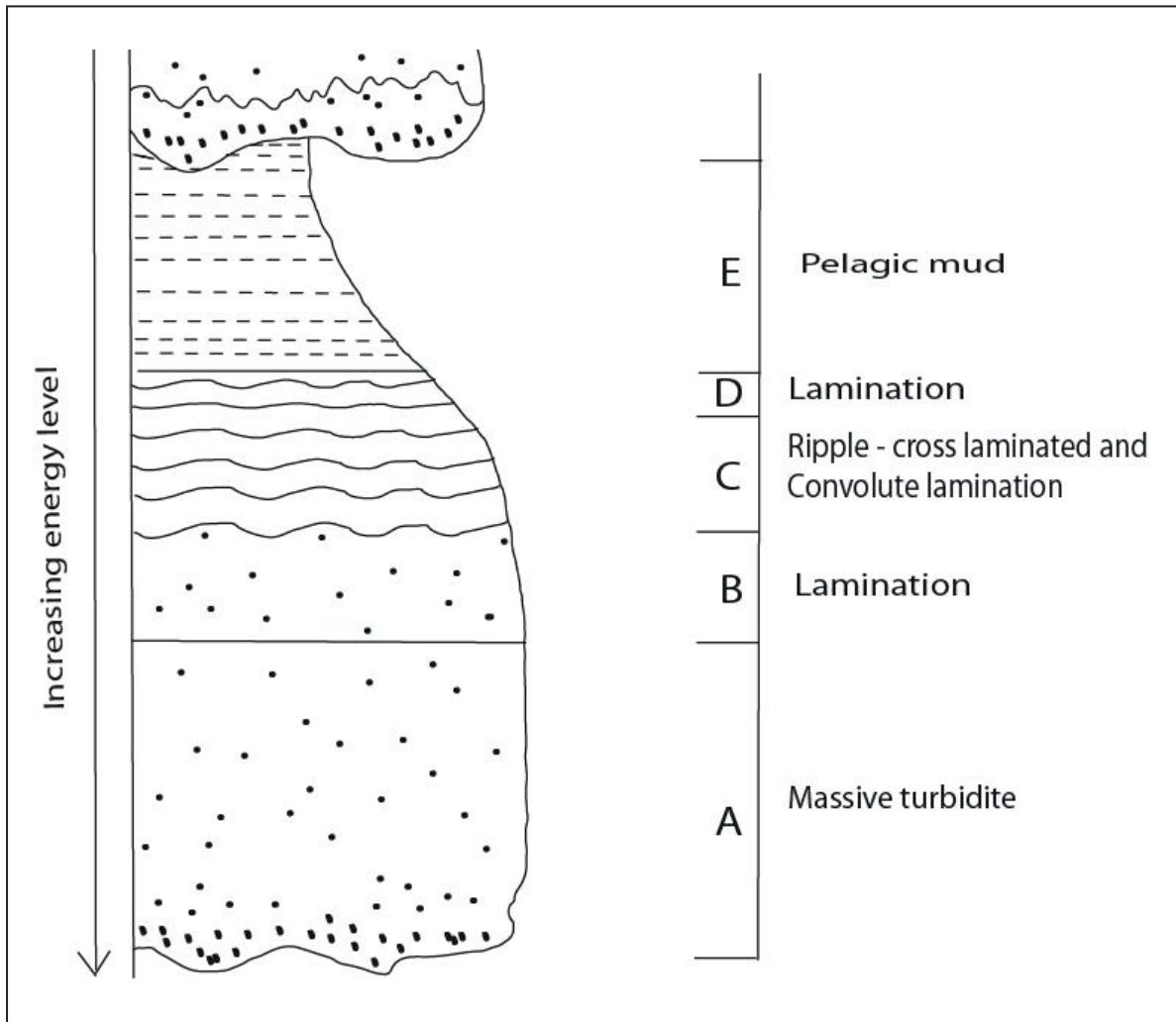


Fig. 6.7: Sketch of the Bouma units in an ideal sequence (Bouma, 1962; Walker, 1965; Middleton and Hampton, 1973).

Table 6.1: Interpretation of the process of formation of an ideal Bouma sequence (Bouma, 1962; Walker, 1965; Middleton and Hampton, 1973) and also of the study area.

| Ideal Bouma unit | | Interpretation | Bouma unit in study area |
|------------------|-------------------------|---|-------------------------------|
| E | Pelagic Mud | Sediments settle from suspension in a basin | Not identified |
| D | Parallel laminae | Sediments settle from suspension in a basin | Parallel laminae present |
| C | Convolute lamination | Penecontemporaneous dewatering | Convolute lamination present |
| | Ripple- Cross laminated | Sedimentation in lower flow regime | Cross lamination present |
| B | Parallel laminae | Sedimentation in high flow regime | Parallel laminae present |
| A | Massive | Rapid deposition of sediment | Massive metagreywacke present |
| | Basal conglomerate | Initial high power erosive phase of the water current | Conglomerate present |

An ideal Bouma sequence has 5 units from A to E. In the present study area there are four units from A to D. The unit A is massive well graded and formed due to the rapid deposition of coarse to fine sediments during the initial surge of turbidity currents. The unit A is succeeded by B unit which is laminated as deposition of planar bed form. This unit is in turn overlain by C unit that formed during low velocity flow deposition and shows convolutions and the various SSDS. Followed by this is D unit with fine laminations that indicate settlement of sediments from suspension in a basin. The E unit of pelagic mud is not identified in the study area. This unit was perhaps eroded (Refer Table 6.1).

The various sedimentary structures and their inferred depositional processes of the metagreywacke in the study area are listed in table 6.1 and 6.2. Based on the various

morphologies of the structures in metagreywacke, the following inferences are drawn regarding the events of formation and evolution (Fig. 6.8) of the basin:

- 1) Turbidite current at continental margin lead to rapid deposition of sediments.
- 2) Initially the coarser deposits produced conglomerates.
- 3) Subsequently the deposition of coarse grained/sand-rich to fine grained/mud-rich sediments occurred.
- 4) Due to the process of liquefaction, during the lithification of these water saturated sediments, the SSDS were formed.
- 5) Deposition of sediments further continued as the SSDS horizon is overlain by undeformed strata.
- 6) Dolerite dykes intruded in the country rocks of metagreywacke leading to the occurrence of cracks and fissures in metagreywacke and along these quartz veins occurred.
- 7) The studied region was locally deformed due to folding and faulting causing a fold and a shear zone. The deformation phase is younger as compared to the dyke emplacement as evident from the sheared quartz veins.

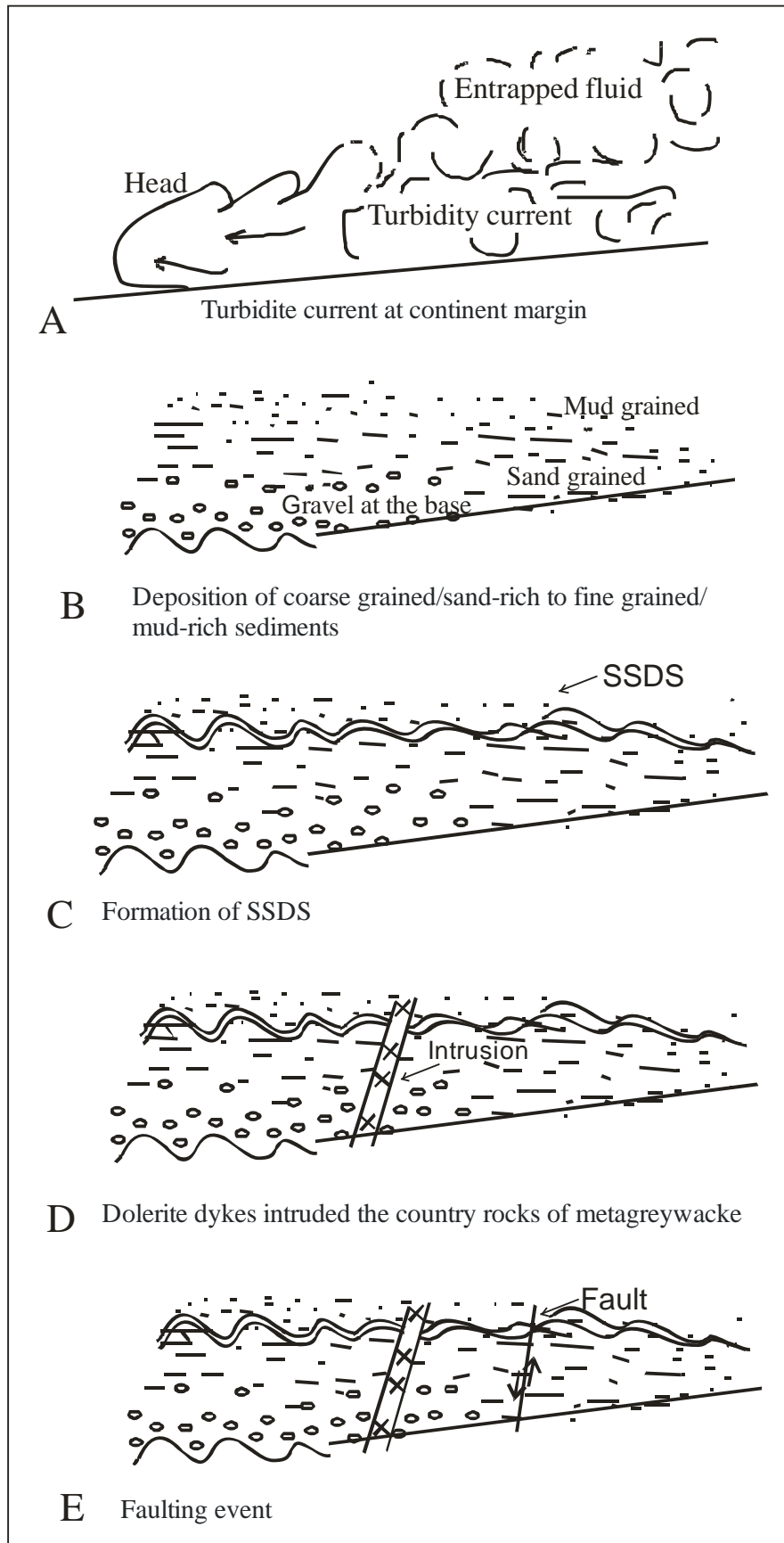













Fig. 6.8: Schematic illustration of a model depicting the phases of basin development in the study area.

Table 6.2: Sedimentary structures and their inferred depositional processes of the heterolithic succession of metaconglomerate and metagreywacke sequence of the study area (Sanvordem Formation).

| Structures | Interpretation | | |
|--|---|---|---|
| Primary depositional structures | | | |
| Dropstone structure (Fig. 3.2B,C) | Dropped fragment cause local distortion and bending of laminae beneath the protuberance |  |  |
| Graded bedding (Fig. 4.3B) | Low density turbidity flow |  | |
| Cross lamination (Fig. 3.2F) | Megaripple bedform migration |  | |
| Liesegang rings (Fig. 3.4A) | Diagenesis or because of rhythmic precipitation |  | |

| Soft sediment deformation structures | | |
|---|---|---|
| Convolute structure (Fig. 3.3A) | Penecontemporaneous dewatering |  |
| Flame and Load structure (Fig. 3.3B) | Differences in viscosity between sediment layers |  |
| Ball and pillow (Fig. 3.3C,D) | Sinking of denser sediments into underlying strata |  |
| Slump Fold (Fig. 3.3E) | When slope of sediments exceed angle of repose, leading to down slope movement of sediments |  |
| Syn-sedimentary faults (Fig. 3.3F) | Brittle deformation when sediments are either unconsolidated or partly consolidated |  |
| Structural deformation structure | | |
| Sheared zone (Fig. 3.4B,C) | Associated with faulting |  |

6.2 Associated rocks

The petrology and geochemistry of the dolerite dykes associated with the metagreywacke aid in interpretation of complex petrogenesis which varies both in space and time. The magmatic behaviour includes fractional crystallization, magma mixing and assimilation which in turn results in triggering of volcanic eruptions (Cox and Hawkesworth, 1985).

6.2.1 Crystallization trend of dolerite dyke

Based on textural and mineralogical observations of the associated dolerite dykes, I now discuss the crystallization process. The texture of dolerite is variable from porphyritic to ophitic / sub-ophitic. The contacts of mineral grains of feldspar and pyroxene commonly have irregular interpenetrating edges indicating simultaneous crystallization of these minerals.

Porphyritic texture in dolerite is exhibited by coarse-grained phenocrysts of plagioclase and also of pyroxene with medium grained groundmass (Fig. 4.5 to 4.7). This texture is attributed to two-stage cooling of the magma that results from the slow crystallization at depth to form phenocrysts, this is followed by rapid cooling of the remaining melt to form the medium grained groundmass. The dolerites exhibit a dominance of plagioclase phenocryst which probably led to commencement of plagioclase crystallization and a delay in pyroxene nucleation leading to supersaturation of pyroxene in the melt. This resulted in formation of many small crystals of pyroxenes in the groundmass. The presence of glomeroporphyritic texture with euhedral plagioclase suggests involvement of feldspar in the evolution of magma (Fig. 4.6D). The plagioclase in dykes is of two generations: medium grained in the groundmass, with simple polysynthetic twinning and coarse grained phenocryst exhibiting oscillatory zoning. Crystallization of plagioclase in the interstices between pyroxene may be

as a result of a higher ratio of nucleation to growth rate of the plagioclase as compared with that of pyroxene.

Besides these various textures, there is presence of plagioclase and apatite as melt inclusions in the host grains of plagioclase and pyroxene (see Fig. 4.5C, 4.6A, B, F). Study of inclusions helps to decipher the order of paragenesis of mineral crystallization. The inference from this texture is:

- 1) The inclusion growth inhibited before the host mineral, only for that particular grain of the host rock.
- 2) The two minerals may have nucleated at exactly the same time, but one grew faster and outlasted the growth of the other.
- 3) The host mineral may have nucleated before the inclusion.

These possibilities depend on the difference in ratio of nucleation rate to growth rate of the two minerals involved. However, elsewhere in the same rock, the included mineral may still be growing.

The comb layering of chert in dolerite (Fig. 4.7B) is a type of unidirectional solidification structure, involving heterogeneous nucleation. Crystallization is forced to occur rapidly in the form of elongate crystals perpendicular to the solid walls of the dolerite producing chert comb layering.

The presence of small, elongate, apatite needles (Fig. 4.5C) in the dolerite dykes attests to their crystallization in the interstitial melt. The stage of their crystallization cannot be determined by textural observations alone. Apatite is seen engulfed by larger grains of plagioclase. However, the occurrence of apatite may reflect the small concentrations of

phosphorus which is relatively insoluble in melts (cf. Watson and Capobianco, 1981; Evans and Hanson, 1993; Vernon, 2004).

Symplectic texture (Fig. 4.7D) seen in dolerites, although rare, is observed as an intergrowth of minerals. It is a replacement texture wherein the plagioclase exceeds pyroxene when unreacted $(\text{Mg, Fe})^{+2}$, together with Na^{+1} from the reacting plagioclase which migrates outward into surrounding plagioclase and reacts with the anorthite molecules to form albite. Ca^{+2} is released in reaction and migrates to evolving symplectites where it enters into clinopyroxene. Similar plagioclase–clinopyroxene intergrowths in dolerites were reported (Gardner and Robins, 1974; Harker, 1909; Ashworth and Chambers, 2000).

The trachytoid texture of plagioclase phenocrysts with the groundmass of plagioclase (Fig. 4.6D) is caused either by flow currents in the magma and/or rotation during crystallisation. The magmatic flow needs sufficient melt for the crystals to passively rotate and align themselves without deforming internally (cf. Paterson et al., 1989; Vernon, 2000).

The plagioclase and pyroxene exhibits concentric zones (Fig. 4.6A, E) which are a type of oscillatory zoning wherein the zones are parallel to the advancing crystal faces. The concentric zones in plagioclase are also seen in which small glass inclusions are present. Minerals such as plagioclase and pyroxene, belonging to solid-solution series continuously react with the surrounding magma melt during crystallization. In order to attain equilibrium during cooling between the growing crystal and the melt, diffusion and ion exchange occur and led to compositional changes giving rise to growth of zones (Allgre et al., 1981). Sector zoning (Fig. 4.5F) identified in dolerites is formed by different crystal faces growing with slightly different chemical compositions (cf. Watson and Liang, 1995; Vernon, 2004). The twins of plagioclase and pyroxene although have same chemical composition, their crystal orientation is different with respect to each other and have a common lattice row or a plane.

The other associated rock identified in the study area is the hornblende schist exhibiting sheafs of ferrhornblende along with quartz-albite aggregates.

6.2.2 Petrogenesis

The geochemistry of dolerite dykes of the study area is compared with related dykes such as: 1) dolerite Deccan-type feeder dyke, Goa (Widdowson et al., 2000) and 2) Desur Lavas, Deccan Traps (Belgaum district, Karnataka) (Hegde et al., 2014). The dolerite samples of the study area plotted on AFM diagram (Fig. 5.5B) indicate a tholeiitic trend indicating well-differentiated magma and defining an iron-enrichment trend (cf. Bose, 1997).

In the plot of MgO against Ni (Fig. 5.6C) the positive correlation of Ni with MgO, suggest that the parent magma is not primary but rather an evolved magma (cf. Mandal et al., 2012). The abundance of the compatible trace element Ni ranges from 38 to 90 ppm which is low as the primary tholeiitic liquids and is consistent with crystallization of olivine fractionation. However, tholeiitic fractionation is significantly controlled by clinopyroxene and plagioclase. Total or high degree of melting of eclogite or amphibolites may give rise to basalts with 5-8% MgO and as such can generate significant amount of liquid leading to rapid flooding and eruption (Hegde et al., 2014). The MgO content of the analysed samples of the study area on an average is 5%, indicating a high degree of melting of the source. The plot of Al₂O₃ vs MgO (Fig. 5.6D) shows positive correlation and is a strong indication of plagioclase fractionation process which is important as MgO content is on an average of 5 wt % (much below 6 wt%; cf. Cox and Hawkesworth, 1985; Riley et al., 2005). The effect of crystallization is quantitatively evaluated using CaO/Al₂O₃ against Mg# plot (Fig. 5.10A) that again suggests plagioclase fractionation.

The high Ba/Zr ratio (average ~2.4) signifies a considerable amount of crustal contamination (typical <1, minimal crustal contamination; Kent and Fitton, 2000). The binary plot of Ce vs

Nd (Fig. 5.10B), elaborates the crustal contaminated magma and also partial melting of the primitive mantle. Plots along the Nd axis would indicate significant range of contamination (Horan et al., 1987). However, the studied dolerite dyke samples plot lie along the calculated melting path between 1% to 5% of the primitive mantle. This range is reported to be consistent within the limits of the tholeiitic magma generation (cf. Langmuir et al., 1977; Bender et al., 1984).

The chondrite normalized REE pattern of the dolerite dykes of the study area (Fig. 5.11) display an LREE enrichment, HREE depletion pattern and a weak negative Eu anomaly. Generally, LREE enrichment and a flat HREE pattern are commonly produced by crustal contamination (cf. Polat et al., 1997). The weak negative Eu anomaly probably owes its presence due to either removal of some plagioclase from a felsic melt by crystal fractionation or by the partial melting of rock in which some feldspar is retained in the source (cf. Rollinson, 1993) and is also indicative of crustal contamination (cf. Sano et al., 2001). In the study area, the Eu anomaly could be as a result of either one or a combination of the above reasons.

Trace elements along with REE data can be used to define the Deccan Trap Basalt Formations so as to provide a comparison with the dykes of Goa and that of the adjacent basalt formation. As such Deccan Formations of Bushe (older), Poladpur, Ambenali and Mahabaleshwar (younger) are comparable to the dykes of Goa (Widdowson et al., 2000). The Poladpur Formation is essentially consistent with contamination by crustal materials probably of granitic type. The Ambenali Formation is less contaminated but is similar to Poladpur. While the Mahabaleshwar Formation consists of basalts derived either from a relatively trace element-enriched mantle source or are contaminated with a different crustal component that affected the Poladpur (Mahoney et al., 1982; Cox and Hawkesworth, 1985).

To correlate the study area samples with the Deccan, bivariate diagrams of TiO_2 against MgO (Fig. 5.6A) and Ba against Sr (Fig. 5.8B) are used. In both bivariate diagrams, among the five dolerite samples, dyke samples from Arambol and Sada plot in Poladpur Formation field.

As the Mg# of Arambol, Sada and Ribandar have a close affinity to the reference samples of Goa dyke and Desur Lava, while the other samples have a lesser range of Mg#. The REE pattern of the dyke of Ribandar and Chimbhel exhibits a weak Eu anomaly. However, Deccan basalts typically do not display Eu anomaly (Widdowson et al., 2000). This indicates that possibly these two dykes (from Arambol and Sada) are of younger generation and related to the post-Deccan Traps that occurred at the end of Deccan volcanism about 63 Ma corresponding to late Mesozoic tectonism, while the other dykes could be the older dykes of Precambrian age. This study can be corroborated by the structural feature of cross cutting relation which is observed at Aguada.

From the above discussion, using the major and trace element geochemistry of the dolerite dykes of Goa, a few dykes show a strong affinity to the Deccan and the related dykes while the other dykes may have been older as that of the Precambrian origin. The dykes showing affinity to Deccan, in particular, resembles the upper stratigraphic unit (Wai Subgroup) of Deccan showing close affinity to the Poladpur Formation. The Wai subgroup comprises about 50% of the Deccan Traps representing a maximum eruptive phase (Widdowson et al., 2000; Self et al., 2006; Rao et al., 2011). Vanderkluyzen et al. (2011) inferred that the dyke systems of western India of Nasik-Pune region and also the coastal swarms are the feeders for the upper Formations of the Wai Sub group (Poladpur, Ambenali and Mahabaleshwar). It is deciphered by various authors (Ernst et al., 2005; Rao et al., 2011) that although Deccan Trap have multiple entry zones through the lithosphere, it is related to a single mantle plume source.

The occurrence of the hornblende schist in the study area owes its formation to be the product of mixing between Deccan basalt magmas and the partial melting of Precambrian amphibolites (cf. Sheth et al., 2009).

6.3 Summary

The metagreywacke suite of rocks comprises of various textures and structures which are a result of the various processes starting from the deposition of sediments to the diagenesis and deformation. Recrystallization and intracrystalline deformation has led to structural deformation of minerals. Low grade metamorphism resulted in green schist facies of rocks with an abundance of chlorite and biotite. With the aid of geochemical signatures of the metagreywacke, the composition, provenance, paleoweathering and tectonic setting were deciphered.

The provenance delineated from the major, trace and REE including Eu anomaly attests to a felsic source. The influence of source rock weathering was determined using chemical index of alteration. The climatic condition during sedimentation of metagreywacke indicates arid type.

Using various major, trace and REE study, it is delineated that the tectonic setting was active continental margin type wherein the sediments are known to be deposited either at subduction arc basins, strike-slip margins, or in proximal portions in back-arc basins.

Based on the textural and structural features of the metagreywacke, the identified Bouma sequence is ascribed to have resulted from turbidity current. A model depicting the phases of basin development is also discussed.

In this chapter, crystallization trend and petrogenesis of dolerite dykes are also discussed. The dykes comprise of plagioclase, pyroxene (augite), apatite, Fe-rich lithic fragment and

ilmenite. The various processes leading to the textural features such as porphyritic, ophitic, presence of inclusions, symplectic and trachytoid are discussed.

Using the geochemical signatures the dykes are found to be tholeiitic and their fractionation was significantly controlled by plagioclase. The effect of crystallization suggests plagioclase fractionation. The rocks have LREE enrichment, HREE depletion and a weak Eu anomaly.

Besides, hornblende schist formation is also reported in the study area with sheafs of ferrohornblende along with quartz-albite aggregates.

Chapter 7

SUMMARY AND CONCLUSION

The State of Goa (India) is situated in the Northwestern part of the Western Dharwar Craton. It is observed that the sedimentary facies and their structures were dependent on the water depth and nature of sediments deposited in the basin.

With the aid of petrological attributes, the metagreywacke of Sanvordem Formation, Goa Group is distinguished into five petrofacies: metagreywacke; quartzo-feldspathic metagreywacke; metagreywacke with biotite; metagreywacke cataclasite and argillite. The Sanvordem Formation of Goa Group is dominated by clastics. This is formed due to deposition of load from a turbulent turbidity current which remained in suspension until it slowed down, leading to deposition of coarse grains to the base of the flow forming a conglomerate with extraneous pebbles. The units grading upwards from a well-graded metagreywacke (A), through a laminated (B), followed by a cross laminated unit (C) and a laminated unit (D). These units are identified in the field to form and resemble a substantial part of the Bouma sequence. The rapid deposition of saturated sediments led to the formation of the SSDS. This event of deposition was followed by folding process. The intrusion of dolerite dykes into the country rock led to the occurrence of various quartz veins which in turn was followed by faulting in the region.

This is for the first time that SSDS have been delineated in the metagreywacke facies of Goa Group and also the presence of dropstone structure seen in conglomerates and liesegang rings in metagreywacke. Regional geology and structural data also attest to the presence of Bouma sequence. All these structures are indicative of a turbidite depositional environment which largely occurred in a deep basin which progressively changed to a shallow basin environment.

The mineralogy, modal data and microstructures are significant parameters to delineate the diagenetic and post-diagenetic modifications. Diagenesis is noted by the presence of variable texture exhibited by the minerals such as:

- 1) The presence of pressure solution stylolites and fracturing of detrital mineral grains that indicates compaction.
- 2) Pitted appearance in detrital grains of quartz and feldspars that suggest dissolution.
- 3) Lobate contacts and overgrowth in quartz formed due to compaction.
- 4) Precipitation along fractures as a result of cementation of silica.

A transition from advanced diagenesis to early metamorphism is noted from the phyllomorphic stage that led to the commencement of mica formation. Recrystallization and the presence of triple junction in quartz are evidences of the initiation of the metamorphic processes. Intracrystalline deformation exhibited by the kink folds identified in feldspars, undulose and wavy extinction in quartz and mica also attest to metamorphism. Further, the metamorphic character is clearly indicated by schistosity. 'Metagreywacke with biotite' exhibits a schistose texture.

To understand the geochemical attributes, the metagreywacke of the study area is compared with the average data of greywacke from Merces, Goa, Goa-Dharwar sector, Late Archaean (3.5-2.5 Ga) greywacke and Fig Tree, Barberton (South Africa). The geochemical characteristics of metagreywacke of the study area indicate a dominance of quartzose sedimentary provenance with subordinate amount of mafic igneous provenance. The trace elements such as La, Sc, Th and Co suggests felsic nature of the source rocks and this is supported by the REE pattern and negative Eu anomaly of 0.73. The felsic source indicates that the main source was that of feldspar-bearing granodiorite rocks.

The trace elements such as Th, U and La are widely used to understand the source of clastic sedimentary rocks. The analyzed metagreywacke shows an average Th/U ratio of 2.25 and La/Th ratio is 4.683. These values indicate a provenance closer to dacitic to quartzose sedimentary rocks composition.

Paleoweathering in the source area affects widely the composition of sedimentary rocks and is in turn governed by source rock composition, duration of weathering, climatic conditions and rate of tectonic uplift of source region amongst the other factors. The chemical index of alteration (CIA) value ranges from 63 to 84. There is a consistent trend of CIA with increasing silica content indicating that CIA is constant during alteration. Evaluating the major oxides mobility of elements on an A-CN-K ternary diagram, indicates absence of potash metasomatism during diagenesis. However, the slight amount of added potassium is due to the presence of clastic grains of K-feldspar, provided as an evidence for detrital nature of K-bearing phases.

The tectonic setting discrimination diagrams and the trace element data of the metagreywacke of the study area attest to active continental margin setting. Further, in the active continental margin settings, the sediments are either deposited at subduction arc basins or strike-slip margins or in proximal portions in back-arc basins. Also, the analysis of trace and REE constrains the average composition of the terrains exposed at the time of deposition to be that of Archean.

The intrusion of **dolerite dykes** within the country rocks of metagreywacke was studied based on field, petrographic and geochemical composition. The dolerite dykes of Goa mainly comprise of plagioclase, pyroxene (augite) with accessories of apatite, Fe-rich lithic fragments and ilmenite. The mineralogy and textural characteristics attest to a higher ratio of nucleation rate to growth rate of the plagioclase as compared with that of pyroxene. The presence of apatite needles in dolerite reflects the small concentrations of phosphorus which is relatively insoluble in melts.

Amongst the dolerite dykes studied from Goa, two of the dykes (Arambol and Sada) represent younger generation dykes and related to the post-Deccan Traps that occurred at the

end of Deccan volcanism about 63 Ma corresponding to late Mesozoic tectonism, while the other dykes could be the older dykes of Precambrian age. This study can be corroborated by the structural feature of cross cutting relation which is observed at Aguada. This indicates the younger dyke to be related to Deccan eruption while the older dyke to be of a much older age, possibly Precambrian age.

The dykes of the study area range in composition from basalt to basaltic andesite. The relation between various major oxides and Mg# as well as trace elements suggests that the dykes formed from an evolved magma and that fractionation was controlled by plagioclase. Plagioclase fractionation is supported by the correlation of MgO with Al₂O₃ and was evaluated from the trend of Mg# with CaO/Al₂O₃. The negative Eu anomaly owes its presence due to either removal of plagioclase from a felsic melt by crystal fractionation or by the partial melting of rock in which feldspar is retained in the source.

The behaviour of trace elements such as Nd and Ce is consistent with the limits of the tholeiitic magma generation. The LREE enrichment, HREE depletion pattern and a weak negative Eu anomaly, possibly imply a low degree of melting than crustal contamination. Further, these dolerite dykes exhibit an affinity to continental basalts and to a lesser extent to ocean island basalt.

The hornblende schist is reported for the first time, comprising of ferrohornblende, quartz and albite with minor presence of biotite and opaques. This owes its occurrence to various dykes and sills that are reported to be product of mixing between Deccan basalt magmas and the partial melting of Precambrian amphibolites.

7.1 Epilogue

The Sanvordem Formation of Goa Group is a turbidite deposit with conglomerate at the base followed by metagreywacke litho units. This resembles a Bouma sequence. The provenance

for the sediments deposition attests to a felsic source. Petrological and geochemical data suggest that the deposition of the metagreywacke largely took place in a deep basin that progressively changed from that of a continental island arc to a shallow basin of active continental setting. Subsequent to the deposition of sediments, the basin underwent tectonic disturbances which led to the three cycles of folding events of the country rocks and intrusion of dolerite dykes.

Future work on the age of metagreywacke and sequence stratigraphy would help to understand the basin and the exact cause of the various SSDS present in the study area. A thorough study on the intrusion of dolerite dykes with respect to its age determination would help to understand the exact timing and the generation of dykes. This would in turn help to delineate the plume or/and the mantle magma activity at the time of its intrusion. Once an integrated study is carried out, the metagreywacke can be well related to Dharwar Group of rocks and the dolerite dykes of Goa can be correlated to the Deccan activity and or the Precambrian dyke emplacement activity.

REFERENCES

1. Allègre, C. J., Provost, A., Jaupart, C. (1981). Oscillatory zoning: a pathological case of crystal growth. *Nature*, 294(5838), 223-228.
2. Allen, J.R.L. (1982). *Developments in Sedimentology: Sedimentary Structures: Their Character and Physical Basis*, II (30), Elsevier, Amsterdam, 343-393.
3. Alsop, G. I, Marco, S. (2013). Seismogenic slump folds formed by gravity-driven tectonics down a negligible subaqueous slope. *Tectonophysics*, 605, 48–69.
4. Alvarez, N. C., Roser, B. P. (2007). Geochemistry of black shales from the Lower Cretaceous Paja Formation, Eastern Cordillera, Colombia: Source weathering, provenance, and tectonic setting. *Journal of South American Earth Sciences*, 23(4), 271-289.
5. Anketell, J.M., Cegla, J., Dzulynsky, S. (1970). On the deformational structures in systems with reversed density gradients. *Annales Societatis Geologorum Pololiae*, 40, 3–30.
6. Araújo, C.E.G., Pinéo, T.R.G., Caby, R., Costa, F.G., Cavalcante, J.C., Vasconcelos, A.M., Rodrigues, J.B. (2010). Provenance of the Novo Oriente Group, southwestern Ceará Central Domain, Borborema Province (NE-Brazil): A dismembered segment of a magma-poor passive margin or a restricted rift-related basin? *Gondwana Res.*, 8, 497- 513.
7. Armstrong-Altrin, J.S., Verma, S.P. (2005). Critical evaluation of six tectonic setting discrimination diagrams using geochemical data of Neogene sediments from known tectonic setting. *Sediment Geol*, 177, 115– 129.
8. Armstrong-Altrin, J.S., Lee, Y.I., Verma, S.P., Ramasamy, S. (2004) Geochemistry of sandstones from the upper Miocene Kudankulam formation, Southern India: Implications for provenance, weathering, and tectonic setting. *Jour. Sed. Res.*, 74(2), 285-297.

9. Armstrong-Altrin, J.S. (2009). Provenance of sands from Cazones, Acapulco, and Bahía Kino beaches, Mexico, *Revista Mexicana de Ciencias Geológicas*, 26(3), 764-782.
10. Ashworth, J. R. Chambers, A.D. (2000) symplectic reaction in olivine and the controls of intergrowth spacing in symplectites. *Journal of Petrology*. 41 (2), 285-304.
11. Asiedu, D. K., Suzuki, S., Nogami, K., Shibata, T. (2000). Geochemistry of Lower Cretaceous sediments, Inner Zone of Southwest Japan: Constraints on provenance and tectonic environment. *Geochem. Jour.*, 34, 155-173.
12. Asiedu, D.K., Dampare, S. B., Asamoah Sakyi, P., Banoeng-Yakubo, B., Osaе, S., Nyarko, B. J. B., Manu, J. (2004). Geochemistry of Paleoproterozoic Metasedimentary Rocks from the Birim diamondiferous field, southern Ghana: Implications for provenance and crustal evolution at the Archean-Proterozoic boundary. *Geochemical Journal*, 38, 215-228.
13. Auden, J. B. (1949). A geological discussion on the Satpura hypothesis and Garo-Rajmahal gap. In *Proc. Natl. Inst. Sci. of India*.15, 55.
14. Bakkiaraj, D., Nagendra, R., Nagarajan, R., Armstrong-Altrin, J.S. (2010). Geochemistry of sandstones from the Upper Cretaceous Sillakkudi Formation, Cauvery Basin, southern India: Implication for provenance. *J Geol Soc India*, 76, 453-467.
15. Baksi, A.K. (1995). Petrogenesis and timing of volcanism in the Rajmahal flood basalt province, northeastern India. *Chemical Geol.*, 121, 73-90.
16. Balakrishnan, S., Hanson, G.N., Rajamani, V., 1990. Pb and Nd isotope constraints on the origin of high Mg and tholeiite amphibolites, Kolar schist belt, southern India. *Contrib. Mineral. Petrol.* 107, 272–292.

17. Balakrishnan, S., Rajamani, V, Hanson, G.N. (1999). U-Pb ages for zircon and titanite from the Ramagiri area, Southern India: evidence for accretionary origin of the eastern Dharwar Craton during the late Archean. *Jour. Geol.*, 107, 69 -86.
18. Balaram, V., Rao, T.G. (2003). Rapid determination of REEs and other trace elements in geological samples by microwave acid digestion and ICP-MS. *Atomic Spectroscopy*, 24, 206-212.
19. Banerjee, A., Banerjee, D. M. (2010). Modal analysis and geochemistry of two sandstones of the Bhandar Group (Late Neoproterozoic) in parts of the Central Indian Vindhyan basin and their bearing on the provenance and tectonics. *Journal of Earth System Science*, 119, 825–839.
20. Bavinton, O.A., Taylor, S.R. (1980). Rare earth element abundances in Archean metasediments from Kambalda, Western Australia. *Geochimica et Cosmochimica Acta*, 44, 639-648.
21. Bender, J.F., Langmuir, C.H., Hanson, G.N. (1984). Petrogenesis of basalt glasses from the Tamayo region, East Pacific Rise. *Jour. Petrol.*, 25, 213-254.
22. Bhatia, M.R. (1983). Plate tectonics and geochemical composition of sandstones. *Journal of Geology*, 91, 611-627.
23. Bhatia, M.R., Crook, K.A.W. (1986). Trace element characteristics of greywacke and tectonic setting discrimination of sedimentary basins. *Contribution to Mineralogy and Petrology*, 92, 181-193.
24. Bhatia, M. R., Taylor, S. R. (1981). Trace-element geochemistry and sedimentary provinces: a study from the Tasman Geosyncline, Australia. *Chemical Geology*, 33(1), 115-125.
25. Blatt, H., Middleton, G.V., Murray, R. (1980). *Origin of sedimentary rocks*. Englewood Cliffs, NJ, Prentice-Hall.

26. Blenkinsop, T. (2000). *Deformation Microstructures and Mechanisms in Minerals and Rock*. Kluwer Academic Press.
27. Bose, M.K. (1997). *Igneous petrology*. Calcutta: World Press, 358.
28. Bouma, A.H. (1962). *Sedimentology of some Flysch Deposits: A Graphic Approach to Facies Interpretation*. Elsevier, Amsterdam, 168.
29. Bouma, A.H. (2004). Key controls on the characteristics of turbidite systems. *Geological Society, Special Publications, London, 222*, 9-22.
30. Bowman, D., Korjenkov, A., Porat, N. (2004). Late-Pleistocene seismites from Lake Issyk-Kul, the Tien Shan range, Kyrghyzstan. *Sedimentary Geology, 163 (3-4)*, 211–228.
31. Brenchley, P. J., Newall, G. (1977). The significance of contorted bedding in upper Ordovician sediments of the Oslo region, Norway. *Journal of Sedimentary Petrology, 44*, 819–833.
32. Brodzikowski, K., Gotowała, R., Hałaszcak, A., Krzyszkowski, D., Van Loon, A.J. (1987). Soft sediment deformations from glaciodeltaic, glaciolacustrine and fluviolacustrine sediments in the Kleszczów Graben (central Poland). In: Jones, M.E., Preston, R.M.F. (Eds.), *Deformation of sediments and sedimentary rocks*. Geological Society Special Publication, 29, 255–267.
33. Brown, C. E., Thayer, T. P. (1963). Low-grade mineral facies in Upper Triassic and Lower Jurassic rocks of the Aldrich Mountains, Oregon. *Journal of Sedimentary Research, 33(2)*.
34. Brück, P. M. (1972). Stratigraphy and sedimentology of the Lower Palaeozoic greywacke formations in Counties Kildare and West Wicklow. In *Proceedings of the Royal Irish Academy. Section B: Biological, Geological, and Chemical Science*, Royal Irish Academy, 25-53.

35. Campbell, I.H., Griffiths, R.W. (1990). Implications of mantle plume structure for the evolution of flood basalts. *Earth Planet. Sci. Lett.*, 99, 79-93.
36. Carl, J.D., Amstutz, G.C. (1958). Three dimensional Liesegang rings by diffusion in a colloidal matrix and their significance for the interpretation of geological phenomenon. *Geological Society of America Bulletin*, 69, 1467-1468.
37. Carozzi, A.V. (1960). *Microscopic sedimentary petrology*. John Wiley & Sons, New York – London, 8-79.
38. Carranza-Edwards, A., Kasper-Zubillaga, J.J., Rosales-Hoz, L., Alfredo-Morales, E., Santa-Cruz, R.L. (2009). Beach sand composition and provenance in a sector of the southwestern Mexican Pacific. *Revista Mexicana de Ciencias Geológicas*, 26(2), 433-447.
39. Chadwick, B., Vasudev, V.N., Hegde, G.V. (1997). The Dharwar Craton, southern India, and its late Archean plate tectonic setting: current interpretation and controversies. *Proc. Indian Acad. Sci. (Earth Planet Sci.)*, 106(4), 249-258.
40. Chakrabarti, G., Shome, D., Bauluz, B., Sinha, S. (2009). Provenance and Weathering History of Mesoproterozoic Clastic Sedimentary Rocks from the Basal Gulcheru Formation, Cuddapah Basin, India. *Jour. Geol. Soc. India*, 74, 119-130.
41. Chakrabarti, R., Basu, A.R., Chakrabarti, A. (2007). Trace element and Nd-isotopic evidence for sediment sources in the mid-Proterozoic Vindhyan Basin, Central India. *Precambrian Res.*, 159, 260-274.
42. Rao, N. C., Burgess, R., Lehmann, B., Mainkar, D., Pande, S. K., Hari, K. R., & Bodhankar, N. (2011). $^{40}\text{Ar}/^{39}\text{Ar}$ ages of mafic dykes from the Mesoproterozoic Chhattisgarh basin, Bastar craton, Central India: implication for the origin and spatial extent of the Deccan Large Igneous Province. *Lithos*, 125(3), 994-1005.
43. Chamley, H. (2013). *Clay sedimentology*. Springer Science & Business Media.

44. Chuhan, F.A., Kjeldstad, A., Bjorlykke, K., Hoeg, K. (2000). Porosity loss by sand grain crushing-experimental evidence and relevance to reservoir quality. *Mar. Petrol. Geol.*, 19, 39-53.
45. Chunga, K., Livio, F., Michetti, A.M., Serva, L. (2007). Synsedimentary deformation of Pleistocene glaciolacustrine deposits in the Albese con Cassano Area (Southern Alps, Northern Italy), and possible implications for paleoseismicity. *Sedimentary Geology*, 196, 59–80.
46. Cojan, I., Thiry, M. (1992). Seismically induced deformation structures in Oligocene shallow-marine and eolian coastal sands (Paris Basin). *Tectonophys*, 206, 79–89.
47. Collier, J.S., Sansom, V., Ishiuka, O., Taylor, R.N., Minshull, T.A., Whitmarsh, R.B., 2008. Age of Seychelles–India break-up. *Earth and Planetary Science Letters* 272, 264–277.
48. Collinson, J.D. (2003). Deformation of sediments. In: Middleton, G.V. (Eds.), *Encyclopedia of sediments and sedimentary rocks*. Kluwer Academic Publishers, Dordrecht, 190–193.
49. Collinson, J.D., Thompson, D.B. (1982). *Sedimentary Structures*. Allen and Unwin, London.
50. Condie, K. C., Wronkiewicz, D. J. (1990). The Cr/Th ratio in Precambrian pelites from the Kaapvaal Craton as an index of craton evolution. *Earth and Planetary Science Letters*, 97(3-4), 256-267.
51. Condie, K.C., Mackie, J.E., Reimer, T.O., (1970). Petrology and geochemistry of Early Precambrian greywacke from the Fig Tree Group, South Africa. *Geological Society of American Bulletin*, 81, 2759-2776.
52. Condie, K. C. (1993). Chemical composition and evolution of the upper continental crust: contrasting results from surface samples and shales. *Chemical geology*, 104(1-4), 1-37.

53. Condie, K.C., Lee, D., Farmer, L. (2001). Tectonic setting and provenance of the Neoproterozoic Uinta Mountain and Big Cootonwood groups, northern Utah: constraints from geochemistry, Nd isotopes, and detrital modes. *Sediment. Geol.*, 141-142, 443-464.
54. Cox, K. G., Clifford, P. (1982). Correlation coefficient patterns and their interpretation in three basaltic suites. *Contributions to Mineralogy and Petrology*, 79(3), 268-278.
55. Cox, R., Lowe, D.R. (1995). A conceptual review of regional-scale controls on the composition of clastic sediment and the co-evolution of continental blocks and their sedimentary cover. *J Sediment Res*, 65, 1–21
56. Cox, K.G., Hawkesworth, C. (1985). Geochemical stratigraphy of the Deccan Traps at Mahabaleshwar, Western Ghats, India, with implications for open system magmatic processes. *Journal of Petrology*, 26, (2), 355-377.
57. Crook, K.A.W. (1974). Lithogenesis and geotectonics: the significance of compositional variations in flysch arenites (greywacke), In: *Modern and ancient geosynclinal sedimentation* Dott, R.H. and Shaver, R.H. (eds), SEPM Special Publication, 19, 304-310.
58. Cullers, R. L. (1995). The controls on the major-and trace-element evolution of shales, siltstones and sandstones of Ordovician to Tertiary age in the Wet Mountains region, Colorado, USA. *Chemical Geology*, 123(1-4), 107-131.
59. Cullers, R. L. (2000). The geochemistry of shales, siltstones and sandstones of Pennsylvanian–Permian age, Colorado, USA: implications for provenance and metamorphic studies. *Lithos*, 51(3), 181-203.
60. Cullers, R.L., Podkovyrov, V.N. (2000). Geochemistry of the Mesoproterozoic Lakhanda shales in southeastern Yakutia, Russia: implications for mineralogical and provenance control, and recycling. *Precambrian Res*, 104(1–2), 77–93

61. Cullers, R.L. (1994). The controls on the major and trace element variation of shales, siltstones and sandstones of Pennsylvanian–Permian age from uplifted continental blocks in Colorado to platform sediment in Kansas, USA. *Geochim Cosmochim Acta*, 58, 4955–4972.
62. Cullers, R.L. (1995). The controls on the major- and trace- elements evolution of shales, siltstones and sandstones of Ordovician to Tertiary age in the Wet Mountains region, Colorado, USA. *Chemical Geology*, 123, 107-131.
63. Cullers, R. L. (2002). Implications of elemental concentrations for provenance, redox conditions, and metamorphic studies of shales and limestones near Pueblo, CO, USA. *Chemical Geology*, 191(4), 305-327.
64. Dayal, A.M., Murthy, S.N. (2006). Geochemistry of Pakhal Shales. *Jour. Geol. Soc. India*, 67, 770–776.
65. Dessai, A.G. (2011). The Geology of Goa: Revisited. *Journal of Geological Society of India*, 78, 233-242.
66. Dessai, A. G., Downes, H., López-Moro, F. J., López-Plaza, M. (2008). Lower crustal contamination of Deccan Traps magmas: evidence from tholeiitic dykes and granulite xenoliths from western India. *Mineralogy and Petrology*, 93(3-4), 243-272.
67. Devaraju, T.C., Huhma, H.C., Kaukonen, R.J., Allapieti, T.T. (2007). Petrology, geochemistry, model Sm-Nd ages and petrogenesis of the granitoids of the northern block of western Dharwar craton. *Jour. Geol. Soc. India*, 70, 889-911.
68. Devaraju, T. C., Sudhakar, T.L., Kaukonen, R. J., Viljoen, R.P., Alapieti, T.T., Ahmed, S.A., Sivakumar, S. (2010). Petrology and geochemistry of graywackes from Goa-Dharwar sector, western Dharwar craton: implications for volcanoclastic origin. *Jour. Geol. Soc. India*, 75, 465-487.

69. Devey, C. W., Lightfoot, P. C. (1986). Volcanological and tectonic control of stratigraphy and structure in the western Deccan Traps. *Bulletin of Volcanology*, 48(4), 195-207.
70. Dey, S., Rai, A.K., Chaki, A. (2009). Palaeoweathering, composition and tectonics of provenance of the Proterozoic intracratonic Kaladgi-Badami basin, Karnataka, southern India: Evidence from sandstone petrography and geochemistry. *Jour. South Asian Earth Sci.*, 34(6), 703-715.
71. Dey, S., Pandey, U.K., Rai, A.K., Anjan Chaki. (2012). Geochemical and Nd isotope constraints on petrogenesis of granitoids from NW part of the eastern Dharwar craton: possible implications for late Archaean crustal accretion. *Jour. Asian Earth Sci.*, 45, 40-56.
72. Dhepe, P.D., (1953). A note on the geology, iron and manganese ore deposits of Goa. *Poona Univ. J. Sci. Tech*, 2(4), 27-36.
73. Dhoundial, D. P., Sarkar, D. K., Trivedi, J. R., Gopalan, K., Potts, P. J. (1987). Geochronology and geochemistry of Precambrian granitic rocks of Goa, southwest India. *Precambrian Res.*, 36, 287-302.
74. Dickinson, W.R., Suczek, C.A. (1979). Plate tectonics and sandstone compositions. *American Association of Petroleum Geological Bulletin*, 63, 2164-2182.
75. Dickinson, W.R., Valloni, R. (1980). Plate settings and provenance of sands in modern ocean basins. *Geology*, 8, 82-86.
76. Dickinson, W.R., (1985). Interpreting provenance relations from detrital modes of sandstones. In: Zuffa, G.G. (Ed.), *Provenance of Arenites*. D. Reidel Publ. Co, New York, N.Y., 333–361.
77. Dunn, J.A. (1942). Manganese ore. *Rec. Geol. Surv. India*, 76, 1-53.
78. Ernst, R.E., Buchan, K.L., Campbell, I.H., (2005). Frontiers in large igneous province research. *Lithos* 79, 271–297.

79. Evans, O. C., Hanson, G. N. (1993). Accessory-mineral fractionation of rare-earth element (REE) abundances in granitoid rocks. *Chemical Geology*, 110(1-3), 69-93.
80. Fadipe, O.A., Carey, P.F., Akinlua, A., Adekola, S.A. (2011). Restricted Access Provenance, Diagenesis and Reservoir Quality of the Lower Cretaceous Sandstone of the Orange Basin, South Africa *South African Journal of Geology*. 114(3-4), 433-448.
81. Feary, D. A. (1979). Geology of the Urewera Greywacke in Waioeka Gorge, Raukumara Peninsula, New Zealand, *New Zealand Journal of Geology and Geophysics*, 22(6), 693-708.
82. Fedo, C.M., Nesbitt, H.W., Young, G.M. (1995). Unraveling the effects of potassium metasomatism in sedimentary rocks and paleosols, with implications for weathering conditions and provenance. *Geology*, 23(10), 921–924.
83. Fedo, C.M., Eriksson, K.A., Krogstad, E.J. (1996). Geochemistry of shales from the Archaean (~ 3.0 Ga) Buhwa Greenstone Belt, Zimbabwe: implications for provenance and source-area weathering. *Geochim. Cosmochim. Acta* 60, 1751-1763.
84. Feng, R., Kerrich, R., (1990). Geochemistry of fine-grained clastic sediments in the Archaean Abitibi greenstone belt, Canada: implications for provenance and tectonic setting. *Geochim. Cosmochim. Acta*, 54, 1061-1081.
85. Feng, R., Kerrich, R., Mass, R., (1993). Geochemical, oxygen, and neodymium isotope compositions of metasediments from the Abitibi greenstone belt and Pontiac subprovince Canada: evidence for ancient crust and Archaean terrain juxtaposition. *Geochim. Cosmochim. Acta*, 57, 641-658.
86. Fermor, L.L. (1909). Manganese ore deposits of India, *Mem. Geol. Surv. India*, 37, 1-371.

87. Fernandes, G.Q., Iyer, S.D., Kotha, M. (2016a). Origin and tectonic setting of Precambrian greywacke of Ribandar-Chimbel, Goa, India: Petrological and geochemical Evidences. *Acta Geologica Sinica, English Edition*, 90(6), 2036–2048.
88. Fernandes, G.Q., Kotha, M., Iyer, S.D. (2016b). Diagenesis and deformation of the metagreywacke-argillite suite (Goa Group). *Proceedings of National Geo-Research Scholars Meet, Wadia Institute of Himalyan Geology, Dehradun, Uttrakhand.*
89. Fernandes, O.A. (2009). Physiography and general geology of Goa. In: *Natural Resources of Goa: A Geological Perspective*. Eds. Mascarenhas A., Kalavampara G. Geological Society of Goa, 11-24.
90. Floyd, P. A., Shail, R., Leveridge, B. E., Franke, W. (1991). Geochemistry and provenance of Rhenohercynian synorogenic sandstones: implications for tectonic environment discrimination. *Geological Society, London, Special Publications*, 57(1), 173-188.
91. Floyd, P. A., Winchester, J. A., Park, R. G. (1989). Geochemistry and tectonic setting of Lewisian clastic metasediments from the Early Proterozoic Loch Maree Group of Gairloch, NW Scotland. *Precambrian Research*, 45(1-3), 203-214.
92. Folk, R. L., Andrews, P. B., Lewis, D. W. (1970). Detrital sedimentary rock classification and nomenclature fm use in New Zealand. *N.Z. Journal of Geology and Geophysics*, 13(4), 937-68.
93. Garcia, D., Ravenne, C., Maréchal, B., Moutte, J. (2004). Geochemical variability induced by entrainment sorting: quantified signals for provenance analysis. *Sediment. Geol.*, 171(1-4), 113-128.
94. Gardner, P.M., Robins, B. (1974). The Olivine-Plagioclase Reaction: Geological Evidence from the Seiland Petrographic Province, Northern Norway. *Contr. Mineral. and Petrol.*, 44, 149-156.

95. Geological Survey of India (GSI) (1996). Geological and Mineral Map of Goa. Government of India.
96. Ghosh, S. K., Pandey, A. K., Pandey, P., Ray, Y., Sinha, S. (2012). Soft-sediment deformation structures from the Paleoproterozoic Damtha Group of Garhwal Lesser Himalaya, India. *Sedimentary Geology*, 261–262, 76–89.
97. Gokul, A.R., Srinivasan, M.D., Gopalkrishnan, K., Viswanathan, L.S. (1985) Stratigraphy and structure of Goa. In: Seminar volume on Earth Resources for Goa's Development, Panaji, Goa.
98. Gruszka, B., Van Loon, A.J. (Tom), (2007). Pleistocene glacio lacustrine breccias of seismic origin in an active graben (central Poland). In: Gruszka, B., Van Loon, A.J. (Tom), Zieliński, T., (Eds.), *Quaternary Geology – Bridging the gap between East and West. Sedimentary Geology Special Issue*, 193, 93–104.
99. Harinadha Babu, P., Ponnuswamy, M.D., Krishnamurthy, K.V. (1981). Shimoga Belt. In: J. Swami Nath and M. Ramakrishnan (Eds.), *Early Precambrian Supracrustals of southern Karnataka. Mem. Geol. Surv. India*, 112, 199-218.
100. Harker, A. (1909). *The natural history of igneous rocks*. Macmillan.
101. Hayashi, K.I., Fujisawa, H., Holland, H.D., Ohmoto, H. (1997). Geochemistry of ~1.9Ga sedimentary rocks from northeastern Labrador, Canada. *Geochim Cosmochim Acta*, 61(19), 4115–4137.
102. Hegde, V.S., Chavadi, V.C. (2009). Geochemistry of late Archaean metagreywackes from the Western Dharwar Craton, South India: implications for provenance and nature of the Late Archaean crust. *Gondwana Research*, 15(2), 178-187.

103. Hegde, V. S., Koti, B. K., Kruger, S. J. (2014). Geochemistry of the Desur lavas, Deccan traps: Case study from the vicinity of Belgaum, Karnataka and their petrogenetic inferences. *Journal of the Geological Society of India*, 83(4), 363-375.
104. Henisch, H.K. (1988). *Crystals in Gels and Liesegang Rings*. Cambridge University, Cambridge, 197.
105. Herron, M.M. (1988). Geochemical classification of terrigenous sands and shales from core or log data. *J Sediment Petrol*, 58(5), 820–829.
106. Picard, M. D., & High, L. R. (1973). *Sedimentary structures of ephemeral streams*, Elsevier, 17.
107. Holland, H. D. (1978). *The chemistry of the atmosphere and oceans*. Wiley, New York, 1.
108. Iyer, S. D., Wagle, B. G. (1987). Morphometric analyses of the river basins in Goa. *Geogr Rev India*.
109. Iyer, S.D., Banerjee, G., Wagle, B.G. (1989). Statistical analysis of lineaments of Goa. *Current Science*. 58(23), 1316-1319.
110. Iyer, S.D., Wagle, B.G., D’cruz, E.E. (1990). Dyke swarms along the Goa coast, India. In: *Proceedings of the National Seminar on Recent Research in Growth of Western India*. M.S. University of Baroda, Vadodara, 14.
111. Jay, A. E., Widdowson, M. (2008). Stratigraphy, structure and volcanology of the SE Deccan continental flood basalt province: implications for eruptive extent and volumes. *Journal of the Geological Society*, 165(1), 177-188.
112. Jayananda, M., Chardon, D., Peucat, J. J., Capdevila, R. (2006). 2.61 Ga potassic granites and crustal reworking in the western Dharwar craton, southern India: tectonic, geochronologic and geochemical constraints. *Precambrian Research*, 150(1), 1-26.

113. Jenner, G. A. (1981). Geochemistry of high-Mg andesites from Cape Vogel, Papua New Guinea. *Chemical Geology*, 33(1-4), 307-332.
114. Kalsbeek, F., Frei, R. (2010). Geochemistry of Precambrian sedimentary rocks used to solve stratigraphical problems: An example from the Neoproterozoic Volta basin, Ghana. *Precambrian Research*, 176(1), 65-76.
115. Kasanzu, C., Maboko, M. A., Many, S. (2008). Geochemistry of fine-grained clastic sedimentary rocks of the Neoproterozoic Ikorongo Group, NE Tanzania: Implications for provenance and source rock weathering. *Precambrian Research*, 164(3), 201-213.
116. Kent, R. W., Fitton, J. G. (2000). Mantle sources and melting dynamics in the British Palaeogene Igneous Province. *Journal of Petrology*, 41(7), 1023-1040.
117. Kerr, A.C., Khan, M., Mahoney, J.J., Nicholson, K.N., Hall, C.M. (2010). Late Cretaceous alkaline sills of the south Tethyan suture zone, Pakistan: initial melts of the Réunion hotspot? *Lithos*, 117, 161–171.
118. Khudoley, A. K., Rainbird, R. H., Stern, R. A., Kropachev, A. P., Heaman, L. M., Zanin, A. M., Sukhorukov, V. I. (2001). Sedimentary evolution of the Riphean–Vendian basin of southeastern Siberia. *Precambrian Research*, 111(1), 129-163.
119. Krogstad, E. J., Hanson, G. N., Rajamani, V. (1991). U-Pb ages of zircon and sphene for two gneiss terranes adjacent to the Kolar Schist Belt, South India: evidence for separate crustal evolution histories. *The Journal of Geology*, 99(6), 801-815.
120. Kröner, A. (1984). Evolution, growth and stabilization of the Precambrian lithosphere. *Physics and Chemistry of the Earth*, 15, 69-106.
121. Kuenen, P.H., Menard, H.W. (1952). Turbidity currents, graded and non-graded deposits. *Journal of Sedimentary Petrology*, 22, 83–96.
122. Kuenen, P.H. (1958). Experiments in geology. *Geological Magazine*, 23, 1–28.

123. Kundu, A., Goswami, B. (2008). A note on seismic evidences during the sedimentation of Panchet Formation, Damodar Basin, Eastern India: Banspetali Nullah Revisited. *Journal of Geological Society of India*, 72, 400–404.
124. Kundu, A., Goswami, B., Eriksson, P.G., Chakraborty, A. (2011). Palaeoseismicity in relation to basin tectonics as revealed from soft-sediment deformation structures of the Lower Triassic Panchet formation, Raniganj basin (Damodar valley), eastern India. *Journal of Earth System Science*, 120 (1), 167-181.
125. Lahtinen, R. (2000). Archaean-Proterozoic transition: geochemistry, provenance and tectonic setting of metasedimentary rocks in central Fennoscandian Shield, Finland. *Precambrian research*, 104, 147-174.
126. Langmuir, C. H., Bender, J. F., Bence, A. E., Hanson, G. N., Taylor, S. R. (1977). Petrogenesis of basalts from the FAMOUS area: Mid-Atlantic Ridge. *Earth and Planetary Science Letters*, 36(1), 133-156.
127. Larsen G., Chilingarian G.V. (1967). *Developments in Sedimentology 8: Diagenesis in sediments*. Elsevier Publishing Company.
128. Larsen, P.H. (1986). Soft sediment deformation structures in Silurian turbidites from North Greenland. *Bulletin of the Geological Society of Denmark*, 35, 19-23.
129. Le Maitre, R. W. B., Dudek, P., Keller, A., Lameyre, J., Le Bas, J., Sabine, M. J., Zanettin, A. R. (1989). A classification of igneous rocks and glossary of terms: Recommendations of the International Union of Geological Sciences, Subcommittee on the Systematics of Igneous Rocks (No. 552.3 CLA). International Union of Geological Sciences.
130. Leggett, J.K. (2012). *Marine Clastic Sedimentology: Concepts and Case Studies*. Springer Netherlands.

131. Li, S., Du, Y., Zhang, Z., Wu, J. (2008). Earthquake-related soft-sediment deformation structures in Palaeogene on the continental shelf of the East China Sea; *Frontiers of Earth Science, China*, 2(2) 177–186.
132. Liesegang, R.E. (1913). *Geologische Diffusionem*. Steinkopf, Dresden, 180 (non vide).
133. Lightfoot, P. C., Hawkesworth, C. J., Hergt, J., Naldrett, A. J., Gorbachev, N. S., Fedorenko, V. A., Doherty, W. (1993). Remobilisation of the continental lithosphere by a mantle plume: major-, trace-element, and Sr-, Nd-, and Pb-isotope evidence from picritic and tholeiitic lavas of the Noril'sk District, Siberian Trap, Russia. *Contributions to Mineralogy and Petrology*, 114(2), 171-188.
134. Lowe, D.R. (1975). Water escape structures in coarse grained sediments. *Sedimentology*, 22, 157–204.
135. Luttinen, A. V., Furnes, H. (2000). Flood basalts of Vestfjella: Jurassic magmatism across an Archaean–Proterozoic lithospheric boundary in Dronning Maud Land, Antarctica. *Journal of Petrology*, 41(8), 1271-1305.
136. Yanping, M., Jinzhou, Z. (2015). Geochemistry and Petrography of Clastic Deposits from the Late Paleozoic Shihezi Formation in the East Central of Ordos Basin, China: Implications for Provenance and Tectonic Setting. *Acta Geologica Sinica (English Edition)*, 89 (supp.), 266–267.
137. Mahoney, J. J. (1988). Deccan traps. In *Continental flood basalts* (pp. 151-194). Springer Netherlands.
138. Mahoney, J., Macdougall, J. D., Lugmair, G. W., Murali, A. V., Das, M. S., Gopalan, K. (1982). Origin of the Deccan Trap flows at Mahabaleshwar inferred from Nd and Sr isotopic and chemical evidence. *Earth and Planetary Science Letters*, 60(1), 47-60.

139. Mandal, A., Ray, A., Debnath, M., Paul, S. P. (2012). Petrology, geochemistry of hornblende gabbro and associated dolerite dyke of Paharpur, Puruliya, West Bengal: Implication for petrogenetic process and tectonic setting. *Journal of earth system science*, 1-20.
140. Manikyamba, C., Naqvi, S. M., Moeen, S., Rao, T. G., Balaram, V., Ramesh, S. L., Reddy, G. L. N. (1997). Geochemical heterogeneities of metagraywackes from the Sandur schist belt: implications for active plate margin processes. *Precambrian Research*, 84(3-4), 117-138.
141. Maravelis, A., Zelilidis, A. (2010). Petrography and geochemistry of the late Eocene–early Oligocene submarine fans and shelf deposits on Lemnos Island, NE Greece. Implications for provenance and tectonic setting. *Geological Journal*, 45(4), 412-433.
142. Marston, R.J. (1978). The geochemistry of the Archaeanvlasticmetasediments in relation to crustal evolution, northeastern Yilgarn Block, Western Australia. *Precambrian Research*, 157-175.
143. Maynard, N. C., Heppner, J. P., Egeland, A. (1982). Intense, variable electric fields at ionospheric altitudes in the high latitude regions as observed by DE-2. *Geophysical Research Letters*, 9(9), 981-984.
144. Mazumder, R., Van Loon, A.J., Arima, M. (2006). Soft-sediment deformation structures in the Earth's oldest seismites. *Sedimentary Geology*, 186, 19–26.
145. Mazumder, R., Rodríguez-López, J.P., Arima, M., Van Loon, A.J. (2009). Palaeoproterozoic seismites (fine-grained facies of the Chaibasa Fm., E India) and their soft-sediment deformation structures. In: Reddy, S., Mazumder, R., Evans, D., Collins, A. (Eds.), *Palaeoproterozoic supercontinents and global evolution*. Geological Society, London, Special Publications, 323, 301–318.

146. McLennan, S.M., Nance, W.B., Taylor, S.R. (1980). Rare earth element thorium correlation in sedimentary rocks, and the composition of the continental crust. *Geochim Cosmochim Acta*, 44, 1833–1839.
147. McBride, E.F. (2003). Pseudofaults resulting from compartmentalized Liesegang bands: update. *Sedimentology*, 50, 725-730.
148. McDonald, B., Shilts, W.W. (1975). Interpretation of faults in glaciofluvial sediments; In: Jopling, A., McDonald, B., (Eds.), *Glaciofluvial and glaciolacustrine sedimentation*. Society of Economic Paleontologists and Mineralogists Special Publication, Tulsa, Oklahoma, USA, 23, 123–131.
149. McLennan, S.M., Taylor, S.R. (1991). Sedimentary rocks and crustal evolution: tectonic setting and secular trends, *J Geol*, 99, 1–21.
150. McLennan, S.M., Nance, W.B., Taylor, S.R. (1980). Rare earth elementthorium correlation in sedimentary rocks, and the composition of the continental crust. *Geochim Cosmochim Acta*, 44, 1833–1839.
151. McLennan, S. M., Taylor, S. R., Eriksson, K. A. (1983). Geochemistry of Archean shales from the Pilbara Supergroup, western Australia. *Geochimica et Cosmochimica Acta*, 47(7), 1211-1222.
152. McLennan, S.M., Taylor, S.R., McCulloch, M.T., Maynard, J.B. (1990). Geochemical and Nd–Sr isotopic composition of deep-sea turbidites—crustal evolution and plate tectonic associations. *Geochim Cosmochim Acta*, 54, 2015–2050.
153. McLennan, S.M., Hemming, S., McDaniel, D.K., Hanson, G.N. (1993). Geochemical approaches to sedimentation, provenance, and tectonics. *Geol Soc Am Spec Papers*, 284, 21–40.
154. McLennan, S. M. (1989). Rare earth elements in sedimentary rocks: influence of provenance and sedimentary processes. *Geochemistry and Mineralogy of Rare Earth Elements*, 169-200.

155. Middleton, G.V., Hampton, M.A. (1973). Sediment gravity flows: mechanics of flow and deposition. In: Middleton, G.V., Bouma, A.H. (Eds.), *Turbidites and Deep-Water Sedimentation*. Pac. Sect. Soc. Econ. Paleontol. Mineral., Los Angeles, CA, 1-38.
156. Milliken, K.L. (2003). Late Diagenesis and Mass Transfer in Sandstone-Shale Sequences. In: (eds) Mackenzie F.T., *Treatise on Geochemistry: Second Edition*, 9, 181206.
157. Mills, P.C. (1983). Genesis and diagnostic value of soft-sediment deformation structures—a review,” *Sedimentary Geology*, 35 (2), 83–104.
158. Mitchell, C., Widdowson, M. (1991). A geological map of the southern Deccan Traps, India and its structural implications. *Journal of the Geological Society*, London, 148, 495–505.
159. Moosavirad, S. M., Janardhana, M. R., Sethumadhav, M. S., Narasimha, K. P. (2012). Geochemistry of Lower Jurassic sandstones of Shemshak Formation, Kerman Basin, Central Iran: provenance, source weathering and tectonic setting. *Journal of the Geological Society of India*, 79(5), 483-496.
160. Morgan, W. J. (1981). 13. Hotspot tracks and the opening of the Atlantic and Indian Oceans. *The oceanic lithosphere*, 7, 443.
161. Moyen, J. F., Martin, H., Jayananda, M., Auvray, B. (2003). Late Archaean granites: a typology based on the Dharwar Craton (India). *Precambrian Research*, 127(1), 103-123.
162. Müller, W., Aerden, D., Halliday, A.N. (2000). Isotopic dating of strain fringe increments: duration and rates of deformation in shear zones. *Science*, 288, 2195–2198.
163. Murphy, J. B. (2000). Tectonic influence on sedimentation along the southern flank of the late Paleozoic Magdalen basin in the Canadian Appalachians:

- Geochemical and isotopic constraints on the Horton Group in the St. Marys basin, Nova Scotia. *Geological Society of America Bulletin*, 112(7), 997-1011.
164. Mutti, E., Ricchi-Luchi, F. (1978). Turbidites of the northern Apennines: introduction to facies analysis. *International Geology Review*, 20, 125–166.
165. Nagarajan, R., Armstrong-Altrin, J.S., Nagendra, R., Madhavaraju, J., Moutte, J. (2007a) Petrography and geochemistry of terrigenous sedimentary rocks in the neoproterozoic rabanpalli formation, bhima basin, southern India: implications for paleoweathering conditions, provenance and source rock composition. *J Geol Soc India*, 70(2), 297–312.
166. Nagarajan, R., Armstrong-Altrin, J.S., Kessler, K.L., Hidalgo-Moral, E.L., Dodge-Wan, D., Taib, N.I. (2015). Provenance and tectonic setting of Miocene siliciclastic sediments, Sibuti formation, northwestern Borneo. *Arabian Journal of Geoscience*, 8, 8549–8565.
167. Nagarajan, R., Madhavaraju, J., Nagendra, R., Armstrong-Altrin, J.S., Moutte, J. (2007b) Geochemistry of Neoproterozoic shales of Rabanpalli formation, Bhima Basin, Northern Karnataka, southern India: implications for provenance and paleoredox conditions. *Rev Mex Cienc Geol*, 24(2), 150–160.
168. Nance, W. B., Taylor, S. R. (1976). Rare earth element patterns and crustal evolution—I. Australian post-Archean sedimentary rocks. *Geochimica et Cosmochimica Acta*, 40(12), 1539-1551.
169. Naqvi, S.M. (2005). *Geology and evolution of the Indian plate*. Capital Publishing Company, New Delhi, 448.
170. Naqvi, S. M., Sawkar, R. H., Rao, D. S., Govil, P. K., Rao, T. G. (1988). Geology, geochemistry and tectonic setting of Archaean greywackes from Karnataka Nucleus, India. *Precambrian research*, 39(3), 193-216.

171. Nesbitt, H.W., Young, G.M. (1982). Early proterozoic climates and plate motions inferred from major element chemistry of lutites. *Nature*, 299(5885), 715–717.
172. Nesbitt, H.W., Young, G.M. (1984). Prediction of some weathering trends of plutonic and volcanic rocks based on thermodynamic and kinetic considerations. *Geochim Cosmochim Acta* 48(7), 1523–1534.
173. Nesbitt, H. W., Young, G. M., McLennan, S. M., Keays, R. R. (1996). Effects of chemical weathering and sorting on the petrogenesis of siliciclastic sediments, with implications for provenance studies. *The Journal of Geology*, 104(5), 525-542.
174. Nesbitt, H.W., Fedo, C.M., Young, G.M. (1997.) Quartz and feldspar stability, steady and non-steady-state weathering, and petrogenesis of siliciclastic sands and muds. *J Geol*, 105, 173–191.
175. Newman, S., Finkel, R. C., Macdougall, J. D. (1984). Comparison of ^{230}Th - ^{238}U disequilibrium systematics in lavas from three hot spot regions: Hawaii, Prince Edward and Samoa. *Geochimica et Cosmochimica Acta*, 48(2), 315-324.
176. Nutman, A.P., McGregor, V.R., Friend, C.R., Bennett, V.C., Kinny, P.D. (1996). The Itsaq gneiss complex of southern West Greenland; the world's most extensive record of early crustal evolution (3900-3600 Ma). *Precambrian Research*, 78(1-3), 1-39.
177. Oertal, G. (1958). A geologia do districto de Goa, *Communicacao do Servico Geologico de Portugal*, Lisboa, 1-40.
178. Ortner, H. (2007). Styles of soft-sediment deformation on top of a growing fold system in the Gosau Group at Muttek of, Northern Calcareous Alps, Austria: Slumping versus tectonic deformation. *Sedimentary Geology*, 196, 99–118.

179. Owen, G. (1987). Deformation processes in unconsolidated sands. In: Jones, M.E., Preston, R.M.F. (Eds.), *Deformation of Sediments and Sedimentary Rocks*. Geological Society of London, 29, 11–24.
180. Owen, G. (1995). Soft-sediment deformation in upper Proterozoic Torridonian sandstones (Applecross Formation) at Torridon. *Journal of Sedimentary Research*, 65(3), 495–504.
181. Owen, G. (1996). Experimental soft-sediment deformation: Structures formed by the liquefaction of unconsolidated sands and some ancient examples. *Sedimentology*, 43(2), 279–293.
182. Owen, G. (2003). Load structures: gravity-driven sediment mobilization in the shallow subsurface. In: Van Rensbergen, P., Hillis, R.R., Maltman, A.J. (Eds.), *Subsurface Sediment Mobilization*. Geological Society of London, Special Publication, U.K., 216, 22–34.
183. Pandey, A.K., Pandey, P. (2015). Soft sediment deformation structures in late Quaternary abandoned channel fill deposit of Yamuna river in NW Sub-Himalaya, India. *Current Science*, 108(9), 1717- 1725.
184. Pande, K., Sheth, H. C., Bhutani, R. (2001). ^{40}Ar – ^{39}Ar age of the St. Mary's Islands volcanics, southern India: record of India–Madagascar break-up on the Indian subcontinent. *Earth and Planetary Science Letters*, 193(1), 39-46.
185. Paterson, S. R., Vernon, R. H., Tobisch, O. T. (1989). A review of criteria for the identification of magmatic and tectonic foliations in granitoids. *Journal of structural geology*, 11(3), 349-363.
186. Patil, S.K., Rao, D.K. (2002). Palaeomagnetic and rock magnetic studies on the dykes of Goa, west coast of Indian Precambrian shield. *Physics of the Earth and Planetary Interiors*, 133, 111-125.

187. Pearce, T.H., Gorman, B.E., Birkett, T.C. (1977). The relationship between major element chemistry and tectonic environment of basic and intermediate volcanic rocks: *Earth and Planetary Science Letters*, 36, 121–132.
188. Peate, D. W. (1997). The Paraná-Etendeka Province. Large igneous provinces: Continental, oceanic, and planetary flood volcanism, 217-245.
189. Pettijohn, F.H., Potter, P.E., Siever, R. (1972). *Sand and sandstone*. Springer, New York, 618.
190. Peucat, J. J., Mahabaleswar, B., Jayananda, M. (1993). Age of younger tonalitic magmatism and granulitic metamorphism in the South Indian transition zone (Krishnagiri area); comparison with older Peninsular gneisses from the Gorur–Hassan area. *Journal of Metamorphic Geology*, 11(6), 879-888.
191. Polat, A., Hofmann, A. W., Rosing, M. T. (2002). Boninite-like volcanic rocks in the 3.7–3.8 Ga Isua greenstone belt, West Greenland: geochemical evidence for intra-oceanic subduction zone processes in the early Earth. *Chemical Geology*, 184(3), 231-254.
192. Potter, P.E., Maynard, J.B., Pryor, W.A. (1984). Overview. In: *Sedimentology of Shale: Study guide and reference source*. Springer-Verlag, 3-73.
193. Potter, P.E., Maynard, J.B., Pryor, W.A. (2012). *Sedimentology of shale: Study guide and reference source*. Springer Science and Business Media.
194. Pram, W. K. B. N., Pohl, J. (1994). Geochemistry of pelitic and psammopelitic Precambrian metasediments from southwestern Sri Lanka: implications for two contrasting source-terrains and tectonic settings. *Precambrian Research*, 66(1), 223-244.
195. Rashid, S.A. (2005). The geochemistry of Mesoproterozoic clastic sedimentary rocks from the Rautgara Formation, Kumaun Lesser Himalaya:

- Implications for provenance, mineralogical control and weathering. *Current Science*, 88, 1832–1836.
196. Richards, M. A., Duncan, R. A., Courtillot, V. E. (1989). Flood basalts and hot-spot tracks: plume heads and tails. *Science*, 246(4926), 103-107.
197. Riley, T. R., Leat, P. T., Curtis, M. L., Millar, I. L., Duncan, R. A., Fazel, A. (2005). Early–Middle Jurassic dolerite dykes from western Dronning Maud Land (Antarctica): Identifying mantle sources in the Karoo large igneous province. *Journal of Petrology*, 46(7), 1489-1524.
198. Roddaz, M., Viers, J., Brusset, S., Baby, P., Boucayrand, C., Hérail, G. (2006). Controls on weathering and provenance in the Amazonian foreland basin: insights from major and trace element geochemistry of Neogene Amazonian sediments. *Chem Geol*, 226, 31–65.
199. Rogers, A.J., Kolb, J., Meyer, F.M., Armstrong, R.A. (2007). Tectono-magmatic evolution of the Hutti-Maski Greenstone Belt, India: Constrained using geochemical and geochronological data. *Jour. Asian Earth Sci.*, 31, 55-70.
200. Rollinson, H.R. (1993). *Using geochemical data: evaluation, presentation, interpretation*. Routledge, United Kingdom.
201. Roser, B. P., Korsch, R. J. (1986). Determination of tectonic setting of sandstone-mudstone suites using content and ratio. *The Journal of Geology*, 94(5), 635-650.
202. Roser, B. P., Korsch, R. J. (1988). Provenance signatures of sandstone-mudstone suites determined using discriminant function analysis of major-element data. *Chemical geology*, 67(1-2), 119-139.
203. Rossetti, D.D.F. (1999). Soft-sediment deformation structures in late Albian to Cenomanian deposits, Sao Luis Basin, northern Brazil: evidence for palaeoseismicity. *Sedimentology*, 46(6), 1065–1081.

204. Rossetti, D.F., Góes, A.M. (2000). Deciphering the sedimentological imprint of paleoseismic events: An example from the AptianCodo Formation, northern Brazil. *Sedimentary Geology*, 135 (1–4), 137–156.
205. Roy, A. B. (2003). Geological and geophysical manifestations of the Reunion Plume-Indian Lithosphere interactions-evidence from Northwest India. *Gondwana Research*, 6(3), 487-500.
206. Samaila, N.K., Abubakar, M.B., Dike, E.F.C., Obaje, N.G. (2006). Description of soft-sediment deformation structures in the Cretaceous Bima Sandstone from the Yola Arm, Upper Benue Trough, North eastern Nigeria. *Journal of African Earth Sciences*, 44, 66–74.
207. Sano, Y., Takahata, N., Nishio, Y., Fischer, T. P., & Williams, S. N. (2001). Volcanic flux of nitrogen from the Earth. *Chemical Geology*, 171(3), 263-271.
208. Sarma, D.S., Mc Naughton, N.J., Belousova, E., Ram Mohan, M., Fletcher, I.R. (2012) Zircon U–Pb ages and Hf-isotope systematic from the Gadag greenstone belt: Archean crustal growth in the western Dharwar craton, India. *Gondwana Research*, 22(3), 843-854.
209. Schmidt, P.W., Prasad, V., Ramam, P.K. (1983). Magnetic ages of some Indian laterites. *Palaeogeography, Palaeoclimatology, Palaeoecology*, 44, 185-202.
210. Selley, R. C. (2000). *Applied sedimentology*. Elsevier.
211. Self, S. (2006). The effects and consequences of very large explosive volcanic eruptions. *Philosophical Transactions of the Royal Society of London A: Mathematical, Physical and Engineering Sciences*, 364(1845), 2073-2097.
212. Sheth, H. C., Ray, J. S., Ray, R., Vanderkluyzen, L., Mahoney, J. J., Kumar, A., Shukla, A. D., P., Adhikari, S., Jana, B. (2009). Geology and geochemistry of Pachmarhi dykes and sills, Satpura Gondwana Basin, central India: problems of dyke-

- sill-flow correlations in the Deccan Traps. *Contributions to Mineralogy and Petrology*, 158, 357.
213. Siegenthaler, C., Finger, W., Kelts, K., Wang, S. (1987). Earthquake and seiche deposits in Lake Lucerne, Switzerland. *Eclogae Geologicae Helvetica*, 80, 241–260.
214. Siever, R. (1979). Plate-tectonic controls on diagenesis. *Journal of Geology*, 87, 127-155.
215. Sinha, S., Islam, R., Ghosh, S. K., Kumar, R., Sangode, S. J. (2007). Geochemistry of Neogene Siwalik mudstones along Punjab re-entrant, India: implications for source-area weathering, provenance and tectonic setting. *Current Science*, 1103-1113.
216. Srinivasan, R., Naqvi, S.M. (1990). Some distinctive trends in the evolution of the Early Precambrian (Archaean) Dharwar craton, South India. *Precambrian Continental Crust and its economic resources - Developments in Precambrian Geology*. Elsevier, 245–266.
217. Storey, M., Mahoney, J.J., Saunders, A.D., Duncan, R.A., Kelley, S.P., Coffin, M.F. (1995). Timing of hot spot- related volcanism and the breakup of Madagascar and India. *Science*, 267, 852-855.
218. Storey, M., Mahoney, J.J., Saunders, A.D., Duncan, R.A., Kelley, S.P., and Coffin, M.F. (1995). Timing of hot spot related volcanism and the breakup of Madagascar and India. *Science*, 267, 852–855.
219. Stow, D.A.V., Reading, H.G., Collinson, J.D. (1996). Deep seas. In: Reading H.G (Eds.), *Sedimentary Environments and Facies*. 3rd edition, Oxford, U.K., Blackwell Science, 395-453.
220. Stow, D.A.V. (2010). Principal characteristics of sedimentary rocks. In: *Sedimentary rocks in the field: A color guide*. Academic press, Elsevier, 77.

221. Stumm, W., Morgan, J. J. (1981). *Aquatic Chemistry*, 780 pp. J. Wiley and Sons.
222. Sugitani, K., Horiuchi, Y., Adachi, M., Sugisaki, R. (1996). Anomalously low Al₂O₃/TiO₂ values for Archean cherts from the Pilbara block, western Australia—possible evidence for extensive chemical weathering on the early earth. *Precambrian Research*, 80(1-2), 49-76.
223. Sukhija, B.S., Rao, M.N., Reddy, D.V., Nagabhushanam, P., Hussain, S., Chadha, R.K. Gupta, H.K. (1999). Timing and return period of major palaeoseismic events in the Shillong Plateau, India. *Tectonophysics*, 308, 53–65.
224. Sun, S., McDonough, W.F. (1989). Chemical and isotope signatures of ocean basalts. In: Saunders AD and Norry MJ (eds.) *Magmatism in the ocean basins*. Geological Society, London, Special Publication, 42, 313-345.
225. Suttner, L. J., Dutta, P. K. (1986). Alluvial sandstone composition and paleoclimate, I. Framework mineralogy. *Journal of Sedimentary Research*, 56(3).
226. Taylor, S.R., McLennan, S.M. (1983). Geochemistry of Early Proterozoic rocks and the Archean/Proterozoic boundary. *Geological Society of American Memoirs*, 161, 119-122.
227. Taylor, S. R., McLennan, S. M. (1985). *The continental crust: its composition and evolution*.
228. Taylor, S. R. (1964). Trace element abundances and the chondritic Earth model. *Geochimica et cosmochimica acta*, 28(12), 1989-1998.
229. Topal, S.G., Özkul, M. (2014). Review article: Soft-Sediment Deformation Structures Interpreted as Seismites in the Kolankaya Formation, Denizli Basin (SW Turkey). *The Scientific World Journal*, 13.

230. Torsvik, T. H., Tucker, R. D., Ashwal, L. D., Carter, L. M., Jamtveit, B., Vidyadharan, K. T., Venkataramana, P. (2000). Late Cretaceous India–Madagascar fit and timing of break-up related magmatism. *Terra Nova*, 12(5), 220-224.
231. Toulkeridis, T., Clauer, N., Kroner, A., Reimer, T., Todt, W. (1999). Characterization, provenance and tectonic setting of Fig Tree greywacke from the Archaean Barberton Greenstone Belt, South Africa. *Sedimentary Geology*, 124, 113-129.
232. Valente, A., Slaczka, A., Cavuoto, G. (2014). Soft sediment deformation structures in seismically affected deep-sea Miocene turbidites (Cilento Basin, southernly Italy). *Geologos*, 20, 67-78.
233. Van Loon, A.J. (2009). Soft-sediment deformation structures in siliciclastic sediments: An overview; *Geologos*, 15, 3–55.
234. Vanderkluysen, L., Mahoney, J. J., Hooper, P. R., Sheth, H. C., Ray, R. (2011). The feeder system of the Deccan Traps (India): insights from dike geochemistry. *Journal of Petrology*, 52(2), 315-343.
235. Vasudev, V.N., Chadwick, B., Nutman, A.P., Hegde, G.V. (2000). Rapid development of late Archaean Hutti schist belt, northern Karnataka: implications of new field data and SHRIMP zircon ages. *J. Geol. Soc. India*, 55, 529–540.
236. Vernon, R. H. (2004). *A practical guide to rock microstructure*. Cambridge university press.
237. Visher, G.S., Cunningham, R.D. (1981). Convolute laminations – a theoretical analysis: Example of a Pennsylvanian sandstone. *Sedimentary Geology*, 28, 175–188.
238. Wagle, B. G. (1982). Geomorphology of the Goa coast. *Proc. Indian Acad. Sci. (Earth Planet Sci.)*, 91 (2), 105-117.
239. Walker, R.G. (1965). The origin and significance of the internal sedimentary structures of turbidites. *Proc. Yorkshire Geol. Soc.*, 35, 1-32.

240. Watson, E. B., Capobianco, C. J. (1981). Phosphorus and the rare earth elements in felsic magmas: an assessment of the role of apatite. *Geochimica et Cosmochimica Acta*, 45(12), 2349-2358.
241. Watson, E. B., Liang, Y. (1995). A simple model for sector zoning in slowly grown crystals: Implications for growth rate and lattice diffusion, with emphasis on accessory minerals in crustal rocks. *American Mineralogist*, 80(11-12), 1179-1187.
242. Watts, A. B., Cox, K. G. (1989). The Deccan Traps: an interpretation in terms of progressive lithospheric flexure in response to a migrating load. *Earth and Planetary Science Letters*, 93(1), 85-97.
243. Wedepohl, K. H. (1991). The composition of the upper earth's crust and the natural cycles of selected metals. *Metals in natural raw materials. Natural Resources*. In: Merian, E. (Ed.), *Metals and Their Compounds in the Environment*. VCH, Weinheim, 3-17.
244. Widdowson, M., (2009). Evolution of laterite in Goa. In: *Natural resources of Goa: a geological perspective*, Mascarenhas, A. and Kalavampara, G. (eds.), Geological Society of Goa, Miramar, Goa, 35-68.
245. Widdowson, M., Pringle, M.S., Fernandez, O.A. (2000). A post K-T Boundary (Early Palaeocene) Age for Deccan type feeder dykes, Goa, India. *Journal of Petrology*, 41, 1177-1194.
246. Wimmenauer, W., (1984). Das prävariskische Kristallin in Schwarzwald. *Fortschritt der Mineralogie*, 62, 6986.
247. Wronkiewicz, D. J., Condie, K. C. (1987). Geochemistry of Archean shales from the Witwatersrand Supergroup, South Africa: source-area weathering and provenance. *Geochimica et Cosmochimica Acta*, 51(9), 2401-2416.

248. Xu, Y. G., He, B., Chung, S. L., Menzies, M. A., Frey, F. A. (2004). Geologic, geochemical, and geophysical consequences of plume involvement in the Emeishan flood-basalt province. *Geology*, 32(10), 917-920.

RESEARCH PUBLICATION

Conferences/Seminars Attended

- Presented a paper titled “**Diagenesis and deformation of the metagreywacke-argillite suite (Goa Group)**” at National Geo-Research Scholars meet 2016 from 1-4 June, 2016, held at **Wadia Institute of Himalyan Geology, Dehradun, Uttrakhand**.
- Presented a paper titled “**Mechanism of formation of sedimentary structures in Metagreywacke-Argillite strata, of Goa Group, Western Dharwar Supergroup, India**” at International Conference on “Geosciences and Environment & 32nd Annual Convention of Indian Association of Sedimentologists” at Department of Earth Sciences, **Annamalai University, Annamalainagar, Tamil Nadu, India** during 7-10, January, 2016.
- Presented a paper (poster) titled “**Role of lithology and structure on the coastal landforms of Goa, India**” at the 4th National Conference of Ocean Society of India (OSICON 2015), held at **CSIR- National Institute of Oceanography, Dona Paula, Goa** from 22-24 March 2015.
- Presented a paper titled “**Petrology and geochemistry of Archaean Greywackes of Ribandar – Chimbhel, Goa: Implication on tectonic setting**” at the National Conference on Sedimentation and stratigraphy & XXXIth convention of Indian Association of Sedimentologists, at **Department of Geology, Savitribai Phule Pune University, PUNE** form *November 12-14, 2014*.

Research Papers Published

Fernandes, G.Q., Iyer, S.D., Kotha, M., 2016. Origin and tectonic setting of Precambrian greywacke of Ribandar-Chimbel, Goa, India: Petrological and geochemical Evidences. *Acta Geologica Sinica, English Edition*, Vol. 90, No. 6, pp. 2036–2048.